

University of Southampton Research Repository ePrints Soton

Copyright © and Moral Rights for this thesis are retained by the author and/or other copyright owners. A copy can be downloaded for personal non-commercial research or study, without prior permission or charge. This thesis cannot be reproduced or quoted extensively from without first obtaining permission in writing from the copyright holder/s. The content must not be changed in any way or sold commercially in any format or medium without the formal permission of the copyright holders.

When referring to this work, full bibliographic details including the author, title, awarding institution and date of the thesis must be given e.g.

AUTHOR (year of submission) "Full thesis title", University of Southampton, name of the University School or Department, PhD Thesis, pagination

UNIVERSITY OF SOUTHAMPTON

Faculty of Physical Sciences and Engineering
Electronics and Computer Science

SPACE CHARGE BEHAVIOUR IN THICK OIL PRESSBOARD INSULATION SYSTEMS FOR CONVERTER TRANSFORMERS

by

Miao Hao

Thesis for the degree of Doctor of Philosophy

June 2015

UNIVERSITY OF SOUTHAMPTON

ABSTRACT

FACULTY OF PHYSICAL SCIENCES AND ENGINEERING

Doctor of Philosophy

Thesis for the degree of Doctor of Philosophy

SPACE CHARGE BEHAVIOUR IN THICK OIL PRESSBOARD INSULATION SYSTEMS FOR CONVERTER TRANSFORMERS

Miao Hao

With increasing desire for renewable energy integration and international power trade, the development and utilization of the high voltage direct current (HVDC) technologies for the long distance and massive power transmission have been boosted in the recent years. The reliability of the converter transformer, which is one the most important components in HVDC transmission, has become a general concern, because of its complex structure and operating conditions. It is well known that the presence of space charge can distort the electric field distribution within the dielectrics, which can potentially influence the reliability of the converter transformer by accelerating the insulation ageing or failure. Therefore, investigation and evaluation of the space charge behaviours within the insulation system similar to those in converter transformers is paramount for delivery of a reliable HVDC transmission system.

Unfortunately, the space charge behaviours in thick oil pressboard insulation systems used in converter transformers have rarely been studied due to its complex solid and liquid mixed insulation structure and severe attenuated signal that cannot be easily measured. Therefore, in this work a purpose built pulsed electroacoustic system (PEA) has been developed to allow the measurement of space charge in a thick oil-gap and pressboard combined insulation system with a total thickness of 2 mm. In order to have a better understanding of the space charge characteristics in converter transformers, three different sample configurations have been used and they are single layer pressboard, oil gap combined with single layer pressboard and oil gap sandwiched between two pressboard layers. Investigations of space charge dynamics in thick oil pressboard insulation systems under various DC stresses, polarity reversal voltages and AC/DC superimposed stresses have been successfully conducted. In addition, the impact of aged oil on the space charge behaviour has been analysed by extracting space charge features using numerical calculations to evaluate the insulation performance of the long time served converter transformer

The results identified that the space charge dependent electric field distribution is significantly distorted in the pressboard bulk or at the oil/pressboard interface under the DC stress. The peak electric stress could be much more severe than the predicted by calculations based on Maxwell-Wagner theory, particularly in the aged oil samples. After polarity reversal, the electric field increase across the oil gap can be significant due to the residual space charge in the pressboard. A method to estimate the maximum electric field enhancement immediately after polarity reversal by using the DC space charge characteristics is proposed in this work, and its effectiveness and accuracy have been experimentally validated. The space charge behaviours under AC/DC superimposed stress, in oil-pressboard insulation system are investigated for the first time in this research. The results revealed the non-linear charge injection behaviour under the superimposed stress in the oil pressboard insulation, which has been evidenced experimentally by the accelerated space charge movement and the increased charge amount when compared with under AC or DC stress separately.

This research demonstrates the severe electric field distortion caused by the space charge accumulation in the thick oil pressboard insulation system under real operating conditions of the converter transformer. This fundamental study paves the way for further improving the reliability of HVDC transmission system, leading to the realization of new rules of design, testing, operation, and maintenance are needed for converter transformers in the power industry.

Contents

Contents	iii
Chapter 1. Introduction	1
1.1 HVDC and convertor transformers	1
1.2 Oil-paper insulation in convertor transformers	6
1.2.1 Insulating oil in convertor transformers	6
1.2.2 Pressboard and paper in convertor transformers	7
1.2.3 Electric field distribution in convertor transformers	7
1.3 Space charges	9
1.4 Research objectives and aims	11
1.5 Contributions of this research work	12
1.6 Outline of the dissertation	14
Chapter 2. Space Charge in Oil-cellulose Insulation Systems	15
2.1 Space charge detection techniques	15
2.1.1 Review of space charge measurement techniques	16
2.1.2 Pulsed electro-acoustic method (PEA)	18
2.2 Characteristic assessments based on the space charge profile	21
2.2.1 Total absolute charge amount	21
2.2.2 Electric field distribution and distortion	22
2.2.3 Apparent charge mobility	23
2.2.4 Trap energy distribution	25
2.3 Space charge in single layer oil-impregnated paper	27
2.4 Space charge in multilayer oil-paper insulation system	30
2.5 Summary	33
Chapter 3. Space Charge Behaviours in Thick Oil-Impregnated Pressboar	d under
HVDC Stresses	34
3.1 Modified PEA system	35
3.2 Sample preparation and experimental setups	37
3.2.1 Sample characteristics and preparation	37
3.2.2 Experimental protocol	41
3.3 Space charge behaviours in 1 mm thick oil-impregnated pressboard	42

3.3.1 Results of pressboard with fresh oil	
3.3.2 Results of pressboard with aged oil	
3.4 Analysis and discussion	54
3.4.1 Total absolute charge amount	54
3.4.2 Electric field distortion	56
3.4.3 Apparent trap-controlled charge mobility	57
3.4.4 Trap energy distribution	58
3.5 Conclusions	60
Chapter 4. Space Charge Behaviour in Multilayer Oil Gap and Thick	Impregnated
Pressboard Systems under HVDC Stresses	61
4.1 Space charge behaviour in an oil gap combined with single layer	er impregnated
pressboard insulation system	62
4.1.1 Experimental setup	63
4.1.2 Acoustic wave transmission and reflection in the combined	system 63
4.1.3 Space charge results	66
4.1.4 Discussions	75
4.1.5 Conclusions	
4.2 Space charge behaviour in an oil gap sandwiched between	two layers of
impregnated pressboard system under HVDC stresses	83
4.2.1 Experimental setup	84
4.2.2 Acoustic wave transmission and reflection in three-layer ins	sulation system
	84
4.2.3 Experiment results	88
4.2.4 Discussions	91
4.2.5 Conclusions	94
4.3 Conclusions	94
Chapter 5 Space Charge Dynamics in a Thick Oil Gap and Pressboa	rd Combined
System under Polarity Reversal Voltages	96
5.1 Experimental setup	98
5.2 Results and Discussions	98
5.2.1 Space charge dynamics under polarity reversal voltage	98
5.2.2 Impacts of the aged oil	101
5.2.4 Impacts of the duration for polarity reversal	107
5.3 Conclusions	113

Chapter 6 Space Charge Behaviour in Oil-pressboard Insulation System	ns under
Combined AC and DC Voltages	115
6.1 Experimental setup	116
6.1.1 AC space charge measurement system	116
6.1.2 Measurement protocol	119
6.2 Results and discussion	120
6.2.1 Space charge under AC electric field	120
6.2.2 Space charge under AC and DC superimposed electric field	124
6.2.3 Impacts of the AC and DC superimposed electric field on the tot	al charge
amount	129
6.3 Conclusions	135
Chapter 7 Conclusions and Future Work	136
7.1 Conclusions	136
7.2 Recommendations for the future work	138
References	140

Definitions and Abbreviations

AC\HVAC	Alternating current\ High voltage alternating current		
Al	Aluminium		
CSC	Current Sourced Converter technology		
DC\HVDC	Direct current\ High voltage direct current		
DP	Degree of polymerization		
GTO	Gate Turn-Off thyristor		
HV	High voltage		
Hz	Hertz		
IGBT	Insulated Gate Bipolar Transistor		
IGCT	Gate-Commutated thyristor		
kV	Kilovolt		
LCC	Line commutated convertor		
LDPE	Low density polyethylene		
LIMM	Laser intensity modulation method		
LIPP	laser induced pressure pulse		
MW	Maxwell-Wagner		
PE	Polyethylene		
PEA	Pulsed electroacoustic method		
PVDF	Polyvinylidene fluorid		
PWP	Pressure wave propagation		
Sc	Semiconducting film		
SCLC	Space charge limited current		
Semicon	Semiconducting polymer		
TL	Thermo luminescence		
TPM	Thermal pulse method		
TSC	Thermally simulated current		
TSM	Thermal step method		
TTL	Transistor-transistor logic		
VSC	Voltage source convertor		
XLPE	Cross-linked polyethylene		
μ	Apparent charge mobility		
3	Permittivity		
τ	Time constant		

σ	Conductivity
ρ	Charge density
E	Electric field
ΔΕ	Distortion factor
\mathbf{E}_{t}	Trap energy level
$V_s(t)$	PEA output signal
F(t)	Pressure wave
Q(t)	Total charge amount
L	Thickness
S	Electrode area
ϵ_0	Vacuum permittivity
ϵ_{r}	Relative permittivity
E_{max}	Maximum electric field
$E_{\text{av}} \\$	Average electric field
υ	Velocity of charge carrier
q(t)	Mean value of accumulated charges
U_{s}	Surface potential
r'	Average charge centroid
$f_0(E_t)$	Original occupation rate of traps
q	Electron charge
k	Boltzmann's constant
T	Absolute temperature
v	Frequency of electron vibration
N	Trap density
Z	Acoustic impedance
G	Generation factor
T	Transmission factor
R	Reflection factor
T_{pr}	Polarity reversal duration

DECLARATION OF AUTHORSHIP

I. Miao Hao

declare that this thesis and the work presented in it are my own and has been generated by me as the result of my own original research.

SPACE CHARGE BEHAVIOUR IN THICK OIL PRESSBOARD INSULATION SYSTEMS FOR CONVERTER TRANSFORMERS

I confirm that:

- 1. This work was done wholly or mainly while in candidature for a research degree at this University;
- 2. Where any part of this thesis has previously been submitted for a degree or any other qualification at this University or any other institution, this has been clearly stated;
- 3. Where I have consulted the published work of others, this is always clearly attributed;
- 4. Where I have quoted from the work of others, the source is always given. With the exception of such quotations, this thesis is entirely my own work;
- 5. I have acknowledged all main sources of help;
- 6. Where the thesis is based on work done by myself jointly with others, I have made clear exactly what was done by others and what I have contributed myself;
- 7. Parts of this work have been published as::

Journals

M. Hao, Y. Zhou, G. Chen, G. Wilson, and P. Jarman, "Space charge behavior in thick oil-impregnated pressboard under HVDC stresses," *Dielectrics and Electrical Insulation, IEEE Transactions on*, vol. 22, pp. 72-80, 2015.

M. Hao, Y. Zhou, G. Chen, G. Wilson and P. Jarman, "Space Charge Behavior in Oil Gap and Impregnated Pressboard Combined System under HVDC Stresses", submitted to *IEEE Trans DEI*, 2015.

Conferences

M. Hao, Y. Zhou, G. Chen, G. Wilson, and P. Jarman, "Space charge behaviour in thick oil-impregnated pressboard under HVDC stresses," *in Solid Dielectrics (ICSD)*, 2013 IEEE International Conference on, 2013, pp. 397-400.

M. Hao, Y. Zhou, G. Chen, G. Wilson, and P. Jarman, "Space charge behaviour in oil and

impregnated pressboard combined insulation system," in Dielectric Liquids (ICDL), 2014 IEEE 18th International Conference on, 2014, pp. 1-4.

- M. Hao, Y. Zhou, G. Chen, G. Wilson, and P. Jarman, "Space charge dynamics in oil and thick pressboard combined system under polarity reversal voltage," *in Electrical Insulation and Dielectric Phenomena (CEIDP), 2014 IEEE Conference on*, 2014, pp. 867-870.
- M. Hao, Y. Zhou and G. Chen, "Charge dynamics in oil/pressboard and HVDC converter transformer", *CIGRE paper A2-PS2-208*, Paris, 2014.
- M. Hao, Y. Zhou, G. Chen, G. Wilson and P. Jarman, "Space charge dynamics in oil-impregnated pressboard under AC electric field", submitted to *CEIDP*, 2014 IEEE Conference on, 2015.
- M. Hao, Y. Zhou, G. Chen, G. Wilson and P. Jarman, "Space charge dynamics in oil/pressboard insulation system under AC and DC superimposed electric field", *CIGRE A2 paper Shanghai Colloquium*, Shanghai, 2015.

Signed:	 	
Date:	 	

Acknowledgment

I would like to present my sincere appreciation to my supervisor Prof. George Chen. He has shown his great patience to my work. He also provides invaluable enlightenment of this study and to firm the confidence and determination for me to complete this thesis. Through frequent meetings and discussions with him, I always could get inspiring ideas about the experiments and designs. I must thank him a lot for his generous assistance and support.

Many thanks also go to my colleagues in the Tony Davies HV lab especially Dr. Yuan Zhou, for his helps on the conductivity measurements for the mineral oil and pressboard. And many thanks to Mike and Neil for their talented and gentle technique support on setting up the modification of my new PEA system.

I would like to thank NGC Company for financial support.

At last, I would like to thank my family members who keep encourage me to go through these years.

Chapter 1.

Introduction

1.1 HVDC and convertor transformers

With the dramatically increasing of power demand and enlarging of the scope of human activity, the desire for long distance power transmission, power trade between asynchronous alternating current (AC) grids and the integration of renewable energy grow stronger day by day. As the result of continuous research and development efforts over the past century, high voltage direct current (HVDC) transmission gradually becomes an optional solution as a competition and supplement to the AC technology. [1-3]

After the development of high voltage mercury arc valve and thyristor valve used for large quantities of DC electric power transmission respectively in 1950s by Lamm [4] and in early 1970s by English Electric and ASEA [5], the development and application of HVDC technologies have been boosted. According to their working principles, today's HVDC converter technologies can be distinguished as Line-Commutated or Current Sourced Converter technology (LCC or CSC) and Voltage Sourced Converter (VSC). The LCC uses half-controllable thyristors as switching devices whereas the VSC uses fully-controllable devices such as Insulated Gate Bipolar

Transistor (IGBT), Gate Turn-Off thyristor (GTO), or Gate-Commutated thyristor (IGCT) as switching devices.

Thyristor based LCC requires a strong AC system in order to commutate. Large amount of reactive power compensators are required to compensate for the reactive power consumed by LCC HVDCs (for a typical LCC HVDC system, the amount of reactive power could be up to 76% of the real power transmitted). Moreover, due to the trapezoidal-shaped converter AC current and high component of DC bias, the HVDC converter transformer design is more complex and expensive comparing to the conventional AC transformers. AC and DC filters are additionally required to minimize the high-frequency harmonics of LCC HVDC. [6-8]

Prior to the development of VSC HVDC, LCC HVDC has played a major role in the bulk power transmission over long distance, either using overhead lines or undersea cables, and the integrations of synchronized AC networks. [9-11] Up to now, most of commercial HVDC projects with more than 1 GW power capacity were using LCC HVDC system, e.g. the BritNed project that exchanges power between UK and Netherland was operational since 2011 with 1 GW power capacity at ± 450 kV. [12]

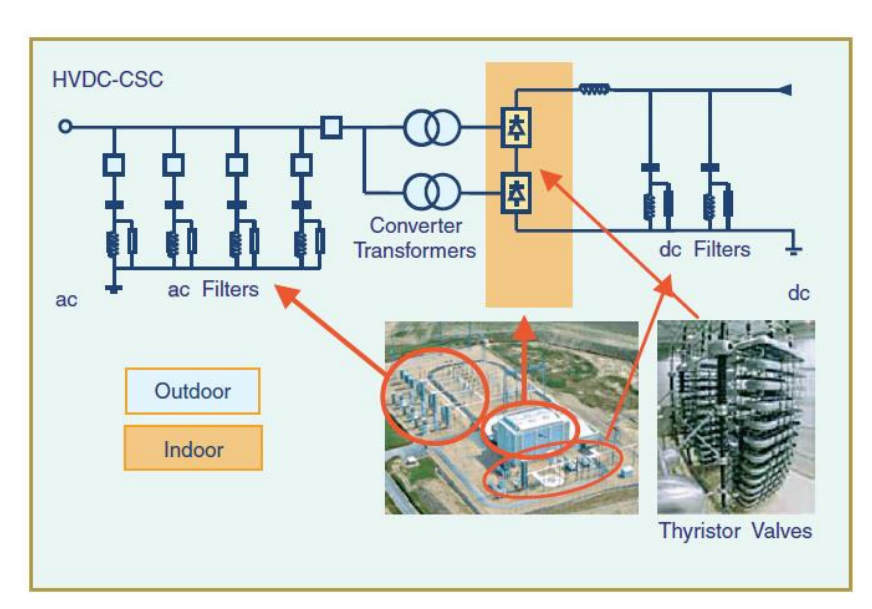


Figure 1-1. Conventional HVDC with current source converters. [7]

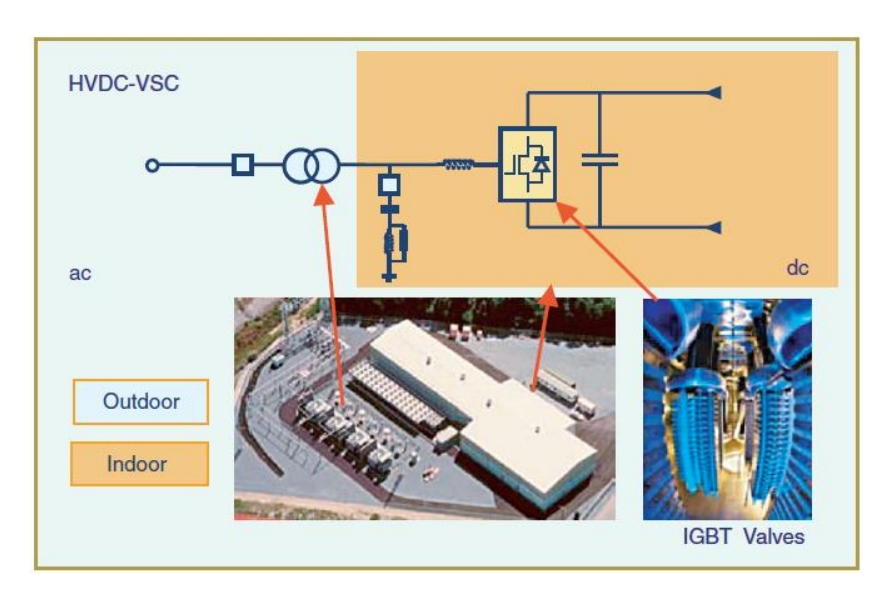


Figure 1-2. HVDC with voltage source converters. [7]

On the other hand, the VSC technology is based on the self-commutated power electronics, e.g. GTO, IGBT. It can overcome some technical limitations in the LCC system and supply a dynamic power quality control and non-drive voltage requirement and so on [13-17].

VSC HVDC can quickly control both active and reactive power independently, and even permit black start. It can be used as a virtual synchronous generator in the AC system to improve overall system stability and performance. Moreover, there are virtually no high frequency harmonics in both converter AC voltage and current, so the converter transformer requirement is not as critical as for the LCC HVDC converter transformer and no significant filters are required between the VSC converter and the converter transformer (refer to Figures 1 and 2 for details). No VSC HVDC DC voltage reversal is required even if a power reversal is required, which in the future makes VSC HVDC technology a preferred option for the construction of future DC grids.

The present limitations with the VSC technology are the voltage and current constraints of individual semiconductor devices [17]. For the same HVDC rating, a converter design using the VSC technology tends to be more expensive, larger, and incur higher losses comparing to a converter design using the LCC technology. A comparison between the power electronics in the two HVDC technologies is shown in Figure 1-3 [18]. Therefore, the applications of VSC HVDC technology are presently limited to relatively lower power applications and the areas where VSC features are more important such as low voltage ride-through capability for wind-farm integrations and the non-voltage reversal feature for future DC grid constructions. [13]

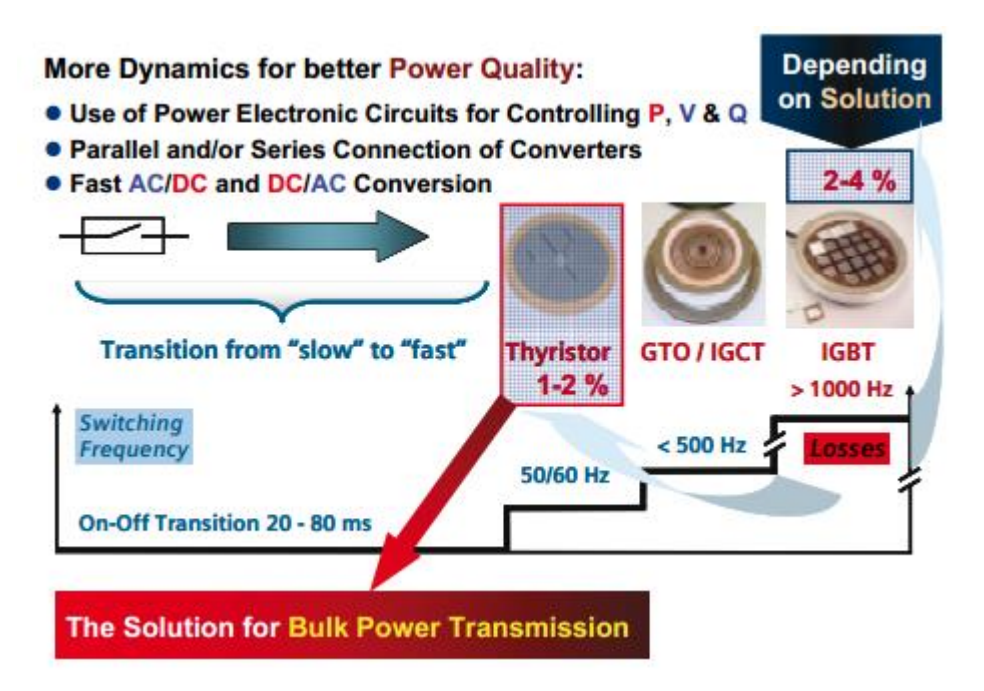


Figure 1-3 Comparison of power electronics in LCC and VSC [18]

As one of the most costly component, HVDC converters play an eminently important role in the LCC HVDC technology which is still dominating the large scale HVDC power transmission system. Unlike normal power transformers, converter transformer need to be specially designed to meet the much more complex operating conditions, including: [19]

1) Combined voltage stresses

The valve windings, connected with the rectifier and the convertor circuit, are object to operating with combined load stress of both DC and AC voltages. In addition, the transient voltages caused by lightning strike and switching operation are also added on the combined stress [19]. Therefore, the voltage distribution, dielectric breakdown strength, and space charge accumulation and distribution in the transformer insulation system are much different from conventional transformer.

2) High harmonics current

High harmonics content current is mainly generated by the operating of power convertor, which brings additional losses in the windings and overheat in tank and other structural parts. High harmonics current can also produce equipment vibration and noise. The low order harmonics, such as the 5th and 7th, can be greatly reduced by the connection of the transformer wingdings with a relative phase shift of 30 electrical degrees [19]. A characteristic distribution of current harmonics in convertor transformer windings is shown in Figure 1-4 [19].

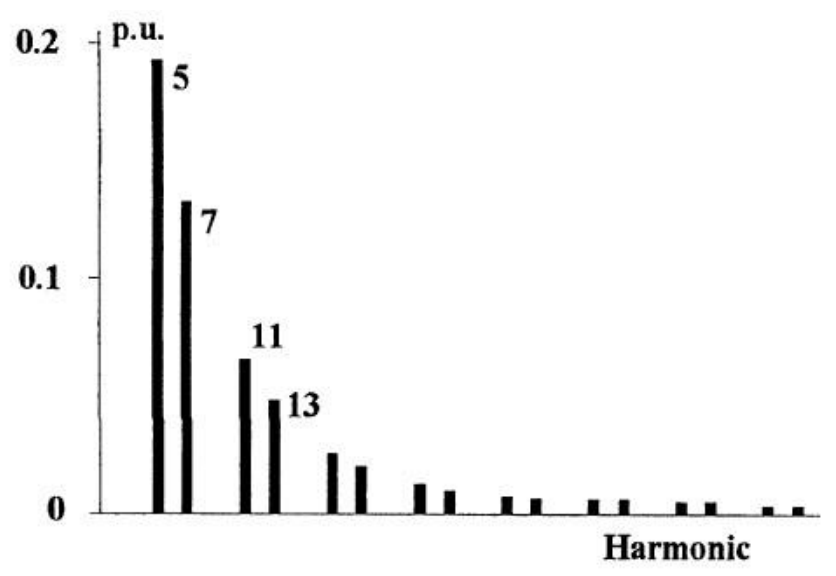


Figure 1-4 Harmonics content characteristic distribution [19]

3) Short circuit impedance

To limit the short circuit current passing through thyristor valves, relatively large short circuit impedance (16%-19%) is usually applied in convertor transformer. In addition, the impedance is a governing factor for the rate of rise of valve current during the commutation. However, the larger impedance will increase the capital cost and reactive power consumed by transformer, leading to a bigger voltage drop and losses. Therefore, industry still prefers to build convertor transformer of relatively lower reactance as a simpler structure and lower costs. [19]

Another specific requirement for convertor transformer is that it is better to ensure small tolerance in impedance between three phases and also between upper and lower bridges. Differences in impedance will lead to distortion in DC voltage form, non-characteristic harmonics, and residual currents between the three phases. The residual currents can act as DC magnetization on the core.

4) DC magnetization

DC magnetization is caused by a small residual DC current oscillating around zero, which can lead to core saturation. Thus, DC magnetization usually plays a role in structural components overheat, high levels of vibration and noise, and marginal increase in the no load loss. [19]

Unexpected failure still occurs in converter transformers, even though their operational functionality is verified and tested per various industry standards, including following:

- The main international standard IEC 61378 Convertor Transformers; [20]
- The specific routine tests: no-load losses and currents (10.3 of IEC 61378-2);
- DC separate source-voltage withstand test including partial discharge and acoustic detection measurements (10.4.3 of IEC 61378-2);

- Polarity reversal including partial discharge measurements (10.4.4 of IEC 61378-2);
 insulation resistance;
- Test of magnetic circuit insulation and associated insulation.

According to the report of CIGRE JWG A2/B4-28 [21], as shown in Table 1-1, the majority of the failures were related to the insulation or dielectric failures of the converter transformers, though the total amount of failures significantly reduced in recent years (**p** presents the failure is prevented following the diagnostic tests before permanently damaging the converter transformer). This clearly suggests that the insulation system of converter transformer need improvements on the aspects of design, maintenance and operation.

1.2 Oil-paper insulation in convertor transformers

Similar to conventional power transformers, oil-impregnated paper insulation system is also used in convertor transformers. The conventional insulation materials, such as Kraft paper and pressboard, mainly containing cellulose combined with mineral oil, have been proved to be suitable for convertor transformers as well. And similarly, oil-impregnated paper is used to cover winding conductors and pressboard sheets perpendicular to the field stress are placed around

Table 1-1. Converter transformer failures report [21]

	1991-2002	2003-2006
Mechanical	8+8P	0
Dielectric	34+10P	25+12P
Thermal	2+3P	2+52P
Induced current	1+3P	0+1P
Operator	1	0+0P
Unknown	7+1P	0+0P
Total	53+25P	27+65P

transformer windings forming a barrier system [22,23].

1.2.1 Insulating oil in convertor transformers

In the majority of cases, transformer oil is a product of petroleum refining and is a complex mixture of paraffin, naphthene, and aromatic and naphtheno-aromatic compounds. Small amount of derivatives of hydrocarbons that include atoms of other elements, such as nitrogen, sulphur and oxygen, also can be found in the composition of transformer oil. To improve its dielectric property,

some additives are also added. The mineral oil will be gradually aged when the gaseous molecules, e.g. oxygen, nitrogen and water vapour, dissolved into the mineral oil under the service condition with high temperature and electric field. The dielectric property of the oil will be then weakened, which will also lead to reduce the reliability of converter transformers and the power transmission systems. Therefore, the researches on the diagnosis and condition assessment of mineral oil under DC stresses have attracted great attentions. [24-27]

1.2.2 Pressboard and paper in convertor transformers

When it comes to the paper, taking typical Kraft paper as example, it contains about 90% cellulose, 6-7% lignin and the rest is pentosans. The natural moisture content of paper is 4-5% by weight and the insulation is dried after winding to less than 0.5%. The dried paper is then impregnated with insulating oil which increases the total dielectric strength and also serves to cool the windings [28]. Pressboards are constructed of multi layers of papers which have been compressed by a combination of heat and pressure to form a stiff and dense media. The dielectric strength and the tensile strength decrease with the ageing status of the pressboard governed by temperature, moisture and oxygen in converter transformers. [29-34] The degree of polymerization (DP) of pressboard is usually applied to indicate the paper degradation, i.e. normally, the DP of fresh paper is greater than 1000; DP 600 indicates the lightly or medium aged paper; DP 400 indicates the strongly aged paper, and the papers with DP below 400 are very strongly or extremely aged papers. [35-37]

1.2.3 Electric field distribution in convertor transformers

The electric stresses in a convertor transformer are much more complex than a conventional transformer. Insulating materials are withstanding not only the normal AC stress, lightning impulse and switching surge, but also DC stress and polarity reversal. Moreover, the properties of insulating materials result in quite different stress distributions for AC and steady state DC voltages in multi-dielectric insulation system.[19, 38] For AC voltage and transient DC voltage, the stress distribution is determined by the permittivity of pressboard and oil. The ratio of relative permittivity for cellulose and oil is about 2:1. Therefore, the capacitive stress distributes approximately double across the liquid insulation as compared to solid insulation. On the other hand, for DC voltage, the stress distribution is determined by the resistivity of insulating materials. The ratio of resistivity for oil and cellulose may vary from 1:10 to 1:500, depending on several factors like oil quality, moisture content, temperature, aging etc. This means in a steady state condition, most of the DC stress is across the solid insulation. Figure 1-5 shows the different stress distributions in oil-paper insulation [19]. Therefore, to enhance the dielectric strength in

DC conditions, a considerable increase in solid insulation is required to increase the number of barriers and their thickness. The additional paper covering is also required for the interconnection between the valve side windings and bushings. These designs could provide a high safety margin to ensure the reliability of converter transformers.

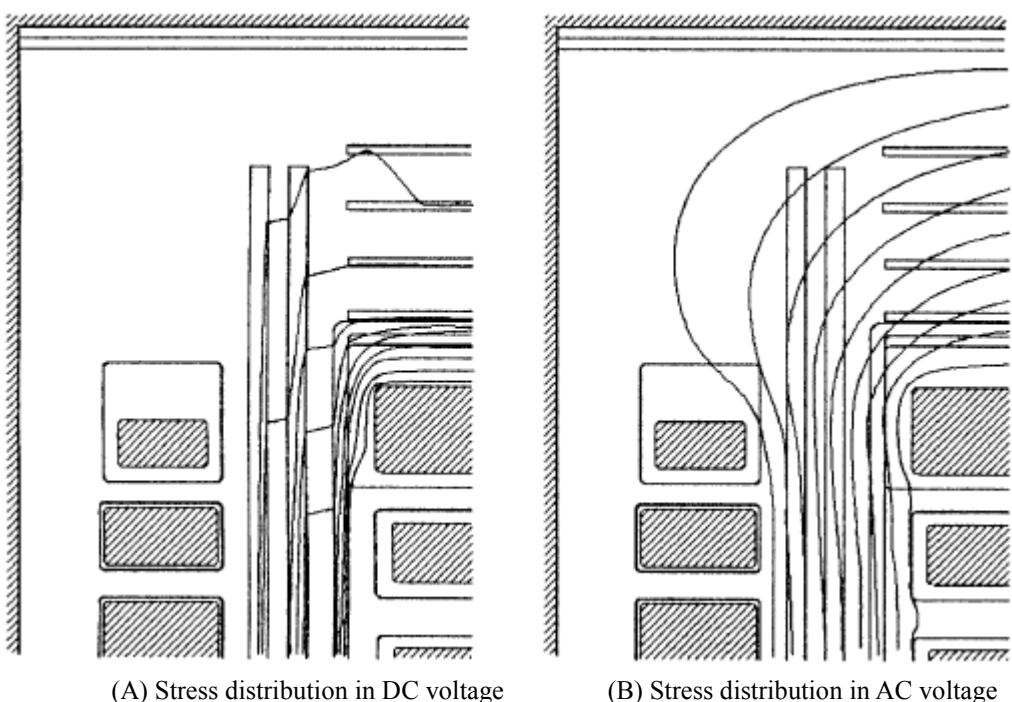


Figure 1-5 Stress distributions in oil-paper insulation under different voltage [19]

Moreover, a sudden change in DC voltage is a critical condition for DC insulation system, such as polarity reversal. When the direction of power flow is changed in HVDC transmission, the direction of current will remain the same for a few power cycles while the voltage is reversed. Many researchers [39-45] have suggested that polarity reversal has great effects on discharge and breakdown of insulation. Polarity reversal could lead to discharge in oil gaps where the electric field is enhanced due to the capacitive distribution, and also flashover along the interface between oil and cellulose. About an hour time is needed to change from capacitive distribution to resistive distribution after a polarity reversal. The voltage distribution during polarity reversal mainly depends on the ratio of the permittivity and resistivity of oil and solid insulation [44], space charge accumulated on pressboard, and stress time [41]. A typical stress distribution pattern in oil paper insulation under different stages of DC voltage is shown in Figure 1-6 [41].

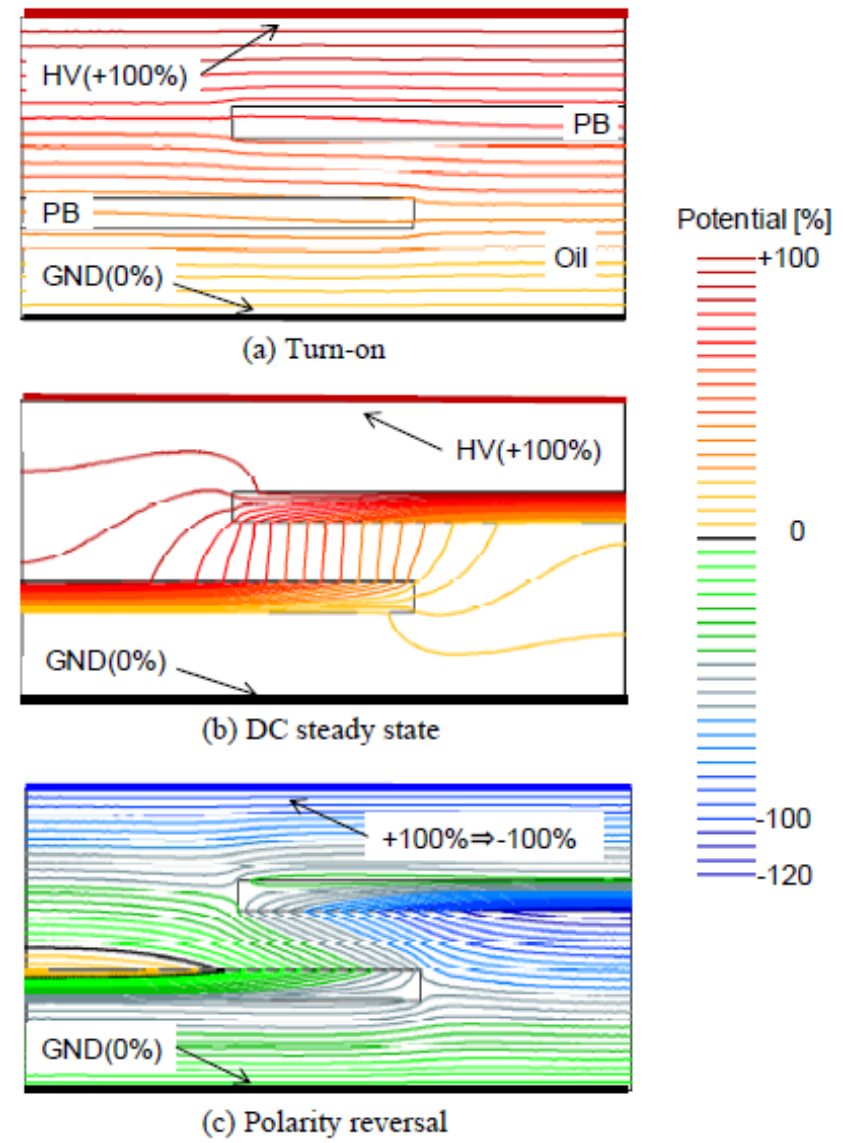


Figure 1-6 Stress distribution under HVDC operation pattern [41]

1.3 Space charges

Space charge was originally used to distinguish excess electric charge distributed in a region of continuum of space from those separate charges. These charges can be all charged carriers, such as electrons, holes, ions and charged particles, which accumulate in the bulk of dielectrics or at the interfaces between metal and dielectrics or the interfaces between two dielectrics. It is generally believed that the presence of space charge can distort the electric field distribution within the insulation bulk and at the interfaces, such as electrode/dielectrics and dielectrics/dielectrics interfaces. The enhanced electric field that beyond the design electric field strength can increase the local conductivity and potentially accelerate the degradation of the dielectric material, and even lead to breakdown [45].

Space charge usually accumulates in a solid dielectric when applied a DC field through it, and is mainly caused by [46,47]:

1) Steady DC current coupled with a spatially varying ratio of permittivity to conductivity. According to the Maxwell's theory, a steady DC current can lead to a space charge in a dielectric with a variable ratio of permittivity to conductivity varying with position, as expressed in following equation:

$$\rho = \sigma \mathbf{E} \cdot \nabla \frac{\varepsilon}{\sigma} \tag{1.1}$$

where ρ is space charge density; σ and ϵ represent the conductivity and permittivity of an insulation material. The gradient of the ratio are mainly due to the inhomogeneous structure of insulation materials, and temperature and electric stress dependent conductivity of materials. Up to now, the calculation of electric field distribution in an oil-pressboard insulation system of a converter transformer is based on the Maxwell theory.

Beside the space charges calculated from the Maxwell theory, the origins of space charge can also result from other phenomena:

- 2) Electronic charge injection. The electrons are injected/extracted from the cathode and anode near the metal/dielectric interface, when the applied electric field strength is beyond the threshold, usually 10kV/mm for LDPE [48]. The threshold electric filed in impregnated papers is strongly depended on the properties of paper and oil, which is usually about 12kV/mm [49]. Charge injection results in a homo-charge distribution- electrons are injected from the cathode while holes from the anode, so the injected charges have the same polarity as injection electrodes, shown in Figure 1-7 (A). The presence of the homo-charges in the dielectric materials usually results in a field enhancement in the middle region of the material.
- 3) Ionic process. Ions might exist in the dielectric materials due to the dissociation of addives or impurities. The degradation of the dielectric may also generate free ions by chemical reactions and dissociation of molecular chains, e.g. the dissociation of the main polymer chain or side groups in polymeric materials [50-51]. The ions move under the influence of the electric field and accumulate near the electrodes with opposite polarities, thus, ionization is responsible for the formation of hetero-charge distribution, as shown in Figure 1-7 (B). The accumulation of hetero-charges can enhance the electric field in the regions in contact with electrodes.

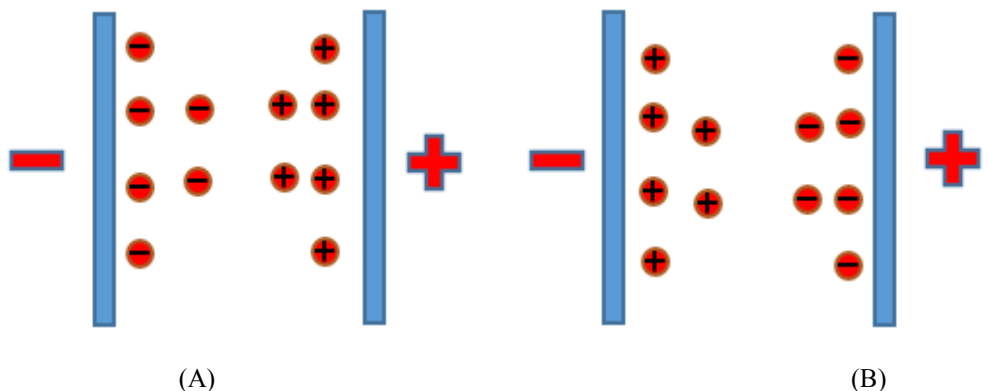


Figure 1-7 Space charge in dielectrics (A) homo charge; (B) hetero charge

Under the superposition of external stress and the stress produced by space charge accumulation, charge carriers can drift across the dielectrics or be captured by traps with different energy depths to form trapped charges [52]. And recombination/neutralization will occur when positive and negative charges meet each other. The net space charge distribution depends on the competition between these phenomena.

The origin of the space charge and its behaviour within a certain dielectric material is highly related to the operating conditions (external electric field, temperature) and the dielectric material properties, e.g. moisture content, degradation status, etc. In a converter transformer under service, the solid and liquid combined insulation system with various additives has to withstand the AC and DC combined stresses with a temperature gradient distribution (normally 70°C, higher near the winding region and lower near the cooling region). Therefore, it is essential to understand the space charge characteristics and their impacts on electrical performance in such complex conditions.

1.4 Research objectives and aims

As one of the key components in large scale HVDC transmission system, the converter transformers are expected to operate with a high reliability. However, the dielectric failure in converter transformers becomes the major concern in recent years. It is well known that the space charge accumulation in the insulation system is one of the major contributors to the dielectric failure. In the past decade, although the characteristics and mechanism of space charge have been well investigated and numerical modelled in polymeric insulation materials used for HVDC cables, the experimental observation and quantitative evaluation of space charge within oil-pressboard insulation system applied for converter transformers are still at the initial stage. Therefore, the general objective of this research work is to obtain a better understanding of space charge dynamics characteristics in oil-pressboard insulation system as break down to the following two aspects.

- 1. The space charge behaviour in oil-pressboard insulation system has rarely been investigated compared with other dielectric materials. This results from two main difficulties: firstly, the oil-pressboard insulation is a kind of mixed insulation system which consists of insulating liquid and impregnated cellulose solid pressboards. This mixed insulation provides a low cost and good dielectric property in power transformers, yet it also results in more complex space charge dynamics characteristics. The second difficulty comes from the severe signal attenuation in thick cellulose pressboards and insulating liquid, leading to an extreme poor signal/noise ratio or even no signal can be detected. This was the main reason that most of the previous studies focused only on the Kraft paper or thin pressboard with the thickness less than 0.5 mm [53-55]. Due to the fact that thick pressboards (≥ 1.0 mm) [37] immersed in mineral oil are usually used in the converter transformers, this research work is to explore and observe the space charge behaviours experimentally in such thick pressboard, as well as in the pressboards and oil gaps (barriers) combined insulation system.
- 2. The relationship between the space charge characteristics and their influence factors, e.g. applied electric fields, moisture, temperature and degradation of dielectric materials, needs to be investigated. The oil-pressboard insulation system has to withstand an AC/DC combined electric field and the polarity reversal voltage when the direction of power flow needs to be reversed. The space charge dynamics is expected to be different compared with under pure DC electric fields, and the accumulation of space charge can result in a critical electric field enhancement when the polarity of the applied electric field is reversed in a short period. Moreover, other influence factors, such as the dielectrics ageing, can further enhance the space charge accumulation resulting in a high risk on the reliability of the insulation system. The lack of the knowledge on the space charge behaviour under these real operating electric fields and the impacts of other influence factors is a major concern for design, manufacture, operation and maintenance of the converter transformers at the different stages of their life time. This research work is to explore and establish the relationship between the space charge characteristics and their influence factors under the real operating conditions aimed to provide the guidelines for power industry.

1.5 Contributions of this research work

In this research work, through the experimental measurements and the feature extractions, the space charge characteristics in oil-pressboard insulation system used mainly in the converter transformers are well understood. The knowledge gained from this fundamental research work lays the foundations for power industry to improve the reliability through design, manufacture, tests, operations, and maintenance of the converter transformers. The contributions of this research work are summarized as follows.

- 1. Since the limitations of the regular pulsed electro-acoustic method (PEA) system for thick insulation, in this research work a special PEA system is successfully designed and built to overcome the severe attenuation of acoustic signals in thick insulation, and it is also modified to enable containing both solid and liquid materials for experiments. The space charge behaviours in thick oil-pressboard insulation system with different structures have been successfully observed by using this purpose- built PEA system. The barriers in the converter transformers consist of multilayer of mineral oil gaps and pressboards. To study their impact on space charge dynamics three basic units of insulation structures are used in this work, i.e. single pressboard layer, an oil gap combined with a layer of pressboard, and an oil gap sandwiched between two layers of pressboards. The space charge profiles in each types of unit have been investigated under DC stresses. The pressboard bulk effect and the oil-pressboard interfacial effect are also studied. In order to provide a more relevant space charge profile in the real converter transformers, thick samples are applied in this work including 1 mm thick pressboards and 0.5 mm thick oil gap.
- 2. Based on the understanding of space charge characteristics in each oil-pressboard unit under DC stresses, the space charge dynamics in oil-pressboard insulation system under polarity reversal voltages and AC/DC combined voltages are investigated and observed. The significant field enhancement in the oil gap and the surfaces of pressboard after reversing the polarity of the applied electric field is experimentally confirmed. Recommendations on the polarity reversal operation and test are expressed based on the space charge dynamics characteristics. Moreover, limited negative charge accumulation in the vicinity of the dielectric/electrode interface in impregnated pressboards has been found under pure 50 Hz AC voltage by using a specially built PEA system with a fast data acquisition system. But when a small DC voltage (much lower than the threshold) is combined with the AC voltage, the amount of space charge accumulated in the insulation system is significantly increased and has to be taken into consideration for the design of insulation system in converter transformers.
- 3. The influence of the degradation of the mineral oil on the space charge behaviours has been investigated in the three insulation units under various electric fields as introduced above. The degradation process is very complex in a real transformer including both physical and chemical ageing processes. Severe aged transformer oil, which was collected from a long term serviced power transformer, is studied in this work in order to obtain the knowledge of space charge behaviours in a converter transformer at the end of its life time. Compared with fresh oil samples, its space charge dynamics characteristics showed evident differences with much higher charge mobility and larger amount of accumulated space charges, suggesting new rules of design, testing, operation, and maintenance are needed for the converter transformers in power industry.

1.6 Outline of the dissertation

This dissertation focuses on the investigation and evaluation of space charge behaviours in thick oil-pressboard mixed insulation system. It is structured in seven chapters outlined as follows.

In Chapter 1, the motivation and objectives of this research work are addressed; the contributions to power industry of this research work are summarized.

In Chapter 2, the space charge detection methods and the existing research on space charge in oil paper insulation system are briefly introduced.

In Chapter 3, the purpose -built PEA system is introduced, which allows to measure space charge within thick, solid and liquid mixed insulation system. By using this modified PEA system, the space charge dynamics in 1.0 mm thick pressboards are investigated respectively while impregnated with the fresh mineral oil and with the severe aged oil under various DC stresses. The impacts caused by the amplitude and the polarity of the applied electric fields, the degradation of the mineral oil have been analyzed by using multiple characteristic assessments based on the space charge profiles.

In Chapter 4, the research focuses on the space charge dynamics in multilayer of pressboards combined with oil gap. The interfacial effects between the pressboard and the oil gap have been studied and compared with the Maxwell theory predications.

In Chapter 5, the electric field enhancement in the pressboard and oil gap combined system has been studied. The influences of the degradation of the mineral oil and the polarity reversal time on the space charge dynamics and electric field enhancement are discussed.

In Chapter 6, the space charge behaviours in the oil-pressboard insulation system subjected to individual AC voltages with the power frequency and AC/DC combined voltages are investigated experimentally using a fast PEA system specially built in this research work. The significant impacts on the space charge accumulations caused by the small DC stress offset are observed and analysed.

In Chapter 7, the conclusions of the overall research work are drawn on the space charge characteristics in oil-pressboard insulation system used in converter transformers. Additionally, the limitations of the current work are discussed and the directions of the future work are also suggested.

Chapter 2.

Space Charge in Oil-cellulose Insulation Systems

This chapter first introduces the various space charge detection techniques and the pulsed electroacoustic (PEA) method is detailed. Then some space charge feature extraction methods that are normally used for evaluation of dielectric materials are reviewed. The existing researches on the space charge in oil-cellulose insulation (oil, paper and pressboard) used for converter transformers and HVDC cables (oil filled cable and mass-impregnated cable) are acknowledged and discussed.

2.1 Space charge detection techniques

The space charge detection techniques are proposed to measure the magnitudes and the locations of the space charges within the dielectric materials. The way used to develop the detection techniques can significantly affect the observation and understanding of the space charge behaviours in dielectrics.

2.1.1 Review of space charge measurement techniques

Space charge phenomena keep attracting increased attentions since the past few decades, due to the rise of HVDC power transmission and renewable energy. The development of the space charge detection and mapping techniques also has been accelerated. From 1970s, various techniques for measuring space charge have been developed and improved in the following years. According to the different ways to treat samples, these techniques can be recognized as two classes, destructive and non-destructive techniques.

The early approaches of destructive measurement to quantify space charge are dust figure method [56] and probe method [57, 58]. The samples used in these methods need to be cut into slabs first, and then polarity sensitive powder or a capacitive probe is used to detect the charges distributed on the surface of slabs. However, the disadvantages are evident for destructive techniques: the destructive sample preparation can affect the charge distribution, and in fact, these methods are measuring the surface charges.

On the other hand, non-destructive techniques have obvious advantages on treating samples to obtain quantitative information of space charge in dielectrics [59]. All these techniques are following a same principle that an external physical quantity is applied and interacts with the accumulated charges within the dielectrics, and then generates another physical quantity detected by other external measurement system. Different physical quantities are used in different methods, which can be temperature, pressure, electrical voltage or current signal. The first non-destructive technique for space charge measurement was introduced by Collins [60] in 1970s, from which modern space charge measurement methods are essentially improved. The basic principle for non-destructive techniques can be concluded as an externally generated wave quantity (thermal or acoustic/pressure) travels through the whole sample to create a temporary and non-destructive displacement of space charge by interacting with charges in the bulk of sample. This displacement can lead to a time-dependent change in charges induced by space charge, and be detected from the electrodes. Therefore, these methods essentially measure the electrical signal. The frequently used techniques that involve thermal expansion or disturbance include: thermal pulse method (TPM) [61], thermal step method (TSM) [62] and laser intensity modulation method (LIMM) [63]. Alternatively, those methods using pressure pulse, normally referred to as PWP (pressure wave propagation method) instead of thermal pulse mainly include: piezoelectrically generated pressure pulse method (PIPP) [64], laser induced pressure pulse method (LIPP) [65].

Table 2-1. Summary of non-destructive space charge detection techniques [59,64]

iabic	_ i. Sammary	or non desti	•		ection techniq	[405 [57,04]
Method	Disturbance	Scan	Detection	Resolution	Thickness	Comments
Method	Distuibunce	mechanism	process	[µm]	[μm]	Comments
TPM	Absorption of short–light pulse in front electrode	Diffusion according to heat conduction equations	Voltage change across sample	2	25	High resolution, requires deconvolution
TSM	Applying Two isothermal sources across sample	Thermal expansion of the sample	Current between sample electrodes	150	2000–20000	Deconvolution is required.
LIMM	Absorption of modulated light in front electrode	Frequency— dependent steady— state heat profile	Current between sample electrodes	2	25	Numerical deconvolution required
LIPP	Absorption of short laser light pulse in front electrode	Propagation with longitudinal sound velocity	Current between sample electrodes	1	100-1000	No deconvolution required. No report on fast- varying space charge measurement.
PIPP	Absorption of piezoelectric ally generated short pulse in metal target	Propagation with longitudinal sound velocity	Current or voltage between sample electrodes	5	5-200	Resolution Improved with deconvolution . Also used for surface charge measurements and fast- varying space charge measurement.
PEA	Force or modulated electric field on charges in sample	Propagation with longitudinal sound velocity	Piezoelectr ic transducer at sample electrode	5-100	50-10000	Deconvolution is required. Also used for surface charge measurements and fast-varying space charge measurement.

Unlike the non-destructive techniques above, in the pulsed electro-acoustic method (PEA), developed in the 1980s by Takada [66], a short electrical pulse is applied to the sample. The acoustic wave can be produced when the space charge is forced by the pulsed field. Then this acoustic wave is detected by a piezoelectric transducer (PVDF foil) that converts the acoustic signal into electrical signal. Therefore, essentially, the PEA method measures acoustic signal. Compared with other non-destructive techniques, as shown in Table 2-1, the PEA method has the advantage on measuring the relative thick samples with a good resolution. Moreover, it can be

simply improved for the specific purposes, hence, it has become to one of the most popular charge measurement technologies. The more detailed description of the PEA method will be introduced in the next part.

2.1.2 Pulsed electro-acoustic method (PEA)

PEA method is widely used in academic research and industrial to profile space charge in solid dielectrics around the world. Since it was developed in 1981, PEA method has been continuously improved for different specific properties. In this work, PEA method is used for measuring the space charge dynamics in oil-paper/pressboard insulation system.

The principle of PEA measurement is illustrated in Figure 2-1, where $V_p(t)$ is the pulsed voltage; q(t) is the electric charge distributed in the sample; F(t) is the acoustic pressure wave as the function of time, the shape of F(t) is same as the pulsed electric field; and $V_s(t)$ is the transducer output as voltage signal. When a pulse voltage is applied to the sample with internal space charge, the charges within the sample or even on the surface will move and generate acoustic waves under the Coulomb force caused by the pulsed electric field. These acoustic waves propagate through the sample and are detected by the attached piezoelectric transducer, which converts the acoustic signal to the electrical signal. Then, this electrical signal is amplified and transferred to an oscilloscope. After the calibration processing and mathematic treatment, the detailed space charge distribution can be acquired. The amplitude of the signal is proportional to the charge quantity, and the signal delay indicates the distance from the sensor, i.e. the position of the charge. In this manner, the space charge distribution is measured quantitatively and non-destructively [67-69].

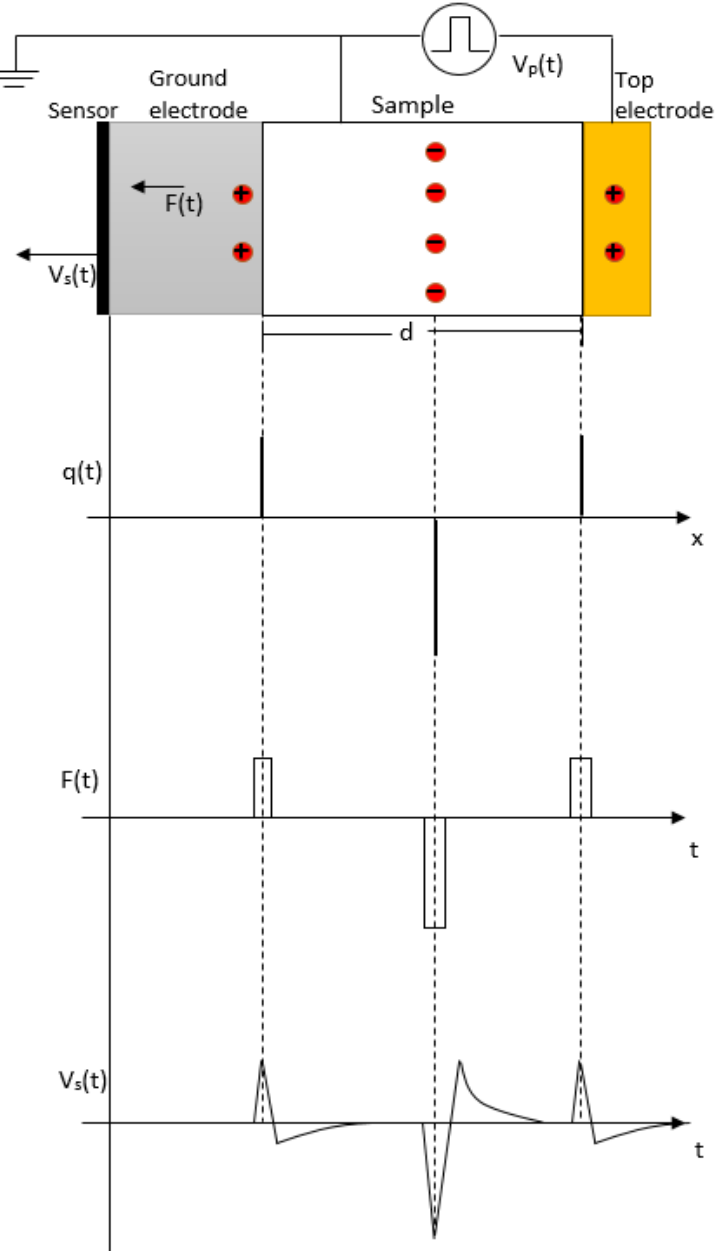


Figure 2-1 Basic principle of PEA method

A typical schematic diagram of PEA setup is shown in Figure 2-2. The system mainly consists of top electrode, ground electrode, piezoelectric sensor and amplifier. The sample is mounted between the top electrode and ground electrode. The different materials of electrodes usually lead to different injection conditions to the sample. For matching the acoustic impedances between sample and electrodes, semiconducting polymer (Sc) is selected as top electrode material while aluminium (Al) as ground electrode material. Biased DC voltage and pulsed voltage are respectively applied from top electrode to the sample through a protecting resistance and a coupling capacitor. The typical pulsed voltage is 0.1-2 kV with a width of 5-200 ns. The acoustic waves produced by the interaction between the pulsed field and space charge are detected by the piezoelectric sensor attached under the ground electrode, and then converted into electrical signal. Normally, there are two materials used for making piezoelectric transducer, lithium niobate

(LiNbO₃) and polyvinylidene fluoride (PVDF). After that, an absorber made of same acoustic property as the sensor is used to absorb the acoustic waves that transfers to the sensor for avoiding the acoustic reflection. The output signal of transducer is amplified by a broadband amplifier (DC to 500 MHz) which is placed close to the sensor and absorber in a shielding box underneath the ground electrode in order to minimize the noise coupling. This amplified electrical signal is then displayed onto a digital oscilloscope. For the normal PEA system, the typical spatial resolution is $10 \mu m$ and the magnitude resolution of charge density is about 0.1 C/m^3 . [70]

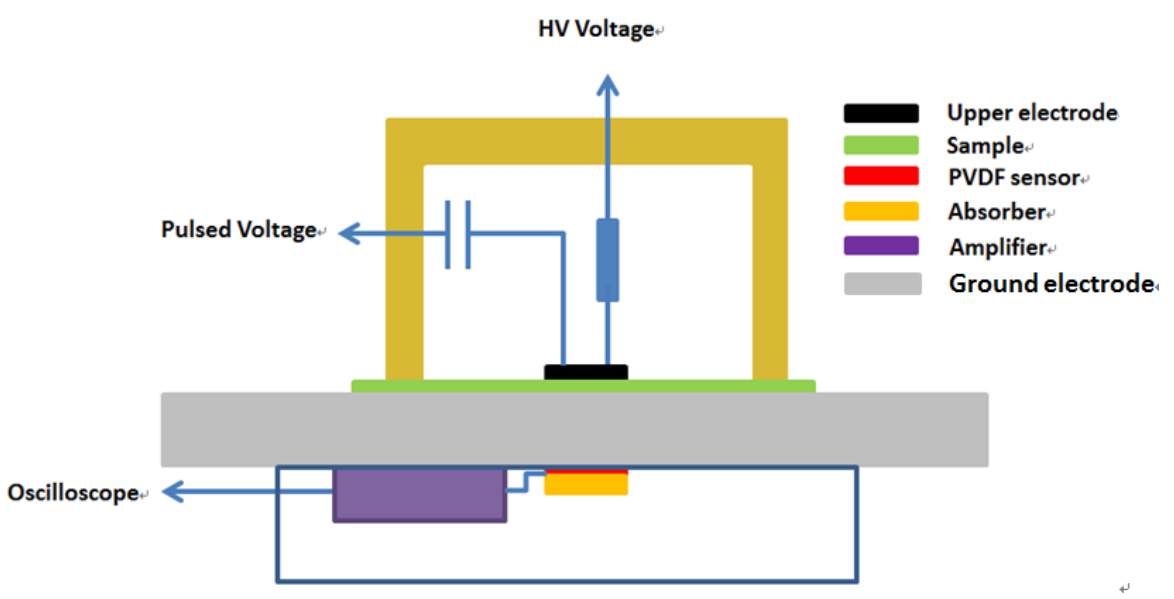


Figure 2-2 Typical structure of PEA system

Normally, the output signal shows a distortion peak immediately after the first peak, as shown in Figure 2-3. However, this distortion peak is not caused by the real space charge, but the system response, so it needs to be eliminated from the output signal through a process named deconvolution. [71]

The relationship of output signal voltage $V_s(t)$ from the transducer and the transmitted pressure wave F(t) can be convoluted as:

$$V_s(f) = H(f) \cdot F(f) \tag{2.1}$$

An impulse force can be used to obtain the transfer function H(f), which has a known wave shape (assuming no space charge in the bulk). The space charge distribution can be obtained from the deconvolution and the inverse Fourier transform process. The calibrated charge profile is demonstrated in Figure 2-4.

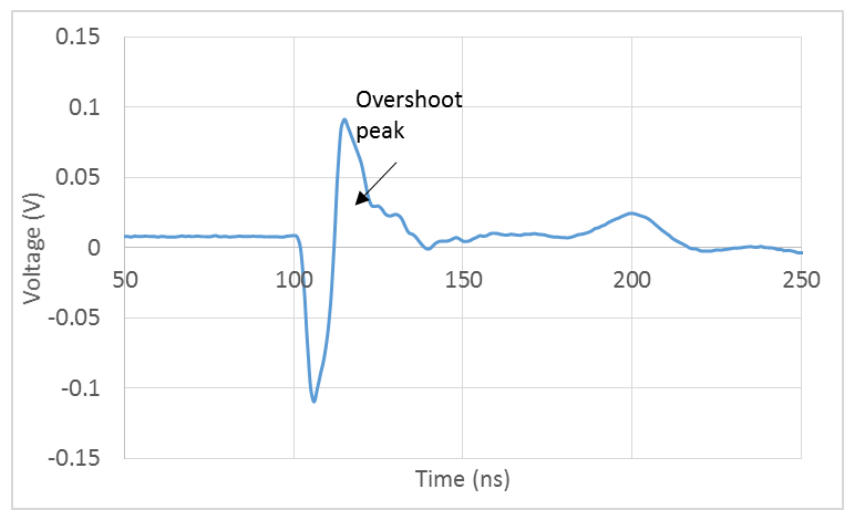


Figure 2-3 Typical PEA output signal in a 0.5 mm thick impregnated pressboard.

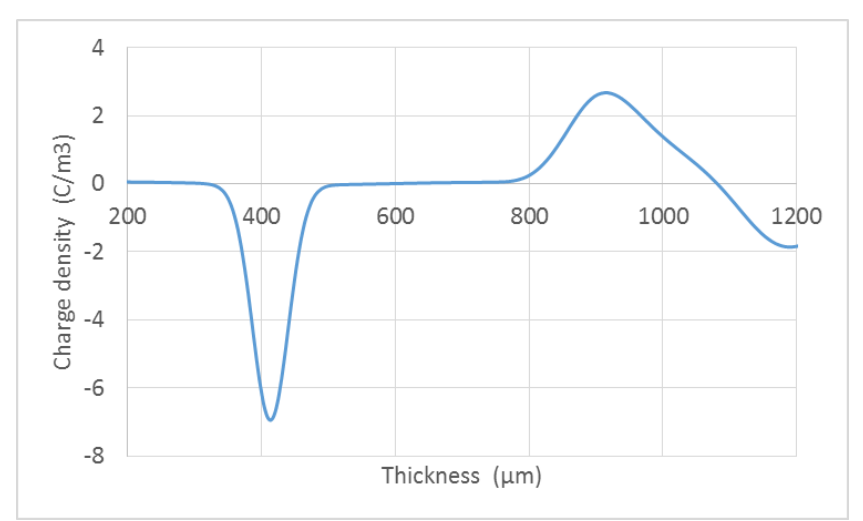


Figure 2-4 Calibrated space charge profile in a 0.5 mm thick impregnated pressboard.

An outstanding advantage of PEA technique is the simple structure that can be conveniently modified for a specific application. In this work, a purpose-built PEA system for investigating space charge dynamics in thick liquid and solid mixed dielectric materials is introduced in Chapter 3.1.

2.2 Characteristic assessments based on the space charge profile

To better understand the space charge characteristics, the space charge profiles obtained from PEA measurements need to be further analysed using various assessment tools. In this section, four typical assessment tools are introduced.

2.2.1 Total absolute charge amount

The accumulation of space charge within the dielectrics is main reason for the electric field distortion. The amount of the accumulated charges, therefore, can obviously indicate the

dielectric properties of the materials. Moreover, by plotting the charge amount vs. the measurement time, a time dependent charge amount dynamics can be obtained, which can be further used to estimate some useful parameters indicating the status of dielectrics, e.g. apparent charge mobility and trap depth.

The total absolute amount of space charge can be calculated using the Equation (2.2) for the measured charge density:

$$Q(t) = \int_0^L |\rho(x, t)Sdx|$$
 (2.2)

where L is the thickness of the sample, $\rho(x, t)$ is the charge density, S is the area of the electrode.

The measured charge density can be obtained during the application of the external voltage (named as volt-on test) or after the removal of the external voltage (named as decay test). Therefore, the calculated time dependent charge amount can be used for describing the build-up or dissipation characteristics for the dielectrics. In some studies related with a certain type of charge carriers, e.g. electrons, the amount of positive charges and negative charges can be calculated separately, rather than absolute amount of all the accumulated charges.

2.2.2 Electric field distribution and distortion

• Based on the electrostatic theory, the electric field is produced by the presence of charges, the relationship is expressed by the Equation (2.3).

$$E(x) = \int_{0}^{x} \frac{\rho(x)}{\varepsilon_0 \varepsilon_r} dx \quad 0 \le x \le L$$
 (2.3)

where $\rho(x)$ is the charge density, ϵ_0 is the vacuum permittivity, ϵ_r is the relative permittivity of the test sample, which is assumed to be constant, L is the thickness of the sample. Therefore, the electric field distribution along the sample thickness can be obtained based on the experimental measured charge density distribution.

Then, the distortion factor ΔE of electric field for the dielectrics can be further calculated by the Equation (2.4).

$$\Delta E = \frac{E_{max} - E_{av}}{E_{av}} \times 100\% \tag{2.4}$$

where the E_{max} is the maximum value of the electric stress in the dielectric bulk in the presence of space charge accumulation; E_{av} is the average applied electric stress.

The distortion factor is also known as the electric field enhancement, which directly shows the impact of the accumulated charges on the electric field distribution within the dielectrics. The larger field enhancement usually indicates a higher local electric field than the designed (or expected) electric field within the dielectric material.

2.2.3 Apparent charge mobility

The mobility of charge carriers in an insulation can indicate the charge transport and extraction mechanisms in a dielectric material [72-75]. It is also applied as a marker of the degradation of the dielectrics [76,77]. Unfortunately it is usually difficult to measure the charge mobility. However, its quantities can be estimated from the depolarization/decay characteristics measured by the PEA system.

The dissipation of the accumulated space charge after removing the external electric field results from the charge extraction from the dielectrics to the electrode or the recombination within the dielectrics. If the recombination can be neglected, the time that the charges drift away from the dielectrics correlates with the time that charges spend within traps and the transit time between traps. With respect to the time that charges are controlled by the traps, the transit time can be negligible. The calculated apparent mobility is only dependent on the time charges spent within traps during the depolarization process, this mobility also named as apparent trap-controlled mobility [52,78].

The derivation of the apparent charge mobility is briefly explained as below [52]:

At relatively high electric field, the apparent charge mobility usually can be expressed as:

$$\mu = v/E \tag{2.5}$$

where v is the velocity of charge carrier and the E is the mean applied electric field.

Then the mean value of the volume density of the space charge at the time t of depolarization can be calculated from the space charge profiles by the following equation:

$$q(t) = \frac{1}{L} \int_0^L |\rho(x, t)| dx$$
 (2.6)

where q(t) is charge accumulated in the sample at the time t of depolarization, $\rho(x, t)$ is charge detected at time t in insulation section x, L is the distance between two electrodes. However, this equation is not very accurate as the total charge revealed by the measurement system comes from the superposition of positive and negative charge layers, so that the measured net charge could be

lower than the real accumulated charge. This usually occurs in high electric field or samples with high conductivity. [52]

Furthermore, recombination can be neglected based on some assumptions, including:, the relationship between charge depolarization time and trap depth (the charges stored in the deep traps moving slower), charge densities are replaced by their average values, and the prevailing charge is unipolar and located close to electrodes. These assumptions also can be expressed as follows:

1. The total current density is all contributed by the dissipation of the accumulated charges measured by the PEA method, according to the charge conservation law:

$$J(t) \cong Ldq(t)/d(t) \cong q(t)v \tag{2.7}$$

where q(t) is the mean charge density through the thickness of the material, calculated from the Equation (2.6), L is the thickness of the sample.

- 2. The charge density is uniform within the insulation thickness, due to the replacement of the mean value.
- 3. According to the Gauss theorem, the electric field at the electrodes can be approximately calculated by applying the mean space charge instead of the local space charge along the insulation thickness:

$$E(x,t) \approx q(t)L/2\varepsilon_r\varepsilon_0 \tag{2.8}$$

where, ε_0 is the vacuum permittivity, ε_r is the relative permittivity of the test sample.

Therefore, considering the assumptions above and the definition of mobility, the mobility can be written as:

$$\mu = \frac{v}{E} = \frac{L}{q(t)E} \frac{dq(t)}{dt}$$
 (2.9)

By combining Equation (2.8) and Equation (2.9), the simplest but severely approximate expression of trap-controlled mobility thus is obtained [52]:

$$\mu(t) = \frac{2\varepsilon_0 \varepsilon_r}{a(t)^2} \frac{dq(t)}{dt}$$
 (2.10)

Due to the space charge measurement process of the PEA technique, the very beginning of the depolarization process is hard to be measured. Therefore, the investigation of the shallow traps or very fast moving charges is limited to this method.

Although the equation above brings large approximations due to the many assumptions, the apparent charge mobility can be simply and directly obtained from the depolarization results by using the PEA method. It has been proved that this method can be used to estimate the characteristics of the dielectric material, especially applied for comparison of different materials by simply obtained the space charge results from depolarization process. [76,78]

2.2.4 Trap energy distribution

The estimation of trap depth is based on the researches on the surface charge depolarization in [79]. The research indicates that the charge density has correlation with the depolarization current in the corona discharging, and generally, charge condition inside dielectrics can be represented according to the measurement of surface potential. Therefore, the average charge centroid after corona charging locates on the traps within a thin layer, and the equivalent surface charge density has a direct proportional relation with the surface potential U_S. The surface potential can be calculated from the following equation:

$$\rho = \varepsilon_0 \varepsilon_r U_s / r' \tag{2.11}$$

where ρ is the equivalent surface charge density; ϵ_0 is the dielectric constant under vacuum; ϵ_r is the relative dielectric constant; U_S is the surface potential; r'is the average charge centroid.

Because the relationship between the decay of surface potential and the current is

$$i(t) = C \frac{dU_s(t)}{dt}$$
 (2.12)

where $C = \varepsilon_0 \varepsilon_r S/L$; S is the surface area; L is the thickness of test sample.

Then, the current density can be obtained by

$$j = \frac{\varepsilon_0 \varepsilon_r}{L} \frac{dU_s(t)}{dt} = \frac{r'}{L} \frac{d\sigma(t)}{dt}$$
 (2.13)

In the corona discharge, the variation of charge density in the trap (potential decay) is approximate to an exponential decay [80], which is

$$\rho = Ae^{-t/\tau} \tag{2.14}$$

where A is a constant; τ is the constant of decay time. The variation law of the current density including the constant of decay time can be obtained by

$$|j(t)| = \frac{r'}{L} \frac{A}{\tau} e^{-t/\tau}$$
 (2.15)

It assumes that the carriers bounded in shallow traps are released firstly, and later the carriers bounded in deep traps are released, when the applied voltage is removed. The release current which changes with decay time at different temperatures illuminates the distribution of trap energy in the sample surface. On the assumption that the carriers will not be trapped again, the relationship among the trap energy level E_t , the current density j and the trap density N_t can be calculated by [80]

$$E_{t} = kTln(vt) (2.16)$$

$$j = \frac{qLkT}{2t} f_0(E_t) N(E_t)$$
 (2.17)

where $f_0(E_t)$ represents the original occupation rate of traps inside the dielectrics. Normally, the value used is 1/2 according to many references based on the experimental observations [80,81]; q is the electron charge; k is the Boltzmann's constant; T is the absolute temperature; v is frequency of electron vibration. The trap energy of electron is calculated from the bottom of the conduction band, and the trap energy of hole is calculated from the top of the valence band.

If
$$C_1 = \frac{qLkT}{2t} f_0(E_t)$$
, $C_2 = \frac{r'A}{L}$, C_1 and C_2 are constant, then

$$N(E_t) = \frac{C_2}{C_1} \frac{t}{\tau} e^{-t/\tau}$$
 (2.18)

Therefore, after obtaining the decay curve of surface charge from PEA data, with the decay time being constant, the surface trap energy distribution can be calculated by equation above. Another derivation of the trap depth based on the similar principle is introduced in [78].

However, similar to the apparent charge mobility, the calculation of the trap depth is also based on the assumptions that 1) the accumulated charges are located on the surface, i.e. the recombination or the net charges will affect the results; 2) the de-trapped charges will not be retrapped; 3) use the average charge density along the thickness of the sample instead of the localized charge density. This estimation method still can provide useful information on the trap depth to distinguish different properties of samples, which has been proved in multiple researches related with polymeric dielectrics as well as oil-paper insulation. [79,82]

Theoretically, all these feature extraction methods can be applied to the space charge characteristics obtained from any space charge detection techniques. With the widely applications of the PEA method in recent years, these feature extraction methods are often used in both academia and industry as the assessments for dielectric materials based on the PEA results.

2.3 Space charge in single layer oil-impregnated paper

Oil-paper insulation systems have been used in power industry for a long time, as the main insulation in various power equipment under both AC and DC voltages, such as the transformers, cables, bushings and other equipment. Space charge has been regarded as one of the major issues related to dielectric ageing and failures of HVDC equipment. It is generally known that space charge accumulated in the bulk or on the interface of dielectric materials can distort the local electric field distribution [83]. This effect will lead to a great increase in the electric stress inside the insulation and accelerate the damage of insulation material, such as ageing processes, partial discharge and even breakdown. Therefore, the research on the space charge behaviours in oil-paper insulation plays a significant role in improving insulation performance and the reliability of HVDC equipment.

Compared with solid dielectrics, such as polyethylene (PE), the published research in oil-paper insulation is quite limited. The space charge measurement in oil-paper insulation system started in 1990s. Liu, et al. [84] first time investigated the space charge accumulation in oil-impregnated pressboard under HVDC by using the pressure wave propagation (PWP) method in 1994. The results, as shown in Figure 2-5, indicate a field dependent space charge behaviour within the single layer impregnated pressboard, i.e. at lower electric field, only negative charges accumulated in the vicinity of both electrodes, while the accumulation of homo charges can be observed under a higher electric field.

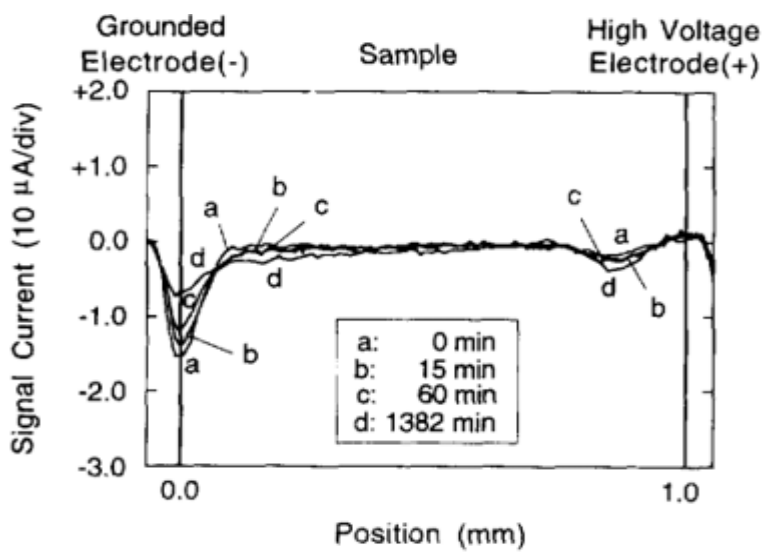


Figure 2-5. Time dependence of current measured in pressboard at 15 kV/mm by PWP [84]

Moreover, a series of experimental works then carried out based on the PWP method, including the oxidized oil [85], moisture content in pressboard [86] as well as the impacts of polarity reversal voltage [87]. The efforts can be summarized as: 1) the ageing of the mineral oil can increase the amount the accumulated charges within a fixed voltage application time; 2) the

moisture concentration in the pressboard results in an increase of hetero-charge accumulation; 3) after polarity reversal, the accumulated negative charges in the vicinity of the ground electrode can enhance the electric field in that region. However, the results are not satisfactory at that time due to the complicated property of oil-impregnated pressboard insulation and the resolution limits of the experimental equipment. Although the PWP technique obtains the correct space charge profiles, similar to the PEA method, the noise caused by the unstable pressure wave is quite large [88], which is a special case in oil-paper insulation with a large attenuation during the pressure wave propagation. Since wide applications of the PEA method, Jeroense et al. investigated the space charge behaviour in thin oil-impregnated paper (around $100 \mu m$) used for HVDC cables in 1997 [53]. They concluded their results in three general trends in oil-impregnated paper: 1) homocharge is always observed for both electrodes; 2) specific charge growth and decay patterns occur, as shown in Figure 2-6; 3) the growth and decay patterns indicate two time constants, short one (< 1 minute) and long one (> 30 minutes) as shown in Figure 2-7. [53]

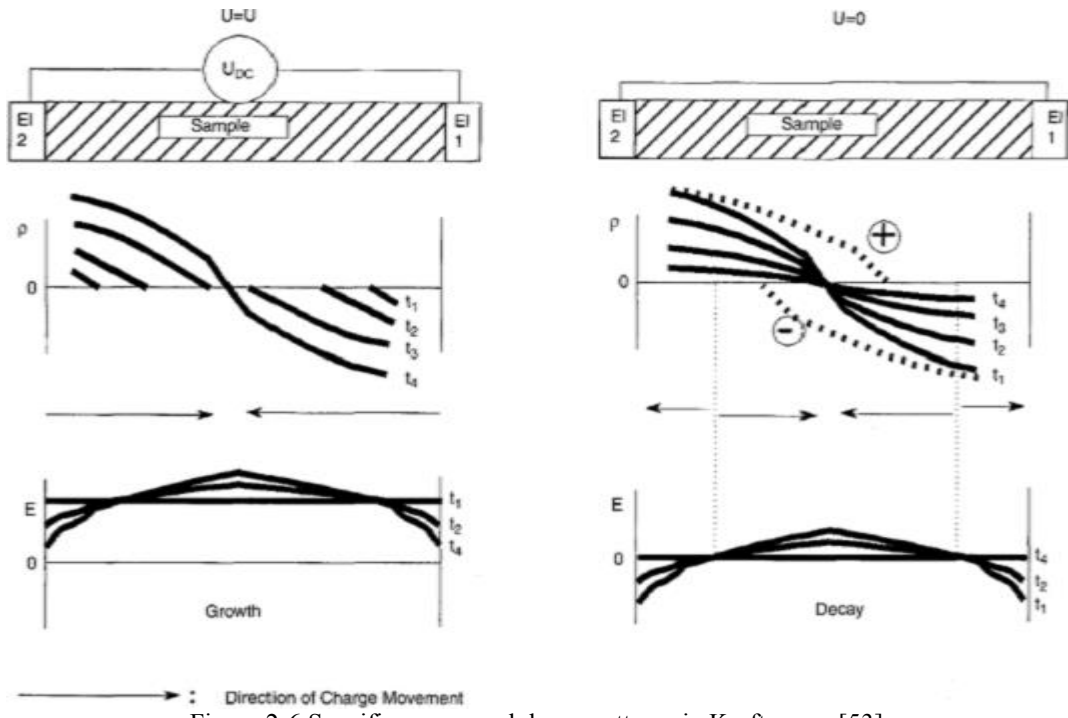


Figure 2-6 Specific grown and decay patterns in Kraft paper [53]

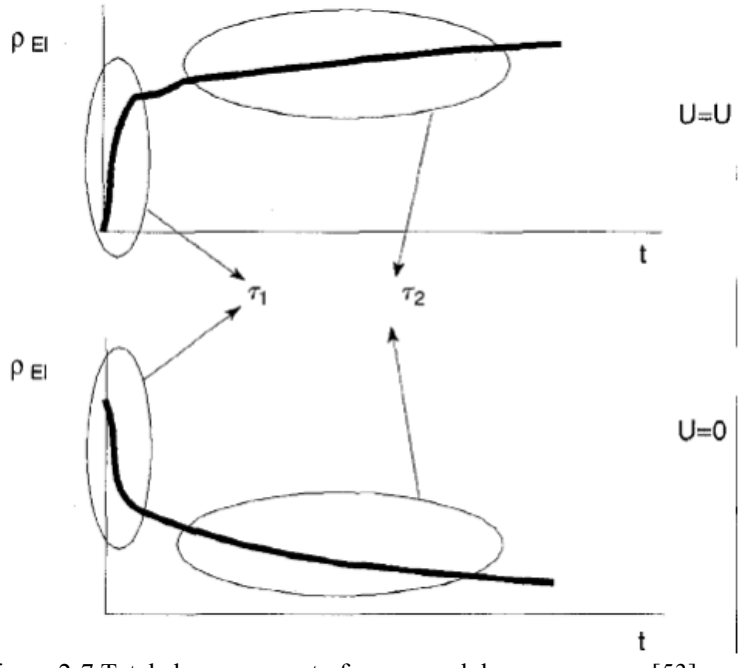


Figure 2-7 Total charge amount of grown and decay processes [53]

Moreover, a physical model of space charge behaviour in 100 µm thick impregnated paper based on the Schottky injection [89] and the hopping mechanism (named the ionic conduction mechanism in [53]) has been built. The model can numerically calculate a symmetrical bipolar charge injection process. However, the model is still at the initial stage: 1) the parameters used in the Schottky injection and hopping mechanism are the parameters used in polymeric material, instead of the oil-paper material; 2) the parameters for both positive and negative charges are set as the same in the model, which is usually not consistent with the experimental results. Ciobanu et al, analyzed the space charge evolution in oil-paper insulation, and associated the mobility phenomena with the mineral content of cable paper (with a thickness of 70 µm) in 2002 [76,90,91], and also investigated the space charge packet in thermal aged impregnated paper [92]. They concluded that the charges parameters derived from the PEA measurements, such as, charge density, apparent trap controlled mobility and variation of trap depth distribution, can be successfully used towards promoting criteria for the best choice of oil-paper insulation technology for DC cables application. However, the space charge profiles still severely suffer from the acoustic attenuation, even though the impregnated paper is very thin. Moreover, the limited resolution of the PEA system can hardly distinguish the accumulated positive charges and negative charges, therefore, it is very difficult to recognise the charge packet phenomena, and no other evidence to validate the charge packet, e.g. current measurement. Zhou, et al. investigated the space charge accumulation and dissipation in thicker (300 µm) oil-paper insulation [54] in 2009. By extending the thickness of the sample, the anode peak and cathode peak can be clearly distinguished. The results showed that: 1) the ionization dominates the space charge dynamics when the electric field is lower than 15 kV/mm, while the charge injection is stronger at the electric field above 15 kV/mm; 2) space charge can increase the electric field more than 40% in

the bulk of dielectrics; and 3) space charge dissipates very fast (within 30s) in oil-paper insulation. The effects of space charge on breakdown and flashover are also discussed [93]. They concluded that space charge can affect the breakdown strength and creeping flashover, and the polarity reversal effect exists in oil-paper insulation. Moreover, the direct measurement of space charge during polarity reversal was reported recently in 2014 [94]. By investigating the space charge accumulation in a single layer of oil-impregnated paper under different polarity reversal voltages with short (30s) and long (4800s) reversal times, they confirmed the electric field enhancement in the region of the electrode/dielectric interfaces. This enhancement is decreasing with the longer reversal time due to the charge dissipation. Moreover, the difference between the natures of positive and negative charges results in an unsymmetrical charge dynamics before and after the polarity reversal process. Since 2011, Zhang, et al. started to investigated the space charge behaviour in a thin layer of oil-impregnate paper with the influences of temperature [95], paper ageing [96] and polarity reversal voltage [97]. They suggested that the high temperature and the lower DP of the paper are related to the enhancement of negative charges and positive charges, respectively. The field enhancement was only observed at the cathode after the polarity was reversed, due to the severe attenuation at the anode. Wu, et al. studied the impacts of temperature gradient along the thin oil-paper on space charge behaviour in 2014 [98], by using a modified PEA system with separate temperature control systems at the two electrodes. They concluded that the homo charge injection was enhanced from the electrode with a higher temperature; while hetero charges appeared at the electrode with a lower temperature. The trend was also simulated by a physical model based on the bipolar space charge model [99]. In this model, only charge injection was taken into consideration. The mobility was obtained from the conductivity of impregnated paper at different temperatures and different electric fields, while other applied parameters remained the same as those used in polymeric materials.

2.4 Space charge in multilayer oil-paper insulation system

The space charge measurements on the multilayer samples play an important role in understanding of the interfacial effects, which is very common in industry applications. Unlike the bulk, the interface usually accumulates space charge quite easily due to the inhomogeneous condition at the interface across the dielectric materials.

The multilayer samples can be classified as the same material and different materials. For the same material, on the oil-paper insulation aspect, the multilayer impregnated papers have been frequently investigated. The space charge profiles within 1 layer to 4 layers of papers are shown in Figure 2-8, produced by Jeroense et al. [100]. The space charge behaviour is significantly influenced by the interfaces between each layer of the papers. Since then the researchers in the

work [49,55,82] did the further tests under different environmental conditions and status of the samples, including applied voltages, temperature, moisture, and aged oil. Tang et al. investigated the space charge behaviours under different DC voltages and temperatures, and studied the space charge features, such as total charge amount, apparent charge mobility and trap energy [49,79]. Hao et al. investigated the combined influence of moisture and temperature on space charge dynamics [55], and also the influence of thermally aged oil [82]. The results provided more information about the space charge behaviours under different conditions in the multilayers. They found that the interface can act like a barrier and prevent space charge from passing through. The comparison between one layer paper and two layers of paper (the total thicknesses of the single layer paper and the combination of two layers of paper were the same) has been researched in [101]. The authors demonstrated the interface effects by calculation and comparison of the charge mobility in the two types of samples. They confirmed that the charge movement in the vicinity of the cathode in the double layers sample was slower than that in the single layer sample. Further research on the space charge in two layers of oil impregnated paper under temperature gradient was studied in [102], which indicated that the polarity of the interfacial charges (the interface between two layers of paper) was always same as the polarity of the electrode at the higher temperature.

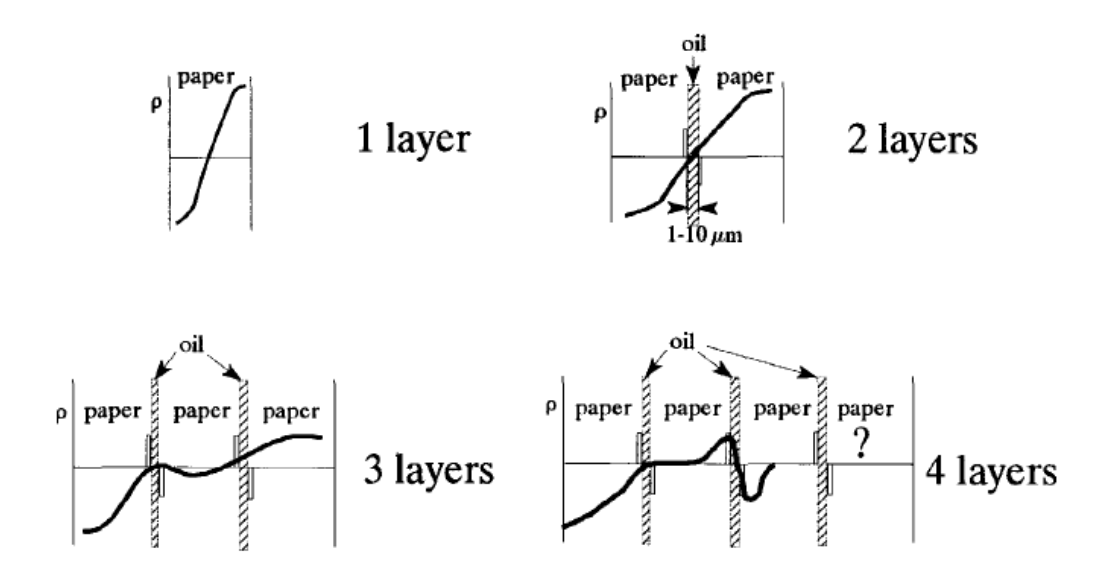


Figure 2-8 Space charge profiles in multi layers of impregnated papers [100]

On the other hand, the multilayer samples with different materials are also very common in the real products, e.g. the oil and impregnated pressboard insulation in transformers. In the past few years, most of the researches on this aspect focused on the solid materials [103-106], the effect of the Maxwell capacitor has been observed, which is the surface built up at the interface due to the inhomogeneous materials. However, the knowledge of the interface between liquid (oil) and solid (impregnated pressboard) is still very limited. The literature in [107] introduced the calibration

process in the laminated samples of transformer oil and epoxy. They suggested that the calibration need to be finished within the time constant of the Maxwell capacitor. Moreover, the effects of the acoustic mismatching in the different materials are shown in Figure 2-9 [107]. The acoustic reflections need to be removed from the space charge profile during the calibration process, based on the calculation of the acoustic wave propagation.

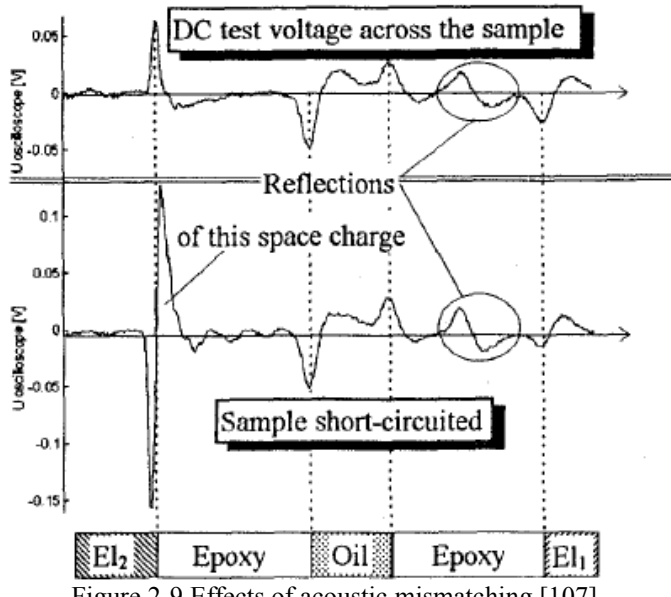


Figure 2-9 Effects of acoustic mismatching [107]

The first attempt of the space charge measurement on the pressboard composited with oil, based on the PWP method, was introduced by Liu, et al. in 1994 [108]. The interfacial charges with the same polarity of the electrode at the oil gap side, indicating a field enhancement in the pressboard. However, due to the limitations of the measurement system, the results were strongly affected by the noise, and only low electric field (4.4 kV/mm) was applied. Recently in 2014, space charge behaviours, based on the PEA method, in the oil gap and a thin impregnated paper combined system was introduced in [109]. The effects of the different voltages as well as the different thicknesses of the oil layer were discussed. They concluded that the high voltage enhanced charge injection, and the thick oil gap decreased the amount of the interfacial charges due to the stronger recombination in the oil. Compared with Maxwell capacitor estimation, the amount of the interfacial charges was significantly larger from the experimental results. This may result from the unideal interface in the real insulation system that the rough interface could potentially generate more traps to accumulate large amount of space charge. However, in their results, the interfacial charges distribute within a broad region (about 150 µm, similar to the paper thickness), due to the limitations of the resolution and the acoustic attenuations. Therefore, it is difficult to separate the interfacial charges and the injected charges from the electrode. Moreover, the measurement time for each test was only 10 minutes, which may be not enough for observations of the space charge accumulation reaching to the steady state. The interface was also introduced into the bipolar space charge model by applying an energy barrier based on the Poole-Frenkel mechanism [110]. Similar to other numerical models, there was no direct reference energy level value for the barrier, instead the parameters of the polymeric materials were used for modelling. Therefore, only a reasonable trend was simulated.

2.5 Summary

The space charge detection techniques and the characteristics assessments were introduced at the beginning of this chapter to set a ground for future space charge measurements and evaluation in oil-pressboard insulation system. Existing researches related to the space charge behaviours in oil-paper insulation were also reviewed. The majority of the past researches only focused on the thin oil-paper insulation used in the HVDC cable insulation. A small acoustic attenuation occurred in thin oil-paper would result in a good signal/noise ratio. On the other hand, the limited resolution of the measurement system would hardly distinguish the distribution of charges with different polarities due to the small scale in thickness of the sample. These difficulties are the main reasons that limit the space charge measurement in thick oil-pressboard. Therefore, a purpose-built PEA system to overcome all these difficulties is essential for the investigation of space charge in thick pressboard insulation.

In the industry converter transformers, the AC/DC combined voltages generally stress on the insulation systems. However, its impact on space charge behaviours has not been investigated and fully understood yet. As a part of the research work, this topic will be addressed in this dissertation.

Although there were few attempts to establish the physical model of space charge behaviours in oil-paper insulation, the modelling now is still at the very initial stage as most of the mechanisms and parameters are directly obtained from the polymeric insulator instead of oil-paper insulation. It still requires tremendous amount of experimental work to determine those parameters for an accurate simulation of the oil-paper insulation system. Therefore, this dissertation only focuses on the experimental works.

Chapter 3.

Space Charge Behaviours in Thick Oil-Impregnated Pressboards under HVDC Stresses

Besides thin impregnated Kraft paper, pressboards are also the common insulation materials used in converter transformers to provide both electrical and mechanical strengths as part of entire insulation system. The thicker sample provides a larger space for charge movements and distributions, which is known as the bulk effect. It is the bulk effect that causes the detection of space charge in pressboards is more difficult than in the Kraft paper, due to the considerable increase of the thickness. The acoustic signal is severely attenuated and dissipated in the impregnated cellulose materials. This is the main reason that most of the studies only focus on the space charge in Kraft paper or thin pressboards, and the bulk effect of space charge in impregnated pressboards is still poorly understood. In order to investigate the space charge behaviours in thick oil-impregnated pressboards (≥ 1.0 mm), a special PEA system is needed to extract the space charge profiles accurately. For this purpose, in this chapter, a new PEA system is proposed and constructed aimed to overcome the severe acoustic signal attenuations encountered by the conventional PEA systems when dealing with the thick pressboards. Then the

sample preparation and the experimental processes are explained, and the space charge profiles in thick oil-impregnated pressboards under different DC stresses are successfully obtained and the results are discussed.

3.1 Modified PEA system

In order to overcome the signal attenuations in thick pressboards, a purpose built PEA system and a 3H (high voltage, high frequency and high resolution) pulse generator were installed. As shown in Figure 3-1, the diameter of the upper electrode shield was enlarged to 10 cm in order to avoid flashover caused by the high external voltage applied on the thick samples. The metal upper electrode is made of brass with an area of about 0.8 cm². The edge of the electrode was smoothly shaped to round angle to avoid the local field enhancement in the vicinity of the electrode, as shown in Figure 3-1. The ground electrode was made of 15 mm thick aluminium plate, which was modified as a container with 11 cm in diameter and 5 mm in depth. This container allows measuring of both solid and liquid materials simultaneously, as shown in Figure 3-2. Both inner and outer surfaces of the ground electrode container were carefully mirror-polished to reduce the acoustics scattering. The piezoelectric sensor used in this system was a thin PVDF film with a thickness of 40 µm and an area of 0.8 cm². The PVDF film used is much thicker than normal PEA system (usually 9 µm) that can greatly enhance the amplitude of the output signals, however, the spatial resolution drops from 10 µm (normal PEA system) to about 40 µm. Since the thickness of the samples used in this project is usually above 1 mm, this spatial resolution drop is acceptable. A thick (1 cm) absorber is firmly attached to the sensor to absorb the acoustic wave propagated through the sensor. The material of the absorber is the non-polarized PVDF to avoid the acoustic reflection at the interface between the sensor and the absorber. The sensor and the absorber were shielded in a brass tube to reduce the noise from other components, as shown in Figure 3-3. The electrical signals generated from the PVDF sensor then enhanced by a broadband amplifier (AU-1332, 50 dB, 0-500 MHz). The shielded sensor system and the amplifier were finally shielded in a brass box to minimize the noise.



Figure 3-1 Top electrode of the new PEA system

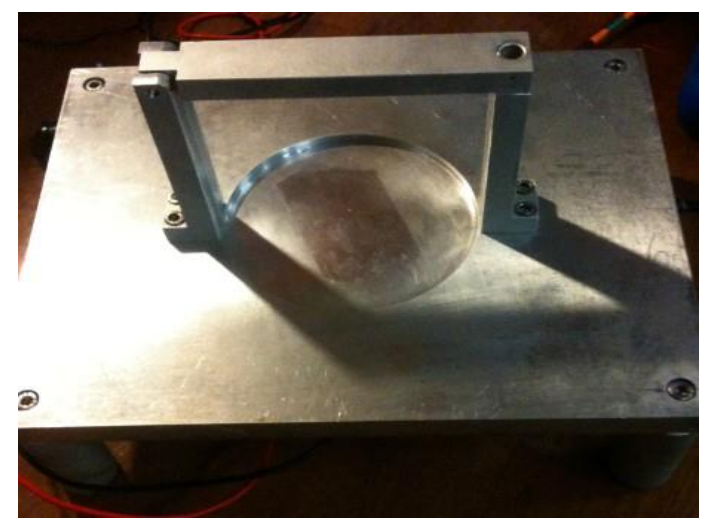


Figure 3-2 Ground electrode of the new PEA system

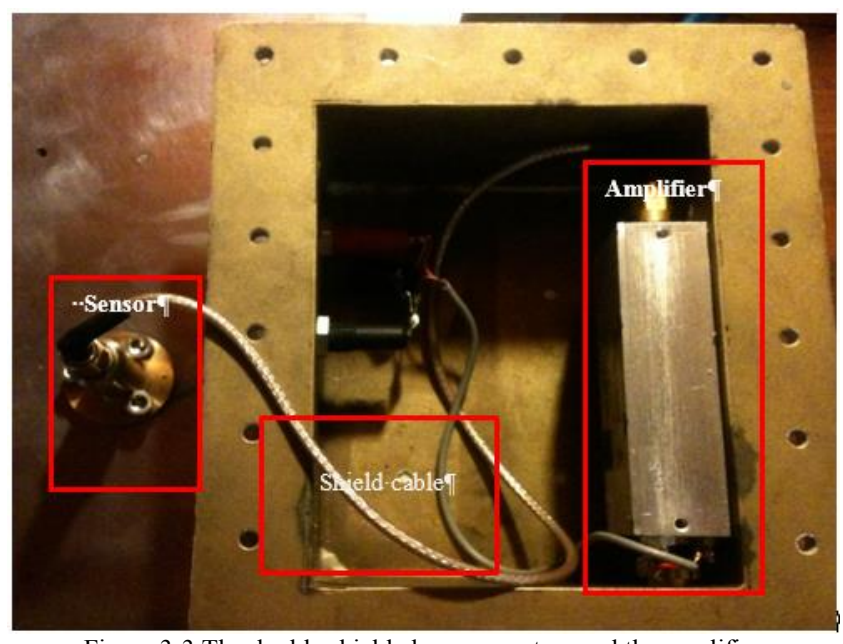


Figure 3-3 The double shielded sensor system and the amplifier

On the other hand, the pulse generator was built based on the Behlke HTS 50-08-UF MOSFET switch [111], as shown in Figure 3-4, which can produce a high voltage (from 500 V to 4 kV) and narrow (5ns width) pulse meeting the requirements of strong and good spatial resolution of the PEA signals. The frequency of the pulses is up to 3 kHz which is fast enough to measure space charge dynamics under alternating voltages, such as polarity reversal or AC voltage.

It has been proved that this special built PEA system can successfully measure space charge dynamics in an insulation system consisting of thick pressboards combined with oil gaps with an overall thickness up to 2 mm.

1) Star-type grounding 2) For high frequency bursts only 3) Impedance matching (0-50 Ohm) 4) Dynamic compensation (0-100 pF)

Figure 3-4 The connection for the pulse generator [111]

3.2 Sample preparation and experimental setups

3.2.1 Sample characteristics and preparation

Connection

The diagnosis and the influence of the degradation of miner oil and pressboard have been studied for a long history. For the HVDC applications, the investigation of the influence of ageing on the dielectric properties has been proposed recently by CIGRE A2/D1.41 working group. A round robin test of the DC conductivity of mineral oil at different stages of degradation has been organized. It is always interesting to know how the aged oil influences the space charge behaviour in the oil-impregnated pressboard insulation system. Meanwhile, the impacts caused by the aged oil, especially the service aged, on the space charge behaviour are also interested by the power industry, e.g. National Grid. Therefore, to meet the industry demands, in this chapter, two types of mineral oils were selected for comparison study: fresh and severely aged. The fresh one was the fresh mineral oil Shell Diala S3 ZX-I, which has a high oxidation stability and a low sulphur content to meet IEC 60296. The severely aged oil provide by National Grid was the service aged

oil collected from a long term serviced power transformer. The significant colour differences between the two types of the oil are shown in Figure 3-5. The transparent oil is the fresh Shell ZX-I oil and the dark brown one is the service aged oil. The result of UV/Vis spectra, as shown in Figure 3-6, also indicates the differences between these two types of oil. The absorption edge of the aged oil shifts from ultraviolet to visible wavelengths comparing to the fresh oil. The chemical changes of the service aged oil, compared with the fresh oil, were measured by the Fourier transform infrared spectroscopy (FTIR), as shown in Figure 3-7. The differences are mainly distributed from 1800 to 500 cm⁻¹: the peak at the 1720 cm⁻¹ indicates the C=O stretch; 1600 cm⁻¹ indicates C-C stretch (in ring); 960 cm⁻¹ indicates O-H bend; 815 to 725 cm⁻¹ indicates C-H bend. These chemical groups clearly show that the oxidation products and acids may exist in the service aged oil. The dielectric properties of the two types of oil are shown in Table 3-1. The moisture content of each type of oil was measured by Karl-Fisher titration after the degasing treatment. The DC conductivity of each oil was measured by a three-electrode system under 10 kV/mm [24,38]. The permittivity was measured by Solartron with a magnitude of electric potential of 1 V [24]. All the measurements were carried out at the room temperature.



Figure 3-5 The two types of mineral oil used in this work, the left one is the fresh oil and the right one is the service aged oil.

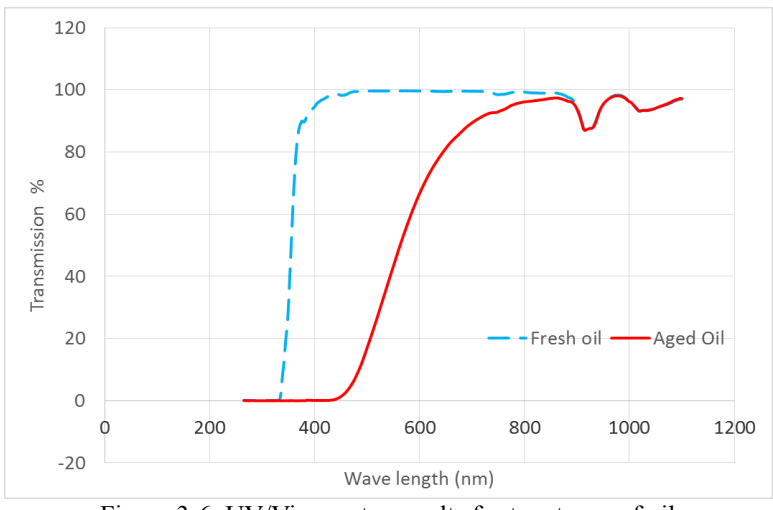


Figure 3-6. UV/Vis spectra results for two types of oil

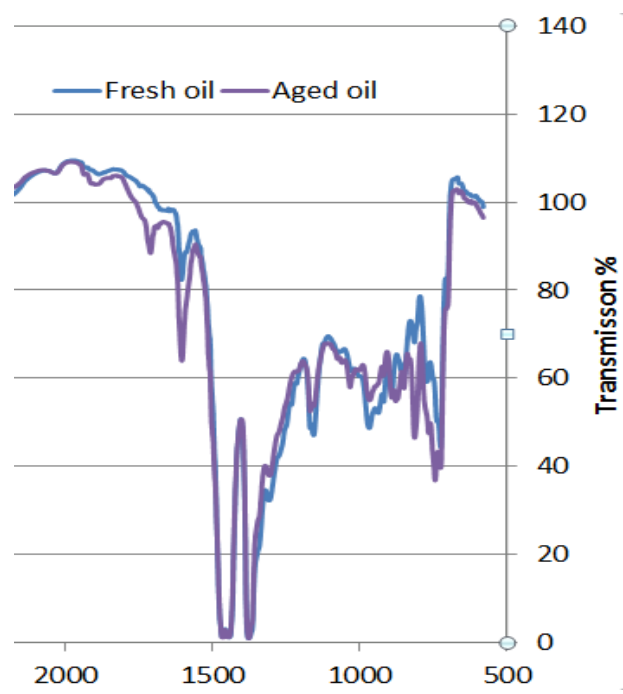


Figure 3-7. Chemical differences between the fresh oil and the aged oil by using FTIR

The pressboards used in this research were the commercially available transformer pressboards supplied by Weidmann Electrical with thicknesses of 0.5 mm and 1 mm. As shown in Figure 3-8 and Figure 3-9, the thinner pressboard has a relatively smooth surface, while the surface of 1 mm is rougher with pressed patterns. The pressboards were cut into circular with a diameter of 9 cm, and then dried at 105°C for 3 days in the fan oven until the mass did not change. After that, the dried pressboards were separately impregnated in the two types of oil under 10 Pa/60 °C for 3 days, which makes the pressboards fully impregnated with oil. Then the samples were natural cooled down to the room temperature. The unused impregnated pressboards were kept in a sealed container under vacuum condition to avoid absorbing of ambient moisture. The dielectric properties of prepared samples of the impregnated pressboards are shown in Table 3-2. The resistivity of the pressboard was measured at the 10 kV/mm [24]. It is noticed that the differences of the resistivity between the two types of impregnated pressboards are even larger than the two types of oil, which may result from the changes of the moisture content between the aged oil and the impregnated pressboard (i.e. the moisture content is the aged oil impregnated pressboard could be much larger than in the fresh oil impregnated pressboard).

Table 3-1. Status of the oil properties [24]

Tenero C II Statems of the on properties [2.]		
	Fresh oil	Aged oil
Moisture (ppm)	<10	25
Resistivity (TΩm) Relative Permittivity Breakdown strength (kV/mm)	7 2.2 32	0.1 2.6 21
Description	transparent	dark brown with sludge

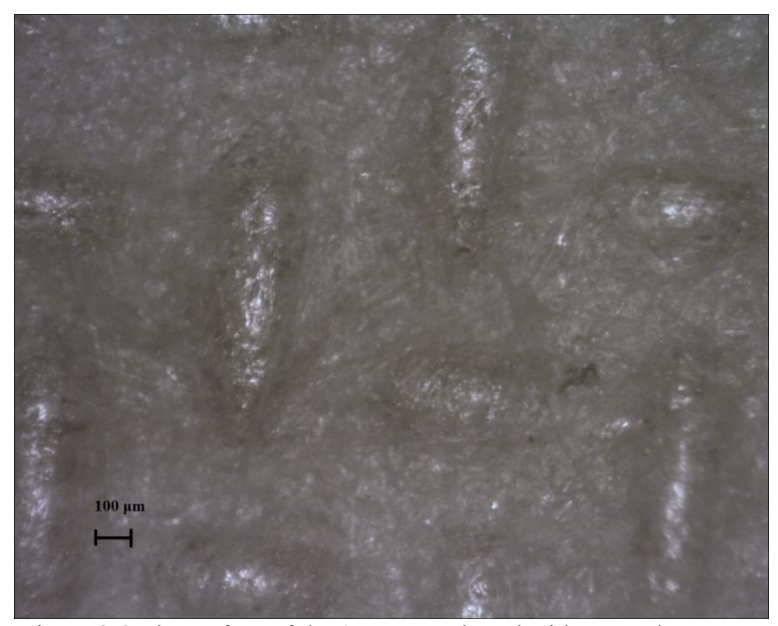


Figure 3-8 The surface of the 1 mm pressboard with pressed patterns.

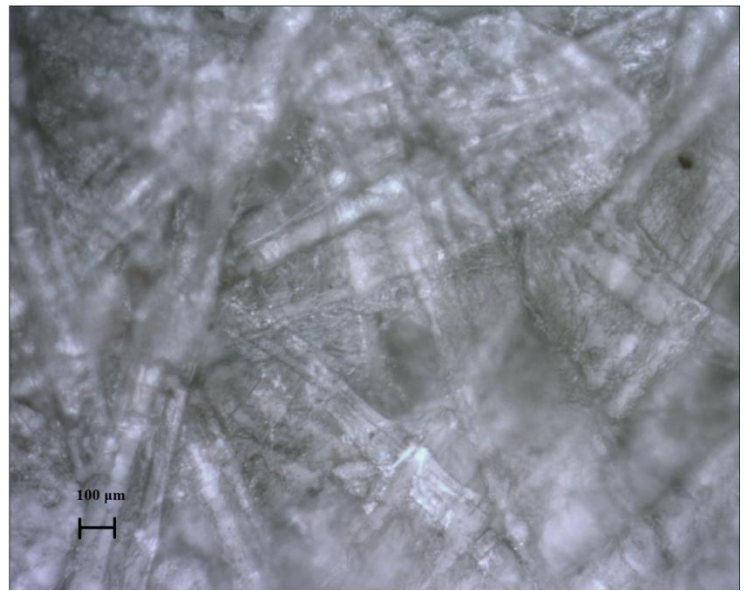


Figure 3-9 The surface of the 0.5 mm pressboard without pressed patterns.

Table 3-2. Dielectric properties of the impregnated pressboards [24]

	1 0	
	Fresh oil-PB	Aged oil-PB
Resistivity (T Ω m)	140	0.3
Relative Permittivity	3.2	4.2
,		
		I

3.2.2 Experimental protocol

To clearly describe the space charge dynamics in the samples, three types of the measurement points are utilized, including volts-on, volts-off and decay, as shown in Figure 3-10.

The volts-on test is measuring the space charge accumulation during the HVDC voltage application, which will show the space charge built-up in service condition. The charges measured at both electrodes, in this case, are the combination of two types of charges: 1) the induced charges caused by the accumulated space charge in the sample; and 2) the charges result from the presence of the DC voltage. The latter usually is very large when the accumulation of space charge is not significant. Therefore, it influences the observation of the space charge dynamics.

To resolve the problems mentioned above, the volts-off test is introduced (different from the 'volt-off test' in the literatures, which refers to decay test or short circuit test). In that, turning off the voltage and measuring the space charge distribution, and then quickly re-applying the voltage. The electrode charges only consist of the induced charges due to the accumulated charges. Therefore, the accumulation of the space charge can be clearly recorded without any influences of the external electric field. However, this method is difficult to measure the very fast moving charges, because the time period used to measure the space charge is only about 15s within which an average of 1024 times of measurements are obtained. It should be noticed that the short period (< 20s) voltage cut-off may also affect the charge dynamics process.

The decay test is carried out after 4 hours of voltage application, by turning off the external voltage permanently. Similar to the volts-off test, the decay test is particular useful to obtain the accumulated space charge profiles. The depolarization characteristics can also be obtained by the decay test, which are further used to estimate the apparent trap-control mobility and the trap energy level distribution.

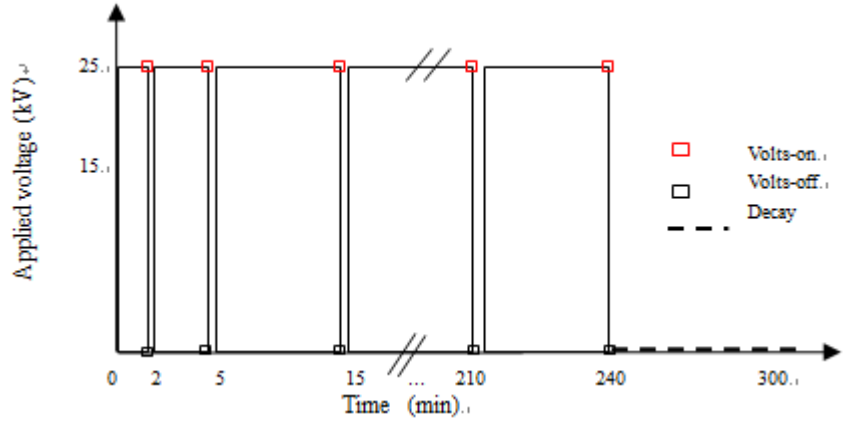


Figure 3-10 Illustration of experiment measurement points

3.3 Space charge behaviours in 1 mm thick oil-impregnated pressboard

When the sample is thin, the surface conditions may dominate the space charge dynamics, and the injected charges from the each electrode are difficult to distinguish due to the limited spatial resolution of the conventional PEA system and the thin thickness of the sample. When the positive charges and negative charges are overlapped, only net charges can be detected by the PEA system. The space charge distribution is supposed to be observed more clearly and accurately in a thick sample. However, it is not straight forward due to the severe acoustics attenuation in the thick pressboards. Therefore, in this work the experiments started from the single layer oil-impregnated pressboards with the thickness of 1 mm, which was also regarded as functional evaluation of the modified PEA system.

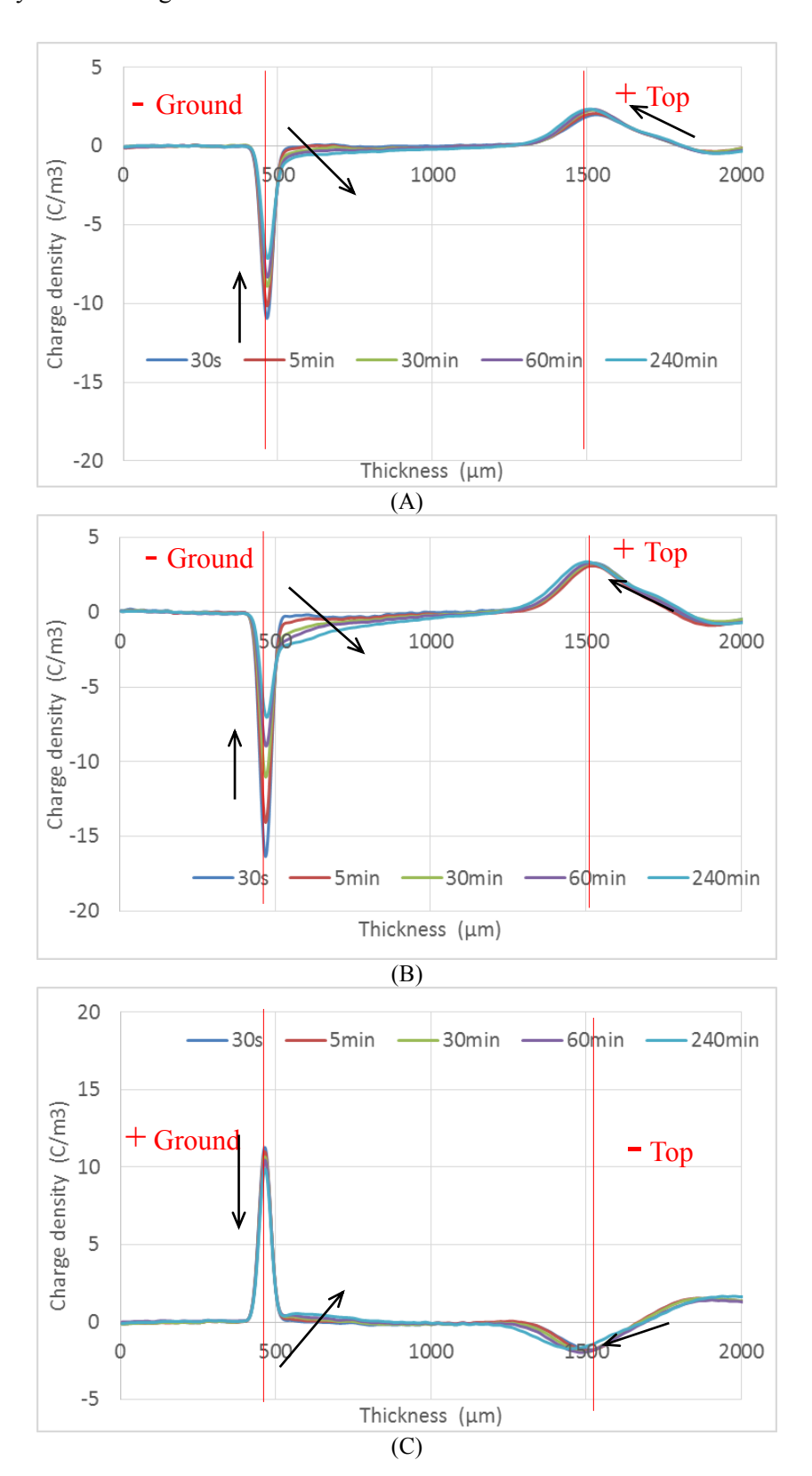
The space charge profiles obtained from the modified PEA system are shown below. It has to be pointed out that the space charge profiles shown in this dissertation are the typical results selected from at least 5 repeated measurements (the results are only slightly different on the value of the charge density, the space charge dynamics trends are the same). The calculated characteristics results are the average values based on all measurements.

3.3.1 Results of pressboard with fresh oil

1. Volts-on

All the measurements were carried out at the room temperature. To identify the effects caused by the applied electric field, including both magnitude and polarity, the followings are chosen +15 kV/mm, +25 kV/mm, -15 kV/mm and -25 kV/mm as the applied electric field. The time for electric field application is 4 hours for each case.

The volts-on results of the space charge distributions in the pressboard impregnated with the fresh oil under the electric fields of +15 kV/mm, +25 kV/mm, -15 kV/mm and -25 kV/mm are respectively shown in Figure 3-11.



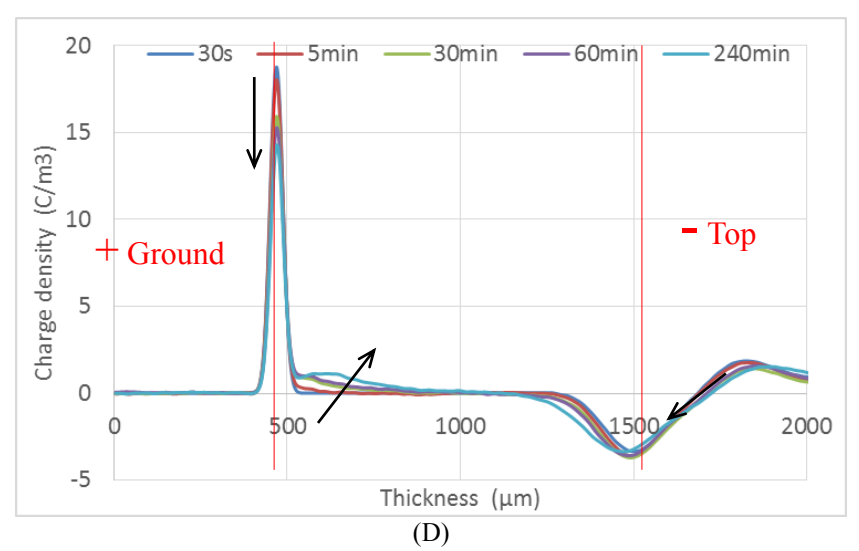


Figure 3-11 Volt-on results of fresh oil samples under different electric fields of (A) +15 kV/mm; (B)+25 kV/mm; (C)-15 kV/mm and (D) -25 kV/mm.

All the results above show that the homo-charge injection occurred in the impregnated pressboard since the charge peak at the electrode is decreasing and moving into the insulation bulk. Moreover, it can be observed that the higher the applied electric field, the more the space charge injected and accumulated in the insulation bulk during the same period.

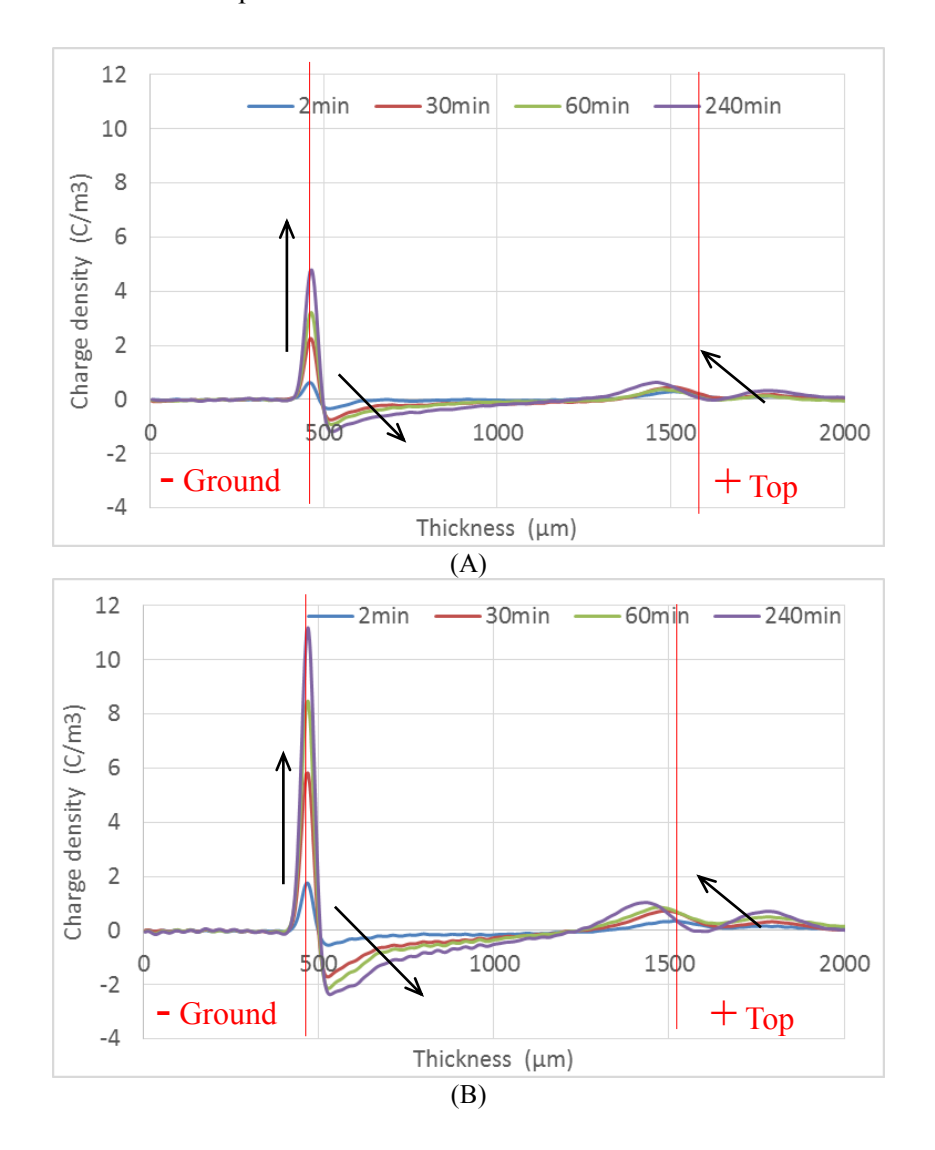
The plots (A) and (B) in Figure 3-11 show the space charge distributions under the positive electric field. When the applied electric field is low, the negative electrode peak is decreasing from about 12 C/m³ at 30s to about 7 C/m³ at 4 hours. However, when the applied electric field is higher, the peak is decreasing from about 16 C/m³ to 7 C/m³ during the same period. Obviously the large amount of negative charge carriers are injected from the cathode into the dielectric bulk. The anode peak is quite stable for both voltages: only very small amount of positive charge carriers are injected from the anode. There are two possible reasons for this: first, the charge injection is influenced by the material and the polarity of the electrode, so the charge injection is different for the anode (semiconducting polymer, covered on metal electrode for the match of acoustic impedances) and the cathode (aluminium); second, there is large acoustic attenuation in the thick impregnated pressboard, so the observation of the charge dynamics at the anode side is not as significant as at the cathode. In this case, the results discussion will be mainly focused on the aluminium electrode side.

On the other hand, the plots (C) and (D) in Figure 3-11 show that the space charge distributions under negative voltages. Generally, comparing to the results under positive voltages, the space charge distribution is a mirror image, i.e. the charge behaviour is almost same, except the difference in the polarity. The anode peak (aluminium) is decreasing from 12 C/m³ at 30s to 10 C/m³ at 3 hours under -15 kV/mm; it is decreasing from 19 C/m³ at 30s to 14 C/m³ at the 3 hours under -25 kV/mm. Therefore, the anode peak (aluminium) under negative voltages is larger than

the cathode peak (aluminium) under positive voltages at the first 30s and also at 3 hours. Moreover, there is smaller peak decrement under negative voltage than positive voltage at the aluminium electrode side. This may indicate that the injection of the negative charge carriers is faster than positive charge carriers at the aluminium electrode side.

2. Volts-off

As shown in Figure 3-12, space charge distributions under the volts-off condition clearly indicate the accumulated charges in the insulation bulk. When the applied voltage is removed, positive charges on the ground electrode is induced by the negative charges accumulated in the pressboard bulk, otherwise, negative charges can be observed on the ground electrode due to the induction of the accumulated positive charges within the sample. With the electric field application, the peak values of the accumulated charges within the pressboard keep increasing and gradually move towards to the middle of the pressboard.



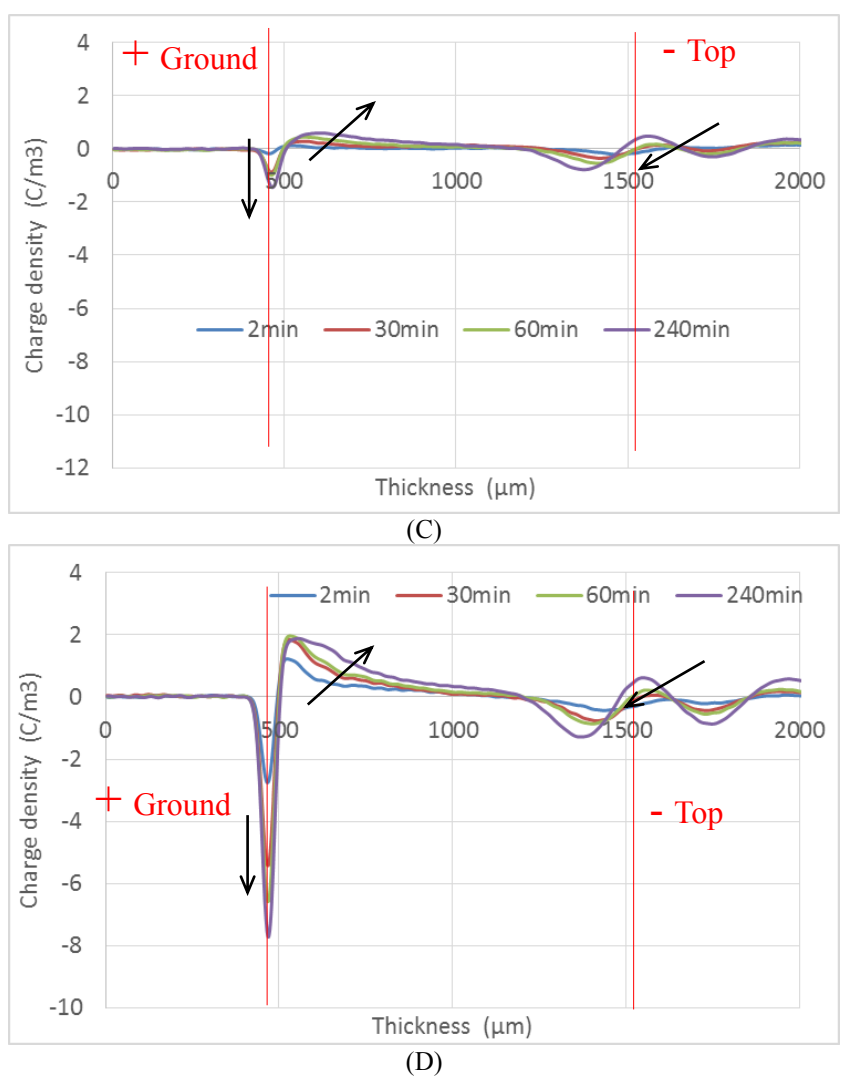


Figure 3-12 Volts-off results of fresh oil sample under different electric fields of (A) +15 kV/mm; (B) +25 kV/mm; (C) -15 kV/mm and (D) -25 kV/mm.

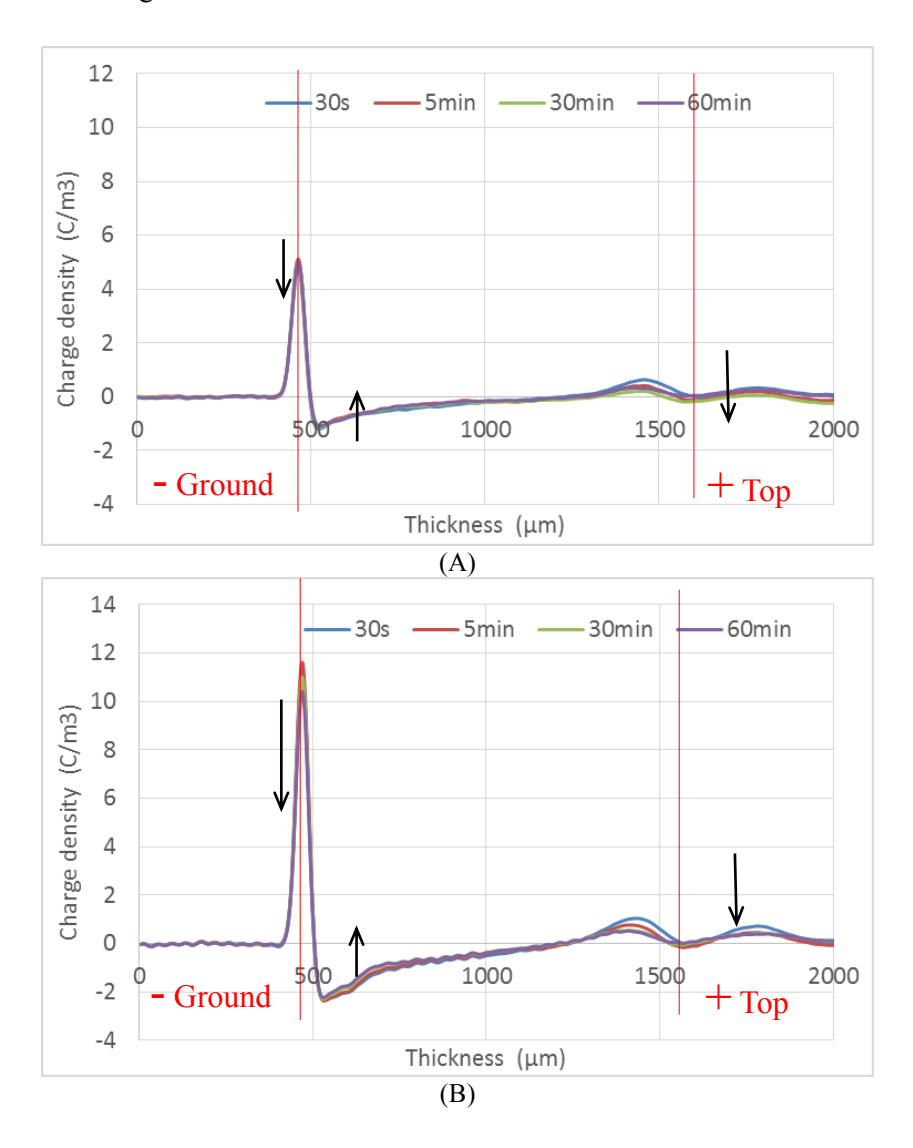
From the plots (A) and (B) in Figure 3-12, the testing results confirm that homo-charge injection occurred with the positive voltage application. The injected charge carriers are accumulating very close to the electrode initially and moving towards to the middle of pressboard with the time. The injected negative charges are accumulated near the cathode in a narrow area: about 54 µm from the cathode under 15 kV/mm; and about 63 µm from the cathode under 25 kV/mm. At the anode side (semiconducting polymer), the peak of the positive charges is overlapped with the induced negative charge due to the large dispersion of the acoustic signals. Since more and more charge injected and accumulated, more and more induced charges can be observed on the electrode. The induced cathode (aluminium) peak is about 4.8C/m³ under 15kV/mm, and about 11.4 C/m³ under 25 kV/mm. This also suggests that the negative charge injection is not proportional to the external electric field, i.e. stronger charge injection occurs under higher electric field.

The plots (C) and (D) in Figure 3-12 demonstrate the charge injection dynamics under negative voltages. The similar trend is observed again: homo-charge injected and moved into the

pressboard bulk. Furthermore, the magnitude of the induced anode (aluminium) peak is generally smaller than the corresponding cathode peaks under positive voltage: about 1.1 C/m³ under -15 kV/mm and 7.9 C/m³ under -25 kV/mm. This is well in agreement with the volts-on results, demonstrating that at the aluminium electrode the injection of the positive charge carriers is weaker than the negative charge carriers. And this phenomenon may be caused by either the difference between the two polarities of charge carriers, or the effect of the aluminium electrode itself [83,100].

3. Decay

The decay tests are carried out after 4 hours voltage stressing when the HVDC voltage is removed. Thus the charge dynamics can be observed without the effects caused by the external electric field. The results, as shown in Figure 3-13, indicate the drifting away and recombination behaviours of the accumulated charges.



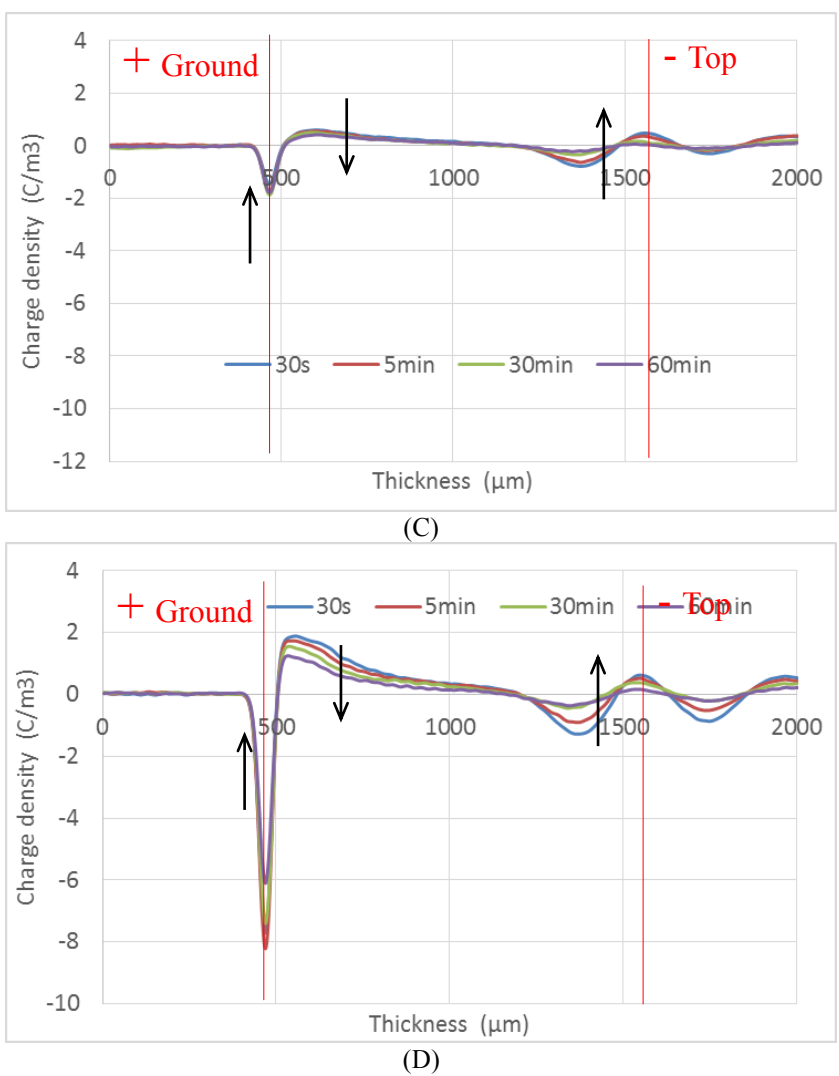


Figure 3-13 Decay results of fresh oil samples under different electric fields of (A) +15 kV/mm; (B) +25 kV/mm; (C) -15 kV/mm and (D) -25 kV/mm.

Generally, as shown above, the injected charges decay very slowly, i.e. very little charge reduction during 1 hour time. This indicates that the most of injected charges in the fresh oil are slow moving charges under both volts-on tests and decay tests. For the samples with the same polarity of the applied voltages (not clear), more space charge accumulated in the insulation bulk during the 4 hours stressing time, and also more charges decayed during the 1 hour distressing time (tense consistence!).

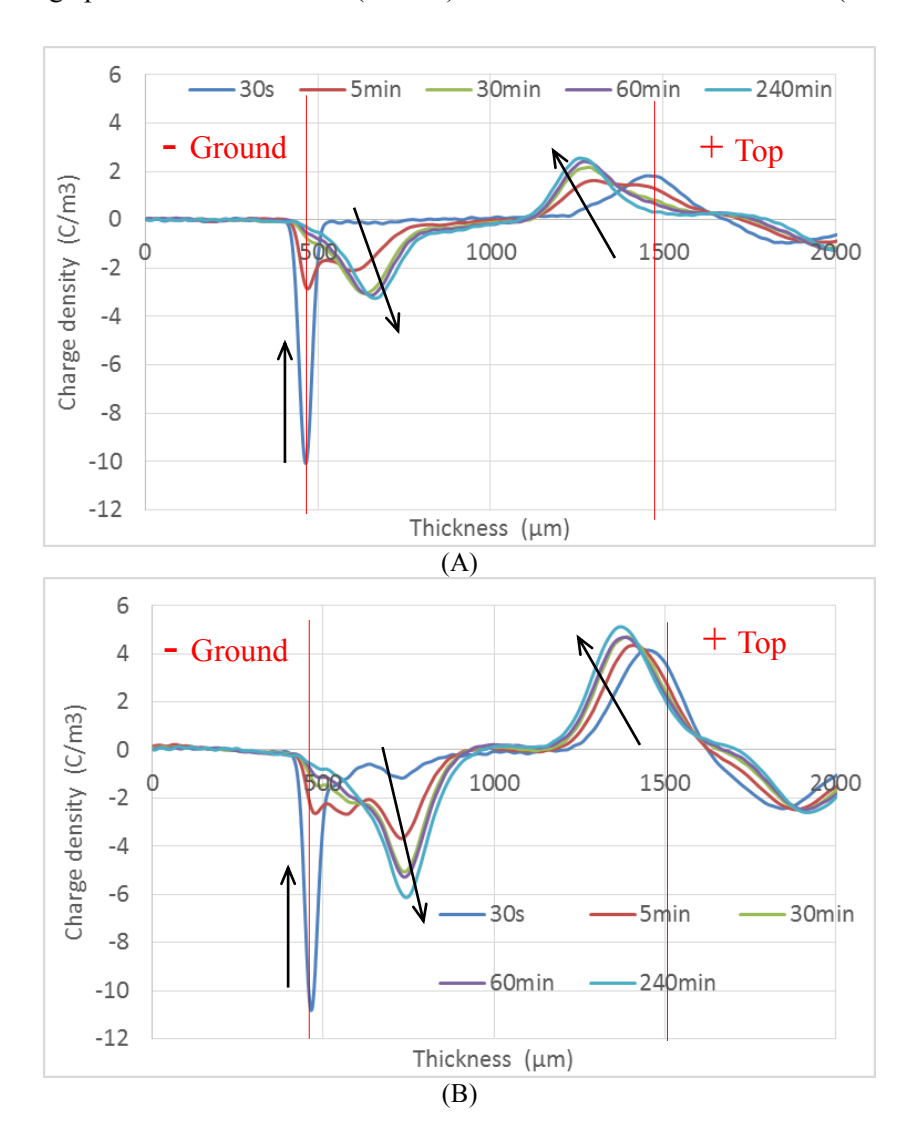
3.3.2 Results of pressboard with aged oil

A. Volts-on

For the purpose of comparison, the space charge dynamics in the pressboards impregnated with the serviced aged oil were also investigated. As shown in Figure 3-14, the volts-on results of the aged oil samples are very different from those observed from the fresh oil samples.

For the plots (A) and (B), under positive voltages, significant amount of homo-charge injection occurred in the aged oil samples: the electrode peaks decrease fast and move towards the dielectric bulk. The cathode (aluminium) peak almost disappears after 30 min, while a negative peak occurs in the insulation bulk near the cathode moving gradually towards to the middle of the pressboard. Similar behaviour occurs at the anode (semiconducting polymer), significant positive charges injection can be observed, compared to the fresh oil samples. This suggests that the status of oil have a significant impact on charge dynamics in the pressboard and the serviced aged oil greatly enhances the charge injection and its mobility.

Moreover, similar trend is observed as in the fresh oil samples, the higher the applied electric stress, the more the space charge accumulated in the insulation bulk. The amplitude of the injected negative charge peak under 25 kV/mm (6 C/m³) is almost doubled of 15kV/mm (3 C/m³).



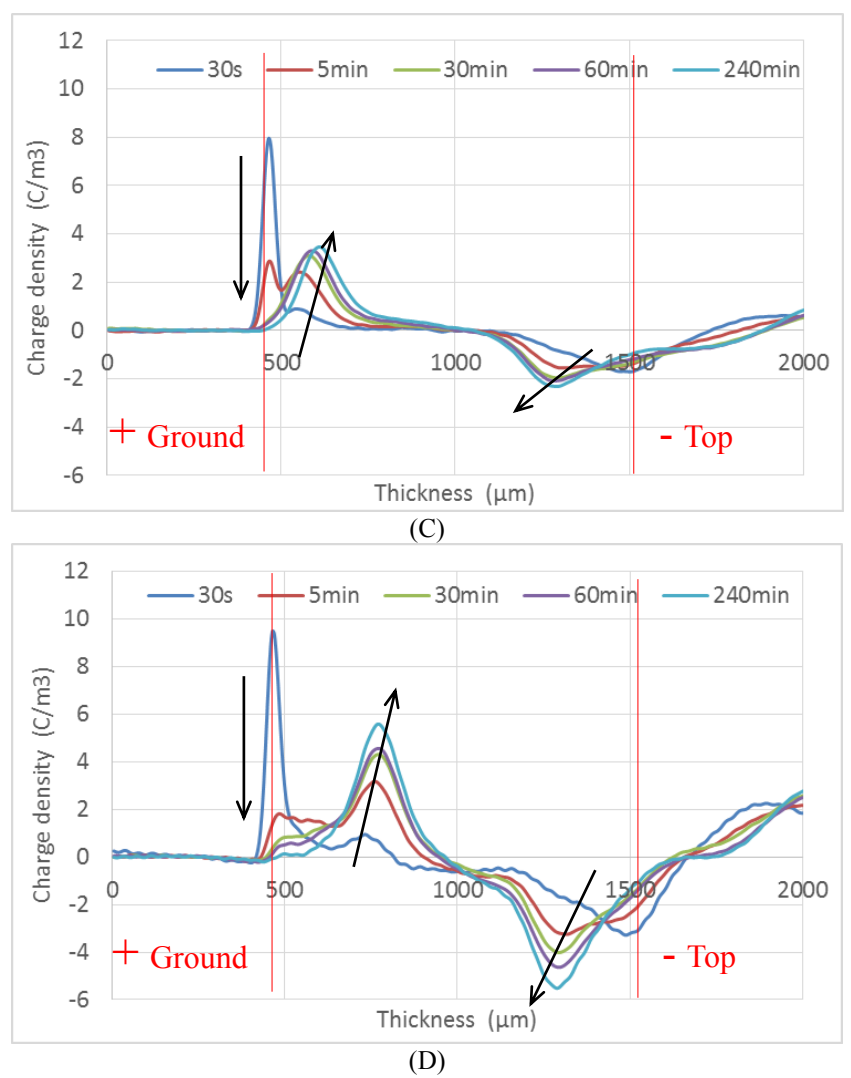
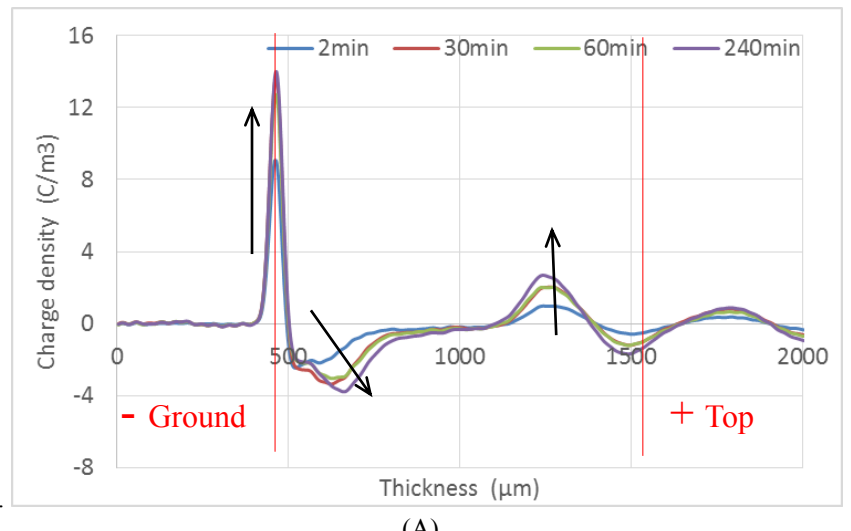


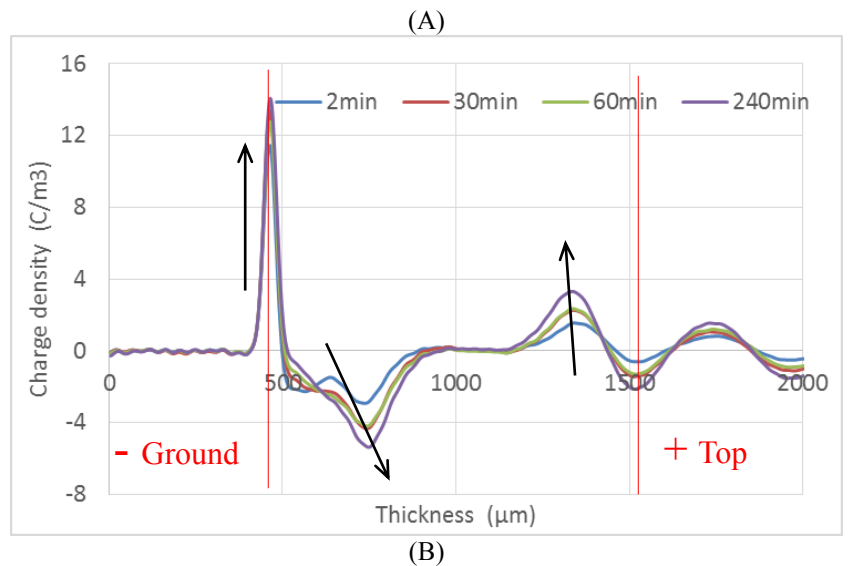
Figure 3-14 Volts-on results of aged oil samples under different electric fields of (A) +15 kV/mm; (B)+25 kV/mm; (C)-15 kV/mm and (D) -25 kV/mm.

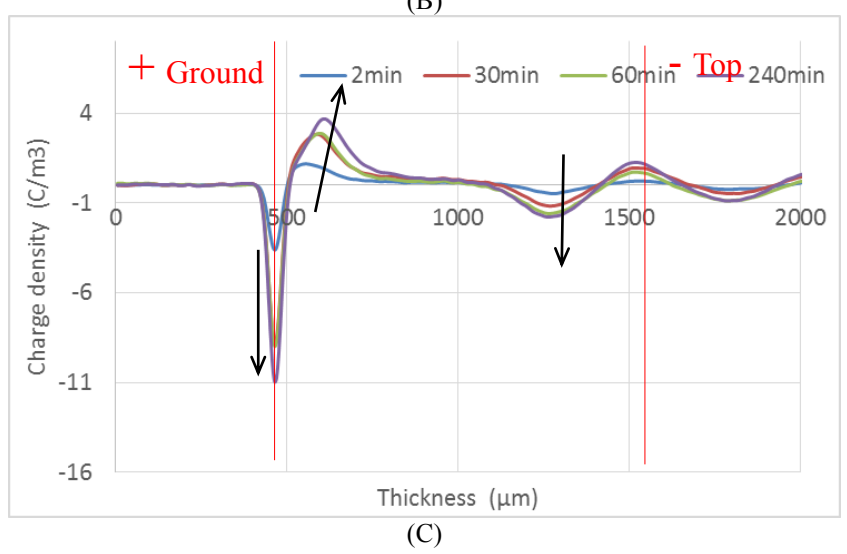
For plots (C) and (D), the trend of the space charge behaviour is almost the same except the polarity deference compared to plots (A) and (B). The electrode peaks almost disappear and move into the insulation bulk in a very short period of time. Moreover, the amplitude of the injected positive peaks at the anode (aluminium) side is about 3.1 C/m³ under -15 kV/mm and 5.9 C/m³ under -25 kV/mm, which is very close to the results from positive voltages. This may indicate that the impact of the polarity of the applied voltage is not significant for aged oil samples.

2. Volts-off

The volts-off results, as shown in Figure 3-15, demonstrate the accumulated charges even more clearly. During the first 2 min, there have already been considerable charges accumulated in the insulation bulk near the electrodes, which suggests that more fast moving charges in the aged oil than the fresh oil due to the higher conductivity of the aged oil. With the voltage application, more accumulated charges are moving towards to the middle of the bulk.







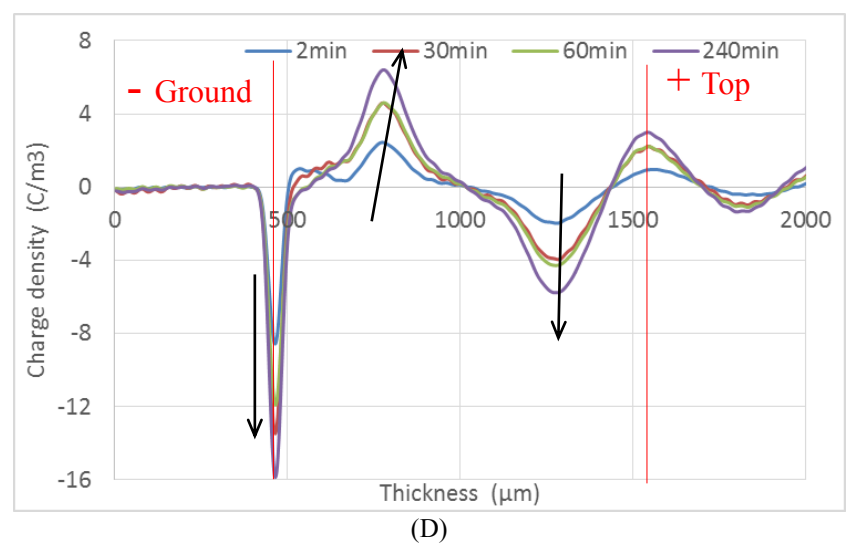


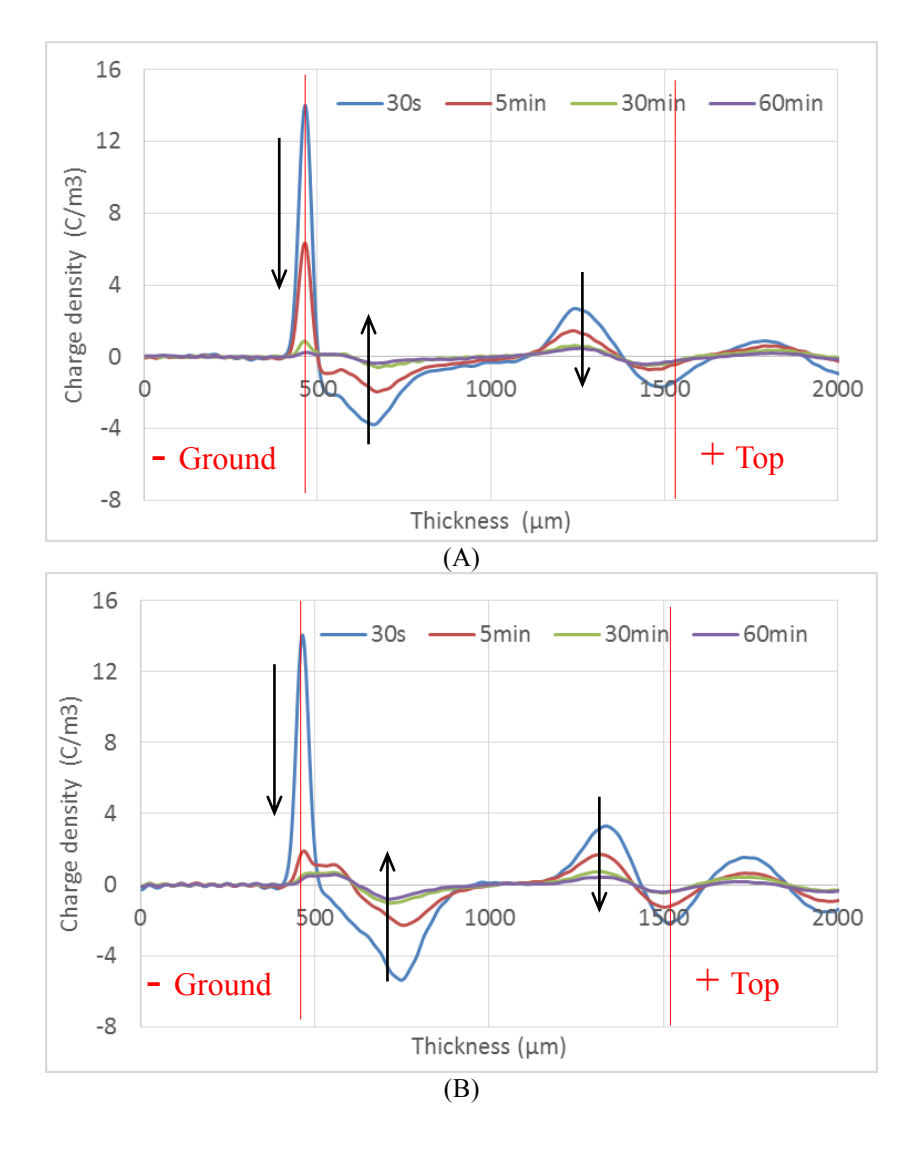
Figure 3-15 Volts-off results of aged oil samples under different electric fields of (A) +15 kV/mm; (B) +25 kV/mm; (C) -15 kV/mm and (D) -25 kV/mm.

As shown in the plots (A) and (B) of Figure 3-15, considerable homo-charges injected and accumulated in the pressboard within the first 2 min. After that, more charge injected deeply into the insulation bulk with the voltage application, therefore, the injected peak is moving towards to the middle of the pressboard. The depth of the negative charges injected from the cathode is closely related to the applied electric field: with applied voltage for 4 hours, the negative peak is about 165 μ m from the cathode (aluminium) under 15 kV/mm and about 186 μ m under 25 kV/mm. For the same amount of charge, the charge deeply injected to the middle will lead to a more significant electric field distortion within the insulation bulk.

In the plots (C) and (D) of Figure 3-15, similarly, the space charge injection occurs very fast once the voltage is applied, indicating the significant effect of the oil property on the charge accumulation. It is also observed that the most of space charge injection occurred within the first 5 min. The injected positive charge peak from the anode (aluminium) is grown with the stress time, and moving into the insulation bulk with a decelerated speed until reaching a dynamic balance. This dynamic balance seems strongly related to the applied voltage and degradation of the sample. For the pressboard impregnated with the aged oil, the peak movement can be observed clearly under the low voltage (from about 80 µm at 2 min to about 160µm at 4 hours). On the other hand, under the high voltage, the peak deeply moves in to the pressboard within the first 2 min (about 190µm), and then just slightly moves to about 192 µm at 4 hours. Compared with the positive voltages, the position of the injected peak is very similar for the same magnitude of the applied negative voltages. This may suggest that the effect caused by the voltage polarity is much smaller than the magnitude of the voltage in the pressboards impregnated with aged oil.

3. Decay

Figure 3-16 shows the decay results for the aged oil samples after the permanent removal of different applied voltages. Generally, the accumulated charges decrease much faster than that from the fresh oil samples. Most of the charges disappear within 30 min, indicating that there are considerable fast moving charges accumulated in the aged oil samples. This validates the hypothesis that the aged oil enhances the dissipation of space charge due to the much higher conductivity of the aged oil impregnated samples.



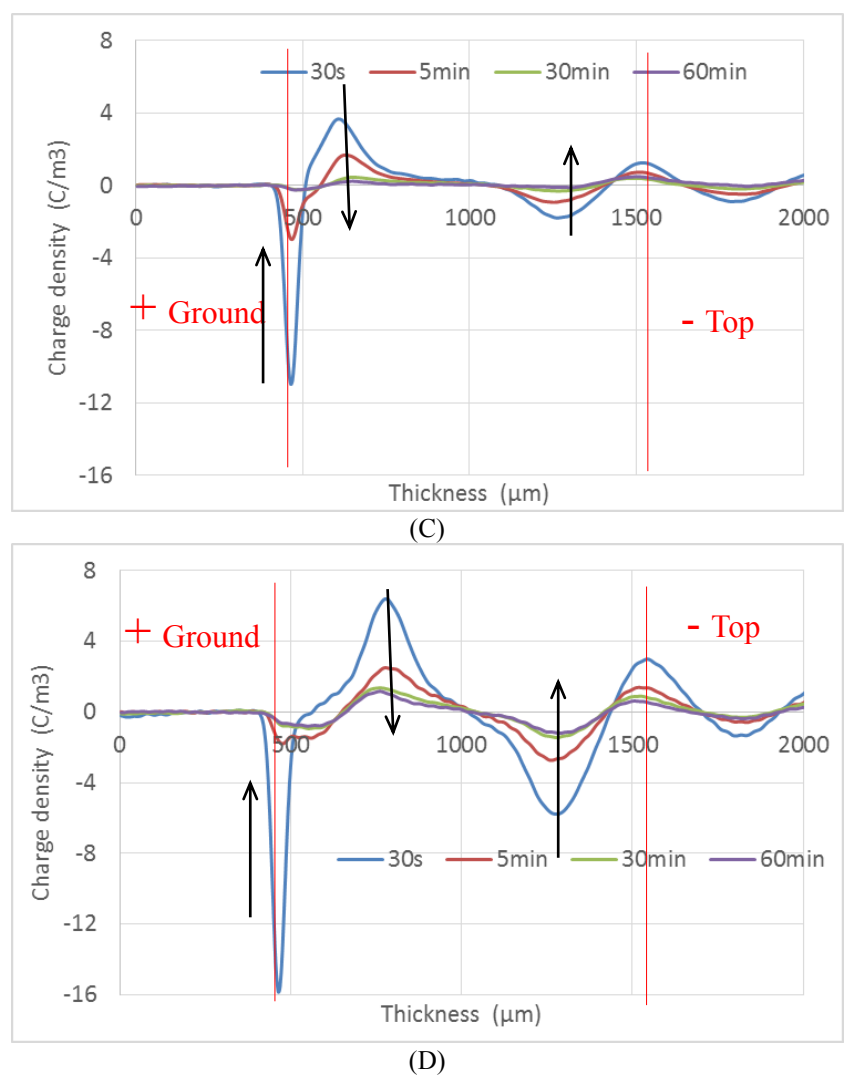


Figure 3-16 Decay results of aged oil samples under different electric fields of (A) +15 kV/mm; (B) +25 kV/mm; (C) -15 kV/mm and (D) -25 kV/mm.

For the samples under lower electric field, the injected positive charge peaks near the aluminium electrode are slightly moving to the middle of the sample with the decay time, which may suggest the most of the injected charges be dissipated from the electrode. In contrast, under higher electric field, the peaks are slightly moving to the electrode side with decay time, which may suggest the most of the injected charges be recombined at the middle of the pressboard due to the space charge accumulated deeper in the pressboard under higher electric field.

3.4 Analysis and discussion

3.4.1 Total absolute charge amount

To have a better understanding of the impact of the oil property on the space charge formation and movement, the total absolute charge amount for each sample is calculated by Equation (2.2).

Then, the total absolute amount of space charge for each sample can be calculated based on the PEA results above, as shown in Figure 3-17.

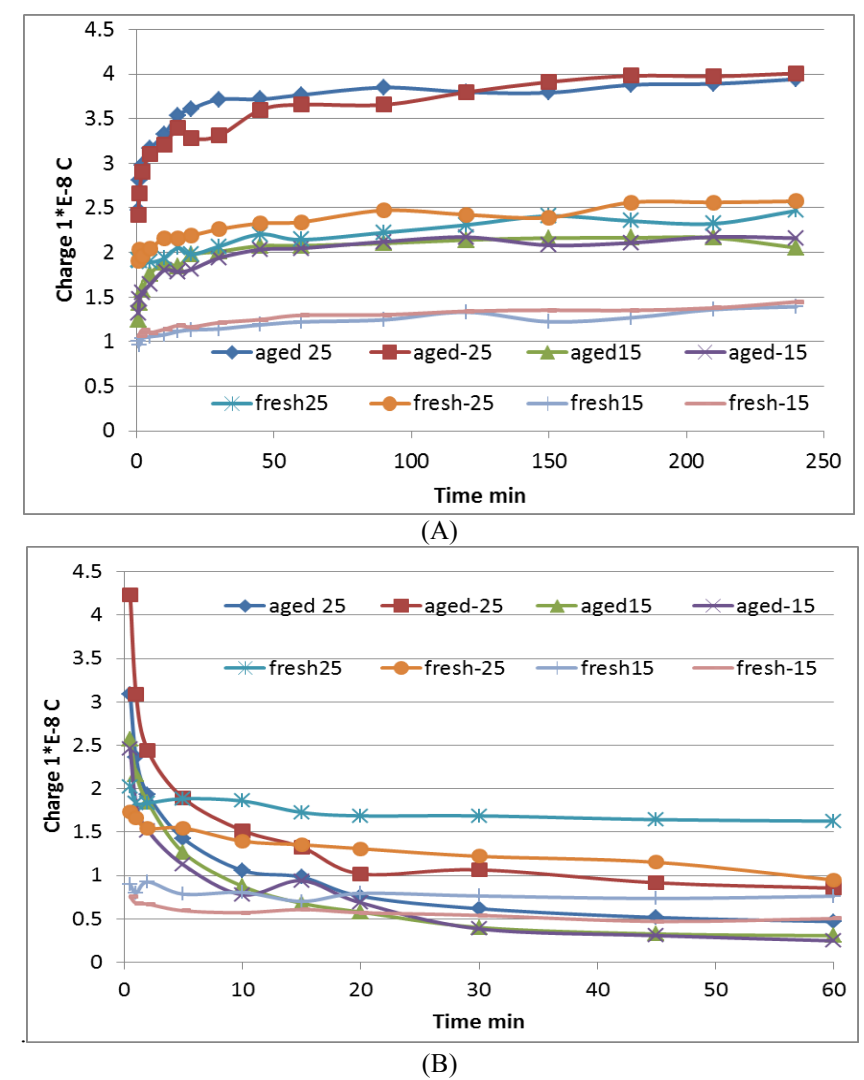


Figure 3-17 Absolute charge amount in the thick pressboard under (A) volts-on and (B) decay processes.

The total charge amount during the volts-on process (plot A) shows three levels of charge accumulation in the samples: the largest charge amount is accumulated in the aged oil sample under ± 25 kV/mm; the aged oil sample under ± 15 kV/mm and the fresh oil sample under ± 25 kV/mm are at the middle level; and the fresh oil sample under ± 15 kV/mm accumulates the least space charge. It is additionally observed that the applied electric stress will initialize the charge injection very similarly for either fresh or aged oil samples, e.g. the charge amounts of both types of oil samples under ± 25 kV/mm and ± 15 kV/mm are very close to each other when the stressing time is short. Furthermore, the charge amounts in the aged oil samples dramatically increase within the first 20 min and then gradually stabilize to a certain level. On the other hand, the charge amounts of the fresh oil samples are generally stable, with gradually increasing during a much longer period.

The total charge amount in the decay process (plot B) shows that the charges accumulated move fast in the aged oil samples, resulting in significant reduction in the first 10 min; however, in the fresh oil samples, most of space charges are slow moving charges which decrease gradually over 1 hour time. It can be seen, after 20 min, large amount of space charges still remain in the fresh oil samples, while only little charges are left in the aged oil samples.

3.4.2 Electric field distortion

One of the major impacts of space charge accumulation is the distortion of the local electric field distribution in the dielectric bulk. The injected homo-charge will reduce the electric field in the region between electrodes and sample. However, with the charges moving deeper towards to the middle of the pressboard, the electric field is gradually increasing in the middle of the insulation bulk. The electric field distributed along the sample can be calculated based on the charge density from the PEA results. As examples, the calculated electric field distributions under +25 kV/mm in the fresh oil pressboard are shown in Figure 3-18, and in the aged oil pressboard are shown in Figure 3-19.

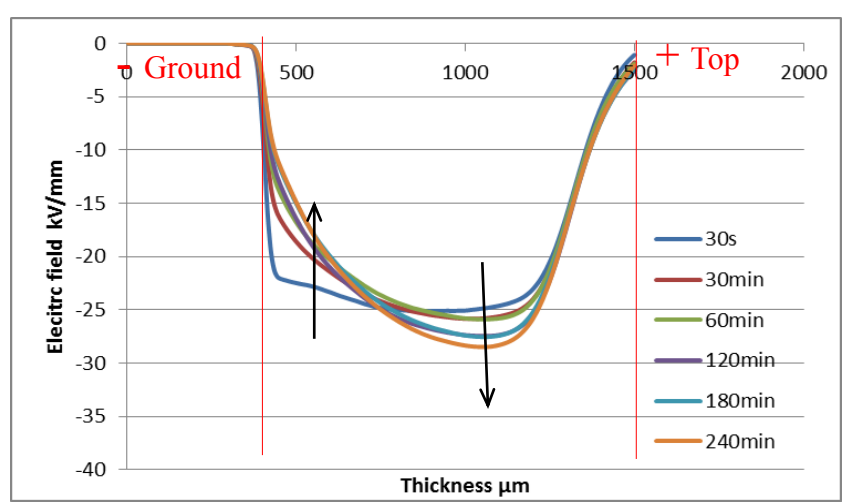


Figure 3-18 Electric field distribution in the fresh oil impregnated pressboard under +25 kV/mm.

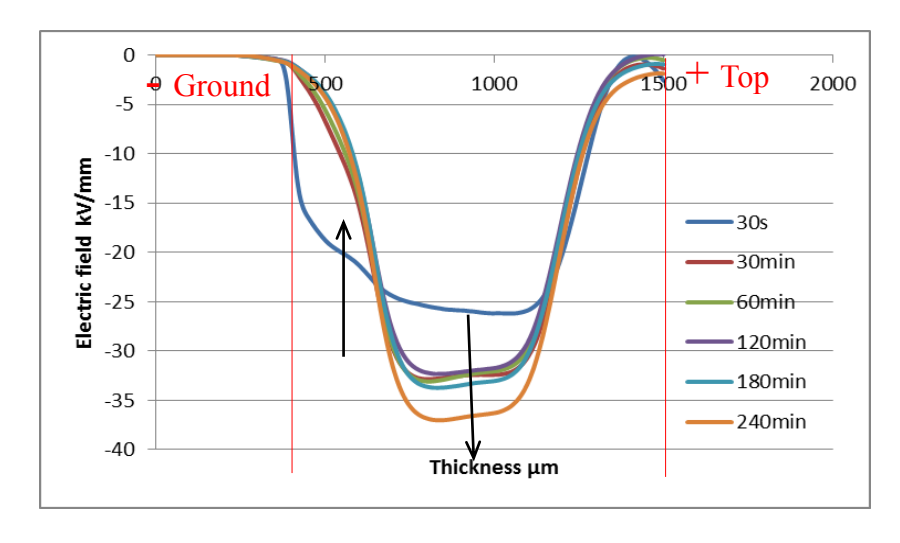


Figure 3-19 Electric field distribution in the aged oil impregnated pressboard under +25 kV/mm.

Therefore, the distortion factor of the electric field ΔE can be further calculated by Equation (2.4). The results, as shown in Figure 3-20, indicate that both the polarity and magnitude of the applied electric stress, and the oil status can affect the electric field distortion in the impregnated pressboard. The oil property is the dominant factor in this experiment: the field enhancement due to the presence of space charge is around 15% for fresh oil and 50% for aged oil. Moreover, the higher applied electric field leads to a larger electric field distortion (usually about 2% difference in the fresh oil samples and 5% in the aged oil samples); the positive voltage usually leads to larger electric field distortion (about 2% difference in the fresh oil samples and 7% in the aged oil samples). However, due to the large conductivity and much more complex status of the aged oil sample, the results usually vary in a relative larger range. In addition, the calculated electric field is probably a little smaller than the real value as the attenuation in the space charge measurement is not considered here.

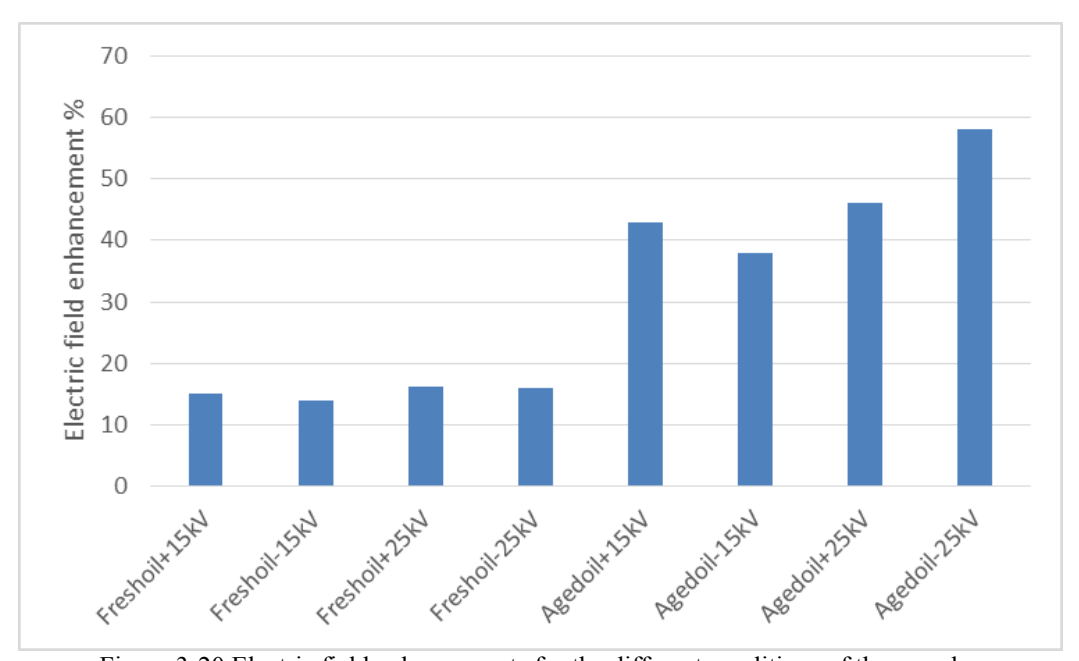


Figure 3-20 Electric field enhancements for the different conditions of the samples

3.4.3 Apparent trap-controlled charge mobility

Apparent trap-controlled charge mobility is used as an index to describe the degradation of the sample, which can be simply estimated by Equation (2.10).

The comparison of the apparent charge mobility for different samples is described in the Figure 3-21. The great mobility difference between the samples with two oil characteristics can be observed, which again indicates the significant impact of the oil property in the impregnated pressboard insulation system. Generally, the charge mobility in the aged oil samples (red lines) is much higher than that in the fresh oil samples (blue lines). The injected charges move fast in

the first 30 min in the fresh samples, and then gradually decrease. On the contrary, in the aged oil samples, the apparent charge mobility is very large in the first 20 min (with more than 5×10^{-11} m²V⁻¹s⁻¹), and then dramatically drops to below 0.1×10^{-11} m²V⁻¹s⁻¹. This result also agree well with the results of the trap depth, i.e. most of the traps in the aged oil are shallow traps, so the charge mobility in the aged oil are much larger than in the fresh oil samples. After 30 min, the residual charges within the insulation system are generally deeply trapped within the pressboard, showing a very small mobility.

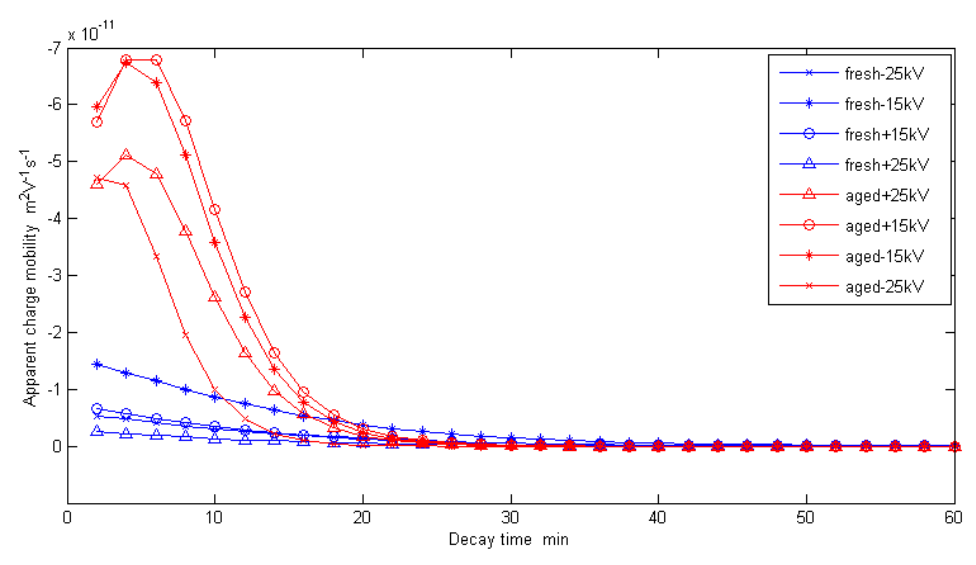


Figure 3-21 Results of the apparent charge mobility

Although this method can clearly describe the dielectric properties in the two groups of samples, however, the charge mobility curves of the aged oil samples show a quick increasing in the first 7 min. This may be due to the limitation of this calculation method. The recombination (or net charge) of the space charge cannot be ignored in this case as they are deeply injected in the insulation bulk. In other words, the considerable amount of charges located in the middle of the sample could be recombined when the depolarization occurs, which will affect the calculation of the charge mobility. Additionally, the mobility of the very fast charges cannot be estimated by this method due to lack of data at the very beginning of the decay test. This is limited by the PEA system which requires about 10 seconds to capture the space charge measurement results.

3.4.4 Trap energy distribution

Another important parameter that can be used to represent the characteristic of the dielectric material is the trap energy distribution of the dielectrics. It is generally believed that the degradation of the dielectric material can result in the change of the trap depth and density. [77]

According to Equation (2.18), the density of trap energy level can be determined by the decay constant of charge density and decay time, which are able to be obtained from the PEA results.

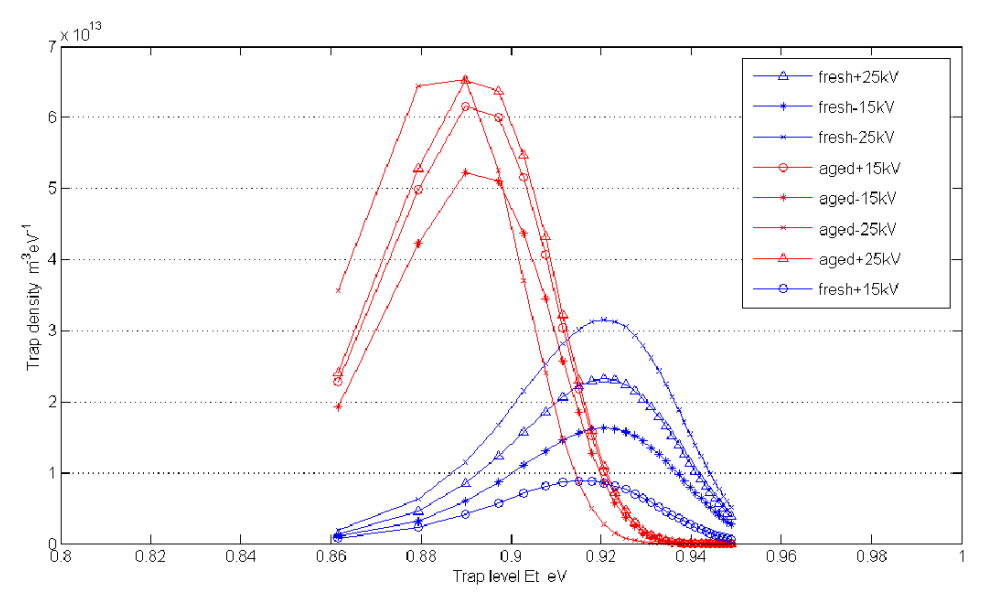


Figure 3-22 Results of the trap energy distribution

The calculation results are shown in the Figure 3-22, which clearly depict the differences between two types of samples (red lines indicate aged oil samples; blue lines indicate fresh oil samples): the energy level of fresh oil samples is mainly distributed in the range of 0.9 to 0.94 eV, and the trap density is in the range from about 1 m⁻³eV⁻¹ to about 3 m⁻³eV⁻¹. It can be seen that there are still certain amount of traps with the energy level above 0.95 eV; for the aged oil samples, the energy level is mainly distributed in the range of 0.86 to 0.92 eV with a much higher trap density from about 5 m⁻³eV⁻¹ to 6.5 m⁻³eV⁻¹. It can also be seen for fresh oil samples that the trap density is increasing with the increasing of the applied voltages due to the voltage excitation theory which is well known in the semiconducting material. However, this method is not very suitable for the aged oil samples as the space charges have been deeply injected into the insulation bulk, therefore, the assumption of this method may not be very suitable in this case; considerable charges are not dissipated from the electrodes but recombined in the middle of the pressboard, so the depolarization current calculation is not accurate; there may be certain amount of space charge re-trapped in the pressboard during the de-trap process as the pressboard samples are very thick and the space charge is deeply distributed into the insulation bulk. Similarly, due to the limitation in the apparent charge mobility at the very beginning of the decay test, the operations to record the first decay data have to consume a few seconds, so the time associated with the trap depth is at least 0.6 eV [112], and in this work it is estimated as 0.86 eV. Although this method has its limitations for the thick samples especially with strong space charge injection, it still can clearly distinguish the differences between the fresh and aged samples in this work.

3.5 Conclusions

In this chapter, the space charge dynamics in 1 mm thick impregnated pressboard has been successfully investigated based a purpose-built PEA system. The distribution of the accumulated charges can be clearly distinguished within the pressboard bulk, though the significant impact of attenuation occurs in the vicinity of the top electrode. The influence of the applied electric stress and the oil status on charge dynamics in the pressboard has been investigated. The total charge amount and the distortion of the electric field are also analysed based on the PEA results.

The homo-charge injection behaviour of the space charge has been observed in the all thick samples with both fresh and aged oils; the higher the applied stress, the more the space charge accumulated in the insulation bulk. It has been found that the service aged oil greatly enhances the charge injection and mobility, resulting in a severe electric field distortion in the middle of the pressboard.

The trap depths in the samples with different oil status are considerably different: the energy level of the fresh oil samples mainly distributes in the range of 0.9 to 0.94 eV with a smaller trap density. On the contrary, the energy level of the aged oil samples is concentrated in the range of 0.86 to 0.92 eV with much higher trap density. This result indicates that there are more space charge in the aged oil samples and most of them are fast moving charges; much less charges injected in the fresh oil samples and most of them are slow moving charges. This is also confirmed by the calculation of the apparent charge mobility in all the samples, even considering the limitation of the calculation method for the trap energy and charge mobility in the thick samples, especially for the aged oil samples within which the space charge recombination cannot be ignored.

Chapter 4.

Space Charge Behaviour in Multilayer Oil Gap and Thick Impregnated Pressboard Systems under HVDC Stresses

In a real life converter transformer, multilayers of pressboards are immersed in the mineral oil forming multiple insulation barriers including the interfaces between the mineral oil and the pressboards. The interface is usually considered as the weakest point in an insulation system. The inhomogeneity of the material and the condition of the interface can easily result in the accumulation of space charge and lead to severe electric field distortion, which is always one of the major issues in the HVDC industry.

Based on the Maxwell-Wagner-Sillars polarization theory, the space charge will build up at the interface between two dielectrics with a different ratio of permittivities and conductivities of the dielectrics, as described in:

$$\rho = \varepsilon_o E_o - \varepsilon_p E_p = \frac{\varepsilon_o \sigma_p - \varepsilon_p \sigma_o}{L_o \sigma_p + L_p \sigma_o} U (1 - e^{-t/\tau})$$
(4.1)

where ε_0 , ε_p are the permittivity of oil film and oil impregnated pressboard, respectively; σ_0 , σ_p are the conductivity of oil and impregnated pressboard, respectively; L_0 , L_p are the thicknesses of the oil gap and impregnated pressboard, respectively; U is the applied voltage; τ is the time constant., which can be calculated by:

$$\tau = \frac{L_o \varepsilon_p + L_p \varepsilon_o}{L_o \sigma_p + L_o \sigma_p}$$
(4.2)

The electric field distribution in different dielectrics thus can be calculated, which now is widely applied in power industry for the insulation design in converter transformers. Some other factors, such as temperature and applied electric field, are considered to be the contributors for the localized variation of the conductivity within the dielectric material [100]. It is expected that a more accurate electric field distribution could be achieved in a converter transformer when the temperature and electric field dependent conductivity of the dielectric material is applied into the Maxwell theory. However, since the space charge mechanisms are not taken into consideration in the Maxwell theory, the actual maximum electric field within the insulation system could be considerably greater than the value predicted by the Maxwell theory prediction as the presence of space charge can enhance the electric field locally. This impact has already been demonstrated for polymeric materials [104].

In this chapter, the space charge behaviours in multilayer oil gap and impregnated pressboards are investigated experimentally, and the results are compared with the Maxwell theory. For convenience of measurement and better understanding of space charge behaviours in a liquid and solid combined system, when conducting the experiments the multilayer barrier system is divided into two configurations: single layer of oil gap combined with a single layer of pressboard and the single layer of oil gap sandwiched between two layers of pressboards.

4.1 Space charge behaviour in an oil gap combined with single layer impregnated pressboard insulation system

In this section, the investigation of the space charge dynamics in a 0.5 mm thick oil gap combined with a 1 mm thick impregnated pressboard under DC stresses is introduced firstly. Then the space charge dynamics with a long time duration of voltage application are further measured to reveal the interfacial effect and the bulk effect.

4.1.1 Experimental setup

Figure 4-1 shows the experimental setup applied in this work to investigate the space charge behaviour in the insulating liquid gap combined with a layer of solid dielectric. The aluminium plate, which is used as the ground electrode in PEA system, was modified to be an oil container that can hold both solid and liquid dielectric materials with a 5 mm in depth and 10 cm in diameter. A 0.5 mm thick PTFE ring was placed on the bottom of the container to create the oil gap, the volume of the oil gap is about 0.05 mL. The area of the oil gap is much larger than the area of the top electrode and the sensor, hence it can be assumed that the electric field is mainly distributed within the gap rather than the PTFE ring. The pressboard was firmly pressed by the top electrode above the oil gap in order to achieve a good contact between the electrode and different layers of dielectrics, which is essential for acoustic signal transmission.

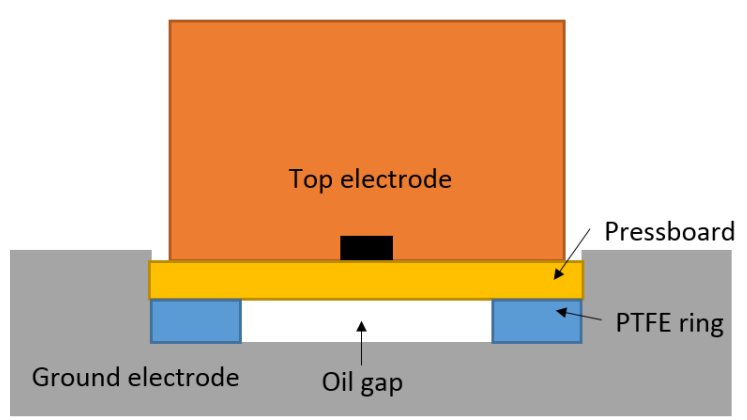


Figure 4-1 The sketch of the measurement setup for oil gap combined with single layer pressboard insulation system

The measurements were carried out at the room temperature. Two different DC electric fields were applied, 12 kV/mm and 20 kV/mm, as comparison. When the voltage was applied, the voltson results were recorded, and after 3 hours, the decay results were recorded during another 3 hours depolarization time. For the long time duration measurement, the space charge profiles were recorded during 48-hour voltage application and 72-hour after voltage removal.

Both fresh oil and service aged oil were measured and the samples prepared follows the same procedures introduced in Ch3.2.

4.1.2 Acoustic wave transmission and reflection in the combined system

The acoustic properties of the oil and the impregnated pressboard are different as shown in Table 4-1. As shown in Figure 4-2, the acoustic wave generated by the space charge within the pressboard with a generation factor G_p propagates towards to the oil gap, and passes through the interface with a transmission factor T. Then this pressure wave transports through the ground electrode, and detected by the sensor. The acoustic signal generated by the space charge at the

interface with the generation factor G_{inter} also propagates through the oil gap and then is detected by the sensor. On the other hand, the acoustic wave generated by the space charge within the oil gap are separated into two parts (assuming the acoustic wave propagation is one-dimensional) with a same generation factor G_o . One part is moving towards to the ground electrode, while the other one moving towards to the pressboard. The latter one is reflected by the oil-pressboard interface with a reflection factor R, due to the unequal acoustic impedances of the oil and pressboard. The reflected acoustic wave then travels through the oil gap and the ground electrode to the sensor. The transmission factors are calculated and shown in Table 4-2. [100]

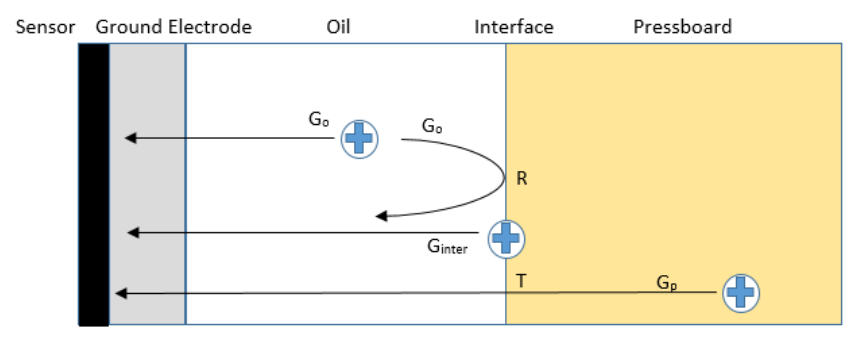


Figure 4-2 The acoustic signal propagations in the oil gap and single layer pressboard combined insulation system

Table 4-1. Acoustic properties [100]

Material	Density ρ (kg/m³)	Acoustic velocity υ (m/s)	Acoustic impedance Z (10 ⁶ kg/m ² s)
Mineral oil	0.85×10^{3}	1400	1.2
Impregnated pressboard	1.2×10³	2000	2.4

Table 4-2. Acoustic transmission factors

Factors	Equation	Value
G_{P}	$\frac{Z_P}{Z_P + Z_P}$	0.5
G_0	$\frac{Z_O}{Z_O + Z_O}$	0.5
G_{inter}	$\frac{Z_O}{Z_O + Z_p}$	0.3
Т	$\frac{2Z_O}{Z_O + Z_P}$	0.7
R	$\frac{Z_p - Z_O}{Z_O + Z_P}$	0.3

The reflected signal may be overlapped with the space charge signal within the pressboard. The whole transmission factor of the reflected signal can be calculated by:

$$F_R = G_O \cdot R = 0.15 \tag{4.3}$$

For the space charge signal, the whole transmission factor can be calculated by:

$$F_P = G_P \cdot T = 0.35 \tag{4.4}$$

The $F_P > F_R$ indicates the reflected signal is smaller than the space charge signal. More importantly, from the pre-test results, no accumulated charges were observed in the oil gap due to the large charge mobility in the oil. The only possible reflection may be reflected from the cathode peak, however, this reflection signal travels through double thickness of the oil gap (where the signal attenuation is much larger than in the pressboard [109]). Therefore, no reflected signal generated by the space charge within oil gap can be observed. As shown in Figure 4-3, no space charge accumulation and reflection signal can be observed within the insulation bulk.

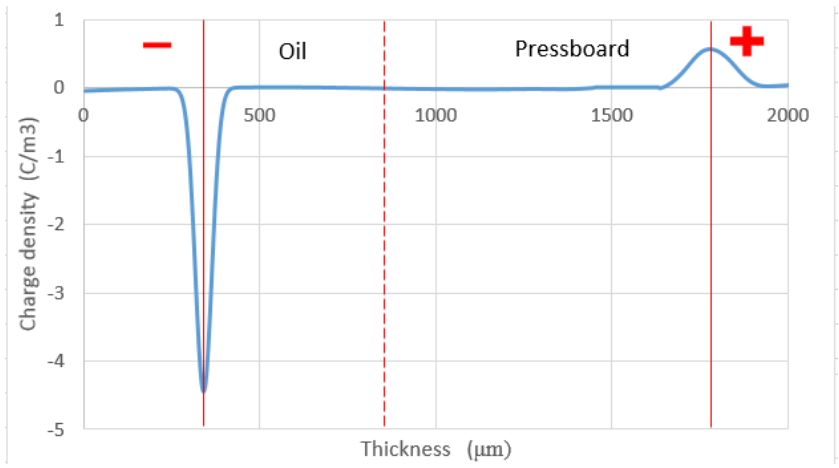


Figure 4-3 The calibrated space charge profile

4.1.3 Space charge results

A. Results of pressboard with fresh oil

1. Volts-on

The volts-on results of the space charge distributions in the pressboard impregnated with the fresh oil at +12 kV/mm and +20 kV/mm are shown in Figure 4-4. The thin solid lines with + and - represent the positions of anode and cathode, and the dash line locates the interface position.

As the oil is directly in contact with the ground electrode, the cathode peak is generally very narrow and large compared with the anode peak. This is because of the large acoustic attenuation along the samples when acoustic waves travel from the anode to the sensor. With the voltage application, the cathode peak keeps decreasing, suggesting homo charge injection occurs from the cathode. The injected negative charges drift very fast within the oil gap due to the higher mobility in the oil [38]. These negative charges move quickly towards to the middle of insulation system, and hindered by the interface between oil and pressboard. Therefore, large amount of negative charges accumulate at the interface with the voltage application. This agrees with the Maxwell-Wagner polarization that charges will be formed at the interface when the dielectrics have discontinuity of the ratio of permittivity and conductivity. And in this case, a negative interfacial peak can be observed.

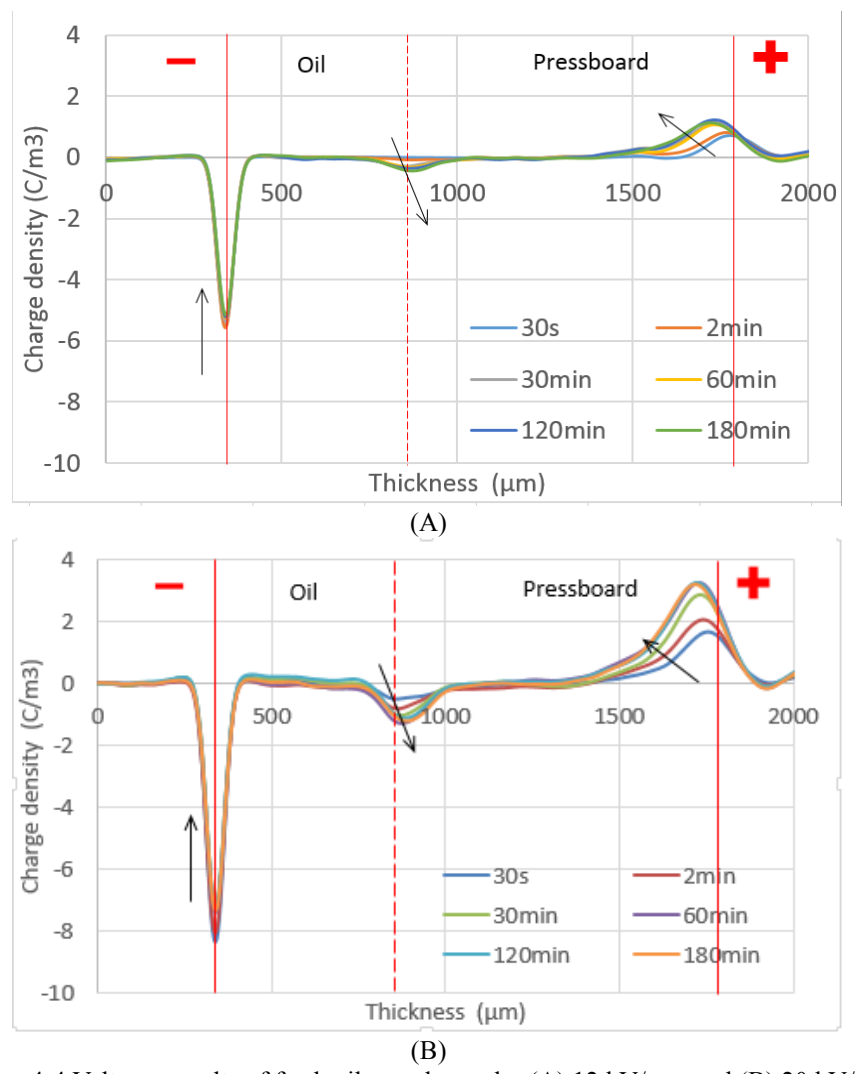


Figure 4-4 Volts-on results of fresh oil samples under (A) 12 kV/mm and (B) 20 kV/mm.

In the fresh oil samples, the build-up of the interfacial charges is slow, i.e. the peak of the interfacial charges is about 0.5 C/m³ after 3 hours voltage application. And under the higher applied voltage, the interfacial peak is slightly higher (about 1.1 C/m³). Moreover, the position of the interfacial peak is not constant at the physical interface between oil and pressboard, but keeps moving into the pressboard bulk, suggesting that the interfacial charges do not only stay at the interface but also move into the pressboard bulk. In the fresh oil samples, the movement is very small during the 3 hours volts-on test, which will be further validated in the long duration tests in the following sections.

At the anode side, homo charge injection also occurs, i.e. positive charges carriers (or extraction of electrons) gradually move into the pressboard bulk, leading to a movement of the anode peak towards to the middle of the pressboard. It should be noticed that the positive peak is much lower and broader compared with the cathode peak due to the large acoustic attenuation and dispersion. Initially, little or none charges are expected to accumulate in the insulation system bulk at 12 kV/mm, therefore, theoretically, if there were no attenuation and dispersion of the involved

materials, the anode peak would be the same as the peak on the cathode with the same amplitude and width. Moreover, the amplitude and width of the peaks located in the bulk of the system are also affected by the acoustic attenuation and dispersion, following the exponential relationship with the distance from the cathode [113]. Therefore, it is difficult to distinguish the injected charges from the anode peak. At 12 kV/mm, the anode peak rises from 0.8 C/m³ to 1.2 C/m³, while from 1.7 C/m³ to 3.1 C/m³ at 20 kV/mm, which may result from the increased negative charge amount at the interface.

2. Decay

The decay tests were carried out after 3 hours voltage stressing by the permanent removal of the external electric field. The results of decay tests can clearly show the accumulated charges inside the insulation system. Therefore, the charge dynamics without the influence of the external voltage can reflect the trap energy levels of the insulation system. The results, as shown in Figure 4-5, indicate the drifting away and recombination behaviours of the accumulated charges at 12 kV/mm (A) and 20 kV/mm (B), respectively.

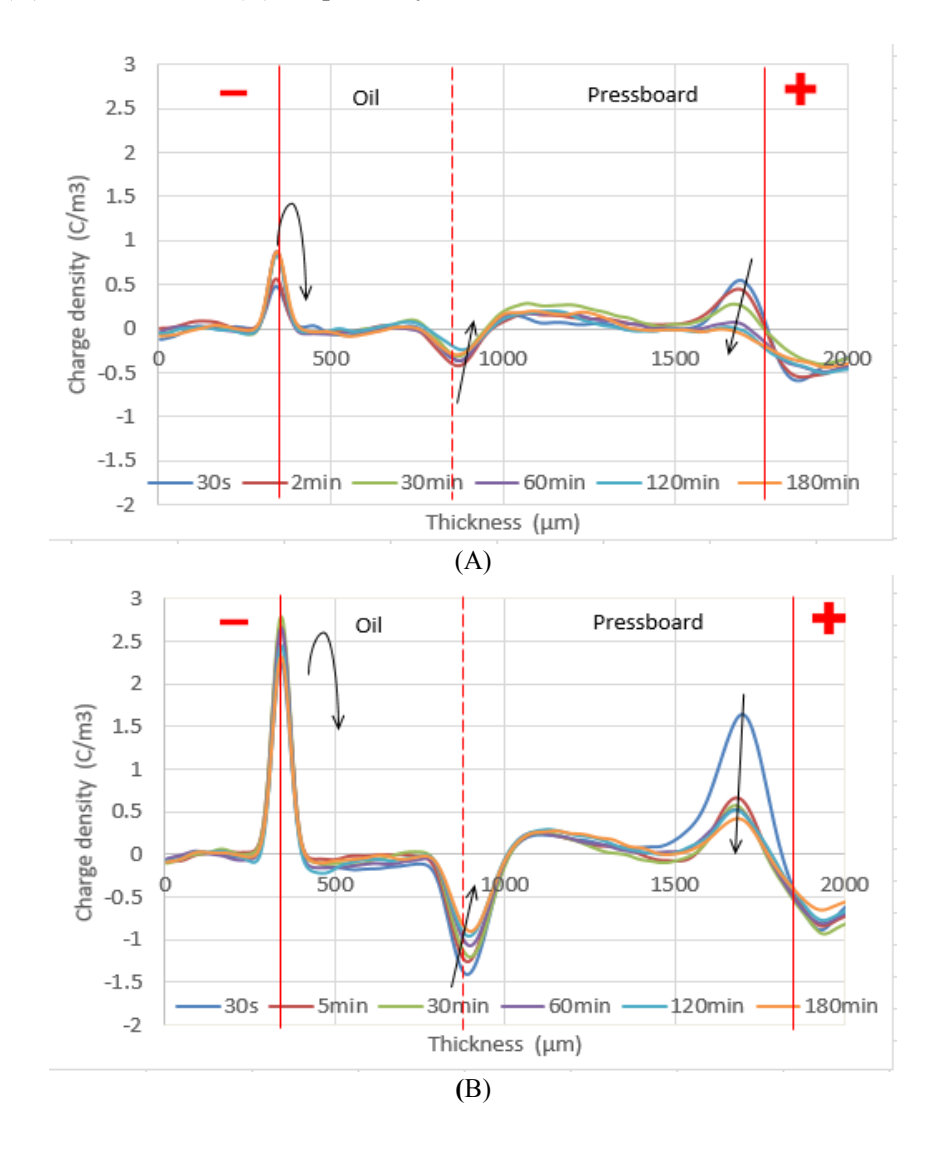


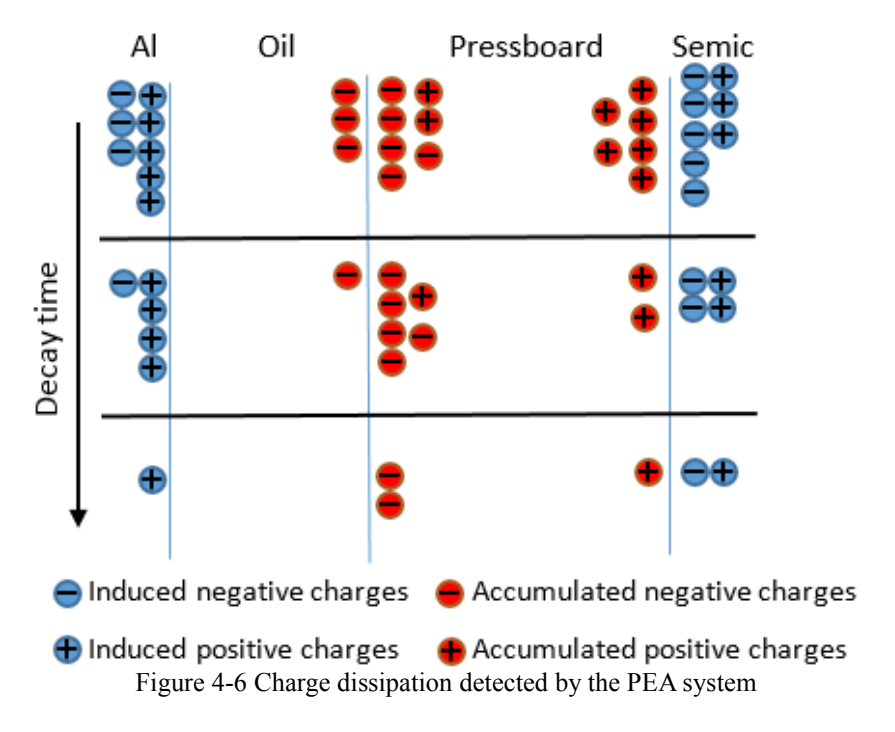
Figure 4-5 Decay results of fresh oil samples under (A) 12 kV/mm and (B) 20 kV/mm

The initial results clearly show that most of the accumulated charges are distributed at the interface and the bulk of pressboard. Large amount of negative charges accumulate at the interface, resulting in a large positive peak induced at the cathode. The amount of negative interfacial charges decreases with the depolarization time, e.g. the interfacial peak drops from 0.46 C/m³ to 0.3 C/m³ under 12 kV/mm and from 1.4 C/m³ to 1 C/m³ under 20 kV/mm. It can be observed that positive charges widely distribute in the pressboard bulk, i.e. a small positive peak locates next to the negative interfacial peak in the pressboard, and significant amount of positive charges accumulate near to the anode as well. The presence of the positive charges near to the interface may be caused by the polarization in the pressboard during the voltage application that positive charges are attracted by the negative interfacial charges under the influence of the applied electric field. These positive charges could also come from the injected positive charges from the anode. These charges travel through the pressboard, which then are blocked by the oil/pressboard interface. The interfacial charges and these positive charges may overlap each other in the narrow vicinity of the interface, which is difficult to be distinguished due to only net charge can be detected by the PEA system. At the anode side, the accumulated positive charges overlap with the induced anode peak due to the large acoustic dispersion, however, the decay of the positive charges can be observed clearly, i.e. the value of the positive peak decreases from 0.54 C/m³ to background noise under 12 kV/mm and from 1.6 C/m³ to 0.5 C/m³ under 20 kV/mm. Therefore, a much faster charge decay process can be observed in the sample under the higher field as more space charge accumulated within the sample which can significantly distort the local electric field in the vicinity of the top electrode and accelerate charge drifting away from the top electrode. And most of the positive charges disappear within 30 minutes. Compared with the interfacial charges, the positive charges near to the anode decay much faster, which affects the dynamics of the cathode peak.

When the external voltage is removed, the charges on the cathode are induced by the accumulated charges within the insulation system including the negative interfacial charges and positive charges near to the anode. However, the amount of the induced charges on each electrode is proportional to source charge amount and inverse proportional to the distance from the accumulated charge to the electrode. [113] Therefore, in this case, most of the induced charges on the cathode are negative charges. In the first 30 minutes, the positive charges near the anode decay much faster than the negative interfacial charges, the induced cathode peak keeps increasing, and then decreasing with depolarization time. This phenomenon may suggest the interface could obstruct the accumulated charges near to the interface to drift away from the pressboard to the electrode, compared with the positive charges that can easily drift away to the anode which is in direct contact with the pressboard.

Moreover, it can be found that the interfacial peak keeps moving into the pressboard bulk during the 3 hours decay time. The reason can be explained as following: the interfacial charge peak may be viewed as the sum of charges from the oil side and charges that in the pressboard. Although all these charges are recognized as the interfacial charges, their characteristics, such as mobility, may be very different due to the different properties of the dielectric materials. Those charges in the oil may quickly drift away from the cathode through the oil gap, while those charges in the pressboard, however, hardly pass through the interface. Thus, they remain in the pressboard near to the interface, showing the interfacial peak moving into the pressboard.

The schematic illustration of the charge dissipation that detected by the PEA system is shown in Figure 4-6.



B. Results of pressboard with aged oil

1. Volts-on

In order to evaluate the dielectric performance in long term service converter transformers, the effects of aged oil on space charge dynamics are also investigated. As shown in Figure 4-7, the volts-on results of the aged oil samples are very different from those observed from the fresh oil samples.

In general, the space charge dynamics are dramatically enhanced by the aged oil. The cathode peak decreases very quickly from 4.8 C/m³ to 1 C/m³ under 12 kV/mm and from 5.8 C/m³ to 1.9 C/m³ under 20 kV/mm in the first 2 minutes, and almost disappears after 30 minutes, indicating very strong homo charge injection from the cathode.

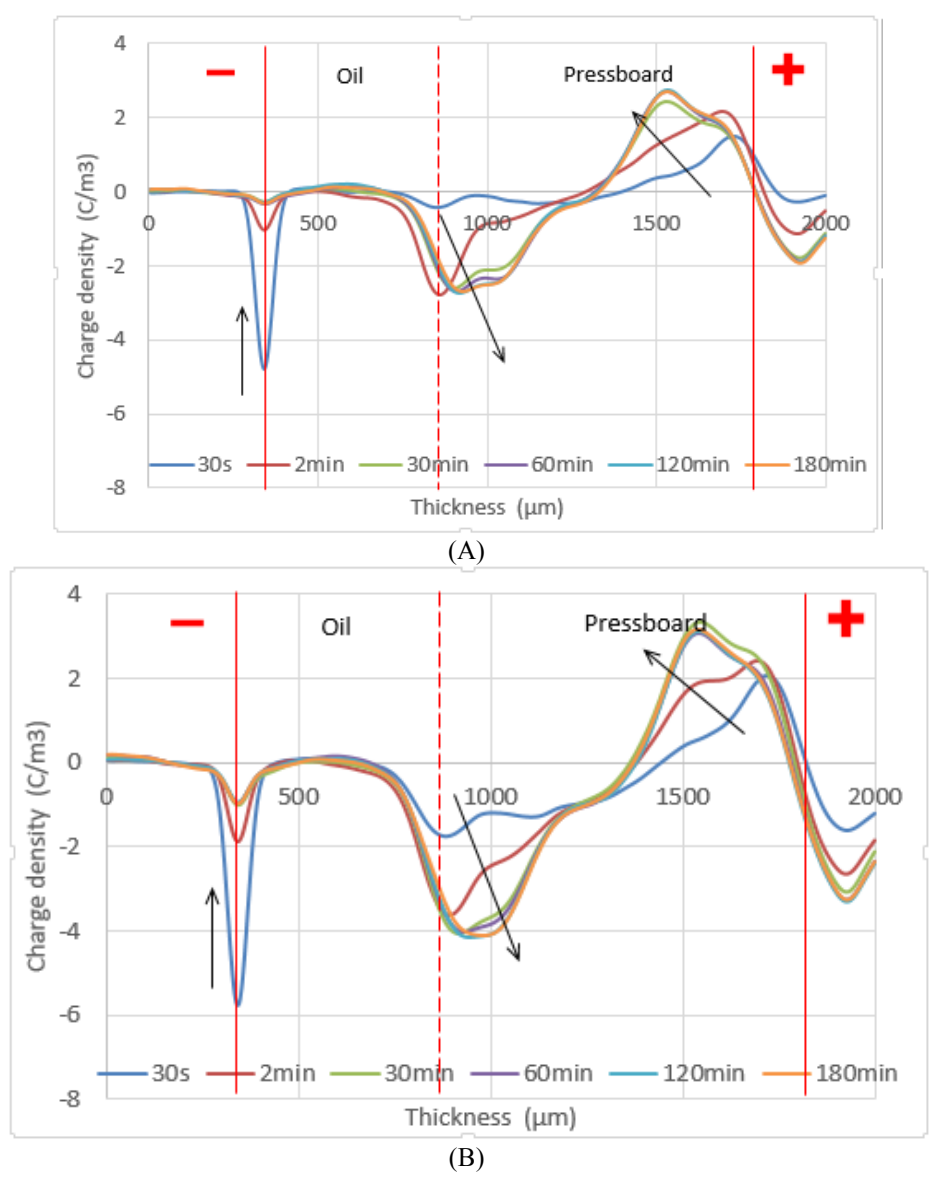


Figure 4-7 Volts-on results of aged oil samples under (A) 12 kV/mm and (B) 20 kV/mm.

Consequently, significant interfacial charge peak quickly occurs and dramatically increases in the first 2 minutes from 0.4 C/m³ to 2.7 C/m³ under 12 kV/mm and 3.8 C/m³ under 20kV/mm, then it gradually increases with voltage application. Meanwhile, large amount of negative charges pass through the interface into the pressboard and move towards to the middle of pressboard. Similarly, strong homo charge injection also happens at the anode, leading to the significant increase of the anode peak value and the obvious movement of the peak position from the electrode into the pressboard bulk. It suggests that both positive charges and negative charges can be easily injected into the aged oil samples, and the movement of these charges is enhanced by the aged oil, leading to a severe electric field enhancement in the middle of the pressboard. The space charge profiles at 30 seconds under different electric fields clear show the effects of the applied fields on space charge dynamics in the aged oil samples. The much larger interfacial peak value in the sample under higher voltage indicates more negative charges are injected from the cathode when higher voltage is applied.

2. Decay

Figure 4-8 shows the decay results for the aged oil samples after the removal of the different applied electric fields.

Due to the enhancement of charge movement in the aged oil samples, the accumulated charges, compared with fresh oil samples, decay very quickly, though the amount of accumulated charges is much larger during the volts-on test. Therefore, the induced positive peak on the cathode keeps decreasing during the decay process. Most of charges disappear shortly after the removal of the applied fields, and there is very little charges remaining in the insulation system after 5 minutes.

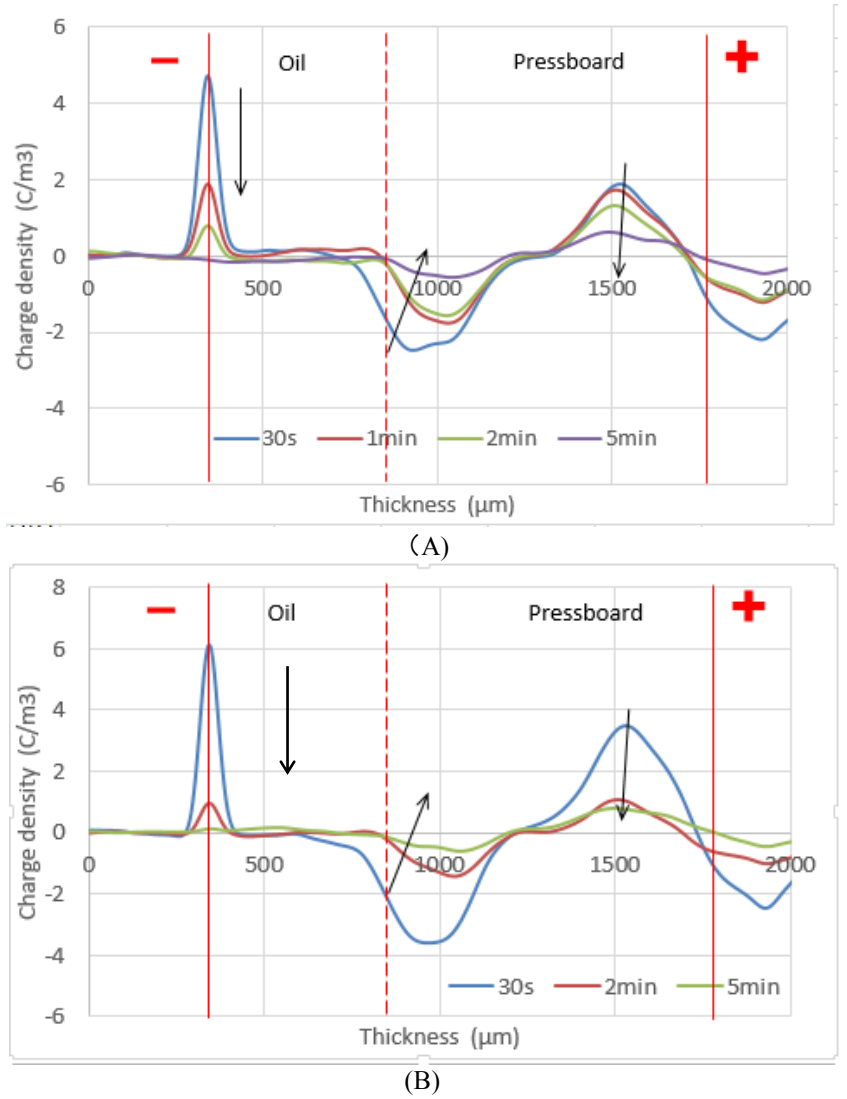


Figure 4-8 Decay results of aged oil samples under (A) 12 kV/mm and (B) 20 kV/mm.

It is interesting to notice that the interfacial charge peak keeps moving into the pressboard during the depolarization process, similar to that in the fresh oil samples. However, in the aged oil samples, this movement is much more obvious. The interfacial charges at the oil side quickly drift away from the aged oil to the cathode, leaving the charges accumulated in the pressboard

near to the interface. These charges may relatively slowly pass through the interface and drift away, or recombine with positive charges in the pressboard bulk. This again shows the interfacial effect, although it is significantly weakened by the aged oil, compared with fresh oil samples.

C. Long-time duration results of pressboard with fresh oil

In order to verify the interfacial effect and bulk effect in fresh oil samples, the space charge profiles have been recorded over 48-hour voltage application and 72-hour after voltage removal, as shown in Figure 4-9 (A) and (B).

The plot (A) shows the space charge dynamics under 12 kV/mm for 48 hours. Significant homo charge injection can be observed at both cathode and anode. The cathode charge peak decreases greatly in the first 24 hours, and then becomes stable with a peak value of 3.5 C/m³. On the hand, as mentioned earlier, the anode charge peak overlaps with the injected positive charges due to the peak broadening. With the voltage application, the positive peak keeps increasing and also reaches to a steady state within 24 hours. Moreover, the movement of the positive charge peak can also be observed clearly, because the pressboard is thick enough to show the bulk effect. The positive charge peak moves to the middle of the pressboard about 110 µm in the first day and then only about 20 µm in the second day, indicating the dynamics balance is gradually reached. Similar to the short time space charge dynamics in fresh oil samples, the charge injection from the interface into pressboard bulk is not significant in the first 3 hours, i.e. the movement of the interfacial peak is small (about 30 µm). After 24 hours, however, large amount of negative charges have been injected and accumulated in the pressboard bulk, resulting the obvious peak movement (about 180 µm). The reason is that the accumulation of negative interfacial charges can reduce the electric field distributed in the oil gap but increase the electric field in the pressboard. Therefore, the negative charge movement from the cathode to the interface is gradually weakened, but the charge movement from the interface to the pressboard is enhanced. However, once the interfacial charges move into the pressboard, the drop of the interfacial peak will again lead to a stronger charge injection from the cathode. This cycle happens continuously until the balance is reached (more than 24 hours in this work), as illustrated in Figure 4-9 (A). Moreover, both the injected positive and negative charges are accumulated near the middle of pressboard resulting in significant field enhancement in the region between these two peaks.

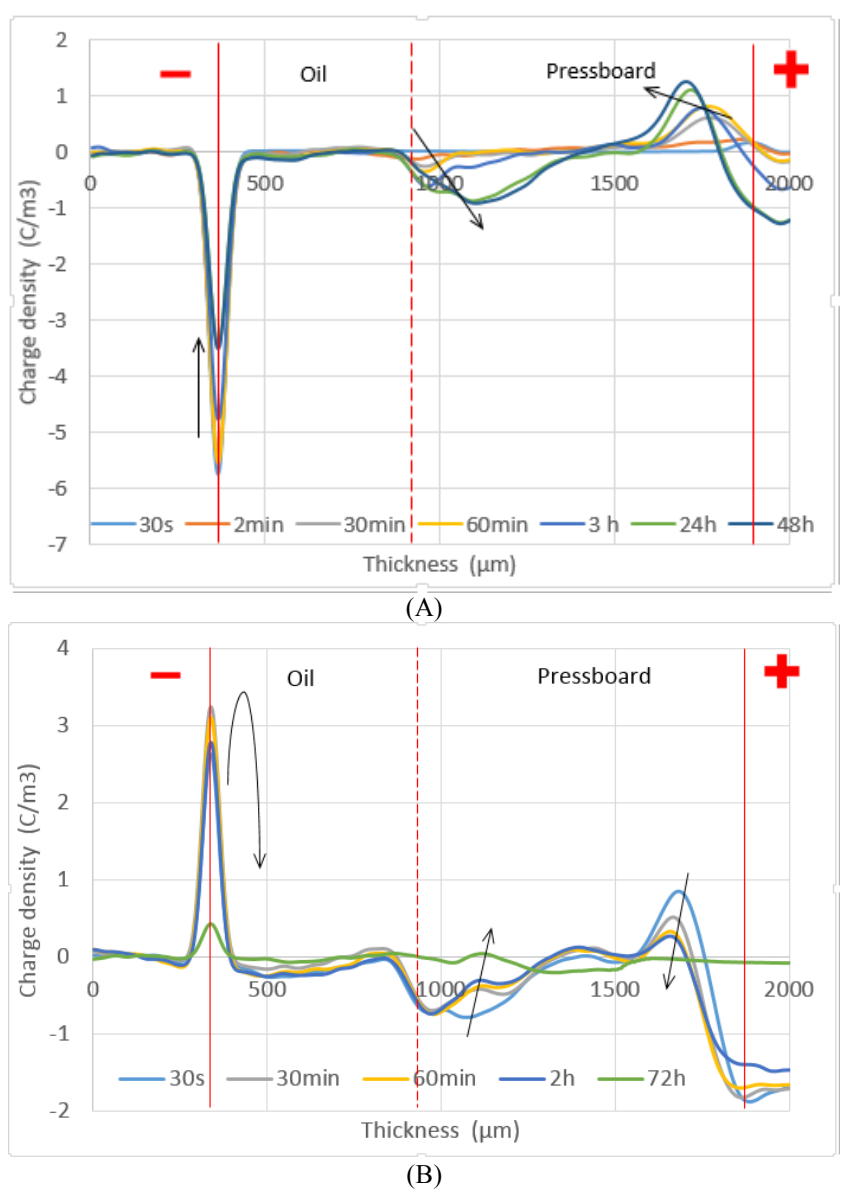


Figure 4-9 Long duration charge dynamics in fresh oil samples under 12 kV/mm under (A) volts-on and (B) decay processes

The result of long time decay test is shown in the plot (B). Similarly, a positive peak can be observed on the cathode, induced by the large amount of negative charges accumulated in the pressboard and interface. There are more negative charges accumulated in the dielectrics during the much longer voltage application compared with the previous results, so the amplitude of the induced cathode peak is also larger. The cathode peak also gradually increases in the first 30 minutes, reaching to the maximum value about 3.1 C/m³, and then starts to decrease. After about 72 hours, the cathode peak drops to about 0.33 C/m³. Meanwhile, the amplitude of the anode peak also drops. Moreover, it can be observed that the anode peak moves towards to the middle of the pressboard during the decay process, which is different from the previous results where the position of the anode peak stays the same during the whole decay process. There may be two reasons to explain this movement: 1) the accumulated positive charges located near to the anode could firstly drift away from the anode, leaving those positive charges in the middle region; 2) the

accumulated positive charges could be attracted by the accumulated negative charges and move towards to the middle of the pressboard following the local electric field direction in the pressboard. The two possible reasons may operate simultaneously, and the charge movement depends on the competition of the two processes in the local area. No positive charges can be observed after 72 hours.

When the decay process starts, it can be seen that large amount of negative charges widely distribute from the interface to the middle of the pressboard. Two negative peaks can be observed, i.e. the first peak is at the interface region; the second peak is in the bulk of the pressboard (about 180 µm from the interface). During the decay process, the second peak decreases quickly and moves towards to the anode, while the first peak only slightly decreases and moves to the bulk of the pressboard within the first 2 hours. After 72 hours, only small amount of negative charges remain in the pressboard near to the interface. The observed charge dynamics may indicate that the most of the accumulated negative charges in the middle region of the pressboard are cancelled or recombined by the accumulated positive charges, resulting the decrease and movement of the second peak. On the other hand, the first peak slowly decays because of the interfacial effect that can form lots of deep traps in the region that prevent charges to de-trap. [114]

It should be noticed that the steady state in the aged oil sample can be quickly reached within the 3 hours of the voltage application duration. Therefore, long duration measurement is not essential for the aged oil sample.

4.1.4 Discussions

A. Total charge amount

By applying Equation (2.2), the total charge amount is calculated for fresh oil samples and aged oil samples. The results are shown in Figure 4-10, the volts-on shown in (A) and the decay shown in (B).

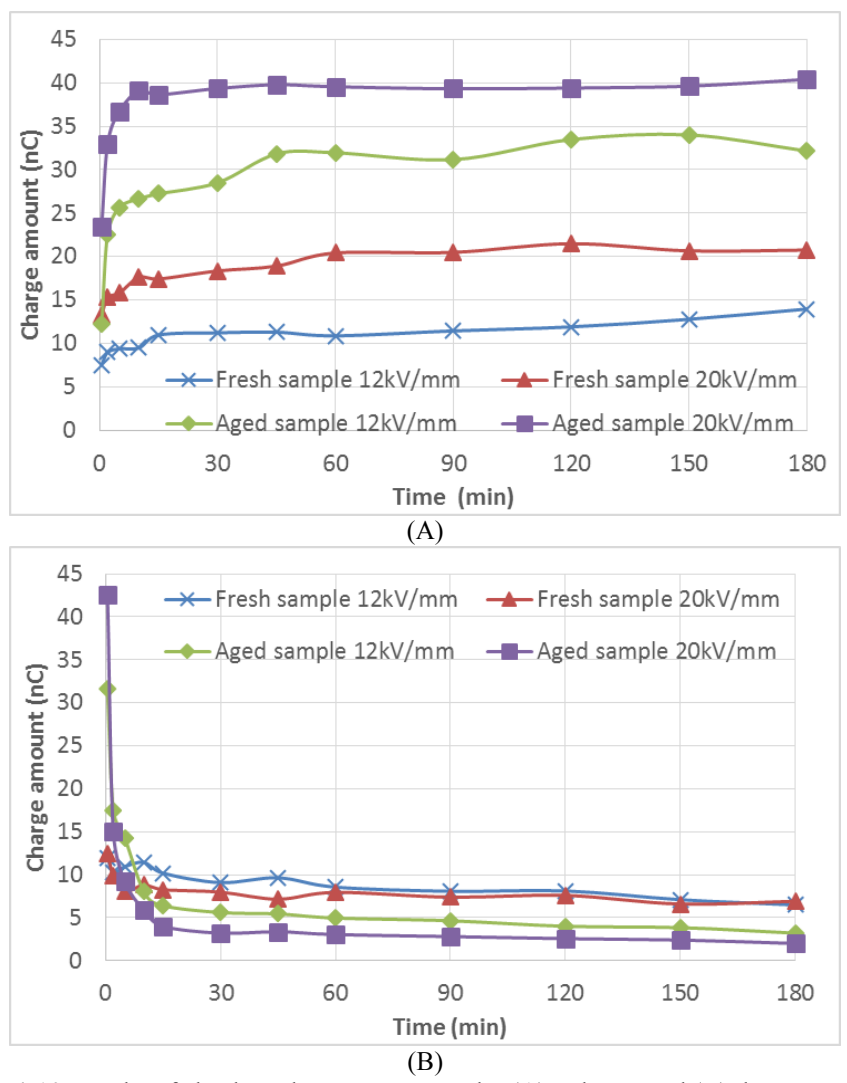


Figure 4-10 Results of absolute charge amount under (A) volts-on and (B) decay processes.

According to the Figure 4-10 (A), the amount of space charge in the samples increases quickly in the first 10 minutes and then the rate of increase slows down gradually during the voltage application for the aged oil samples, while the charge amount keeps increasing slowly for the fresh oil samples. Moreover, compared with other factors, e.g. the amplitude of applied voltage, the status of the oil property dominates the charge amount during the volts-on test, e.g. the charge amount in the aged oil samples under 12 kV/mm is much larger than in the fresh oil samples under 20 kV/mm.

The charge amount during the depolarization process is shown in the plot (B). The amount of the accumulated charges decreases rapidly in the first 10 minutes in the aged oil samples (from 44.3 nC to about 5 nC), and only very little charges remain after 20 minutes. On the contrary, there is no obvious significant decrease of charge amount in the fresh oil samples. Consequently, significant amount of charges (compared with the accumulated charges in the aged oil samples) remain in the fresh oil samples. It is also noticed that the differences of the aged oil samples and the fresh oil samples are much smaller, even though the great differences in the conductivity. This

can be explained as: 1) the relationship between conductivity and space charge amount may not be linear because the charges measured by the PEA method are trapped in the dielectric material; 2) Only 'net charge' can be measured by the PEA method, therefore, it is possible that a large amount of positive charges and negatives charges may overlap and cannot be distinguished by the PEA measurement.

B. Maxwell-Wagner polarization vs. PEA measurement

Based on the Equation (4.2) and Equation (4.1), the time constants and the charge amount in the oil gap combined with single layer pressboard insulation system can be calculated. It should be noticed that the oil conductivity and pressboard conductivity used in the calculation are measured at 10 kV/mm, respectively. The time constant of the fresh oil samples is about 230 s, while it is about 4 s for the aged samples. Normally, it is regarded as the steady state that can be reached after a period that is longer than 4-5 times of the time constant (the error is less than 5%) [115]. This means that the fresh oil samples reach the steady state in about 920 s, while about 16 s for the aged oil samples. Based on the equation (4.2) the interfacial charge density which is the only space charge in the whole insulation system is about 480×10^{-6} C/m² (charge amount is 38.4 nC when the area of the electrode is 0.8 cm²) in the fresh oil samples and 455×10^{-6} C/m² (36.4 nC when the area of the electrode is 0.8 cm²) in the aged oil samples. The space charge amount in the fresh oil samples is slightly higher than in the aged oil samples, because the space charge in the whole system estimated by the MW polarization is mainly determined by the ratio of dielectric properties of the different material.

On the other hand, the space charge profiles from PEA measurements show a much more complex space charge dynamics. Firstly, the origins of space charge are not only due to the discontinuity of the permittivity and conductivity of the dielectrics, but also other space charge mechanisms such as charge injection from electrodes. These mechanisms are usually strongly related with degradation of the dielectrics. Therefore, the charge amount is only 13.8 nC in the fresh oil samples under 12 kV/mm, while about 34.8 nC in the aged oil samples under 12 kV/mm. Secondly, the injected space charges distribute in the whole insulation system, including the interface and the pressboard bulk. The movement and injection of the interfacial charges from the interface into the pressboard bulk are also observed. Thus, the electric field distributed in the pressboard will be further distorted and enhanced, compared with the results purely based on the MW polarization. Thirdly, due to the charge injection and movement, the time to reach the steady state (or the space charge dynamic balance state) is generally longer than the estimated time from MW polarization, e.g. the long term space charge dynamics indicate the fresh oil samples may need about 24 hours to reach the steady state; it still needs about 10 minutes to reach steady state for the aged oil samples, though the aged oil greatly enhances the movement of the injected

charges. Correspondingly, the time for charge dissipation is also much longer due to the interfacial effect. Deep traps at the interface prevent charge dissipation, e.g. there is still little amount of charges remaining near the interface after 72 hours in the long duration test of fresh oil samples; most of charges are dissipated within 10 minutes for the aged oil samples.

C. Effects caused by adding oil gap

The results of this work are also compared with the previous work in Ch.3.2 that investigated the space charge dynamics in the impregnated pressboards without the oil gap under similar HVDC electric fields. Due to the large acoustic attenuation at the anode side, the following discussions mainly focus on the cathode side. When the external voltages are applied, the negative charges are injected from the cathode into the system, i.e. the negative charges accumulate at the interface between oil gap and pressboard then move into the pressboard, or they can directly accumulate in the pressboard if the oil gap does not exist. Therefore, by comparing the charge amount and the charge peak position of the negative charges accumulated in the pressboard within the same time period in the samples with and without the oil gap, the effects on the space charge dynamics caused by the presence of the oil gap can be revealed.

Firstly, the amount of the accumulated negative charges in the impregnated pressboard within 180 minutes in different samples, including insulation system with and without the oil gap, is summarized in Table 4-3. In general, the negative charge amounts in the samples with oil gap is larger than the samples with the matched conditions without the oil gap, although slight higher electric fields were applied in the samples without oil gap. This suggests that more negative charges can be injected and accumulated in the insulation system when an oil gap is present.

Table 4-3. Negative charge amount in different samples by PEA measurement

Insulation Structure	Conditions	Charge amount (nC)
	Fresh oil 12kV/mm	4.8
With oil film	Fresh oil 20kV/mm	7.9
	Aged oil 12kV/mm	16.9
	Aged oil 20kV/mm	26.6
	Fresh oil 15kV/mm	4.1
Without oil film	Fresh oil 25kV/mm	6.2
	Aged oil 15kV/mm	14.2
	Aged oil 25kV/mm	18.6

Secondly, the space charge dynamics usually can be described by the peak movement of the accumulated charges, i.e. the alternation of the peak position can present the major movement of the accumulated charges. For the homo charge injection in oil-pressboard insulation system, the peaks of accumulated charges move towards to the middle of sample. Thus, the peak of the negative charges will gradually move inside the pressboard bulk towards to the middle of the pressboard, and this movement over 180 minutes is recorded in Figure 4-11.

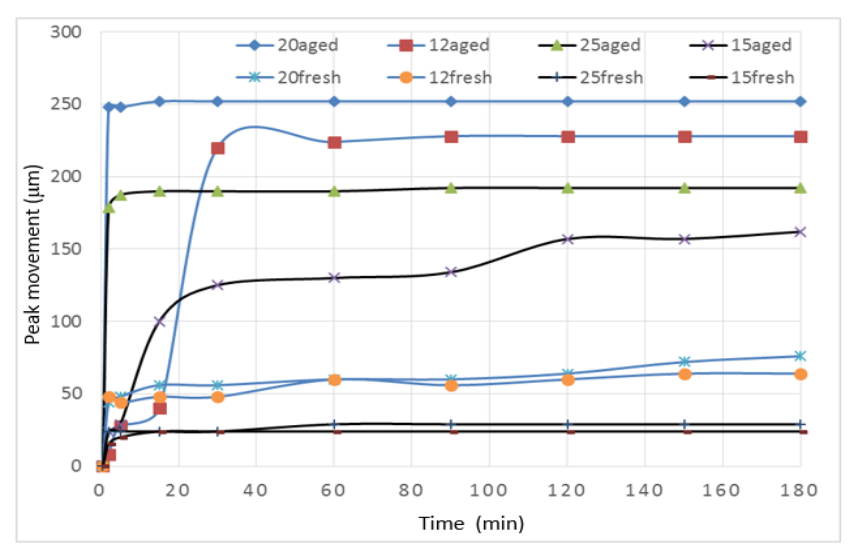


Figure 4-11 Movement of the interfacial peak under voltage applications.

The blue lines indicate the samples with oil gap, while the black lines indicate the samples without oil gap (only impregnated pressboard). The bottom two lines are the fresh oil samples without oil gap, the distances of their peak movements from the original position are only about 25 μ m. Above them, the two blue lines are the fresh oil samples combined with oil gap. Within 180 minutes, the charge peak moves more than 50 μ m, and continues increasing with time. In the fresh oil samples, the charge movement is generally very slow, so the effect caused by the applied electric field is not obvious. The third level from the bottom contains the aged oil samples without oil gap. Unlike the fresh oil samples, the charge movement is greatly enhanced by the aged oil, so the difference of the peak movements under higher electric field can be easily distinguished from the lower electric field. Under 25 kV/mm, the negative peak moves about 180μ m, while under 15 kV/mm, the peak moves about 160μ m. The top two lines are the aged oil samples combined with oil gap. The peak moves about 250μ m under 20 kV/mm, and about 228μ m under 12 kV/mm. It is also found that the peak needs much less time to reach its final position under higher electric field in the aged oil samples.

The results above indicate that the presence of the oil gap may enhance the space charge injection and accumulation in the pressboard under external electric field. The reason for this may be that the decrease in the electric field due to the homo charge injection at the interface between the electrode and the oil gap is smaller than without the oil gap, i.e. the electrode directly contacts with the pressboard. This is because the charges drift much faster in the oil than in the pressboard, so the negative charges can quickly drift to the oil/pressboard interface once the negative charges inject into the oil gap from the electrode. Therefore, more charges can inject into the insulation system. Another possible explanation could be the different Schottky barrier for oil and pressboard, which means more charges could be injected from the electrode to the oil gap. However, it has to be verified by measuring the Schottky barrier for such materials. Moreover, the ionization of the oil could generate additional positive and negative charge carriers. The

positive charge carriers could drift to cathode and further increases the negative charge injection. Meanwhile, the negative charges drift to the oil/pressboard interface, acting like the injected negative charges. These ionized charges may also contribute to the increase in the charge amount when the oil gap is presented.

The previous decay charge dynamics in the fresh oil samples (as shown in Figure 4-5 and Figure 4-9) show the positive charges adjacent to the electrode dissipate much faster than the interfacial negative charges. This suggests that the interface may be considered to possess many deep traps that prevent charge dissipation. On the other hand, in the aged oil samples, the charge dissipation is not significantly affected by the interface, because the aged oil greatly enhances the charge movement due to its higher conductivity, so charges can easily drift away.

D. Electric field distribution and distortion

The electric field distribution within the combined insulation can be calculated from Equation (2.3) with a position dependant permittivity based on the space charge profiles when the external electric field is applied. As the interfacial peak can further move into the pressboard bulk, therefore, it is very difficult to distinguish the interfacial charges from the accumulated charges within the bulk of the pressboard. An estimation to determine the amount of the interfacial charges in proposed in Figure 4-12. It is assumed that a surface charge is broadened to a symmetric peak by the PEA system. As no bulk charge can be observed in the oil gap, therefore, the interfacial charge amount can be calculated by integrating a symmetric charge density from the interface to the start point of the interfacial peak in the oil gap (red region). The charge amount in the bulk of the pressboard can be then calculated by the subtraction of the measured to the half of the symmetric interfacial peak (grey region).

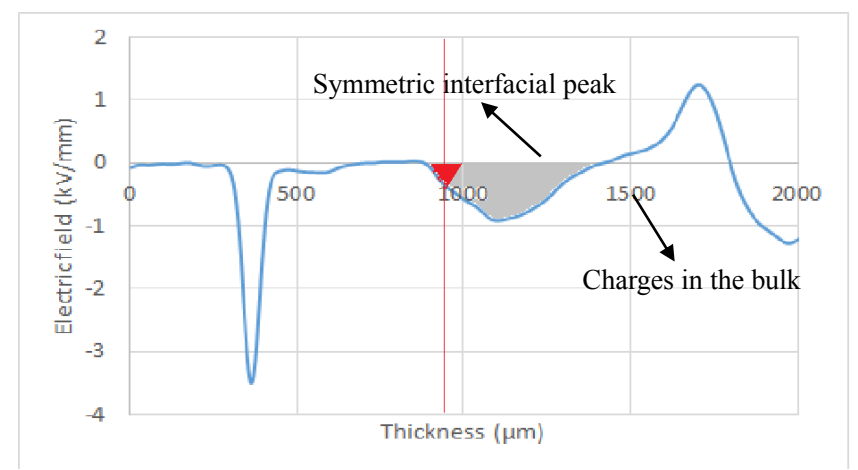


Figure 4-12 Estimation of the amount of the interfacial charge and accumulated charges in the bulk of pressboard.

As shown in Figure 4-13, the electric field distribution in fresh oil sample (A) and aged oil sample (B) under 12 kV/mm. The electric field in the oil gap is higher than the pressboard quickly after

the external voltage is applied. With the voltage application, the electric field in the oil gap gradually decreases while increases in the pressboard. During 3 hours voltage application, the electric field almost uniformly distributed in the solid and liquid insulation. Then the electric field in the pressboard becomes higher than the oil gap, suggesting the dielectric is gradually changing from the polarization process to the conduction process. Compared with the MW calculations based on permittivity (initial state) and resistivity (steady state), the electric field calculated from the real space charge is significantly distorted in the bulk of the pressboard at the steady state (48h). It can be clearly observed that the electric field in the middle of the pressboard is greatly enhanced and the maximum value is much larger than the MW calculation (resistivity).

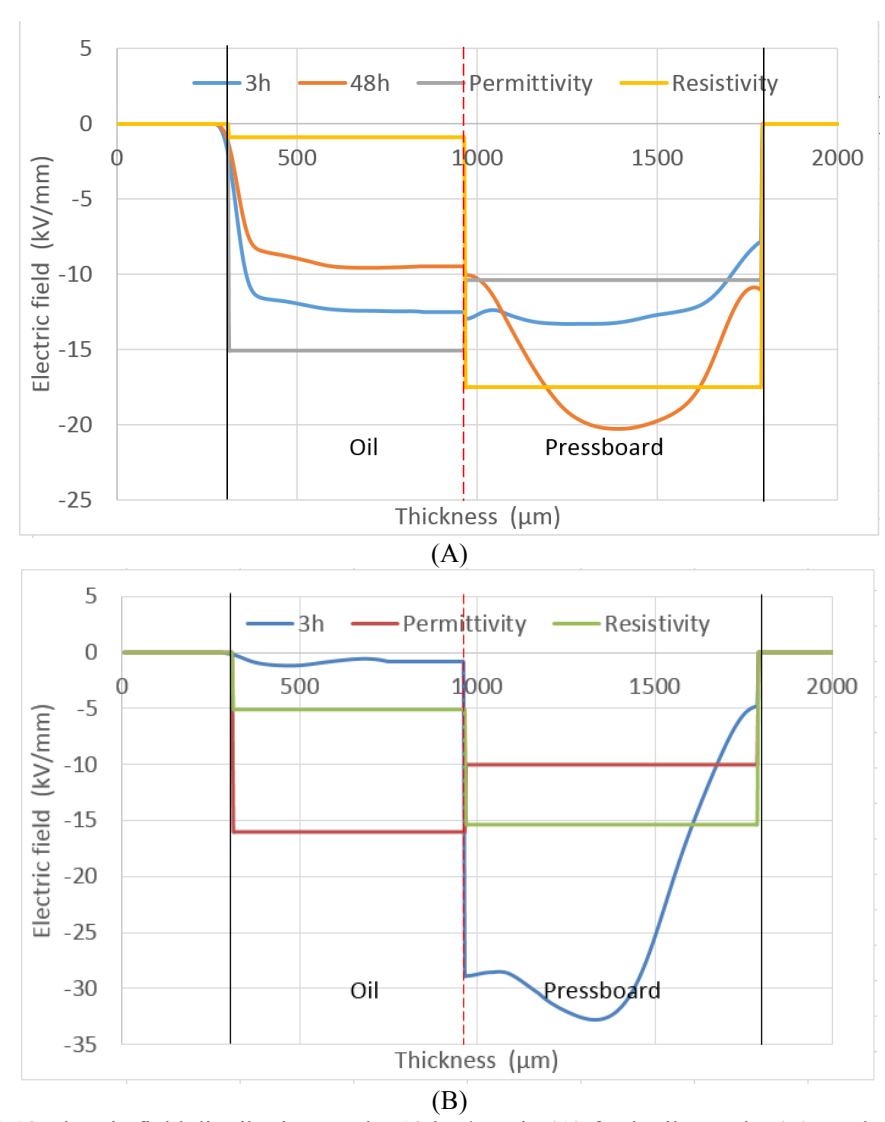


Figure 4-13 Electric field distributions under 12 kV/mm in (A) fresh oil sample; (B) aged oil sample compared with the MW calculations.

By applying Equation (2.4), the electric field enhancement for each sample can be calculated. Figure 4-14 shows the electric field enhancement in the Maxwell-Wagner (MW) polarization, only one layer of impregnated pressboard and an oil gap combined with impregnated pressboard under four different conditions including different external electric fields and oil aging statuses.

The blue bars are the field enhancements at the steady state based on the electric field distributions that are calculated by MW method. The results show the field enhancements in the fresh oil samples are much larger than in the aged oil samples. This is because the electric field at the steady state distribution is mainly determined by the ratio of the conductivities of the oil and pressboard, but not the absolute value of their conductivities. In this work, the aged oil has significant impacts on the conductivities in both oil and the impregnated pressboard, so the conductivity ratio is much smaller in the aged oil samples, leading to a much smaller electric field enhancement.

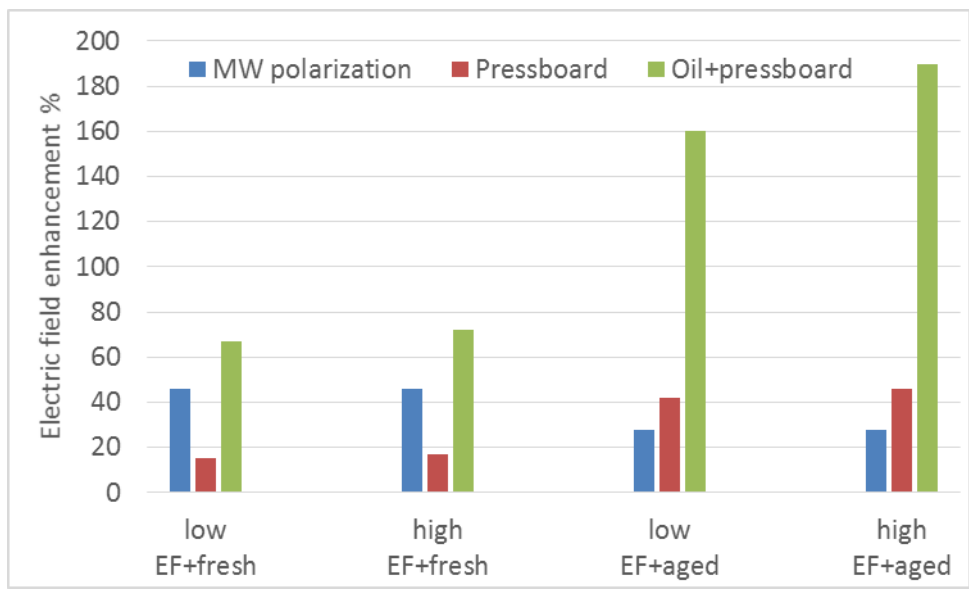


Figure 4-14 Electric field enhancements under the different conditions

The electric field enhancement for the samples that combined with an oil gap (green bars) is generally much larger than only pressboard samples (red bars) under each condition. For the fresh oil samples, the field enhancements for the samples without an oil gap are about 15%, which jump to about 70% in the samples combined with an oil gap when the external voltage is applied for 48 hours. For the aged oil samples, the electric field is greatly enhanced to about 42% only in the pressboard samples, and more than 160% in the samples combined with an oil gap. This clearly shows the significant impact of the aged oil on the electric field enhancement, which also shows the obvious difference with the estimation based on MW polarization.

4.1.5 Conclusions

This section introduces the successful application of the PEA method for investigation of the space charge behaviour in an oil gap combined with single layer of impregnated pressboard. The results are also compared with the Maxwell-Wagner polarization and with the situation of only impregnated pressboard (without oil gap). The following conclusions can be drawn:

- Homo charge injection is enhanced by the magnitude of the applied electric field and the aging status of the oil, and the aged oil is the dominant factor.
- The aged oil can greatly enhance the charge movement. The dynamics balance of space charge in the aged oil samples is reached within 10 minutes, while it needs about 24 hours for fresh oil samples.
- Compared with MW polarization, it can be observed that the space charges distribute not
 only at the interface, but also within the pressboard bulk. The charge amount is much
 larger than the estimation based on MW polarization, especially in aged oil samples. It
 also has been observed that longer time is needed to reach steady state, due to the
 movement of the interfacial charges from the interface to the pressboard bulk.
- When an oil gap is added to pressboard, the negative charge amount and its movement distance indicate that the oil gap enhances the negative charge injection and movement in the pressboard bulk when the external voltage is applied. On the other hand, the interface can also prevent the charge dissipation when external voltage is removed, acting as a barrier. However, this barrier effect is significantly weakened by the aged oil.
- The electric field enhancement in the pressboard combined with oil gap is most significant compared with the estimation based on MW polarization and samples without an oil gap. Particularly, the electric field enhancement in the middle of the pressboard is larger than 100% in the aged oil samples, which may bring severe risk to the reliability of the insulation system.

4.2 Space charge behaviour in an oil gap sandwiched between two layers of impregnated pressboard system under HVDC Stresses

Based on the understanding of space charge behaviour in the insulation system consisting of an oil gap and single layer of pressboard, the other barrier unit is introduced in the section: an oil gap formed between two layers of pressboards.

Two oil/pressboard interfaces exist in this insulation unit. The interfacial charges with same magnitude and opposite polarities separately build up at the two interfaces, according to the Maxwell-Wagner polarization. If the space charge mechanisms are further considered, according to the observation and understanding of the previous work, homo-charge injection occurs within the pressboard in the vicinity of the electrodes. These injected charges could move inside the pressboard bulk towards to the oil gap. Meanwhile, the interfacial charges may also move towards to the pressboards under the external electric field. However, this movement may be very slow

due to the interfacial barrier effect. Therefore, the electric field in the vicinity of the interfaces in the pressboard may be enhanced. This enhancement is expected to be larger than the estimation by the Maxwell-Wagner polarization.

In this section, this hypothesis is experimentally proved by investigating the space charge dynamics in such three-layer insulation system.

4.2.1 Experimental setup

Similar to the previous works, the oil samples are the service aged oil supplied by National Grid and the fresh insulating mineral oil. Their properties are already listed in the Table 3-1 and Table 3-2 in Chapter 3.1.

As shown in Figure 4-15, a layer of impregnated pressboard with a thickness of 0.5 mm was placed on the ground electrode. An oil gap was formed above on the pressboard by a PTFE ring with a thickness of 0.5 mm. The diameter of the hole was 2 cm. Another impregnated pressboard with a thickness of 0.5 mm was then placed on the PTFE ring, and then firmly pressed by the top electrode.

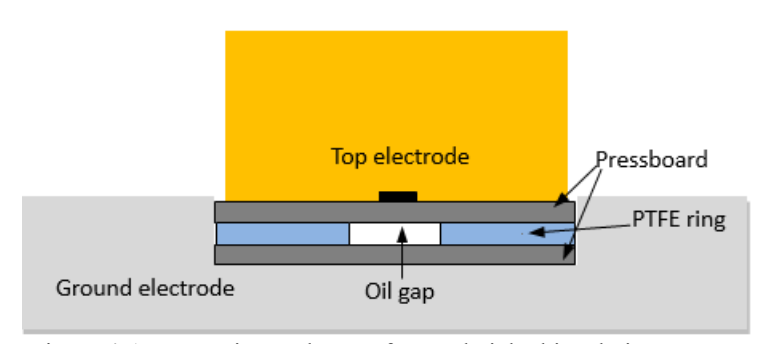


Figure 4-15. Experimental setup for sandwiched insulation system.

Both fresh oil samples and aged oil samples were investigated in this work, as comparison. The expected external electric field is 20 kV/mm, however, flashover occurs in the aged oil samples when the electric field is higher than 16.7 kV/mm. Therefore, the space charge dynamics in the aged oil samples under 16 kV/mm were recorded.

4.2.2 Acoustic wave transmission and reflection in three-layer insulation system

Considering the acoustic wave generated from the accumulated charges within the bulk of each layer of dielectric material, as shown in Figure 4-16, the transmission and reflection of the five acoustic sources have to be considered separately.

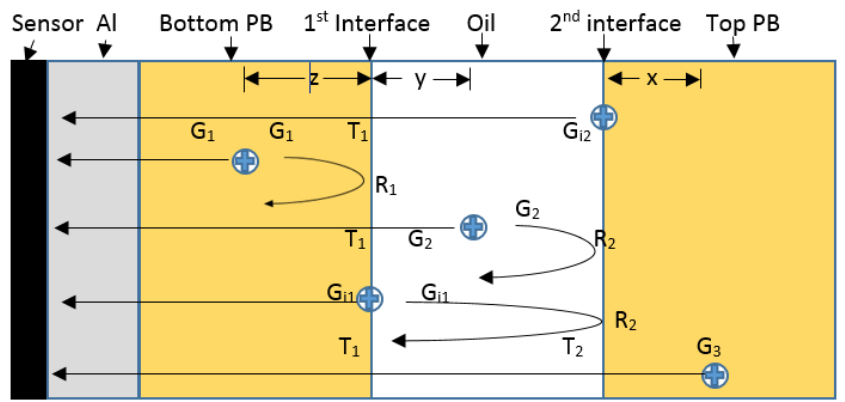


Figure 4-16. Acoustic propagations within the sandwiched insulation system.

The acoustic wave generated by the charges within the top layer pressboard with a generation factor G_3 , travels through the 2^{nd} interface with a transmission factor T_2 and into the oil gap, and then travels through the other interface with T_1 into the other pressboard. The whole transmission factor is:

$$F_3 = G_3 T_2 T_1 \tag{4.5}$$

The whole travel time t₃ is:

$$t_3 = \frac{x}{v_p} + \frac{d}{v_o} + \frac{d}{v_p} \qquad 0 \le x \le d \tag{4.6}$$

where x is the distance between the accumulated charge and the 2^{nd} oil/pressboard interface; v_p is the acoustic velocity of pressboard; v_o is the acoustic velocity of oil; and d is the thickness of each layer.

Similarly, the acoustic wave generated at the 2^{nd} interface with the generation factor G_{i2} also travels through the oil gap and the bottom pressboard to the sensor. Its transmission factor is:

$$F_{i2} = G_{i2}T_1 (4.7)$$

And its travel time t_{i2} is:

$$t_{i2} = \frac{d}{v_o} + \frac{d}{v_p} \tag{4.8}$$

When the acoustic waves generated by the charges within the oil gap with a generation factor G_2 , the acoustic waves travel in two opposite directions: one travels to the bottom layer pressboard with a transmission factor T_1 ; the other travels towards to the top layer pressboard, and reflected by the 2^{nd} interface with a reflection factor R_2 , and then travels towards to the bottom layer pressboard with a transmission factor T_1 . Therefore, the whole transmission factor for the first part of the acoustic wave F_2 is:

$$F_2 = G_2 T_1 (4.9)$$

The whole travel time t₂ is:

$$t_2 = \frac{y}{v_o} + \frac{d}{v_p}$$
 $0 \le y \le d$ (4.10)

where y is the distance between the accumulated charge within the oil gap and the 1st oil/pressboard interface.

And the whole transmission factor for the reflected acoustic wave F_{R2} is

$$F_{R2} = G_2 R_2 T_1 \tag{4.11}$$

The whole travel time of the reflected acoustic wave t_{R2} is:

$$t_{R2} = \frac{d-y}{v_o} + \frac{d}{v_o} + \frac{d}{v_p}$$
 $0 \le y \le d$ (4.12)

The space charge located at the 1^{st} interface also generate two parts of the acoustic waves with the generation factor G_{i1} . One part directly travel through the bottom layer pressboard and detected by the sensor; while the other part travels towards to oil gap and reflected by the 2^{nd} interface. The travel time for the latter reflection signal is:

$$t_{i1} = \frac{2d}{v_o} + \frac{d}{v_p} \tag{4.13}$$

This time is always longer than the travel time t₃ of the acoustic signal sourced from the space charge within the top layer pressboard, due to the acoustic velocity is smaller in the oil gap than the pressboard. This means this reflection signal is always delayed behind the acoustic signals from the top layer pressboard. Therefore, this reflection signal can be ignored.

When the acoustic waves generated by the charges within the bottom layer pressboard with a same generation factor G_1 , one acoustic wave directly moves towards to the sensor, while the other one propagates back to the 1^{st} oil/pressboard interface. The latter one then is reflected by the interface with a reflection factor R_1 , and then travels through the bottom layer pressboard to the sensor. The whole transmission factor for the reflected wave is:

$$F_{R1} = G_1 R_1 \tag{4.14}$$

And its travel time is:

$$t_{R1} = \frac{z}{v_p} + \frac{d}{v_p} \qquad 0 \le z \le d \tag{4.15}$$

where z is the distance between the accumulated charge and the 1st oil/pressboard interface.

Therefore, the acoustic waves can overlap with the other signal when the following conditions are fulfilled, separately:

$$t_{R1} < t_2 \tag{4.16}$$

$$t_{R2} < t_3 \tag{4.17}$$

By applying the acoustic properties in Ch.4.1, the transmission factors can be calculated, as shown in Table 4-4.

Therefore, the reflection wave F_{R2} compared with the acoustic wave F₃ is smaller. And based on

Table 4-4. Acoustic transmission factors				
Factors	Equation	Value		
G ₃	$\frac{Z_P}{Z_P + Z_P}$	0.5		
G_2	$\frac{Z_O}{Z_O + Z_O}$	0.5		
G_1	$\frac{Z_P}{Z_P + Z_P}$	0.5		
G_{i2}	$\frac{Z_o}{Z_o + Z_P}$	0.3		
G_{i1}	$\frac{Z_p}{Z_o + Z_P}$	0.7		
T_2	$\frac{2Z_O}{Z_O + Z_P}$	0.7		
T_1	$\frac{2Z_P}{Z_O + Z_P}$	1.3		
R ₂	$\frac{Z_p - Z_O}{Z_O + Z_P}$	0.3		
R_1	$\frac{Z_p - Z_O}{Z_O + Z_P}$	0.3		

the knowledge from the previous work, no accumulated charges can be observed within the bulk of the oil gap. Then, the reflection F_{R2} is ignored.

On the other hand, the reflection wave F_{R1} is 0.23 times of the acoustic wave from the oil gap and the 1st interface, which is also ignored in this work. The travel times of the other reflection waves are all obviously larger than t₃, so they do not overlap with the space charge signal in this work.

4.2.3 Experiment results

A. Volts-on results

Figure 4-17 shows the space charge dynamics in fresh oil sample under 20 kV/mm. In the first layer of pressboard that is in direct contact with the ground electrode, homo charge injection occurs, i.e. negative charges inject from the electrode into the pressboard bulk. The cathode peak drops with the external voltage application from 12 C/m³ to 9.8 C/m³. The injected negative charges move from the cathode side to the oil gap side, and widely distributes in the pressboard within 1 hour. On the other hand, in the second layer of pressboard that contacts directly with the anode, the positive charge peak moves towards the oil gap, indicating positive charges injected from the anode into the pressboard bulk. However, the injected charges are difficult distinguished from the electrode peak due to large acoustic dissipation at the anode side.

Considerable charges accumulate gradually at the interfaces between oil gap and pressboards with the voltage application. Positive charges accumulate at the first interface between the oil gap and the first layer of pressboard (adjacent to the ground electrode), while negative charges accumulate at the other interface between the oil gap and the second layer of pressboard (adjacent to the top electrode). The amplitudes of the both interfacial peaks keep increasing during the 1 hour volts-on test, which enhances the electric field distributed in the regions within the two layers of pressboards near the interfaces, but decreases the electric field in the oil gap. This agrees qualitatively with the Maxwell-Wagner polarization that charges will be formed at the interface when the dielectrics have discontinuity of the ratio of permittivity and conductivity [116]. These charges may result from the ionization process within the oil, while the charge injection is blocked by the two interface layers of pressboards.

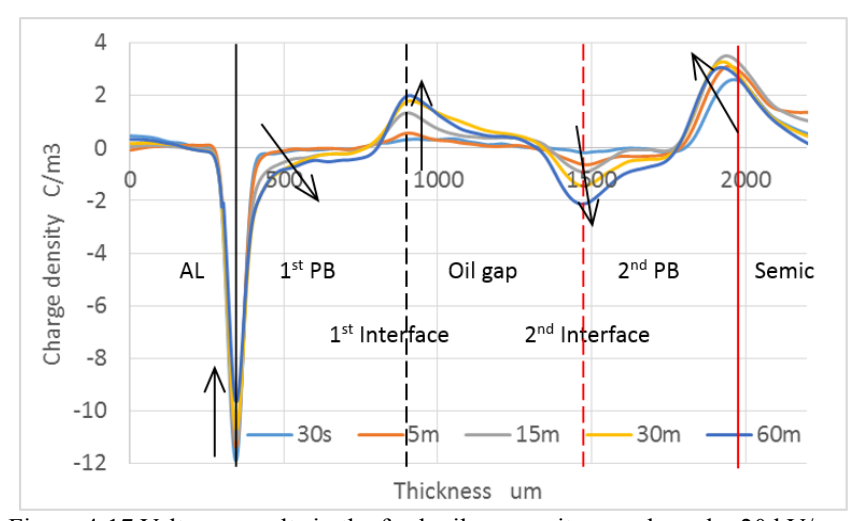


Figure 4-17 Volts-on results in the fresh oil composite sample under 20 kV/mm.

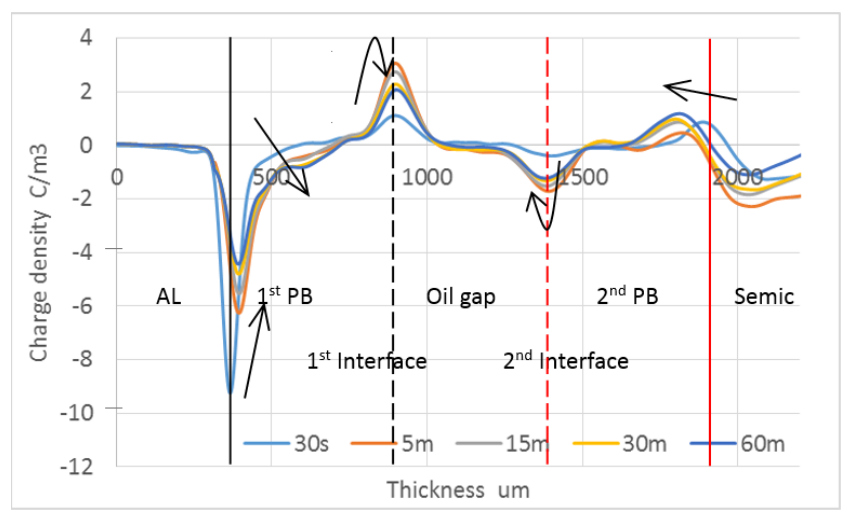


Figure 4-18 Volts-on results in the aged oil composite sample under 16kV/mm.

As shown in Figure 4-18, the space charge dynamics in the aged oil sample under 16 kV/mm is significantly enhanced. It can be observed that homo charge injection occurs in the first 5 min, e.g. the cathode peak drops from about 9.2 C/m³ to 6.2 C/m³ in the first 5 min, and then to about 4.3 C/m³ at 60 min. Both the cathode peak and anode peak move into the bulk of the pressboards.

Similar to the fresh oil sample, positive charges accumulate at the first interface and negative charge accumulate at the second interface. However, the amplitudes of the two interfacial peaks in the aged sample quickly increase within the first 5 min and then gradually decrease until the saturation state is reached. For example, the amplitude of the first interfacial peak rises rapidly from about 1 C/m³ to 3 C/m³ within the first 5 min and then drops to about 2 C/m³ during the 1 hour voltage application. This may result from the homo charge injection moving from the pressboards, and neutralized with interfacial charges ionized from the oil.

It also has to be noticed that the charges with opposite polarities distribute within a narrow area near the oil/pressboard interfaces, which may lead to a significant electric field enhancement at the interfaces, even the flashover. However, this narrow area may be smaller than the resolution of the PEA system that cannot be clearly detected.

B. Decay results

After the 1 hour voltage application, the decay tests were carried out by removing the external electric field. It is usually believed that the space charge dynamics without the influence of the external voltage can reflect the trap energy levels of dielectric materials [52].

The space charge decay characteristics in fresh oil sample are shown in Figure 4-19. It can be observed that negative charges distribute in the bulk of the first layer pressboard, while positive charges accumulate in the second layer pressboard. This confirms the homo charge injection when the external voltage is applied. It is also found that positive charges present at the first

interface between oil gap and pressboard, while negative charges locate at the second interface. With the 1 hour depolarization time, the accumulated charges only slightly decrease, suggesting the charge mobility of the accumulated charges in fresh oil is generally small. In the vicinity of the anode (semiconducting polymer), the positive charges decay faster than the negative charges in the vicinity of the cathode (aluminium), which may be the impacts of the different electrode materials on the space charge behaviour.

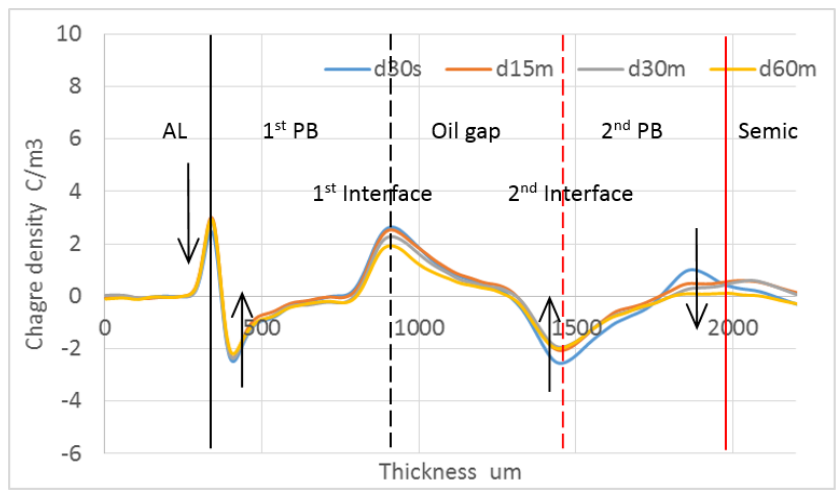


Figure 4-19 Decay results in the fresh oil sample under 20 kV/mm.

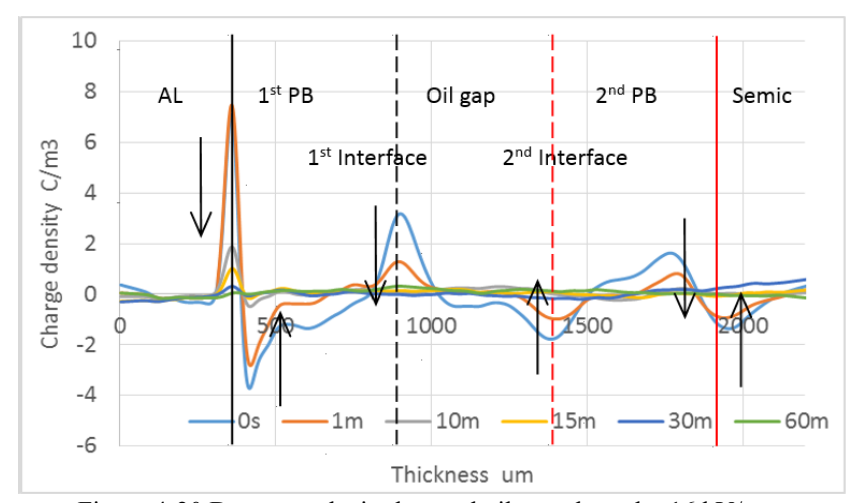


Figure 4-20 Decay results in the aged oil sample under 16 kV/mm.

On the other hand, Figure 4-20 shows the charge dissipation dynamics in aged oil sample. At the beginning, compared with fresh oil, more space charges accumulate in the multi-layer insulation system, e.g. in the first layer of pressboard, the amplitude of the negative peak is about 3.9 C/m³ and the negative charges widely distribute in the whole bulk of the pressboard. Similarly, significant positive charge distribution can be observed in the second layer of pressboard. Electric field near the two interfaces of the oil gap is greatly enhanced due to the opposite polarity charges distribute near to the interfaces in the oil gap and pressboard. With the increasing decay time, the accumulated charges dissipate very quickly, and leave only background noise after 30 min, indicating the mobility of accumulated charges is greatly enhanced by the aged oil.

4.2.4 Discussions

A. Total charge amount

The total charge amount is calculated based on Equation (2.2) from the space charge profiles. The results of absolute charge amount vs. time for volts-on and decay processes are shown in Figure 4-21 and Figure 4-21.

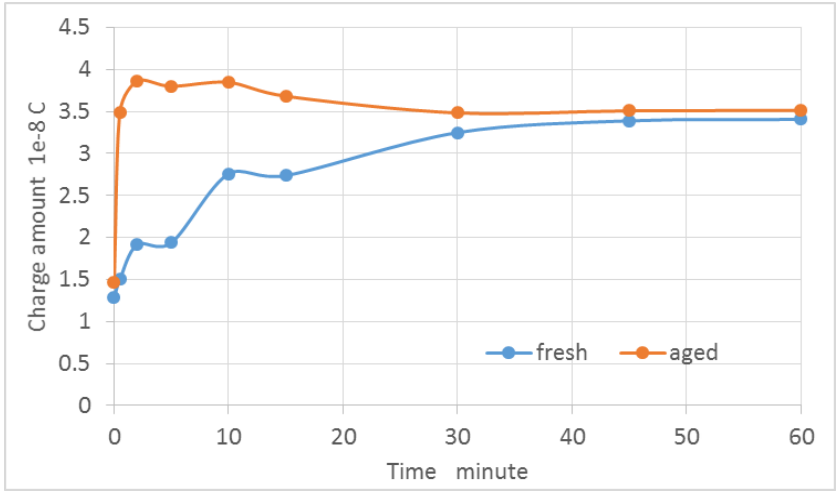


Figure 4-21 Total charge amount vs. voltage application time.

The blue line in Figure 4-21 indicates the total charge amount in the fresh oil sample under 20 kV/mm, while the red line is the charge amount in aged oil sample under 16 kV/mm. The charge amount in fresh oil sample is gradually increasing with the voltage application time, and becomes stable after 40 min. On the contrary, the charge amount in the aged oil sample jumps to the maximum value (about 3.9×10^{-8} C) in the first 2 min, then slowly decreases to a stable value (about 3.5×10^{-8} C).

The results of charge amount reduction during the decay process are shown in Figure 4-22. The charge dissipation in the fresh oil sample is very slow, i.e. the charge amount decreases from about 3.5×10^{-8} C to 2.5×10^{-8} C over 1 hour. On the other hand, the charges in aged oil sample decay much faster, i.e. most of the charges disappear within the first 5 minute, the charge amount drops significantly from about 3.6×10^{-8} C to 0.6×10^{-8} C, and then gradually reduces to about 0.3×10^{-8} C in the rest 55 minutes.

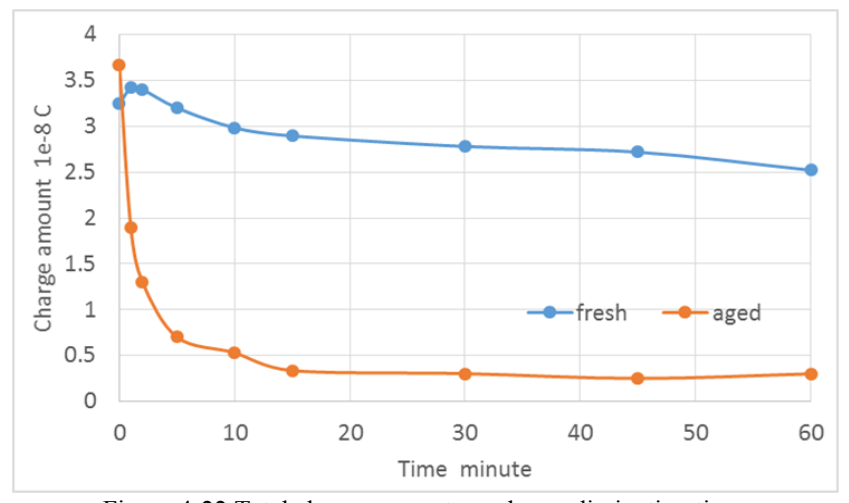


Figure 4-22 Total charge amount vs. charge dissipation time.

B. Electric field distribution and distortion

As shown in Figure 4-23 and Figure 4-24, the electric field distributed within the pressboards are generally increased, while deceases in the oil gap, due to the polarities of the interfacial charges. Moreover, the homo charge injection from the both electrodes can reduce the electric field distributions in the region between electrodes and pressboards. However, the opposite polarity charges accumulated near to the interfaces between oil gap and pressboards can greatly enhance the electric field near to the interfaces. Particularly, this may be the case in the aged oil samples, i.e. the large amount homo charges can be quickly injected and move through the pressboard bulk and cause the interfacial peak at the interfaces as a result of the high conduction of aged oil. This results in a considerable field enhancement at the interfaces which may be the reason for the flashover in aged oil when the external voltage is larger than 16.7 kV/mm. Moreover, the maximum electric field in the aged oil sample occurs at the first 5 minutes, and after that, the electric fields at the two interfaces are decreasing with the voltage application time. This may be related to the charge neutralization at the two oil/pressboard interfaces. This indicates that the aged dielectrics withstand the highest risk (from the electric field distortion view) shortly after the voltage application. However, the reduction of the electric field may also result from the limited resolution of the PEA system that cannot distinguish the charges distributed within a narrow region. In that case, a significant large electric field enhancement may occur within the narrow region. Therefore, a further verification with a high resolution space charge detection system is essential.

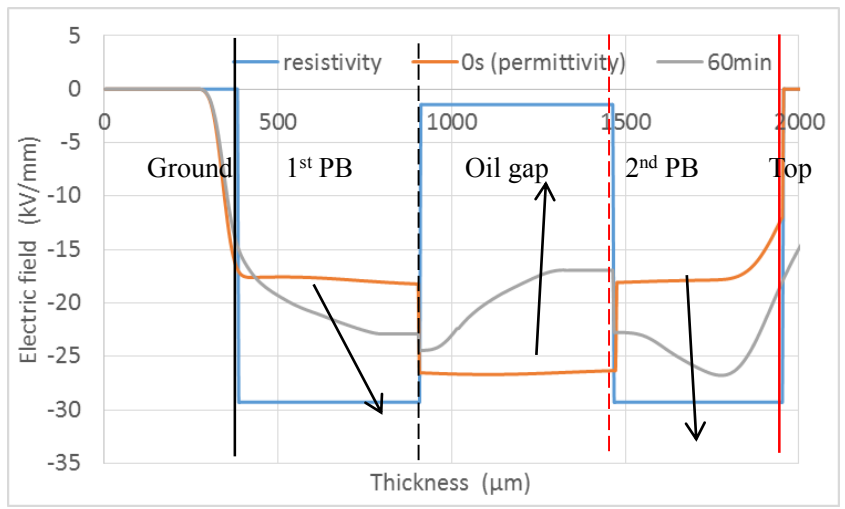


Figure 4-23 Electric field distribution in fresh oil sample under 20 kV/mm.

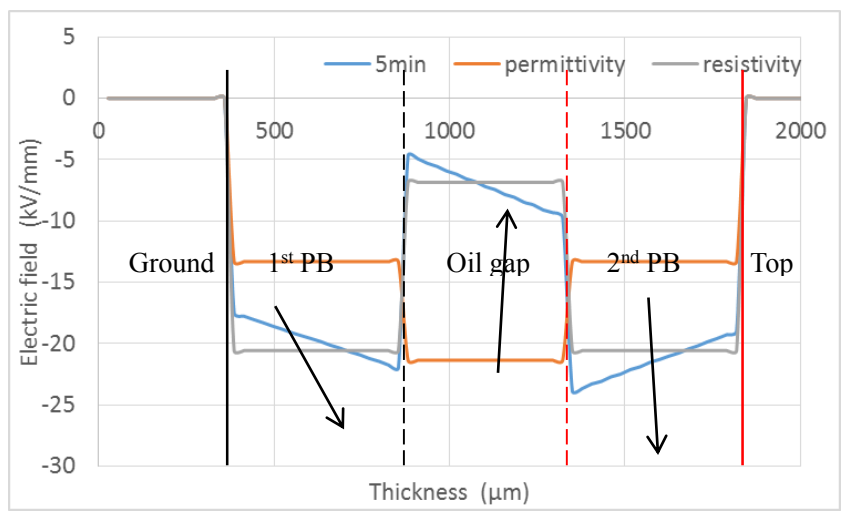


Figure 4-24 Electric field distribution in aged oil sample under 16 kV/mm.

Therefore, a comparison of electric field enhancement between the calculation based on the space charge measurement and the estimation based on the Maxwell theory is shown in Figure 4-25.

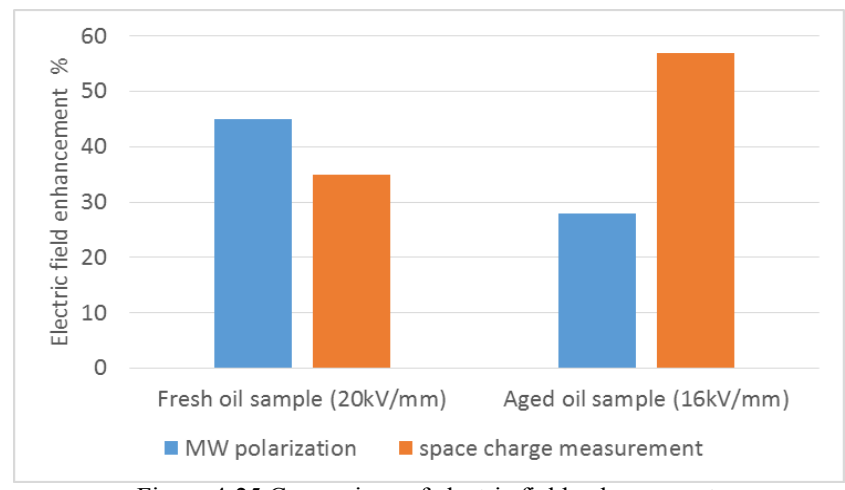


Figure 4-25 Comparison of electric field enhancement.

For the fresh oil sample, the field distortion based on the space charge profiles is smaller than the Maxwell theory. According the results from the previous section Ch. 4.1, the space charge dynamic balance may require a longer stressing time (about 24 h). In this work, the 1 hour voltage application time may be not sufficient for the charge accumulation, leading to a small electric field distortion.

On the other hand, the electric field enhancement in the aged oil sample shows the great difference between the two methods. It indicates that the severe electric field distortion is more related with the dielectric properties, rather than the ratio of the conductivity.

4.2.5 Conclusions

In this section, the space charge dynamics within three-layer insulation (pressboard-oil-pressboard) system has been experimentally investigated by the PEA method. The homo charge injection from the both electrodes to the pressboards has been observed. The hetero interfacial charges accumulate separately at the two oil/pressboard interfaces, which may result from the ionization from the oil and lead to an electric field reduction within the oil gap. The maximum electric field occurs in the vicinity of the oil/pressboard interfaces, due to the accumulation of the homo charges in the pressboards and the hetero charges localized at the interface. These homo charges and hetero charges can be neutralized in the aged oil samples after 5 minutes, resulting in a decrease of the interfacial charges and electric field in the vicinity of the interfaces.

4.3 Conclusions

In this chapter, the space charge characteristics in the two types of the multi-layer oil gap combined pressboard insulation systems have been experimentally investigated by the PEA method. The comparison between the space charge measurement results and the Maxwell-Wagner polarization are discussed in terms of charge amount, time constant and the electric field distortion. Some important conclusions can be summarized as follows:

- 1. Homo-charge injection can always be observed in the pressboard.
- 2. For the oil gap, the charge injection process and ionization may exist in the same time. The final charge distribution depends on the competition of the two processes. When the oil gap is in direct contact with the electrode, charge injection achieves the dominance over the ionization. On the other hand, when the injected charges are blocked by the pressboard, the ionization dominates the charge dynamics in the oil.

- 3. Although the polarity of the interfacial charges in the estimation and the experiment is consistent, the space charge distribution and the electric field distribution are very different due to the characteristics of space charge dynamics.
- 4. The oil/pressboards interface generally behaves as a barrier to prevent charge moving through. However, this barrier effect is related with the time of the voltage application and the degradation of the dielectrics. This effect could explain that the location of the maximum electric field within the multi-layer insulation occurs in the vicinity of the interface or pressboard bulk.
- 5. The time for reaching the space charge dynamic balance in the thick insulation system, such as the insulation units in this work, is much longer than the prediction based on the Maxwell-Wagner polarization. And the electric field distortion has proved much larger when the time of the electric field application is sufficiently long.
- 6. The space charge characteristics are highly related with degradation of the dielectrics. The significant space charge accumulation usually leads to a severe electric field distortion. However, it is very different from the calculation based on the Maxwell-Wagner polarization using the ratio of the conductivities in each dielectric material at the steady state.

Chapter 5.

Space Charge Dynamics in a Thick Oil Gap and Pressboard Combined System under Polarity Reversal Voltages

The polarity reversal is an important operation in HVDC transmission to control the direction of the power flow. It is generally believed that a transient electric field enhancement within the oil immediately after the voltage reversal, as the charges with the opposite polarity remains in the cellulose in a real converter transformer. This temporary voltage is governed by the conductivity and permittivity of the dielectrics.

From the point of the space charge phenomena, the whole polarity reversal operation can be divided as three stages, as shown in Figure 5-1, based on the understanding from the previous works. Considering the two-layer insulation unit (an oil gap combined with single layer pressboard), the first stage is the DC electric field application, as the same as the introduced in Ch.4.1. In this stage, homo-charges are injected from the electrodes, then accumulate at the

oil/pressboard interface and the bulk of the pressboard. The amount of accumulated charges are to a great extent dependent on the magnitude and duration of the electric field application, ageing. The second stage is the polarity reversal process. The applied voltage during this process is not described in detail by the IEC-61378-2. It only requires the whole polarity reversal process should be completed within 2 min [117]. In fact, the power industry usually directly turn off the applied voltage, and turn on the voltage with the opposite polarity after 2 min. Therefore, this process can be simply regarded as the charge decay process within the polarity reversal period. The third stage is the voltage application with the opposite polarity. The residual charges in the insulation bulk become to hetero charges (in the currently reversed electric field) and enhance the electric field in the vicinity of the two electrodes. The enhanced electric field may lead to a stronger charge injection that could neutralize those accumulated hetero charges and reach to a new balance of space charge.

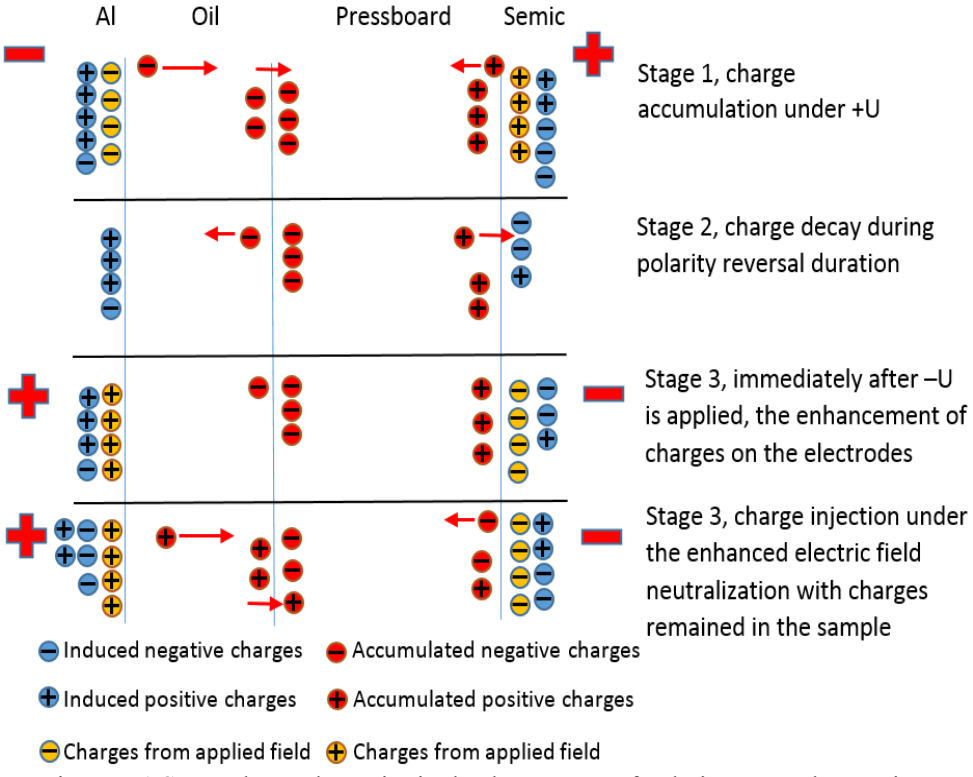


Figure 5-1 Space charge dynamics in the three stages of polarity reversal operation.

Therefore, the characteristics of space charge play a vital role in the magnitude of the enhanced electric field immediately after the polarity reversal, which, particular in this work, are related with the magnitude of the applied electric field, the time for charge dissipation during the polarity reversal process (the second stage), and the degradation of the oil.

In this chapter, the space charge dynamics in the oil and impregnated pressboard combined insulation system are experimental investigated by the PEA method. The effects caused by the three factors are also discussed.

5.1 Experimental setup

In this chapter, the oil gap and impregnated pressboard composite system is applied, which has been introduced in Ch.4.1.

The applied voltages are shown in Figure 5-2. At first, +U voltage is applied for 60 min, and then turn off the voltage and waited T_{pr} for charge decay. After that, turn on the voltage –U for another 60 min, then repeating the processes to reverse the voltage from –U to +U again. The double polarity reversal where U is the applied voltage, 18 kV (12 kV/mm) or 30 kV (20 kV/mm); T_{pr} is the duration of the polarity reversal, 0.5 min, 2min, 5 min are investigated in this work. Two reversals are required in IEC-61378-2, to test the unsymmetrical insulation structure and other impact caused by the polarity dependent phenomena. [117]

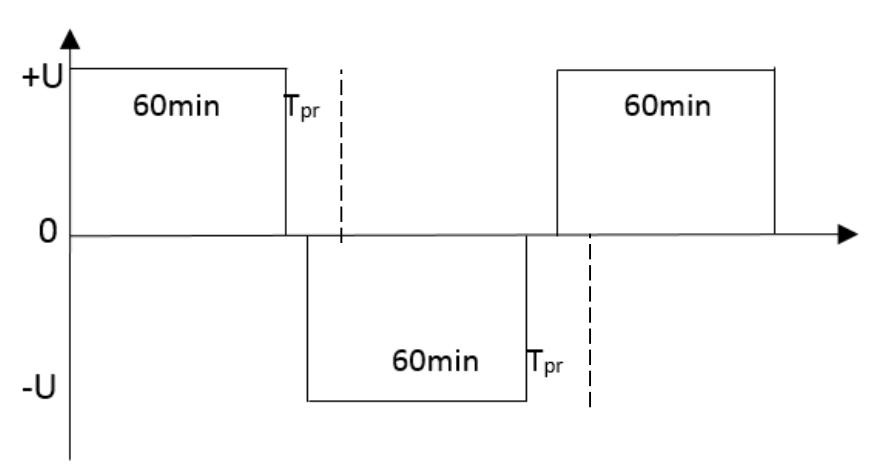


Figure 5-2 Procedures of voltage polarity reversal

5.2 Results and Discussions

5.2.1 Space charge dynamics under polarity reversal voltage

In this section, the proposed space charge dynamics during the polarity reversal operation have been verified by the PEA measurements in both fresh oil samples. The applied electric field is 20 kV/mm, and the duration of the polarity reversal process is 2 min.

The charge dynamics in the fresh oil sample before and after the 1st polarity reversal (+U to -U) are shown in Figure 5-3 (A), while before and after the 2nd polarity reversal (-U to +U) are shown in Figure 5-3 (B). The black arrows indicate the trend before polarity reversal, while the red arrows show the trend after polarity reversal.

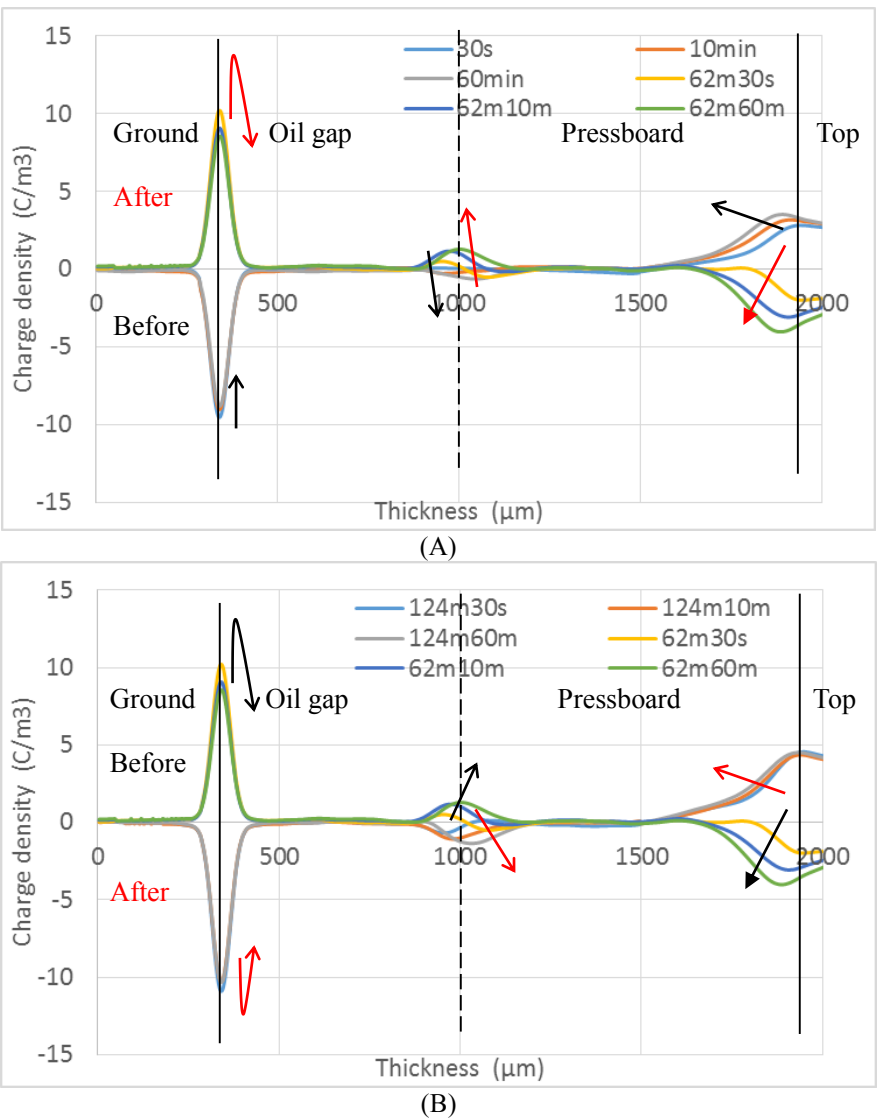


Figure 5-3 space charge dynamics before and after (A) the 1st polarity reversal and (B) the 2nd polarity reversal

According to Figure 5-3 (A), negative charges are injected from the ground (Al) electrode and accumulated at the oil/pressboard interface. However, the amount of the interfacial charge is small due to the short duration of DC voltage application and the good dielectric properties. So after the polarity reversal, the charge density at the Al electrode is enhanced at about 10 C/m³ as the accumulated charges remains in the insulation bulk, especially in the vicinity of the interface. Immediately after the application of the revered voltage, the interfacial peak is divided into two parts. The first part seems to locate in the oil gap, which can be quickly reversed to same polarity with the applied voltage. The other part is the charges accumulated within the pressboard bulk, which cannot quickly dissipate and enhance the electric field across the oil gap. The electric field across the oil gap is positively proportional to the magnitude of the ground electrode peak, which has been shown in Ch.4.1. The enhanced electric field also results in more positive charges accumulated at the interface after the 1st polarity reversal. In the vicinity of the top (semiconducting polymer) electrode, the amount of the accumulated negative charges under the

negative voltage is also more than the positive voltage, though the signal is severely attenuated. This could also result from the enhanced electric field at the interface between pressboard and the top electrode. Moreover, the differences between the positive and negative charges also could be another possible reason. However, these differences are usually very small as mentioned in Ch.3.3.

When the 2nd polarity reversal operation is finished, the applied electric field reverses to +20 kV/mm again, as shown in Figure 5-3 (B). An almost symmetric space charge profile can be observed, compared with the 1st polarity reversal, which is also known as the 'mirror image effect' [118]. Again, the interfacial charges in the oil gap can quickly change to negative charges following the polarity of the ground electrode. The positive charges within the pressboard induce more negative charges at the ground electrode, leading to a slightly larger negative peak (about 1.1 C/m³), compared with the peak after the 1st polarity reversal process. The negative charges are then injected from the ground electrode. These injected negative charges gradually neutralize and replace the accumulated positive charges remains in the pressboard bulk in the vicinity of the interface until reaching the new charge dynamics balance.

Based on the understanding of the long duration measurements in Ch.4.1.3, the time for the dynamics balance of the space charge in the fresh oil sample is about 24 hours, though it is particular for 12 kV/mm. However, only 1 hour is applied in this work, resulting in the limited space charge accumulated in the insulation bulk and the small field enhancement (which can be simply and approximately related with the amplitude of the peak at the ground electrode) after polarity reversal process.

At the other hand, a simply calculation of space charge profile based on the previous results of the fresh oil samples under 20 kV/mm in Ch.4.1 is introduced as follows.

According to the proposed charge dynamics process, the space charge distribution $\rho_d(x)$ after 2 min charge decay process can be collected from the previous charge decay result. The reversed voltage can be calculated from the reference data with a voltage difference ratio.

The voltage ratio can be simply calculated by

$$R = \frac{U_{pr}}{U_{ref}} \tag{5.1}$$

where U_{pr} is the polarity reversal voltage, -30 kV in this work; U_{ref} is the reference voltage in Ch.3.1, +15kV.

Therefore, the space charge profile after 2 min polarity reversal process can be calculated by:

$$\rho_{pr}(x) = \rho_d(x) + R \cdot \rho_{ref}(x) \tag{5.2}$$

where $\rho_{pr}(x)$ is the space charge profile after polarity reversal; $\rho_{ref}(x)$ is the space charge profile of the reference data.

The comparison of the estimated result and the experimental result is shown in Figure 5-4. The estimated magnitude of the ground electrode is slightly higher than the experimental result. Moreover, only negative interfacial charges can be observed within the estimated result, while both positive charges and negative charges can be found in the vicinity of the interface. As explained before, these positive charges are quickly injected from the ground electrode due to the enhanced electric field across the oil gap during the 30s (including the time to collect the experimental data), which also slightly reduce the magnitude of the peak of the ground electrode. Therefore, the estimated result may be more close to the real condition when the reversed voltage is applied. It also has to be noticed that, the estimated data is calculated based on the results of 3 hours voltage application which obviously leads to more accumulated charges within the insulation system to induce more positive charges on the ground electrode. However, considering the total charge amount in the fresh oil sample is very small, this difference is also very limited.

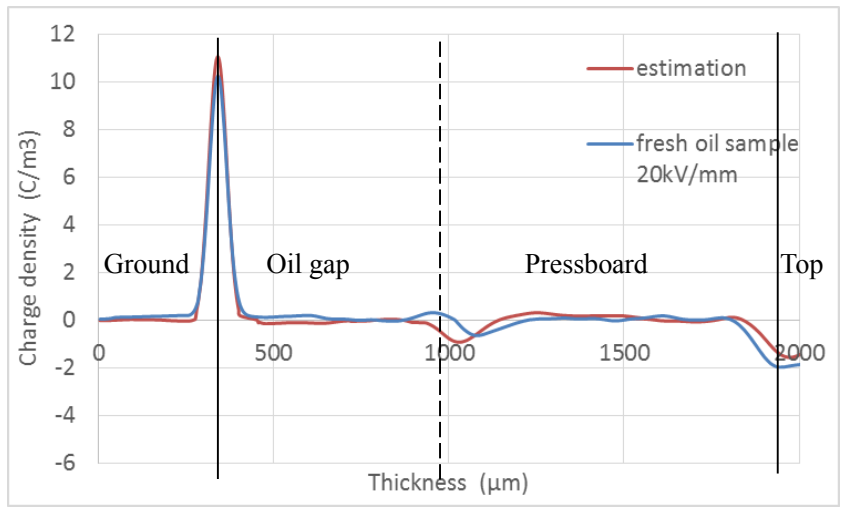


Figure 5-4 Comparison between the measurement and estimated space charge distribution immediately after the 1st polarity reversal in the fresh oil sample under 20 kV/mm with T_{pr} =2 min.

5.2.2 Impacts of the aged oil

As the whole space charge dynamics before and after the polarity reversal operation has been proved to approximately agree with the proposed charge dynamic process, the impacts caused by the degradation of the mineral oil are further investigated in this section.

As shown in Figure 5-5, the space charge profiles in the samples with the fresh oil, and aged oil, separately, are recorded immediately after the first polarity reversal process, i.e. from +12 kV/mm to -12 kV/mm, with a fixed T_{pr} of 30s.

After 30s for charge decay, a large amount of hetero charges still remains in the insulation bulk, particularly, at the two surfaces of the impregnated pressboard. Therefore, the charge density at the two electrodes are much larger, compared with the fresh oil sample, e.g. the charge density of the peak of the ground electrode is 9.2 C/m³ in the aged oil sample, while only 5.1 C/m³ in the fresh oil sample. The different amount of hetero charges also result in the considerable differences in the electric field across the oil gap, as shown in Figure 5-6. The maximum electric field in the fresh oil gap is about 15.7 kV/mm, while it is 20.6 kV/mm in the aged oil gap.

Therefore, by using Equation (2.4), the electric field enhancement within the fresh and aged oil gap is shown in Table 5-1. The positive proportional relationship between the peak value of the ground electrode, the maximum electric field in the oil gap and the field enhancement are confirmed.

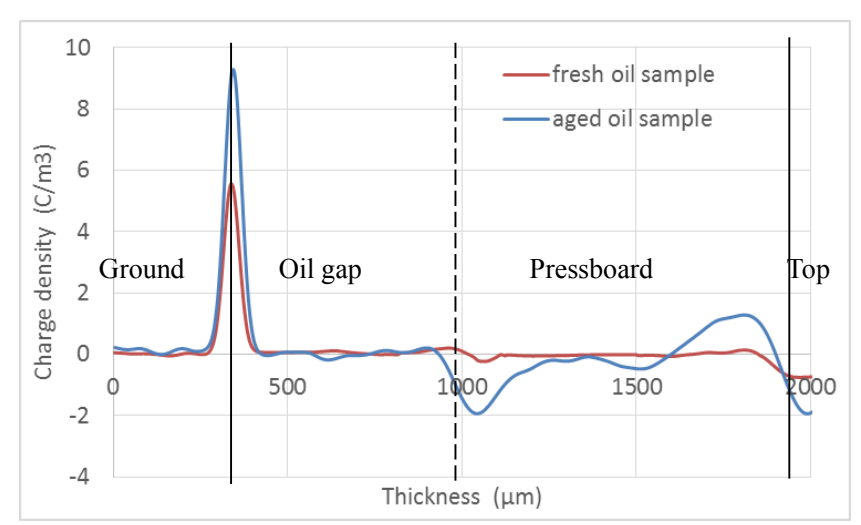


Figure 5-5 Space charge distribution immediately after the 1^{st} polarity reversal in the fresh oil sample and aged oil sample under 12 kV/mm with $T_{pr} = 30 \text{s}$.

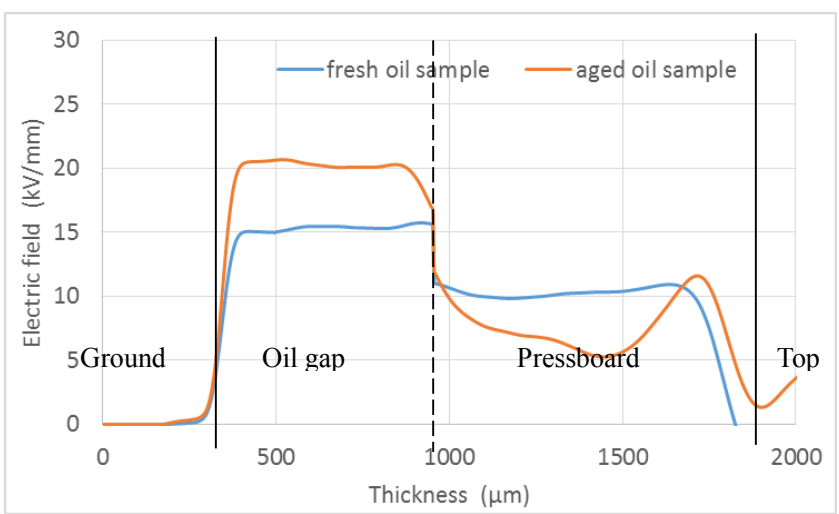


Figure 5-6 Electric field distribution immediately after the 1^{st} polarity reversal in the fresh oil sample and aged oil sample under 12 kV/mm with $T_{pr} = 30 \text{s}$.

Table 5-1. Impacts of the aged oil under polarity reversal voltage

Oil type	Peak value of the ground electrode (C/m³)	Maximum electric field in the oil gap (kV/mm)	Field enhancement in the oil gap (%)
Fresh oil	5.1	15.7	30.8
Aged oil	9.2	20.6	71.7

5.2.3 Impacts of the magnitude of the applied electric field

It is generally believed that the high electric field could enhance the space charge amount within the dielectric material by both increasing the charge injection based on the Schottky injection, and enhancing the charge mobility which also leads to a larger conductivity. This suggests that more hetero charges are accumulated in the insulation system which could potentially increase the electric field distortion after the polarity reversal process.

In this section, the impacts caused by the electric fields of 12 kV/mm and 20 kV/mm in fresh oil sample and aged oil sample are investigated, separately. The duration of the polarity reversal process is fixed to 30s.

Figure 5-7 shows the space charge distributions in the fresh oil sample under different electric fields immediately after the 1st polarity reversal process (from +U to -U). It can be clearly observed that more hetero charges (negative charges) remains in the vicinity of the oil/pressboard interface, which could induce more positive charges at the ground electrode. More positive charges can also be found at the interface on the oil side. As explained before, these positive charges are injected from the ground electrode during the short period (30s) for the operations of the data acquisition. Therefore, the more amount of these positive charges can directly indicate

the enhancements caused by the higher electric field on the charge injection and mobility, compared with the result under lower electric field.

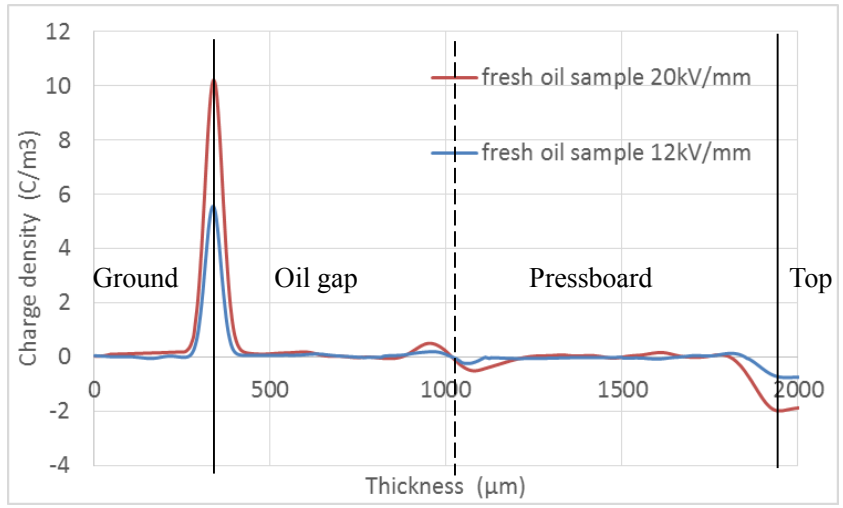


Figure 5-7 Space charge distribution immediately after the 1^{st} polarity reversal in the fresh oil sample under 12 kV/mm and 20 kV/mm with T_{pr} =30s.

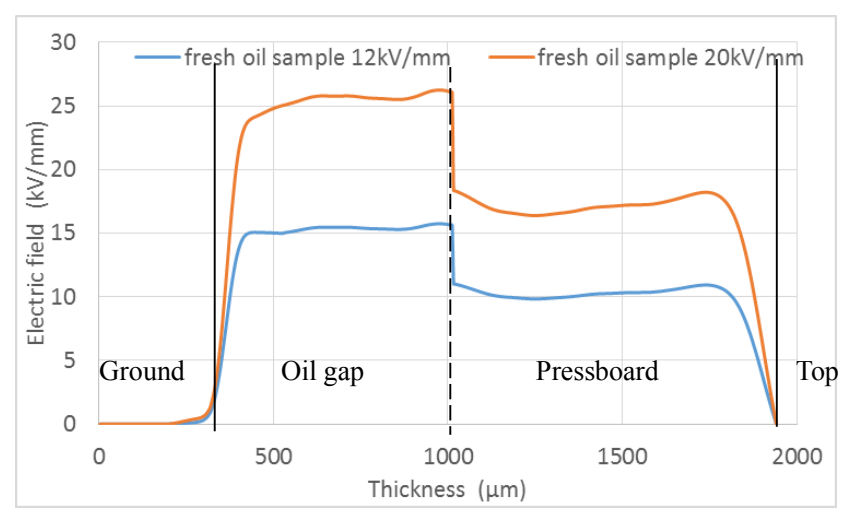


Figure 5-8 Electric field distribution immediately after the 1^{st} polarity reversal in the fresh oil sample under 12 kV/mm and 20 kV/mm with T_{pr} =30s.

The electric field distributions under 12 kV/mm and 20 kV/mm can be calculated from the space charge profiles by using Equation (2.3), as shown in Figure 5-8. Immediately after the polarity reversal process, the electric field within the oil gap is generally higher than in the pressboard. The maximum electric field locates at the oil/pressboard interface as the positive charges are injected and accumulated at the interface where is close to the residual negative charges in the pressboard.

Table 5-2 shows the electric field enhancement in the oil gap under different magnitude of the applied electric field. The electric field enhancement under higher electric field is slightly larger than the lower electric field. It also needs to aware that the electric field enhancement calculations is based on the space charge distributions in Figure 5-7, which can be affected by those positive charges injected in the 30s. These charges can reduce the electric field across the oil gap, especially under higher electric field. Therefore, the 'real' difference of the electric field enhancement caused by the different magnitude of the applied electric field could be larger.

Table 5-2. Impacts of the magnitude of applied electric field in the fresh oil sample

			•
Applied electric field (kV/mm)	Peak value of the ground electrode (C/m³)	Maximum electric field (kV/mm)	Field enhancement in the oil gap (%)
12	5.1	15.7	30.8
20	10.2	26.3	31.5

On the other hand, in the aged oil sample, the space charge distributions under different applied electric field are shown in Figure 5-9. Under 12 kV/mm, considerable hetero charges can be observed in the vicinity of the oil/pressboard interface and the pressboard/top electrode interface, which greatly increase the magnitude of the both peaks on the electrodes. However, no hetero charges can be observed in the insulation system, therefore, the limited increase of the magnitude of the ground electrode peak can be observed. Similar with the fresh oil sample under higher electric field, the positive charge injection during the 30s for data acquisition is significantly enhanced by both of the high reversed electric field and as well as the severe aged oil. A significant drop of the peak on the ground electrode during the data acquisition process in the experiments has been observed. Therefore, a more accurate way to describe the impact caused by the high electric field in the aged oil is using the estimation method based on the results in Ch.4.1. The estimation method has been introduced in the previous section, and the result is also shown in Figure 5-9. It can be observed that the significant amount of hetero charges exists in the insulation system, and results in a boosted peak value on the ground electrode (about 15 C/m³). The result confirms the significant impact caused by the high electric field in the aged oil sample, and also shows the superiority of the estimation method over the measurement, when the space charge dynamics is very fast, particularly in the aged oil sample under high electric field.

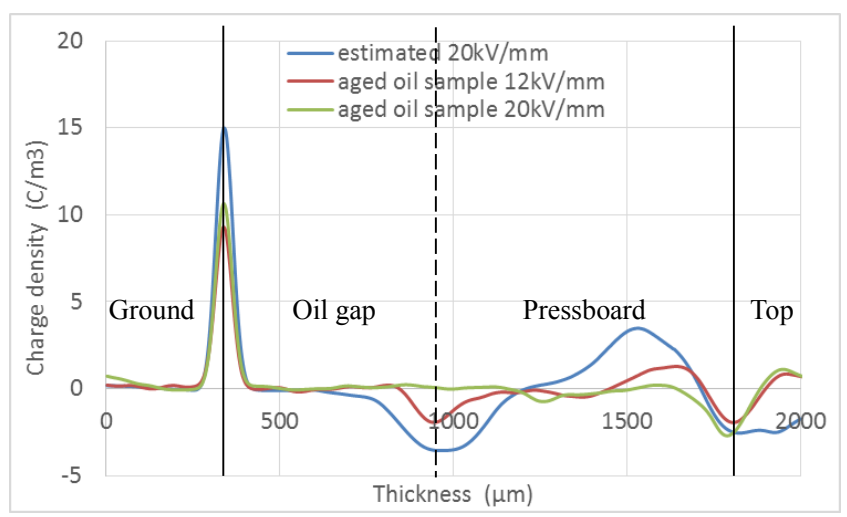


Figure 5-9 Space charge distribution immediately after the 1^{st} polarity reversal in the aged oil sample under 12 kV/mm and 20 kV/mm with T_{pr} =30s.

The electric field distributions in the aged sample under different magnitudes of the applied electric fields are shown in Figure 5-10. Significant differences between the estimated electric field distribution and the calculated electric field distribution based on the measure space charge profile under 20 kV/mm can be observed. The estimated electric field in oil gap is around 40 kV/mm, and the maximum value is 42.1 kV/mm. However, the electric field calculated from the space charge distribution is around 20 kV/mm in the oil gap, and the maximum value (25.2 kV/mm) occurs in the pressboard bulk, suggesting the considerable homo charges have been injected in the pressboard bulk. Under 12 kV/mm, the injection of the positive charges within 30s could also reduce the electric field in the oil gap. However, this reduction is not as significant as in the 20 kV/mm because the lower applied electric field can only enhance limited the charge injection from during the short period.

Table 5-3 describes the impacts caused by the different magnitudes of the applied electric field in the aged oil sample. The great difference of the electric field enhancement between the lower electric field and the estimated result under higher electric field indicates that the electric field impacts could be enlarged in the aged oil sample, compared with the slightly differences in the fresh oil sample.

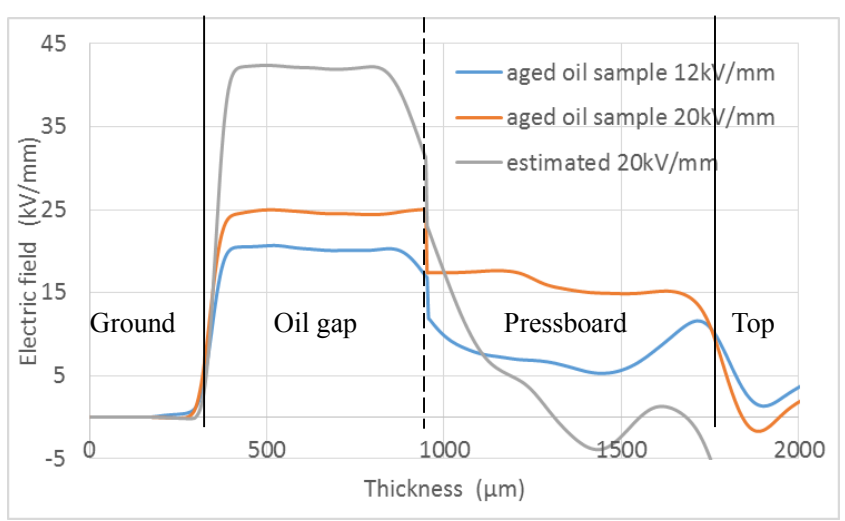


Figure 5-10 Electric field distribution immediately after the 1^{st} polarity reversal in the aged oil sample under 12 kV/mm and 20 kV/mm with $T_{pr} = 30 \text{ s}$.

Table 5-3. Impacts of the magnitude of applied electric field in the aged oil sample

Applied electric field (kV/mm)	Peak value of the ground electrode (C/m³)	Maximum electric field (kV/mm)	Field enhancement in the oil gap (%)
12	9.2	20.6	71.7
20	10.2	25.2	26
20 (estimated)	15.1	42.1	110.5

5.2.4 Impacts of the duration for polarity reversal

The accumulated charge dissipation usually describe as an exponential decrease with the decay time [100]. However, based on the understanding from the Ch.4.1, the charge dissipation is greatly dependent on the degradation of the mineral oil as well, i.e. the charges dissipate very slow in the fresh oil sample; while they decays very fast in the aged oil. Moreover, the oil/pressboard interface can potentially prevent charges drifting away from the vicinity of the interface, acting like a barrier. However, this charge block effect is also greatly weakened in the aged oil. Therefore, the duration for charge dissipation could affect the space charge distribution, differently, in the fresh oil sample and the aged oil sample. As a result, the electric field enhancement in the oil gap could be further influenced after the polarity reversal process.

In this section, the impacts caused by the duration for polarity reversal process were investigated from both experimental work and estimation in the fresh oil sample and the aged oil sample.

A. The fresh oil sample under 20 kV/mm

Figure 5-11 show the space charge distributions in the fresh oil sample immediately after the application of the revered electric field (from $\pm 20 \text{ kV/mm}$) with different polarity reversal duration T_{pr} , i.e. 30s, 2 min and 5 min.

In general, the different polarity reversal durations have very little impacts in the fresh oil sample, because the charge dissipation is generally very slow in such fresh material. A slightly increase of the peak value at the ground electrode can be observed. This phenomenon is also reported in Ch.4.1. It is caused by the more positive charges dissipated than negative charges within the same period, due to the positive charges can drift away much easier from the directly contacted electrode, while the accumulated negative charges in the vicinity of the oil/pressboard interface could be blocked (or deeply trapped), refers to Figure 4-5. Based on the result from Ch.4.1, this phenomenon usually occurs in the first 30 min of the charge dissipation in the fresh oil sample. This could result in the increase of the electric field across the oil gap, but decrease the electric field in the vicinity of the interface between the pressboard and the top electrode, as shown in Figure 5-12. However, the general impacts are very limited due to the amount of hetero charges in the fresh oil sample is very small. The impacts of the duration of the polarity reversal are summarized in Table 5-4. Very limited impacts on the electric field enhancement in the oil gap can be found, generally smaller than 40% (the displacement field after the polarity reversal dominates the field enhancement in the oil gap). It also needs to be noticed that the impacts of the polarity reversal duration are even smaller in the fresh oil sample under 12 kV/mm, in which the amount of the hetero charges is much smaller, refers to the previous section in Ch.5.2.3. Therefore, the results are not shown in this section.

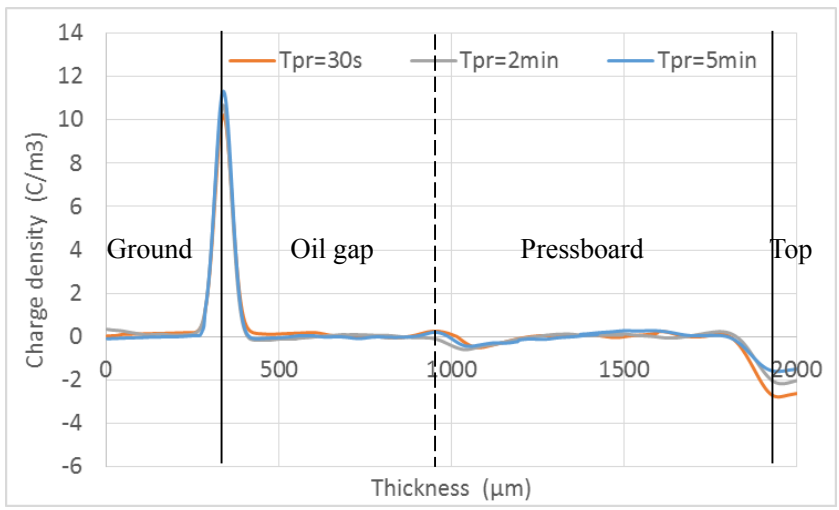


Figure 5-11 Space charge distribution immediately after the 1^{st} polarity reversal in the fresh oil sample under 20 kV/mm with T_{pr} =30s, 2min and 5min

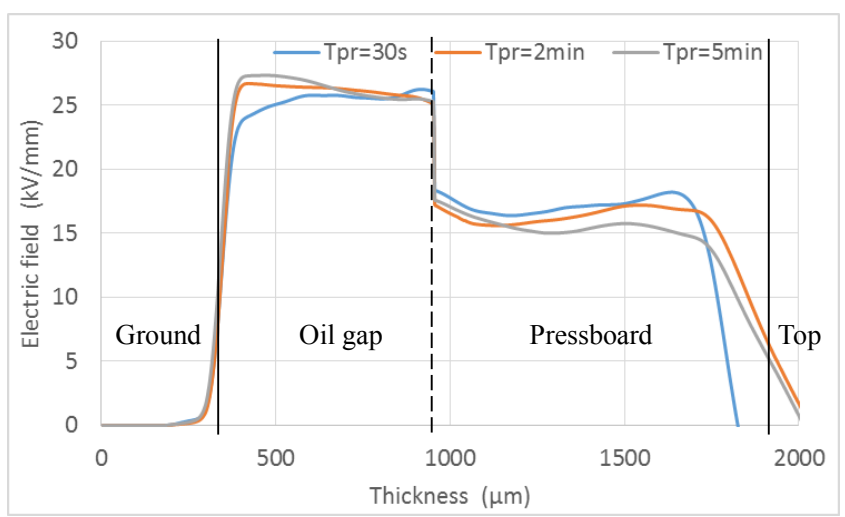


Figure 5-12 Electric field distribution immediately after the 1^{st} polarity reversal in the fresh oil sample under 20 kV/mm with T_{pr} =30s, 2min and 5min

Table 5-4. Impacts of the duration of polarity reversal process in the fresh oil sample under 20kV/mm

Duration T _{pr} (minute)	Peak value of the ground electrode (C/m³)	Maximum electric field (kV/mm)	Field enhancement in the oil gap (%)
0.5	10.2	26.3	31.5
2	10.7	27.1	35.5
5	11.3	27.4	37

B. The aged oil sample under 12 kV/mm

In the aged oil sample, the aged oil greatly enhance the mobility of the charges (refers to Ch.3.2), therefore, the different durations of the polarity reversal process can significantly influence the amount of the hetero charges remained in the insulation system. As shown in Figure 5-13, considerable hetero charges distributed in the vicinity of the oil/pressboard interface and the pressboard/electrode interface, when the T_{pr} is 30s. Therefore, the both electrode peaks are greatly enhanced, e.g. the peak value of the ground electrode is about 9.2 C/m³. When the Tpr is 2 min, the considerable hetero charges have dissipated, and the peak value of the ground electrode drops to 6.8 C/m³. For the condition that the Tpr is 5 min, most of the hetero charges have decayed. Therefore, the peak value of the ground electrode is only 5.4 C/m³. Correspondingly, the electric field distribution shows a same trend, as shown in Figure 5-14. The electric field across the oil gap quickly decreases with the increase of the polarity reversal duration. On the contrary, the electric field distributed within the pressboard keeps increasing when a longer polarity reversal duration is applied. This means a more uniform electric field distribution in the whole combined insulation system after polarity reversal operation can be reached, when the polarity reversal duration is sufficiently long (about 5 min in the aged oil sample). The summary of the impacts caused by the polarity reversal duration in the aged oil sample is shown in Table 5-5. The electric field enhancement in the oil gap dramatically drops from 71.7 % to 33.3 % when the T_{pr} rises from 30s to 5 min.

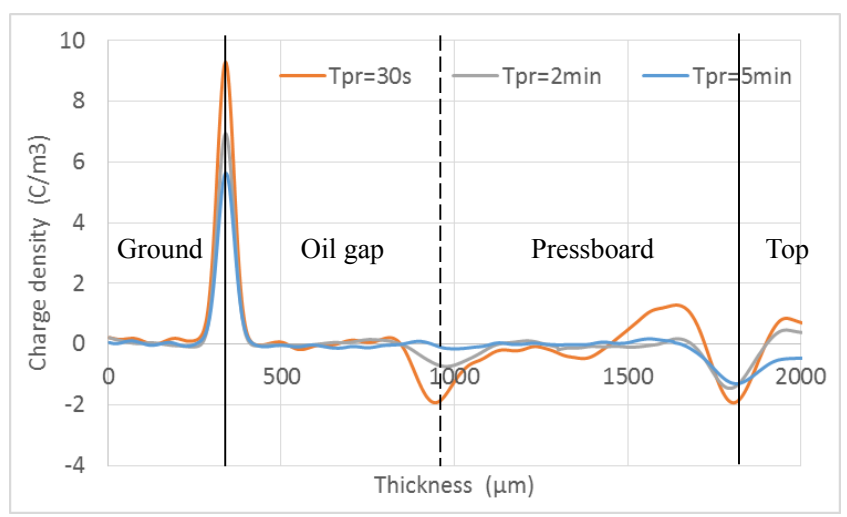


Figure 5-13 Space charge distribution immediately after the 1^{st} polarity reversal in the aged oil sample under 12 kV/mm with T_{pr} =30s, 2min and 5min.

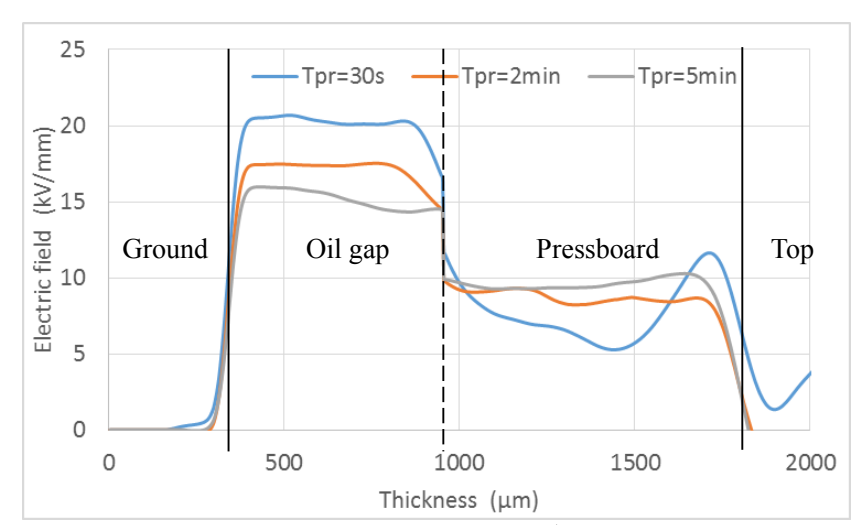


Figure 5-14 Electric field distribution immediately after the 1^{st} polarity reversal in the aged oil sample under 12 kV/mm with $T_{pr} = 30s$, 2min and 5min.

Table 5-5. Impacts of the duration of polarity reversal process in the aged oil sample under 12kV/mm

Duration T _{pr} (minute)	Peak value of the ground electrode (C/m ³)	Maximum electric field (kV/mm)	Field enhancement in the oil gap (%)
0.5	9.2	20.6	71.7
2	6.8	17.5	45.8
5	5.4	16	33.3

C. The aged oil sample under 20 kV/mm

Under the high electric field, large amount of the hetero charges exist in the insulation system, which potentially can greatly enhance electric field across the oil gap. However, as explained before, the charge dynamics in the aged oil sample under such highly enhanced electric field can

also inject large amount homo charges into the insulation system to neutralize those hetero charges remained in the insulation system. This process could be very fast and completed during the data acquisition process of the PEA system (about 30s). Therefore, such quick space charge dynamics are difficult to be correctly recorded by using the current data acquisition system for the PEA system. However, based on the previous results under pure DC electric field, the space charge distributions in the aged oil sample under 20 kV/mm with different polarity reversal durations can be estimated. As shown in Figure 5-15, the estimated space charge profiles with different T_{pr} consist the similar trend with the 12 kV/mm results, i.e. the amount of hetero charges and the peak value of the ground electrode quickly decrease when a longer polarity reversal duration T_{pr} is applied. As the charge decays exponentially with the decay time, the peak value of the ground electrode dramatically decreases from 15 C/m³ to 9.3 C/m³ when the T_{pr} increases from 30s to 2 min. It further slightly decreases to 8.5 C/m³ when the T_{pr} increases to 5 min. The experimentally recorded space charge profile with a polarity reversal duration of 30s is also shown in Figure 5-15, as comparison. A small peak of hetero charges can be observed in the insulation system. Figure 5-16 shows the electric field distributions in the aged oil sample calculated from the space charge profiles in Figure 5-15. When the T_{pr} is 30s, a significant distortion of the electric field distributed in the oil gap and the pressboard can be observed. The maximum electric field in the oil gap is about 42 kV/mm. When the polarity reversal duration increases to 2 min, the maximum electric field in the oil gap drops sharply to 27.2 kV/mm, and it further reduces to 26.6 kV/mm when the T_{pr} is 5 min. The electric field enhancement in the oil gap in each condition is calculated and shown in Table 5-6.

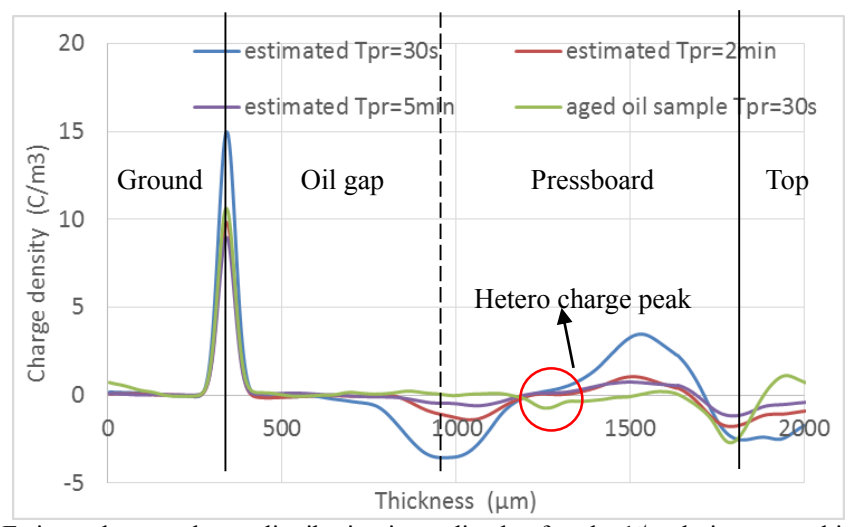


Figure 5-15 Estimated space charge distribution immediately after the 1st polarity reversal in the aged oil sample under 20 kV/mm with T_{pr} =30s, 2min and 5min.

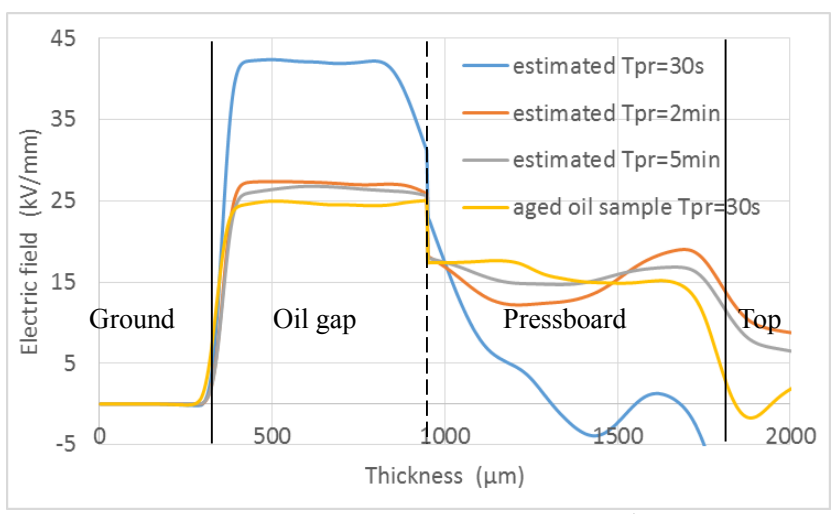


Figure 5-16 Estimated electric field distribution immediately after the 1^{st} polarity reversal in the aged oil sample under 20 kV/mm with T_{pr} =30s, 2min and 5min.

Table 5-6. Impacts of the duration of polarity reversal process in the aged oil sample under 20kV/mm

- 011 ()			
Duration T _{pr} (minute)	Peak value of the ground electrode (C/m³)	Maximum electric field (kV/mm)	Field enhancement in the oil gap (%)
0.5	15	42.1	110.5
2	9.3	27.2	36
5	8.5	26.6	33

Table 5-7. Impacts caused by the polarity reversal durations on the electric field enhancement

Duration T _{pr} (min)	Electric field enhancement %		
	Fresh oil sample 20kV/mm	Aged oil sample 12kV/mm	Estimated aged oil sample 20kV/mm
0.5	31.5	71.7	110.5
2	35.5	45.8	36
5	37	33.3	33

Table 5-7 summarizes the impacts of the different polarity reversal durations on the electric field enhancement in the oil gap within both fresh and aged oil samples under 12 kV/mm and 20 kV/mm. The results clearly show that the longer polarity reversal duration has very limited impacts in the fresh oil sample. On the contrary, for the aged oil sample, the electric field enhancement can be effectively controlled by increasing the polarity reversal duration, i.e. 5 min is sufficient to reduce the electric field enhancement to less than 33% in the oil gap (only displacement field exists). However, it has to be noticed that the space charge accumulation also closely depends on the voltage application time. Compared the results of the long duration measurement in the fresh oil sample (refers to Ch.3.2), it needs about 24 hours to reach the space charge balance in the fresh oil sample, while the voltage application duration for the polarity

reversal measurements is only 1 hour. Therefore, the electric field enhancement in the fresh oil gap could be potentially much higher than the currently results (< 40%), and may result in unexpected risks.

5.3 Conclusions

In this chapter, the space charge dynamics in the oil gap combined with single layer pressboard insulation system before and after the polarity reversal voltage are investigated by the PEA method. The impacts of the aged oil, magnitude of the applied electric field and the polarity reversal duration are investigated and discussed. A proposed space charge dynamics before and after the polarity reversal operation has been experimentally proved, which allows to estimate the space charge distribution immediately after the polarity reversal process based on the volts-on and decay results under pure DC electric field in Ch.4.1. Some important conclusions are summarized as follows:

- 1. For the fresh oil sample, the electric field enhancement in the oil gap is generally smaller than 10% immediately after the application of the revered voltage. This is because the amount of the accumulated hetero charges in the fresh oil sample is generally small, when the voltage application time is 1 hour, i.e. steady state has not been reached. A higher applied electric field can increase the amount of the hetero charges in the sample, and result in a higher electric field enhancement. However, compared with the results obtained under 12 kV/mm, the increase of the field enhancement is negligible under 20 kV/mm. On the other hand, the charge dissipation is very slow in the fresh oil sample, the oil/pressboard interface can deeply trap charges to prevent charges drifting away. Therefore, the electric field enhancement is only slight affected by the different polarity reversal durations.
- 2. For the aged oil sample, the space charge dynamics are greatly enhanced by the aged oil. Large amount of hetero charges are accumulated within the insulation system during the 1 hour voltage application time, and the amount of the charges can be further dramatically risen when a higher electric field is applied. Therefore, potentially, the electric field across the oil gap could be significantly enhanced after the application of the reversed voltage. However, the electric field enhancement in the aged oil gap is also to a great extent dependent on the polarity reversal duration, which can drop from 71.7 % to 33.3 % under 12 kV/mm and from 110.5 % to 33 % if the reversal duration is extend from 30s to 5 min.
- 3. The greatly enhanced electric field in the aged oil can significantly accelerate the homo charge injection to neutralize the large amount of hetero charges accumulated in the insulation system. These space charge dynamics is too fast to record for the current data acquisition system for the

PEA system. One of the way to solve this problem is using the proposed estimation method which has been applied in this chapter. It has been shown that this method can generate reasonable space charge distributions without the influence caused by the delay of the data acquisition.

4. Based on the results of the space charge profiles of the fresh oil sample in long duration measurement, it requires about 24 hours to reach the space charge balance (steady state). And considerable charges can be accumulated in the insulation bulk during such long period, it could potentially result in a much larger electric field enhancement across the oil gap. The voltage application time for the polarity reversal test in IEC-61378-2 is 1.5 hour, which may not sufficient long for a new converter transformer, according to the current investigation on space charge behaviour under polarity reversal voltages.

Chapter 6.

Space Charge Behaviour in Oilpressboard Insulation Systems under Combined AC and DC Voltages

It is well known that the AC and DC superimposed voltages are applied on the valve winding of the converter transformer in the LCC HVDC transmission system. Compared with the DC voltage, very limited research has been done on the space charge behaviour under AC voltage in both polymeric materials and oil-cellulose materials. The reasons could come from two aspects: firstly, the quantity of the space charge under AC fields is very small that is usually assumed to be much less problematic than that under DC field [119-121]; secondly, a very fast data acquisition system is essential for recording the space charge dynamics under the alternating electric field, particularly in the AC field with the power frequency (50 Hz or 60 Hz).

The small quantity of the space charge under AC field is mainly because the charges could be injected into the system during the half cycle of the AC voltage and extracted (or neutralized by the charges with the opposite polarity) during the other half cycle. Therefore, the amount of AC space charge greatly depends on the unsymmetrical characteristics of the positive charges and

negative charges. In other words, if only electrons are considered (positive charges are regarded as the extraction of the electrons), the AC space charge accumulation can be assumed as the result from the differences of the injection and extraction characteristics of the electrons.

Moreover, in the practical applications, the insulation system is usually equivalent to an R-C network to determine the dielectric performance based on the conductivity and permittivity of the dielectrics. The dielectric performance under AC and DC combined stress is usually obtained by combining the calculation of the AC and DC components separately [122]. This may not be sufficiently accurate as the dielectric materials usually could be non-linear systems. In fact, the research in [123] has already shown the significant space charge accumulation under the superimposed electric fields in the LDPE, compared with the sum of the DC impact and AC impact separately. However, up to date no publications report the space charge behaviour in oil/pressboard insulation system subject to the superimposed stresses.

In this chapter, the impacts of the charge mobility on the space charge behaviour under the AC voltage (50 Hz) are experimentally investigated by using the PEA system with a fast data acquisition system, based on the understanding from previous works that the charge mobility could be very different in the fresh oil sample, aged oil sample and in the oil gap. After that, the impacts of the superimposed electric field are investigated and discussed from the point of views of the total charge amount.

6.1 Experimental setup

6.1.1 AC space charge measurement system

In order to capture the fast space charge dynamics under the AC voltage with a frequency of 50 Hz, a faster data acquisition system is introduced to the PEA system, which consists of two essential component: a fast HV pulse generator (2 kHz) that allows to detect space charge under AC voltage with a frequency up to 100 Hz; and a high performance digital signal averager 'Eclipse' which has a maximum sampling frequency of 2 GS/s, and a large memory to record/store huge amount of space charge data. The whole experimental setup is illustrated in Figure 6-1. A low AC voltage is generated from the function generator (a superimposed voltage can also be generated from the function generator), which is then amplified 2000 times by the HV amplifier. This amplified high voltage AC voltage is applied to the top electrode of the purposed built PEA system used for the thick oil pressboard insulation system. Meanwhile, a series of high voltage pulse signals externally triggered by the Eclipse are applied on the top electrode, which make the charges in the sample to generate the acoustic signals. The acoustic signals are then transferred into electrical signals by the piezoelectric sensor. The PEA signals are acquired and stored by the

Eclipse in a high sampling frequency. And then these raw data are sent to the computer for signal processing.

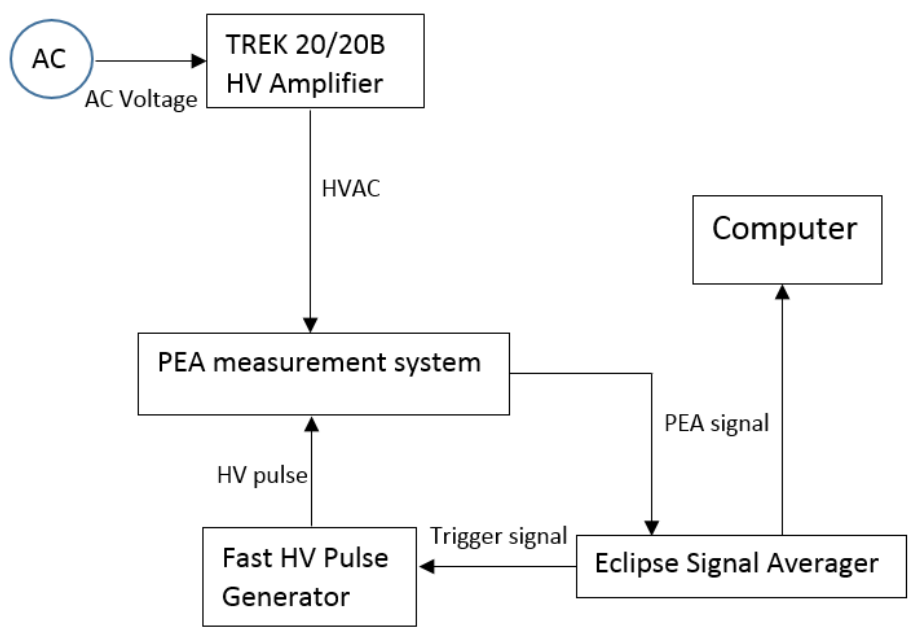


Figure 6-1 AC space charge measurement system

There are two main steps for the signal processing, phase resolved PEA signal and calibration. The Eclipse can record 20 measurement points in a full AC cycle (including 50 Hz AC voltage) with a fixed interval phase angle of 18°, and each measurement point is a data series of the space charge profile. The data acquisition is consecutively repeated for about 100 cycles of the AC voltage, by doing this, sufficient data can be used for averaging. As the sampling is not synchronized with the AC voltage, i.e. the start of the data acquisition is not synchronized with the zero-crossing point (0° or 180°) of the AC voltage, the phase angle of the each measurement point in the AC voltage cycle has to be distinguished. Considering the capacitive charge on the electrodes is mainly determined by the applied voltage, it can be used to identify the phase angle of each measurement point. Technically, the capacitive charge could be referred to the peak value of the ground electrode (which suffers less from the severe acoustic attenuation) in each space charge profile. The procedures for distinguishing the phase angle of the PEA signal are briefly described as follows:

- 1. The data of the measurement points at a same phase angle within the 100 consecutive AC cycles are averaged to denoise. Therefore, 20 denoised signals can be obtained, which are distributed in a full AC cycle, and each signal is averaged about 100 times.
- 2. The peak value of the ground electrode in each denoised signal is recorded and ploted in sequence. Then this plot is fitted with a Sine curve by Matlab, as shown in Figure 6-2. Therefore, the phase angle of each measurement point can be directly calculated by the fitted equation.

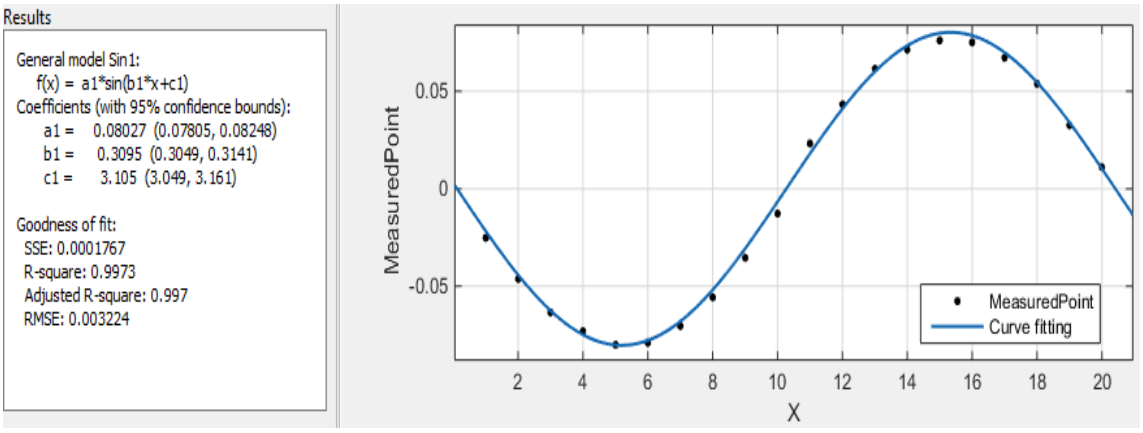


Figure 6-2 Determination of the phase angle for each measurement point.

Once the phase angle of each measurement point is determined, the space charge results can then be calibrated by the reference data with a same phase angle by using the same calibration procedures in the DC measurements.

A demonstration of the space charge distribution in the single layer fresh oil impregnated pressboard under a cycle of AC electric field of 9.6 kV/mm is shown in Figure 6-3. The phase angle can be correctly distinguished during the full cycle of the AC voltage with 50 Hz, however, the peaks of the top electrode are much smaller and boarder compared with the ground electrode, due to the severe acoustic attenuation.

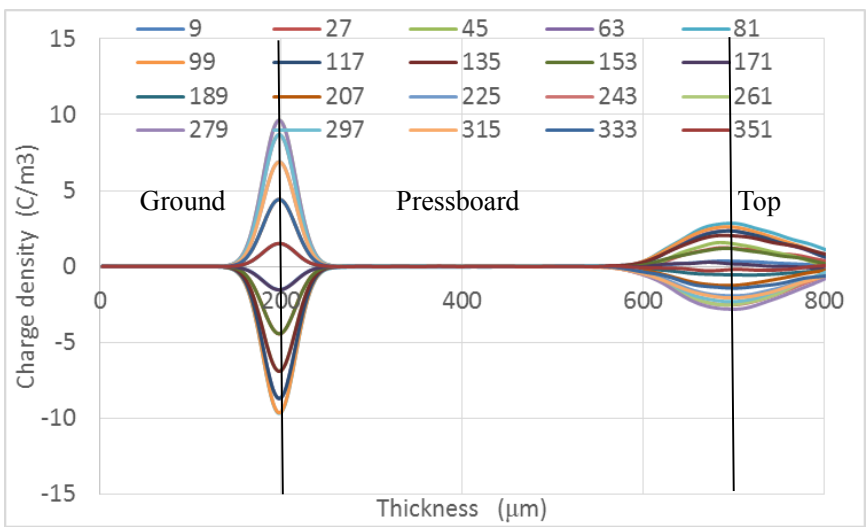


Figure 6-3 Space charge in single layer fresh oil impregnated pressboard within a full cycle of AC field at

Another demonstration of the space charge profiles in the single layer fresh oil impregnated pressboard under a superimposed electric field (consisting of 9.6 kV/mm AC stress and +4.8 kV/mm DC stress) at the 1 hour of the field application is shown in Figure 6-4. The effect of homo charges accumulation (corresponding with the applied DC stress) can be obviously observed at the two surfaces of the pressboard. These demonstrations clearly show the PEA

system with the fast data acquisition system can be successfully applied on the space charge measurement under the alternating voltage with the 50 Hz in the oil pressboard insulation system.

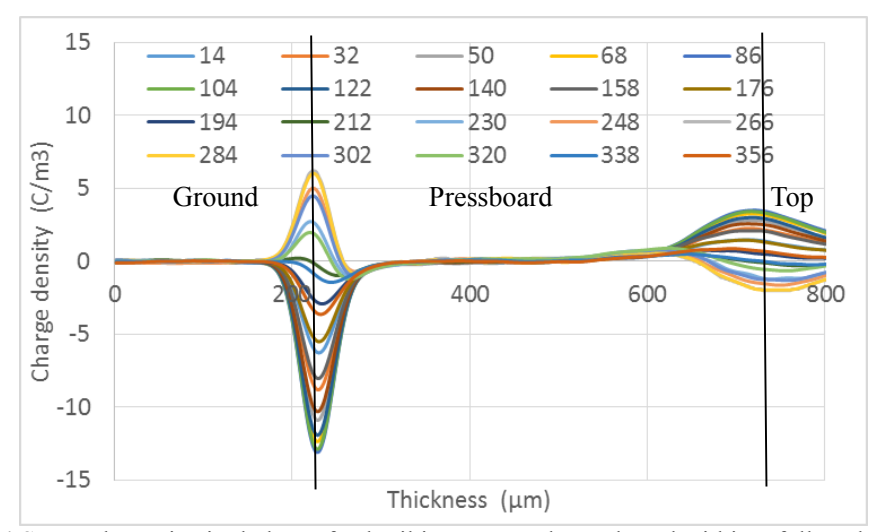
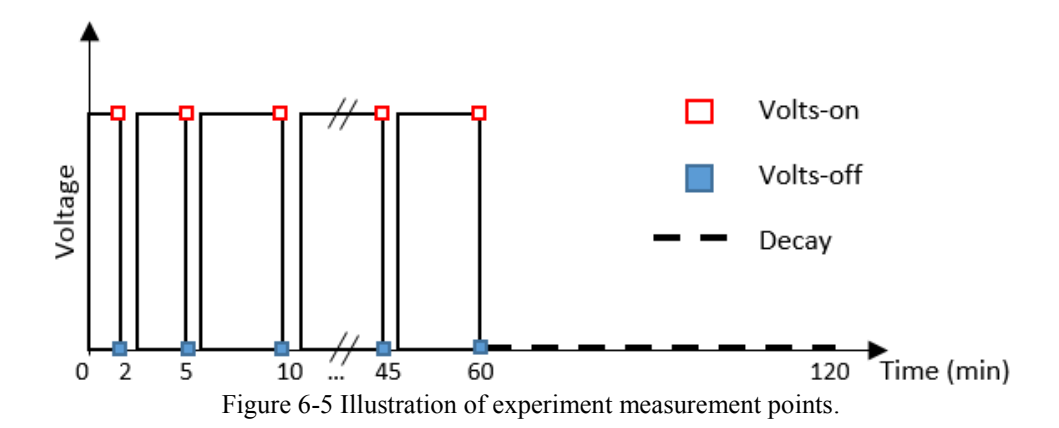


Figure 6-4 Space charge in single layer fresh oil impregnated pressboard within a full cycle of AC/DC combined stresses at 60min.

6.1.2 Measurement protocol

Considering the amount of the AC space charge could be very small, the volts-off measurements are applied to verify the space charge build up. As shown in Figure 6-5, volts-on measurement means the AC voltage is continuously applied during the data acquisition process. After each volts-on measurement, the applied external voltage is temporarily turned off. The residual space charge in the sample can be measured in a short period (about 30s by using the normal oscilloscope with an average of 1024 times). The external voltage is then turned back on immediately after the completion of the volts-off measurement. The external voltage is applied for 1 hour, and after that, the voltage is permanently removed, and the decay of the space charge is measured. All the measurements are completed at the room temperature.

The applied electric field include pure DC field ($\pm 4.8 \text{ kV/mm}$, far smaller than the threshold 10 kV/mm), pure AC field (9.6 kV/mm r.m.s) and superimposed electric field (DC 4.8 kV/mm + AC 9.6 kV/mm r.m.s).



6.2 Results and discussion

In this section, the space charge behaviour under AC electric field is firstly investigated. The impacts caused by the different charge mobility in fresh oil impregnated pressboard, aged oil impregnated pressboard and the oil gap combined with single layer pressboard insulation system are discussed. Then the investigations focus on the comparison of the space charge under superimposed stress, pure DC stress and pure AC stress. The total charge amount under various stresses are calculated and compared.

6.2.1 Space charge under AC electric field

Based on the assumption that the space charge under AC stress is greatly related with the mobility of the charge carriers within the dielectrics, the samples with different charge mobility are selected to verify the impacts of the charge mobility on the space charge behaviour under AC stress. According to the understanding of the previous work (refers to Ch3 and Ch4), the charge mobility in the aged oil impregnated pressboard is obviously larger than in the fresh oil impregnated pressboard, while the charge mobility in the oil gap could be regarded as very large in that charges keeps drifting in the oil gap and cannot be detected by the PEA system. Therefore, those samples mentioned above are selected in this work. The pressboards used in this chapter are 0.5 mm thick, having the same thickness as the oil gap.

A) Space charge in the single layer of fresh oil impregnated pressboard

Figure 6-6 shows the space charge profiles at a phase angle of 81° of the AC cycle during the 1 hour of the AC voltage application, in order to show the time dependent charge dynamics more clearly. It can be observed that a small amount of negative charges are injected from the ground electrode in to the pressboard in the vicinity of the ground electrode/pressboard interface. The accumulated AC space charge is also validated by the volts-off results, as shown in Figure 6-7. The negative charges are accumulated in the narrow vicinity of the interface between the ground electrode and the pressboard, which also induce a positive peak with a similar charge density on

the ground electrode. The peak of the accumulated charges keeps increasing with AC voltage application and reaches to about 0.3 C/m³ during 1 hour. However, no accumulated charges can be observed in the vicinity of the top electrode, which may be due to the limited resolution of the PEA system at the top electrode side that is unable to distinguish the accumulated charges and the capacitive charges when they are distributed within a narrow area.

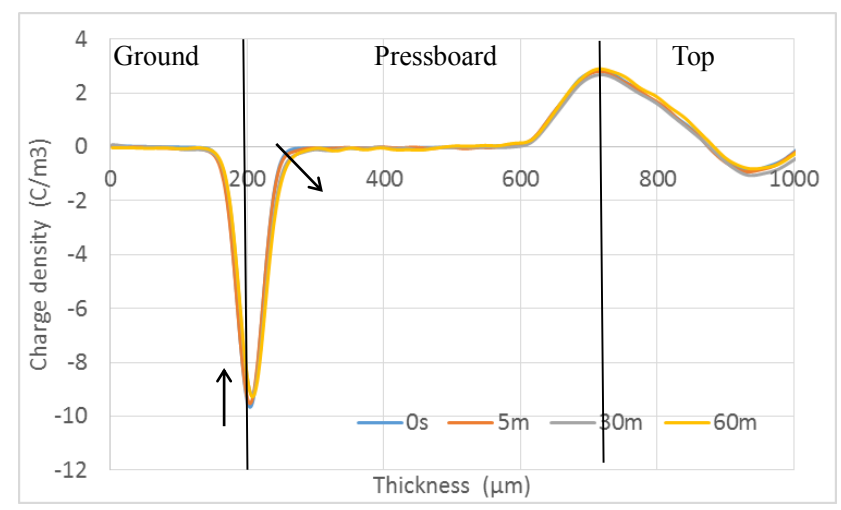


Figure 6-6 Volts-on results of space charge in single layer fresh oil impregnated pressboard under 9.6 kV/mm AC field at 81°.

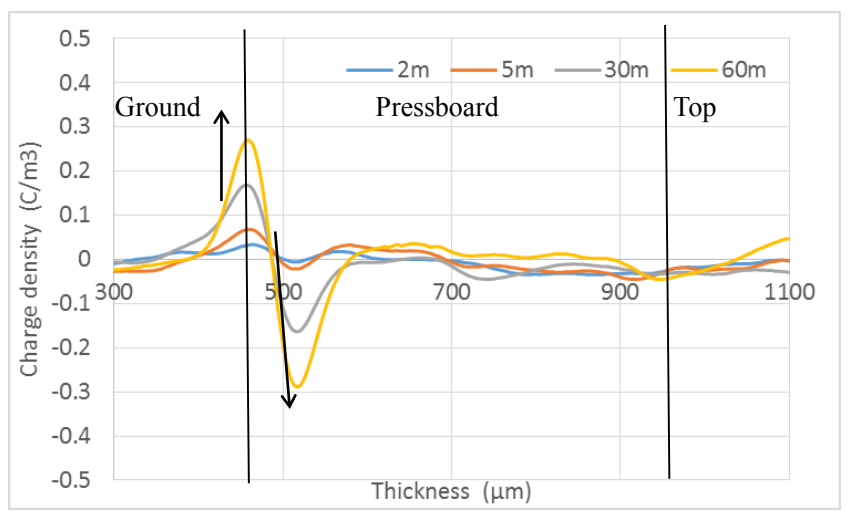


Figure 6-7 Volts-off results of space charge in single layer fresh oil impregnated pressboard under 9.6 kV/mm AC field.

B) Space charge in the single layer of aged oil impregnated pressboard

Figure 6-8 shows the space charge profiles at a phase angle of 81° of the AC voltage with 50 Hz frequency in the aged oil impregnated pressboard. No obvious space charge accumulation can be observed, compared with the fresh oil impregnated pressboard. Only some small oscillations can be observed within the pressboard bulk. The volts-off results as a validation of the little accumulation of space charge are shown in Figure 6-9. A smaller negative charge peak (about 0.08 C/m³) can be observed, compared with the fresh oil sample. Moreover, the smaller positive

charge peak (about 0.07C/m³) can be observed at the 60 min within the pressboard bulk. This may suggest that the space charge within the aged oil sample may distribute in a much boarder area in the sample bulk due to the large mobility of the charges. These injected charges could be overlapped or recombined in the pressboard bulk that is difficult to be distinguished due to the limited resolution of the PEA system, and only some oscillations can be detected.

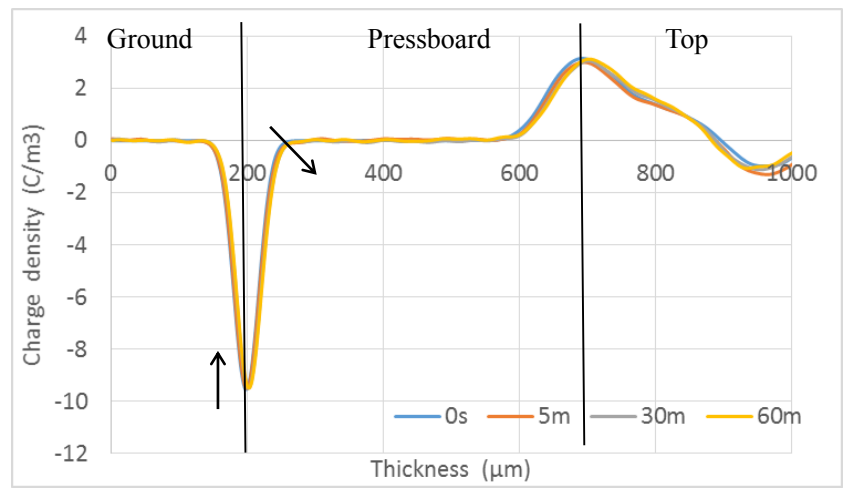


Figure 6-8 Volts-on results of space charge in single layer aged oil impregnated pressboard under 9.6 kV/mm AC field at 81°.

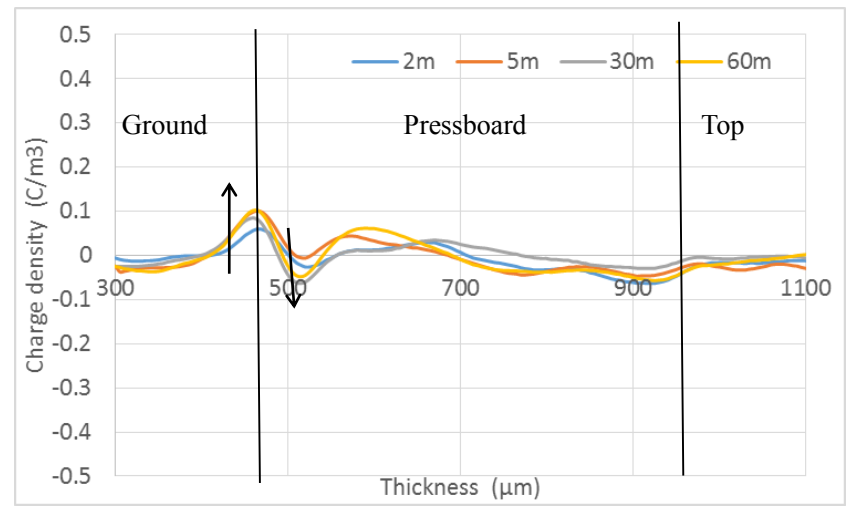


Figure 6-9 Volts-off results of space charge in single layer aged oil impregnated pressboard under 9.6 kV/mm AC field.

C) Space charge in the oil gap combined with a single layer impregnated pressboard

When a fresh oil gap is applied between the fresh oil impregnated pressboard and the ground electrode, the space charge profiles at an 81° phase angle of the AC voltage are shown in Figure 6-10. No accumulated space charge can be observed in the insulation system, only oscillations within the insulation bulk. The volts-off results also confirm that no space charge accumulation in the insulation system when an oil gap is applied, as shown in Figure 6-11 and Figure 6-12 (aged oil sample). The range of the oscillations are from +0.03 C/m³ to -0.03 C/m³, which is believed as the background noise.

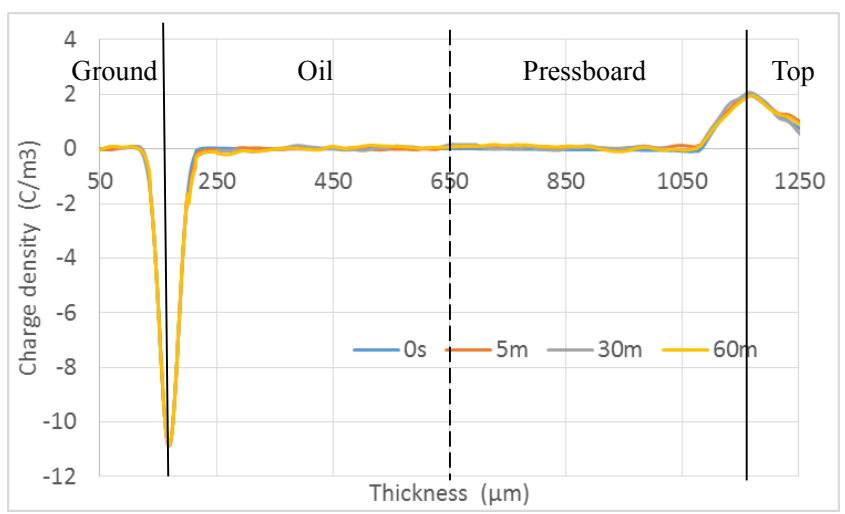


Figure 6-10 Volts-on results of space charge in fresh oil combined with impregnated pressboard insulation system under 9.6 kV/mm AC field at 81°.

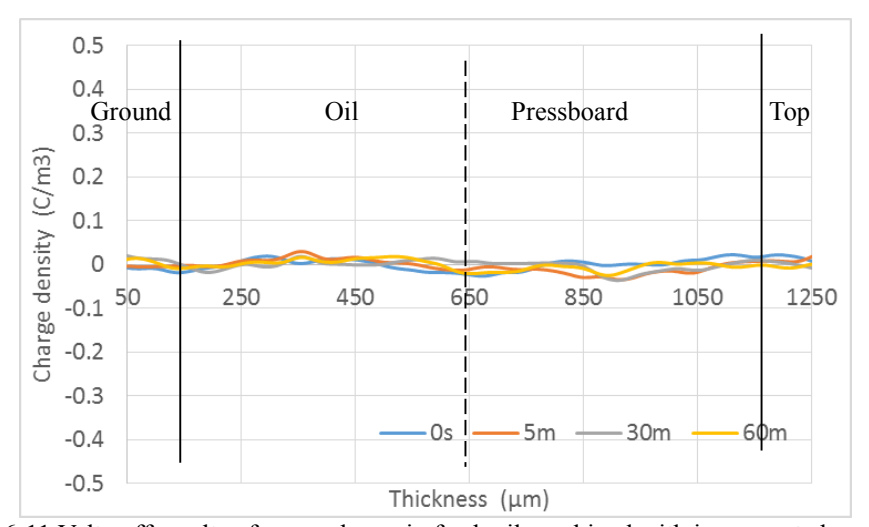


Figure 6-11 Volts-off results of space charge in fresh oil combined with impregnated pressboard insulation system under 9.6 kV/mm AC field.

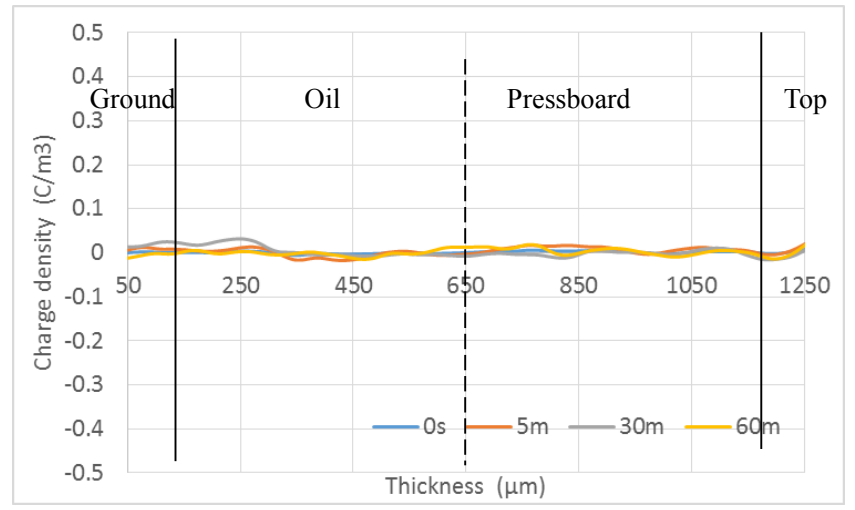


Figure 6-12 Volts-off results of space charge in aged oil combined with impregnated pressboard insulation system under 9.6 kV/mm AC field.

The results above clearly indicate that 1) the amount of the space charge accumulated in the single layer pressboard is generally very small; 2) the space charge behaviour in oil/pressboard

insulation system is related with the charge mobility in the dielectric materials, i.e. when the charge mobility is small in the single layer of the fresh oil impregnated pressboard, the accumulated charges (mainly negative charges) distribute in the narrow vicinity of the pressboard/ground electrode interface; when the charge mobility is higher in the single layer of the aged oil impregnated pressboard, the positive and negative charges could distribute broadly within the pressboard bulk; when the oil gap is applied, in which both positive charges and negative charges are believed to drift much faster than in the pressboard, hence the injected charges may keep drifting within the oil gap rather than being trapped by the oil/pressboard interface.

6.2.2 Space charge under AC and DC superimposed electric field

In this section, the space charge behaviour in the single layer pressboards respectively impregnated with fresh oil and aged oil under superimposed electric field (+4.8 kV/mm DC stress combined with 9.6 kV/mm AC stress) are firstly investigated. Experiments also have been repeated on the oil gap combined with pressboard insulation system.

A) Space charge in the single layer of fresh oil impregnated pressboard

Based on the previous experiments under AC electric field (9.6 kV/mm), a very small DC offset electric field (+4.8 kV/mm) is superimposed, which is generally believed below the threshold of the charge injection in the oil pressboard insulation system (the threshold means the space charge accumulation is dramatically increasing when the applied electric field is higher than a particular value). The space charge profiles within a whole cycle of the superimposed stress are shown in Figure 6-4 when the electric field application time is 60 min. The time dependent space charge dynamics at a phase angle of 86° is shown in Figure 6-13. Compared with the space charge profiles under pure AC electric field, it can be clearly observed that both of the peaks at the electrodes are moving towards to the middle of the pressboard, indicating the negative charge injection from the ground electrode and the positive charge injection from the top electrode. This agrees with space charge dynamics in the single layer of impregnated pressboard under +15 kV/mm DC electric field (refer to Ch.3), suggesting these charges may mainly result from the small DC offset, particularly, the positive charge injection (which has not been observed from the space charge profiles under the pure AC stress).

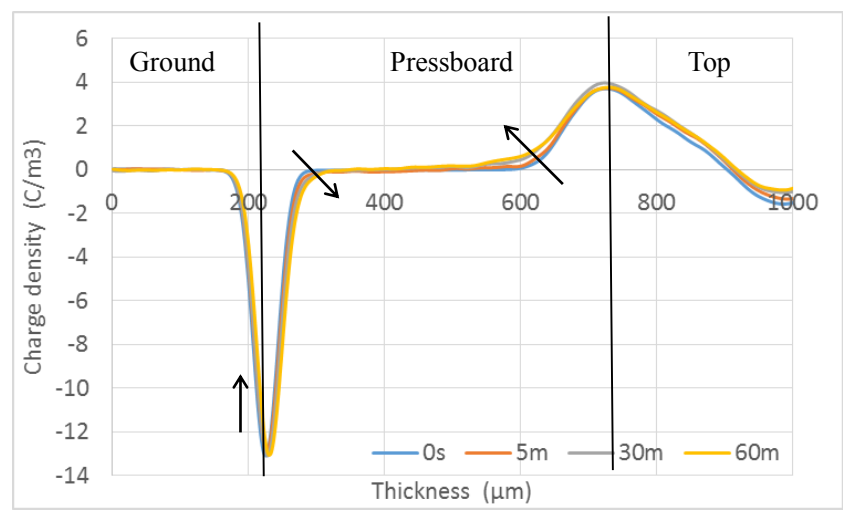


Figure 6-13 Volts-on results of space charge in single layer fresh oil impregnated pressboard under AC/DC combined stresses at 86°.

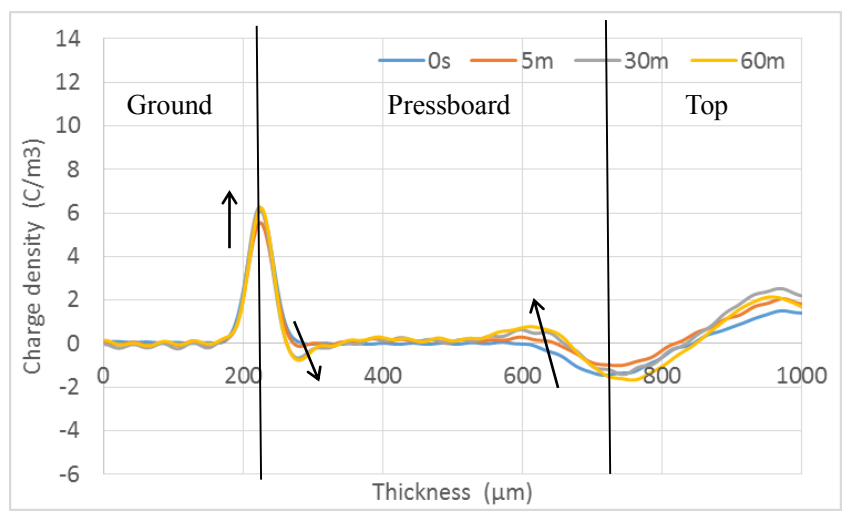


Figure 6-14 Volts-on results of space charge in single layer fresh oil impregnated pressboard under AC/DC combined stresses at 266°.

Figure 6-14 shows the space charge dynamics at a phase angle of 266° during the electric field application duration of 1 hour. Both of the peak values on the electrodes are smaller compared with the results at 86°, due to the polarity of the DC stress is opposite to the AC stress at a phase angle of 266°. The accumulation of the space charge in the vicinity of the two electrode/pressboard interfaces can also be observed. However, at a phase angle of 266°, these accumulated charges behave as the hetero charges that increase the peak values of the both electrodes. This indicates that the accumulated charges could enhance the electric field in the vicinities of the pressboard surfaces.

B) Space charge in the single layer of aged oil impregnated pressboard

The impacts caused by the aged oil on the space charge behaviour under the superimposed electric field are investigated as well, as shown in Figure 6-15 and Figure 6-16. Figure 6-15 shows the space charge dynamics at a phase angle of 81° that the DC stress and the AC stress are in the same

polarity. Significant negative charge injection from the ground electrode can be observed. These negative charges can quickly move into the pressboard bulk and distribute in a broad region, which is different from the charges in the fresh oil sample where charges only distribute in a narrow vicinity of the two surfaces of the pressboard. As shown in Figure 6-16, the space charge dynamics at a phase angle of 261° validate the large amount of negative charges broadly distribute within the pressboard bulk shortly after the application of the superimposed stress. Moreover, the significant increase of the charge density on the two electrodes can be observed, indicating a much severe electric field distortion in the vicinities of the electrode/pressboard interfaces.

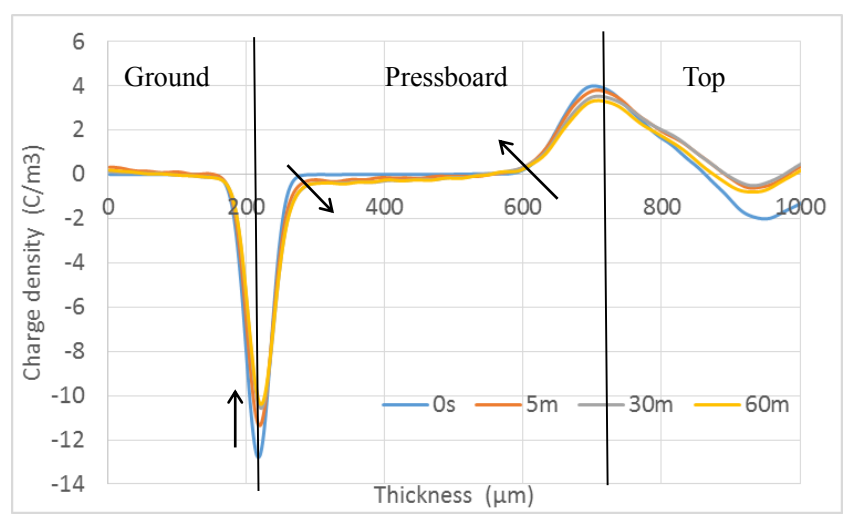


Figure 6-15 Volts-on results of space charge in single layer aged oil impregnated pressboard under AC/DC combined stresses at 81°.

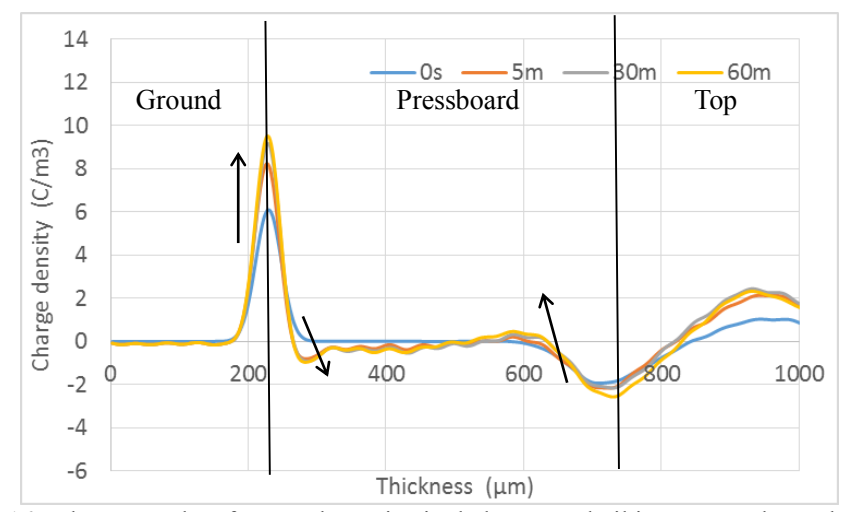


Figure 6-16 Volts-on results of space charge in single layer aged oil impregnated pressboard under AC/DC combined stresses at 261°.

C) Space charge in the oil gap combined with pressboard insulation system

Considering the practical condition in converter transformers, the space charge behaviour in the oil gap and pressboard composited insulation system under the superimposed stress is investigated. The impacts caused by the aged oil is also discussed in this section.

As shown in Figure 6-17, the amount of space charge at a phase angle of 81° are greatly increased when an oil gap is introduced in the insulation system with fresh oil. When a small DC stress (much smaller than the threshold) is combined with the AC stress, large amount of the negative charges presence is observed at the oil/pressboard interface immediately after the application of the superimposed stress. This negative interfacial peak is quickly increasing to the maximum value (about 4.3 C/m³) within the first 5 min. Compared with the space charge dynamics under pure DC electric field (refers to Ch.4.1), the increase of the interfacial peak is much faster when the superimposed electric field is applied. Then the peak value keeps decreasing which may result from the neutralization by the positive charges injected from the top electrode. Correspondingly, as shown in Figure 6-18 (the space charge dynamics at a phase angle of 261°), the peak value of the ground electrode increases to the maximum value (about 7.3 C/m³) at 5 min then gradually decreases to about 6.1 C/m³ at 60 min. This indicates the electric field distributed across the oil gap could be greatly enhanced at 5 min, then this enhancement starts to decrease.

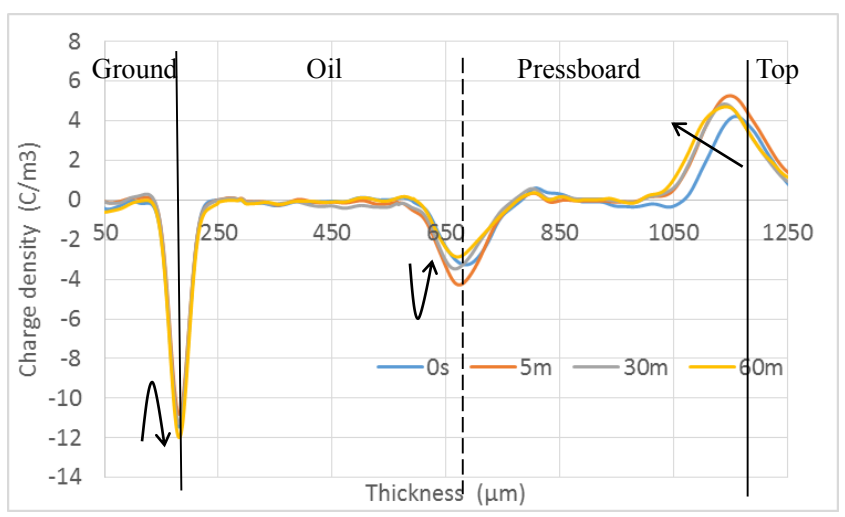


Figure 6-17 Volts-on results of space charge in fresh oil combined with impregnated pressboard insulation system under AC/DC combined stresses at 81°.

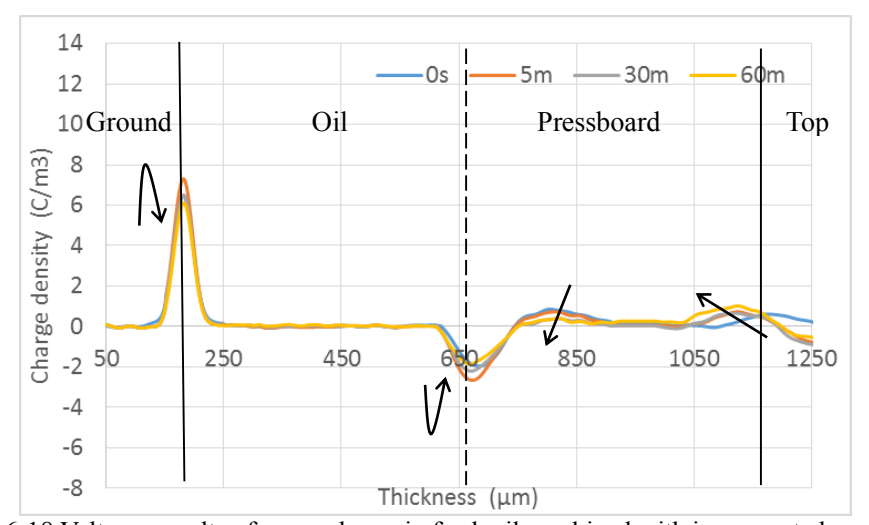


Figure 6-18 Volts-on results of space charge in fresh oil combined with impregnated pressboard insulation system under AC/DC combined stresses at 261°.

When the aged oil is applied, the space charge behaviour becomes very complex due to the large mobility of the charge carriers, as shown in Figure 6-19 (81°) and Figure 6-20 (261°). It can be observed that the negative interfacial peak instantly reaches to the maximum value after the application the combined stresses. Then the interfacial peak keeps decreasing. When the AC stress is opposite to the DC stress, i.e. at a phase angle of 261°, the charge density on the ground electrode has been dramatically enhanced to about 12.4 C/m³ within the first 5 min, suggesting that significant negative charges are accumulated within the whole insulation system. However, both positive charges and negative charges could broadly distribute within the insulation system due to the large mobility by the aged oil. Therefore, the overlapped charges with the opposite polarities are difficult to be separated by the current PEA system, and the severe oscillations can be observed in the insulation bulk.

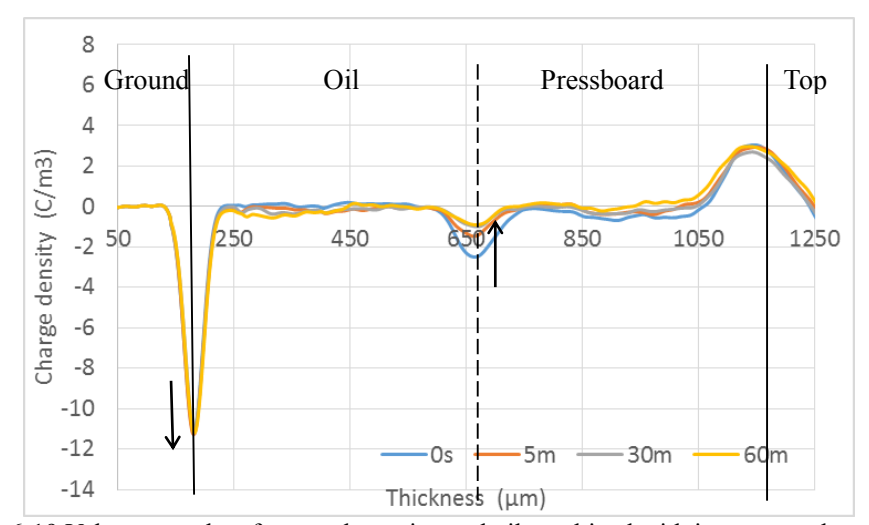


Figure 6-19 Volts-on results of space charge in aged oil combined with impregnated pressboard insulation system under AC/DC combined stresses at 81°.

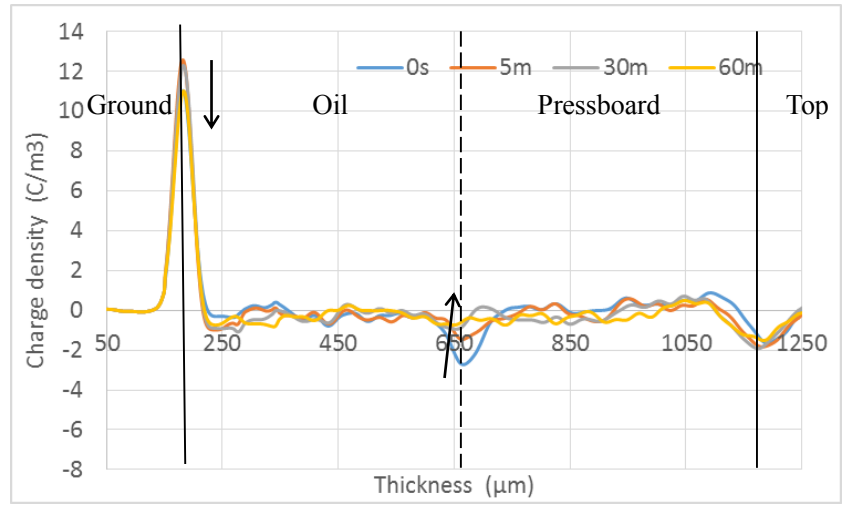


Figure 6-20 Volts-on results of space charge in aged oil combined with impregnated pressboard insulation system under AC/DC combined stresses at 261°.

In this section, the differences of the total charge amount within the insulation system between the superimposed stress and the combination of the pure AC stress and DC stress are discussed. The charge amounts in the pure DC stress (4.8 kV/mm), pure AC stress (9.6 kV/mm) and the superimposed stress (9.6 kV/mm AC and 4.8 kV/mm DC offset) are calculated respectively based on Equation (2.2). To avoid the influences caused by the applied electric field, the charge amount from the volts-off measurements are used for comparison. However, it should be always aware that some fast charges could dissipate during the volts-off measurement.

A) Single layer impregnated pressboard

Figure 6-21 and Figure 6-22 show the volts-off space charge dynamics in the pressboard impregnated with the fresh oil and the aged oil, respectively, under the pure DC electric field 4.8 kV/mm. Homo charge injection can be observed in all the samples. Negative charges are quickly accumulated within the pressboard in aged oil sample, compared with the fresh oil sample under such low electric field. The negative charges distribute in a broad region within the pressboard bulk with a peak value of 0.15 C/m³ in the fresh oil sample and 0.26 C/m³ in the aged oil sample. Little amount of positive charges have been observed in the vicinity of the top electrode/pressboard interface with a peak value of 0.08 C/m³ in the fresh oil sample and 0.06 C/m³ in the aged oil sample.

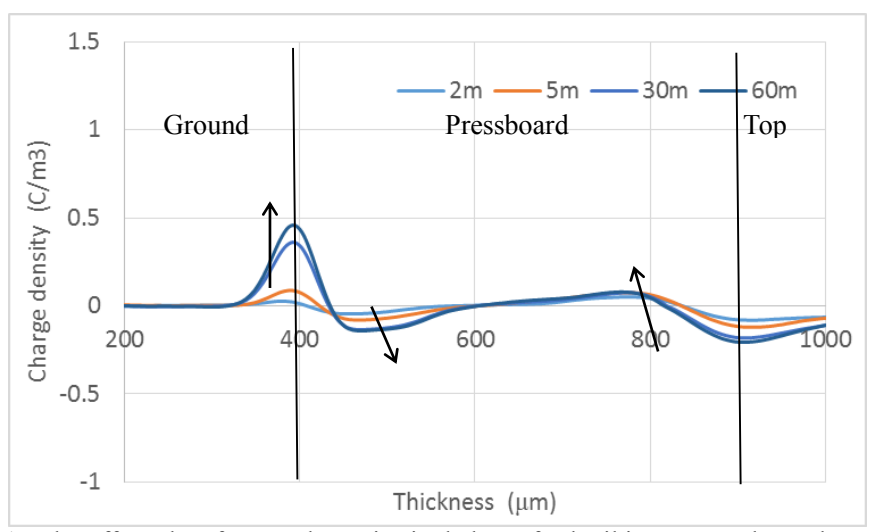


Figure 6-21 Volts-off results of space charge in single layer fresh oil impregnated pressboard under 4.8 kV/mm DC field.

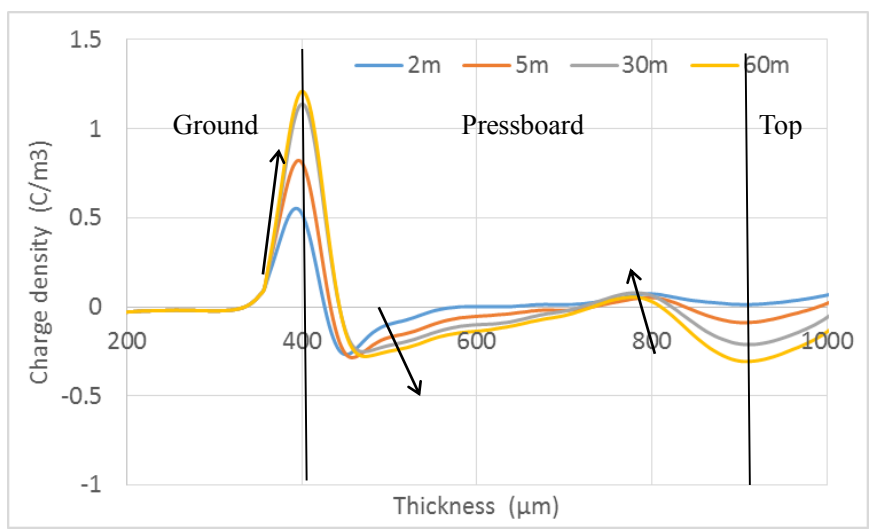


Figure 6-22 Volts-off results of space charge in single layer aged oil impregnated pressboard under 4.8 kV/mm DC field.

When the AC electric field (9.6 kV/mm) is superimposed on the DC field, as shown in Figure 6-23 and Figure 6-24, the amount of the accumulated space charge in the pressboard is generally increased. Compared with the space charge profiles under pure DC field, the amount of the negative charges is greatly increased in the vicinity of the ground electrode/pressboard interface. The peak value of the accumulated negative charges is about 0.4 C/m³ in the fresh oil sample and 0.5 C/m³ in the aged oil sample. Considering the space charge under AC stress that distribute in a narrow region of the surfaces of the pressboard, the increased negative charge peak in this region may be caused by the AC component. Moreover, more positive charges can also be clearly observed in the vicinity of the top electrode/pressboard interface with a peak value of 0.15 C/m³ in the fresh oil sample and 0.2 C/m³ in the aged oil sample.

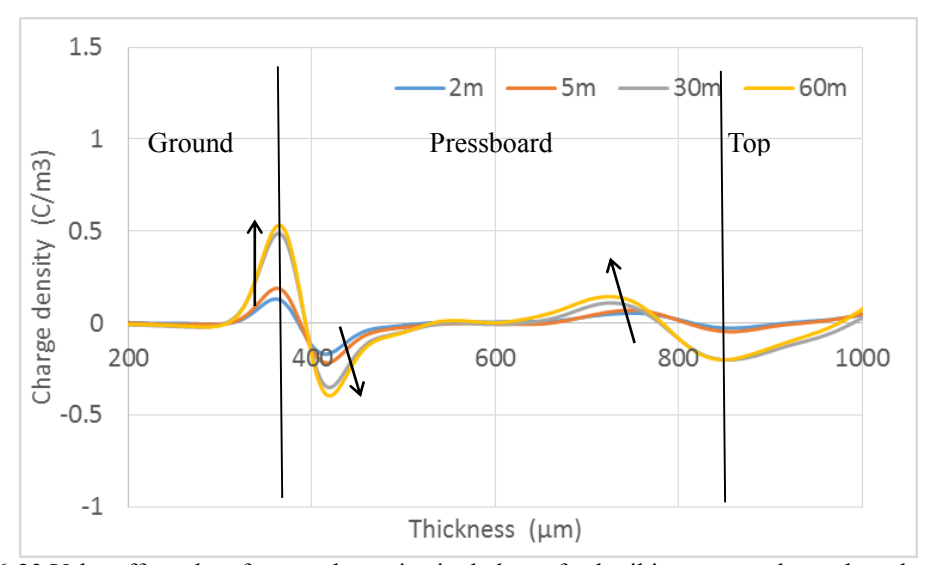


Figure 6-23 Volts-off results of space charge in single layer fresh oil impregnated pressboard under AC/DC combined stresses.

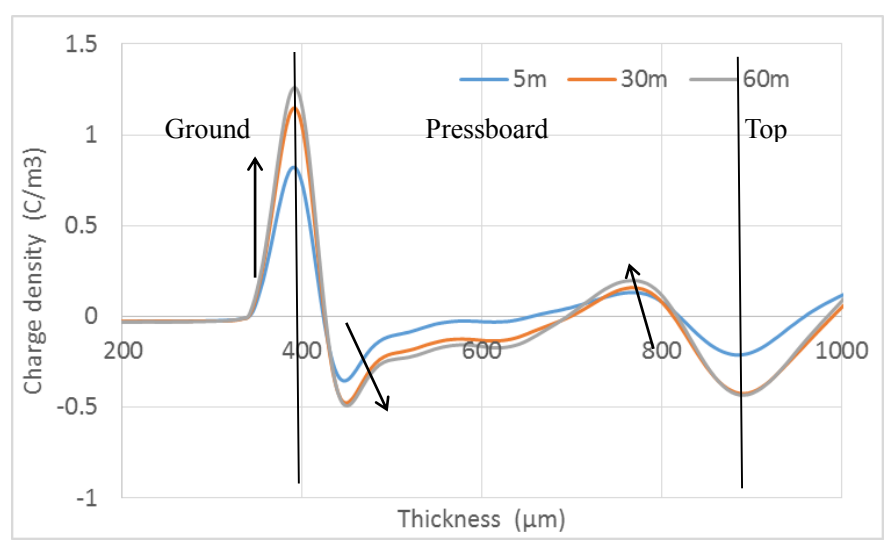


Figure 6-24 Volts-off results of space charge in single layer aged oil impregnated pressboard under AC/DC combined stresses.

Figure 6-25 compares the total charge amount within the fresh oil sample under the pure AC stress, pure DC stress, superimposed stress and the sum charge amount of the AC and DC space charge, respectively. It can be observed that the charge amount under superimposed stress is generally larger than the direct charge sum of charge amount of AC and DC space charge, indicating the charge injection into the impregnated pressboard is non-linear. Moreover, the charge amount at the 2 min is much larger under the superimposed stress than the others, suggesting the acceleration of charge injection caused by the superimposed stress.

On the other hand, as shown in Figure 6-26, the acceleration of the charge injection caused by the superimposed stress cannot be observed as the charge mobility is generally enhanced by the aged oil. The differences of the total charge amount at the 60 min between the superimposed stress and the sum of the AC and DC space charge is much larger in the aged oil sample, compared with the fresh oil sample.

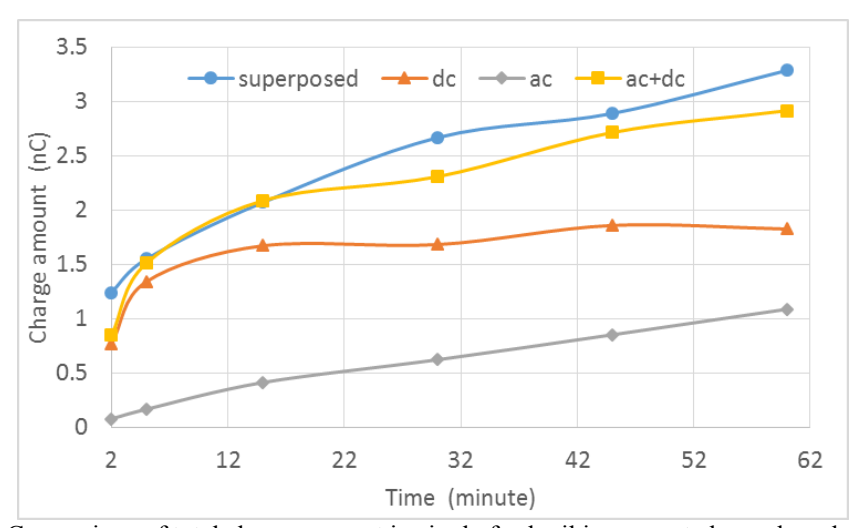


Figure 6-25 Comparison of total charge amount in single fresh oil impregnated pressboard under various stresses.

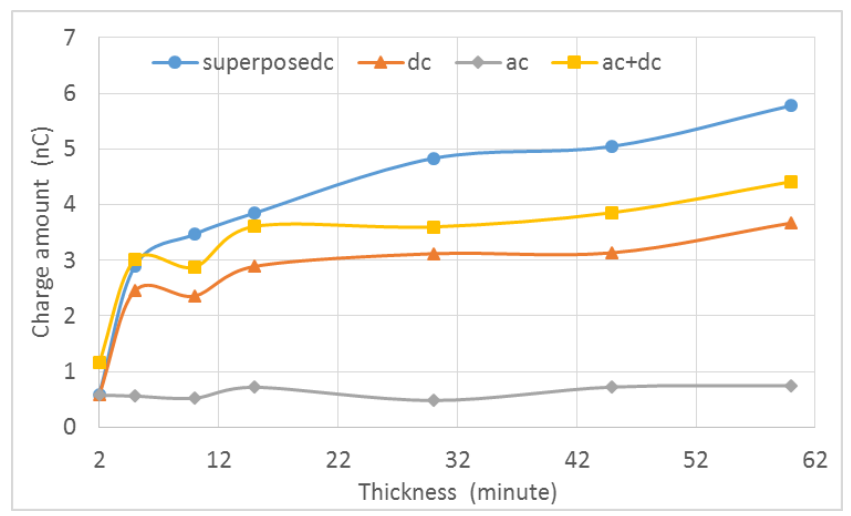


Figure 6-26 Comparison of total charge amount in single aged oil impregnated pressboard under various stresses.

B) Oil gap and pressboard combined insulation system

When an oil gap is combined with the pressboard, the volts-off results under pure DC electric field in the fresh oil sample and aged oil sample are shown in Figure 6-27 and Figure 6-28, respectively. In the fresh oil sample, no obviously space charge accumulation can be observed in the insulation bulk under such low electric field, only small amount of the positive charges locate in the vicinity of the interface between the top electrode and the pressboard. However, in aged oil sample, space charge can be clearly observed. The negative interfacial peak quickly occurs after the application of the DC voltage, which increases to the maximum value within the first 5 min. Meanwhile, the positive charges are injected from the top electrode, and quickly move into the pressboard bulk towards to the oil/pressboard interface due to the large conduction of the aged oil. The neutralization may occur in the vicinity of the oil/pressboard interface, leading to the gradual decrease of the interfacial peak.

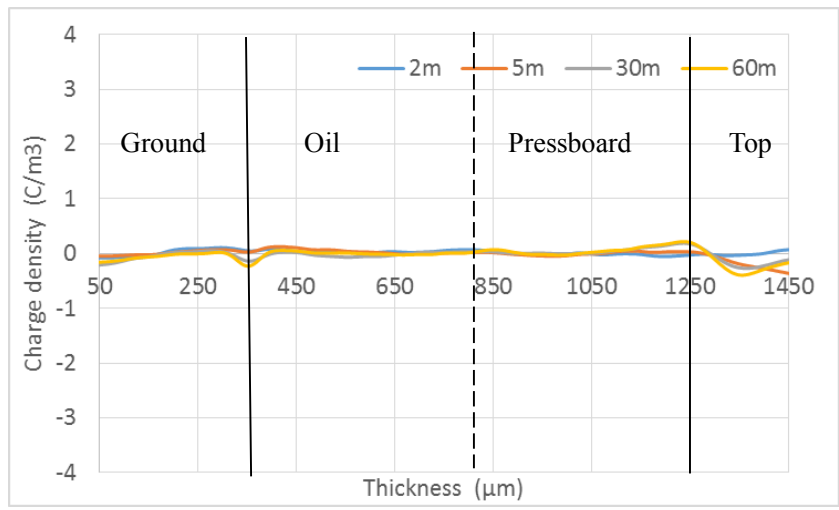


Figure 6-27 Volts-off results of space charge in fresh oil combined with impregnated pressboard insulation system under 4.8 kV/mm DC field.

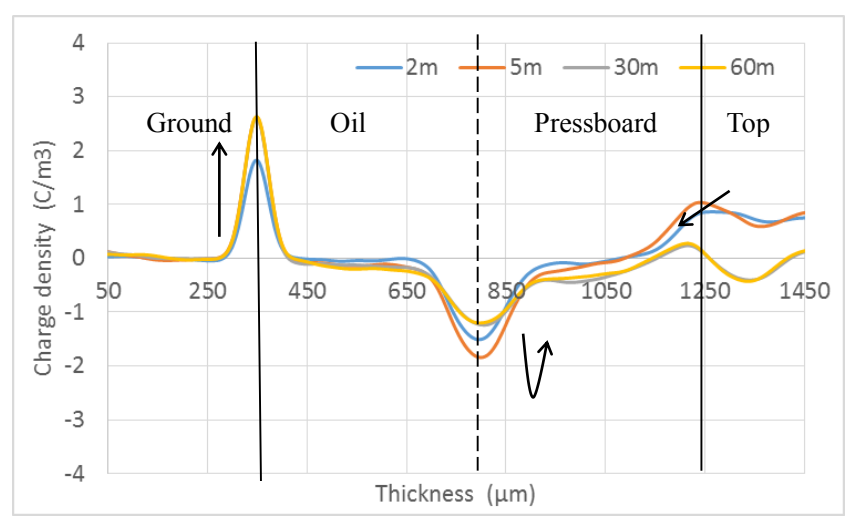


Figure 6-28 Volts-off results of space charge in aged oil combined with impregnated pressboard insulation system under 4.8 kV/mm DC field.

When the superimposed stress is utilized, the space charge injection is significantly enhanced in the fresh oil sample, as shown in Figure 6-29. The negative interfacial peak quickly occurs at the oil/pressboard interface, and keeps increasing in the first 5 min. Meanwhile, large amount of the positive charges can also be observed in the vicinity of the top electrode. On the other hand, in the aged oil sample, charge movement is also accelerated by the superimposed electric field as shown in Figure 6-30. The interfacial peak keeps decreasing during the application of the applied electric field, suggesting the significant neutralization or overlap of the positive charges and negative charges at the interface due to large charge mobility caused by both aged oil and the superimposed stress. The charge amount in the aged oil sample is much less than the fresh oil sample, because only net charges can be detected by the PEA system.

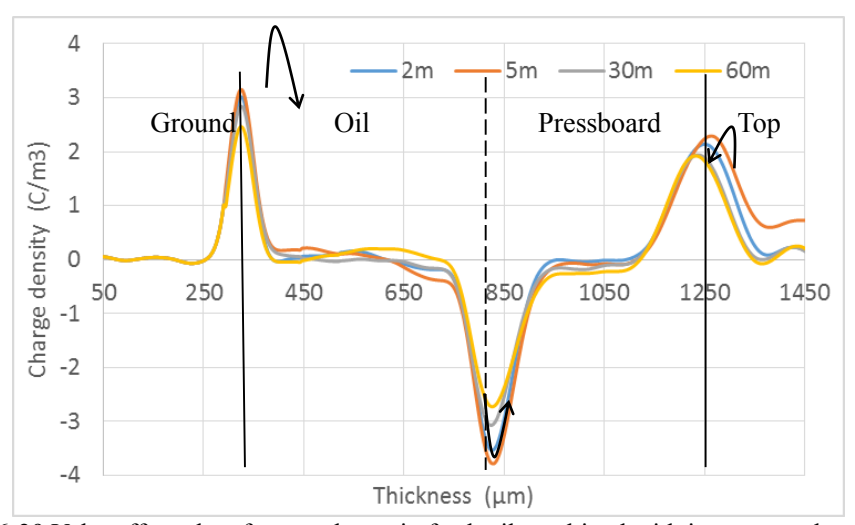


Figure 6-29 Volts-off results of space charge in fresh oil combined with impregnated pressboard insulation system under AC/DC combined stresses.

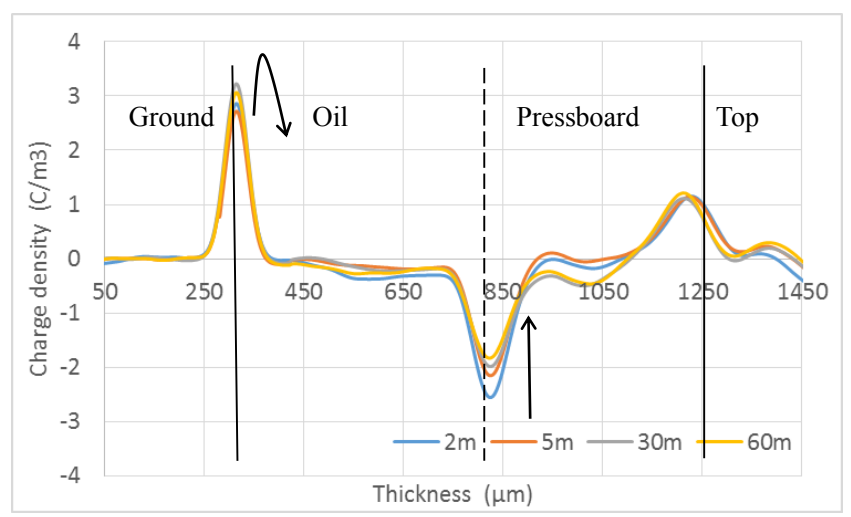


Figure 6-30 Volts-off results of space charge in aged oil combined with impregnated pressboard insulation system under AC/DC combined stresses.

The summary of the total charge amount in the oil gap and pressboard combined insulation system under various electric fields is shown in Figure 6-31. As no AC space charge can be observed in the system, the charge amount under superimposed stress is compared with the pure DC stress. For the fresh oil sample, the maximum total charge amount under pure DC stress is only about 3 nC at 60 min, while it is about 56.4 nC at 5 min of the application of the superimposed stress. For the aged oil, the charge amount under the superimposed stress is slightly larger than the pure DC stress. However, the charge amount keeps deceasing under the superimposed stress due to the neutralization of the positive and negative charges with a very large mobility in the aged oil sample. Therefore, it is reasonable to assume that the maximum charge amount occurs at the very beginning of the voltage application.

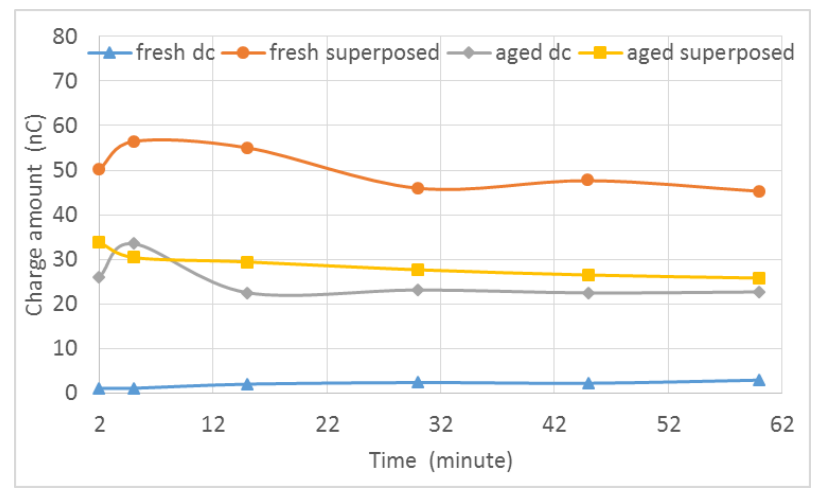


Figure 6-31 Comparison of total charge amount in oil gap combined with impregnated pressboard insulation system under various stresses.

The results above generally validate the oil-pressboard insulation is a non-linear system from the point view of the total charge amount. The charge amount under the superimposed stress is generally larger than the sum of the AC and DC space charge. Moreover, the space charge

movement can be significantly accelerated under the superimposed stress, particularly in the fresh oil sample.

6.3 Conclusions

In this chapter, the dynamics of the space charge in oil pressboard insulation system subjected to the superimposed AC (50 Hz) and DC stresses have been experimentally investigated using the PEA method with a fast data acquisition system. Based on the observations and discussions of the space charge dynamics, this work for the first time revealed the characteristics of the space charge in oil pressboard under the superimposed stresses directly related with the operating condition in real life converter transformers. The major conclusions can be drawn as follows:

- 1. The accumulation of the space charge under pure AC electric field is generally very small compared with DC fields, which depends greatly on the charge mobility in the dielectrics. In the single layer of the fresh oil impregnated pressboard, negative charges are distributed in a narrow vicinity of the ground electrode/pressboard interface. And no space charge accumulation can be observed when an oil gap is combined with the pressboard.
- 2. Homo charge injection (corresponding to the polarity of the applied DC field) can be observed by applying a small DC stress superimposed with the AC stress. Theses accumulated charges could potentially enhance the electric field in the middle of the pressboard when the polarity of the superimposed AC field is same as the DC field. On the other hand, when the polarity of the superimposed AC field is opposite to the DC field, they could increase the electric field at the surface of the pressboard and across the oil gap.
- 3. The total charge amount in the oil pressboard insulation system subjected to the superimposed electric field is generally larger than the sum of the charge amount in the same sample subjected to the DC component and the AC component, respectively. Moreover, the space charge movement can be evidently accelerated by the superimposed stress, particularly, in the fresh oil gap and pressboard combined insulation system. From the point view of the space charge characteristics, this difference validates that the superimposed stress will cause more significant impacts than the sum of the AC space charge and the DC space charge in the oil pressboard insulation system.

Chapter 7.

Conclusions and Future Work

7.1 Conclusions

This dissertation focuses on the investigation of the space charge dynamic characteristics in oil-pressboard under various electric stresses. As an effort to reveal the space charge behaviour for the first time in the thick oil-pressboard insulation system utilized in real life converter transformers, this research work has successfully measured and extracted the features of the space charge dynamics experimentally using a purposed built PEA system in the thick oil impregnated pressboard, multilayer oil gap and pressboards combined insulation system under DC electric fields, polarity reversal stresses, and AC/DC superimposed stresses. The impacts caused by the service aged mineral oil on the space charge behaviour are also investigated and discussed. Some major conclusions can be drawn on the basis of this essential fundamental research work.

A purpose build PEA system has been developed that can successfully detect space charge signal from the thick oil pressboard insulation up to 2 mm in thickness. The homo charge injection in the 1mm thick single layer oil impregnated pressboard has been observed by using the new PEA system. It has been found that the space charge dynamics is related with the amplitude and polarity of the applied DC electric field, as well as the status of the mineral oil. The aged oil in this work is the dominant factors that significantly enhances the space charge dynamics, i.e. the

amount of the accumulated charges is enlarged, and the charge injection and migration are accelerated, resulting in a severe electric field distortion in the middle of the pressboard up to 58%. By applying the characteristics assessments, the results indicate that the aged oil significantly increases the total charge amount and the mobility of the charges, which are related with the large trap density and low trap depth.

Considering the multilayer liquid-solid insulation system utilized in the real life converter transformer, two basic insulation structures are extracted from the multilayer system, i.e. the oil gap combined with the single layer pressboard insulation system and the oil gap sandwiched between two layers of pressboards insulation system. The space charge dynamics have been respectively investigated in these two insulation structures with a total thickness of 1.5 mm (0.5 mm for the liquid gap and 1 mm for the solid part). The space charge cannot be directly measured by the PEA system, due to the large charge mobility in the oil, hence only the charge trapped at the oil/pressboard interface can be detected. The origins of the charge carriers in the oil gap can be from either charge injection or ionization process or both. The charge injection dominates over the ionization when the oil gap is directly contacted with the electrode, otherwise, the ionization dominates the charge dynamics in the oil gap when the injected charges are blocked by the pressboards. These charges could be blocked by the oil/pressboard interface which acts as a barrier to prevent charge from moving through. However, this barrier effect could be weakened by the aged oil. Significant differences have been observed between the space charge profiles and the calculation based on the Maxwell-Wagner polarization on the time constant to reach the steady state and the electric field enhancement. A much longer duration (24 hour) is required to reach the space charge balance in the fresh oil sample. The electric field enhancement is much larger than the calculation value when the steady state is reached.

The impacts caused by the polarity reversal of the applied voltage on the space charge dynamics and electric field enhancement across the oil gap have been studied in the oil gap and single layer pressboard combined insulation system. The experimental results validate that the electric field enhancement across the oil gap immediately after the application of the reversed electric field is directly dependent on the residual charge amount within the insulation system at the moment of the application of the revered stress. Therefore, the larger electric field enhancement could result from the higher applied electric field, the shorter polarity reversal duration and the degradation of the mineral oil. An estimation of the enhanced electric field immediately after the polarity reversal process based on the charge decay characteristics has been proposed and successfully applied to estimate the electric field enhancement in the aged oil sample under 20 kV/mm which cannot be accurately measured due to the very fast space charge dynamics in the aged oil under the greatly enhanced electric field. Based on the measurement results, some recommendations can be made: For a new converter transformer, the polarity reversal duration shows little impact

on the electric field enhancement. However, considering the time for the balance of the space charge is about 24 hours in the fresh oil sample, the voltage application duration for the polarity reversal test may be extended from 90 minutes to 24 hours. For an aged converter transformer, the longer polarity reversal duration could dramatically decrease the electric field across the oil gap after the polarity reversal operation.

It is generally believed that no or small amount of space charge exists in the dielectrics under AC stress. The relationship between the AC space charge and the charge mobility has been investigated using the PEA method with a fast data acquisition system. It has been found that more AC space charges show within the sample with the lower charge mobility, i.e. fresh oil impregnated pressboard. And no space charge can be observed in the oil gap and pressboard combined insulation system. From the point view of space charge dynamics, the non-linear space charge characteristics has been validated in the oil pressboard insulation subjected to the superimposed stresses. The total charge amount and the space charge dynamics can be enhanced by the superimposed stresses, particularly in the fresh oil gap combined with pressboard insulation system. Moreover, electric field distortion has to be taken into consideration as the accumulated space charge could potentially distort the electric field distribution in different regions of the insulation system related with phase angle of the AC stress.

7.2 Recommendations for the future work

As an initial research effort for the space charge behaviour in thick oil pressboard insulation system utilized in converter transformers, this works provides a leading understanding of the space charge dynamics characteristics in the complex solid and liquid composed insulation system under the various stresses related with the real operating conditions in the new and long serviced converter transformers, respectively. However, further detailed investigations of the space charge behaviour in the thick oil pressboard insulation system are still needed in order to have a full understanding of the space charge in the converter transformers.

1. Temperature. The normal working temperature in a converter transformer is usually around 70 °C, which may also dramatically increase to a higher value due to the variable loads. The temperature gradient also exists in the converter transformer from the conductor to the cooling system. The temperature is generally believed an important factor that enhances the space charge dynamics. Hence, potentially for an operating converter transformer, the electric field distortion caused by the presence of the space charge should be much severer than under the room temperature, leading to a higher unexpected risk on the reliability of the insulation system in converter transformers.

- 2. Moisture. For a new converter transformer, the moisture content could be very low in the insulation system. However, the moisture content could rise with the degradation of the dielectrics, which also leads to the increase of the space charge. Moreover, the moisture balance within the liquid and solid composite insulation system is usually related with temperature [37]. When the load increases, the working temperature in the converter transformer rises, the moisture could quickly transfer from the pressboard into the oil. The oil with a high conductivity could result in more charges drift through the oil/pressboard interface into the pressboard bulk, leading to severely enhanced electric field in the middle of the pressboard, which potentially increases the risk of the of the converter transformer with a higher load.
- 3. Different stages of the degradation of the oil pressboard insulation. The differently degraded dielectrics could result in various space charge behaviours. Although the impacts of the fresh insulation and the long term service aged oil have been investigated in this work, it is still worthy of investigating the space charge behaviour in different stages of the degradation for the insulation diagnosis and a better operation strategy to avoid failure.
- 4. Once the space charge behaviour in converter transformers has been better understood, it is important to apply the space charge dependent electric field distribution into the calculation and the design of the electric field distribution in the whole converter transformer. The research in this work has demonstrated the considerable limitation of the electric field calculation based on the Maxwell theory and the superimposed principle which are supposed to be applied in the linear system. The impacts caused by the space charge accumulation are generally neglected in the currently practical power industry, which could seriously threat the reliability of the insulation system in the converter transformer. Considering the complex space charge dynamics under the operating conditions, an accurate but practical method to introduce the impacts caused by the space charge on the electric field estimation is desired.
- 5. On the other hand, the physical model of the space charge behaviour in oil pressboard combined insulation system is helpful for the better understanding of the space charge behaviour in such complex insulation system. However, the accuracy of the model is highly related with the measurements with higher resolution and less signal attenuation. Therefore, a further improved space charge detection system is needed.

References

- [1] E. W. Kimbark, *Direct current transmission*, vol. 1. John Wiley & Sons, 1971.
- [2] D. C. T. Links, D. C. Side, and C. Stations, Power transmission by direct current. Springer, 1975.
- [3] W. Long and S. Nilsson, "HVDC transmission: yesterday and today", *Power Energy Mag. IEEE*, vol. 5, no. 2, pp. 22–31, 2007.
- [4] U. Lamm, "Mercury-arc valves for high-voltage dc transmission", in *Proceedings of the Institution of Electrical Engineers*, 1964, vol. 111, no. 10, pp. 1747–1753.
- [5] H. Alstom, "Connecting to the future", Alstom, 2010.
- [6] J. Arrillaga, *High voltage direct current transmission*, Institution of Electrical Engineers, London, UK, 1998.
- [7] M. P. Bahrman and B. K. Johnson, "The ABCs of HVDC transmission technologies", *Power Energy Mag. IEEE*, vol. 5, no. 2, pp. 32–44, 2007.
- [8] A. G. Siemens, "High voltage direct current transmission-proven technology for power exchange", Energy Sect. Ger., 2011.
- [9] C.-K. Kim, V. K. Sood, G.-S. Jang, S.-J. Lim, and S.-J. Lee, *HVDC transmission: power conversion applications in power* systems, John Wiley & Sons, 2009.
- [10] B. Andersen and C. Barker, "A new era in HVDC?", IEE Rev., vol. 46, no. 2, pp. 33–39, 2000.
- [11] R. Majumder, C. Bartzsch, P. Kohnstam, E. Fullerton, A. Finn, and W. Galli, "Magic bus: High-voltage DC on the new power transmission highway", *Power Energy Mag. IEEE*, vol. 10, no. 6, pp. 39–49, 2012.
- [12] S. P. Teeuwsen and R. Rossel, "Dynamic performance of the 1000 MW BritNed HVDC interconnector project", in *Power and Energy Society General Meeting*, 2010 IEEE, 2010, pp. 1–8.
- [13] O. Saksvik, "HVDC technology and smart grid", in *Advances in Power System Control, Operation and Management (APSCOM 2012), 9th IET International Conference on*, 2012, pp. 1–6.
- [14] M. Davies, M. Dommaschk, J. Dorn, J. Lang, D. Retzmann, and D. Soerangr, "HVDC plus–basics and principle of operation", in *Special Edition for Cigré Exposition*, 2008.
- [15] M. P. Bahrman, J. G. Johansson, and B. A. Nilsson, "Voltage source converter transmission technologies: the right fit for the application", in *Power Engineering Society General Meeting*, 2003, *IEEE*, 2003, vol. 3.
- [16] E. M. Callavik, P. Lundberg, M. P. Bahrman and R. P. Rosenqvist, "HVDC technologies for the future onshore and offshore grid", in *CIGRE*, Paris. 2012
- [17] D. A. N. Jacobson, P. Wang, C. Karawita, R. Ostash, M. Mohaddes and B. Jacobson, "Planning the next nelson river HVDC development phase considering LCC vs. VSC technology", in *CIGRE*, Paris. 2012
- [18] J. M. P. de Andrés, J. Dorn, D. Retzmann, D. Soerangr, and A. Zenkner, "Prospects of VSC converters for transmission system enhancement power grid Europe", June 26–28, 2007, Madrid, Spain.
- [19] A. Carlson, "Specific requirements on HVDC converter transformers", *ABB Transform. AB*, Ludvika, Sweden, 1996.
- [20] IEC 61378-1:2011 Convertor transformers. Transformers for industrial applications, 2011.
- [21] JWG A2/B4. 28, "HVDC converter transformers design review, test procedures, ageing evaluation and reliability in service", *CIGRE*, brochure 406, 2010
- [22] Heathcote and J. Martin, J&P transformer book, 13th ed., Oxiford: Elsevier Ltd, 2007.
- [23] E. Kuffel, W. S. Zaengl and J. Kuffel, *High voltage engineering: fundamentals*, 2nd ed., Oxiford: Butterworth-Heinemann, 2000.
- [24] T. J. Gallagher, Simple dielectric liquids: mobility, conduction, and breakdown, Oxford University Press, 1975.
- [25] T. O. Rouse, "Mineral insulating oil in transformers", Electr. Insul. Mag. IEEE, vol. 14, no. 3, pp. 6-

- 16, 1998.
- [26] J. C. Whitaker, AC power systems handbook, CRC Press, 2006.
- [27] Y. Zhou, "Electrical properties of mineral oil and oil/impregnated pressboard for HVDC converter transformers", Doctoral, School of Electronics and Computer Science, University of Southampton, 2014
- [28] A. M. Emsley and G. C. Stevens, "Review of chemical indicators of degradation of cellulosic electrical paper insulation in oil-filled transformers", in IEE Proc.-Sei. Meas. Technol, 1994.
- [29] A. M. Emsley, X. Xiao, R. J. Heywood, and M. Ali, "Degradation of cellulosic insulation in power transformers. Part 3: Effects of oxygen and water on ageing in oil", *IEE Proceedings-Science, Meas. Technol.*, vol. 147, no. 3, pp. 115–119, 2000.
- [30] T. V Oommen and T. A. Prevost, "Cellulose insulation in oil-filled power transformers: Part II-maintaining insulation integrity and life", *IEEE Electr. Insul. Mag.*, vol. 22, no. 2, 2006.
- [31] D. M. R. Vanegas and S. M. Mahajan, "Correlation between hot-spot temperature and aging factor of oil-immersed current transformers", in *Power and Energy Society General Meeting-Conversion and Delivery of Electrical Energy in the 21st Century, IEEE*, pp. 1–5, 2008.
- [32] D. Linhjell, L. Lundgaard, and U. Gafvert, "Dielectric response of mineral oil impregnated cellulose and the impact of aging", *Dielectr. Electr. Insul. IEEE Trans.*, vol. 14, no. 1, pp. 156–169, 2007.
- [33] S.-Q. Wang, G.-J. Zhang, J.-L. Wei, S.-S. Yang, M. Dong, and X.-B. Huang, "Investigation on dielectric response characteristics of thermally aged insulating pressboard in vacuum and oilimpregnated ambient", *Dielectr. Electr. Insul. IEEE Trans.*, vol. 17, no. 6, pp. 1853–1862, 2010.
- [34] M.-H. Ese, K. B. Liland, and L. E. Lundgaard, "Oxidation of paper insulation in transformers", *Dielectr. Electr. Insul. IEEE Trans.*, vol. 17, no. 3, pp. 939–946, 2010.
- [35] Thomas A. Prevost and T. V. Oommen, "Cellulose insulation in oil filled power transformers: Part I: History and Development", Electrical Insulation Magazine, Vol. 22 No 1, Jan/Feb 2006
- [36] A. M. Emsley, R. J. Heywood, M. Ali, and X. Xiao, "Degradation of cellulosic insulation in power transformers. Part 4. Effects of ageing on the tensile strength of paper", in *Science, Measurement and Technology, IEE Proceedings*-, vol. 147, no. 6, pp. 285–290, 2000...
- [37] P. M. Mitchinson, "Surface tracking in the inter-phase region of large transformers", Doctoral, School of Electronics and Computer Science, University of Southampton, 2008.
- [38] F. Schober, A. Küchler, and C. Krause, "Oil conductivity—an important quantity for the design and the condition assessment of HVDC insulation systems", 2014.
- [39] C. H. Krause and R. Woschitz, "The temperature dependence of the dielectric strength of transformer oil and pressboard insulation at HVDC polarity reversal stress" in *14th International Conference on Dielectric Liquids (ICDL 2002)*, Graz, 2002.
- [40] B. Wang, Q. Wang and Y. Sun, "Calculation and analysis of polarity reverse transient electric field in valve winding end of convertor transformer", *Transformer*, vol. 44 (6), pp. 11-15, 2007.
- [41] H. Okubo, T. Nara, H. Saito, H. Kojima, N. Hawakawa and K. Kato, "Breakdown characteristics in oil/pressboard composite insulation system at HVDC polarity reversal", in *Annual Report Conference on Electrical Insulation and Dielectric Phenomena*, Japan, 2010.
- [42] X. Lu, S. Chen and Z. Fang, "Numerical computation of polarity reversal electric field in the converter transformer ending and its insulation design", *Journal of Xi'an Jiaotong University*, vol. 33(11), pp. 8-12, 1997.
- [43] M. Fu, L. A. Dissado, G. Chen and J. C. Fothergill, "Space charge formation and its modified electric field under applied voltage reversal and temperature gradient in XLPE cable", *IEEE Transactions on Dielectrics and Electrical Insulation*, vol. 15(3), pp. 851-860, 6 2008.
- [44] W. Lao, N. Yan, Q. Chen and Y. Wang, "Analysis of electrical field on oil-paper insulation system under polarity reversal voltage", *Electric machines and control*, vol. 14 (11), 11 2010.
- [45] W. Choo, G. Chen and S. G. Swingler, "Space charge accumulation under effects of temperature gradient and applied voltage reversal on solid dielectric DC cable", in *the 9th International Conference*

- on Properties and Applications of Dielectric Materials, Harbin, 2009.
- [46] T. L. Hanley, R. P. Burford, R. J. Fleming and K. W. Barber, "A genetal review of polymeric insulation for use in hvdc cables", *IEEE Electrical Insulation Magazine*, vol. 19(1), Jan 2003.
- [47] M. S. Kahlil, "International research and development trends and problems of hvdc cables with polymeric insulation", *IEEE Electrical Insulation Magazine*, vol. 13(6), pp. 35-47, Nov. 1997.
- [48] G. C. Montanari, G. Mazzanti, F. Palmieri, A. Motori, G. Perego, and S. Serra, "Space-charge trapping and conduction in LDPE, HDPE and XLPE", *J. Phys. D. Appl. Phys.*, vol. 34, no. 18, p. 2902, 2001.
- [49] C. Tang, G. Chen, M. Fu and R. Liao, "Space charge behavior in multi-layer oil-paper insulation under different dc voltages and temperatures", *IEEE Transactions on Dielectrics and Electrical Insulation*, vol. 17(3), pp. 778-788, 2010.
- [50] J. C. Fothergill, Electrical degradation and breakdown in polymers, no. 9. IET, 1992.
- [51] N. Hussin and G. Chen, "Space charge accumulation and conductivity of crosslinking byproducts soaked LDPE", in *Electrical Insulation and Dielectric Phenomena (CEIDP), 2010 Annual Report Conference on,* 2010, pp. 1–4.
- [52] G. Mazzanti, G. C. Montanari, F. Palmieri, and J. Alison, "Apparent trap-controlled mobility evaluation in insulating polymers through depolarization characteristics derived by space charge measurements", J. Appl. Phys., vol. 94, no. 9, pp. 5997–6004, 2003.
- [53] M. Jeroense and P. Morshuis, "Space charge measurements on impregnated paper: a review of the pea method and a discussion of results", *IEEE Electrical Insulation Magazine*, vol. 13(3), pp. 26-35, May 1997.
- [54] Y. Zhou, Y. Wang, G. Li, X. Wang, Y. Liu, B. Li, P. Li and H. Cheng, "Space charge phenomena in oil-paper insulation materials under high voltage direct current", *Journal of Electrostatics*, vol. 67, pp. 417-421, 2009.
- [55] J. Hao, G. Chen, R. Liao, L. Yang and C. Tang, "Influence of moisture on space charge dynamics in multilayer oil-paper insulation", *Dielectrics and Electrical Insulation*, vol. 19(4), pp. 1456 - 1464, Aug 2012.
- [56] N. Ando and F. Numajiri, "Experimental invrstigation of space charge in xlpe cable using dust figure", *IEEE Trans. Electri. Insul.*, vol. 14(1), pp. 36-42, 1979.
- [57] M. S. Khalil and B. S. Hansen, "investigation of space charge in low-density polyethylene using a field prob technique", *IEEE Trans. Electr. Insul*, vol. 23(3), pp. 441-445, 1988.
- [58] M. S. Khalil, A. A. Zaky, "The effect of cable structure on space charge formation", IEEE Trans. Electr. Insul., Vol. 23, No. 6, pp. 1043 1046, 1988.
- [59] N. H. Ahmed and N. N. Srinivas, "Review of space charge measurements in dielectrics," *Dielectrics and Electrical Insulation, IEEE Transactions on*, vol. 4, pp. 644-656, 1997.
- [60] R. E. Colins, "Analysis of spatial distribution of charges and dipoles in electrets by a transient heating technique", *J. App. Phys.*, vol. 47(11), pp. 4804-4808, 1976.
- [61] Y. Suzuoki, H. Muto, T. Mizutani and M. Ieda, "Investigation of space charge in high-density polyethylene using thermal pulse response", *Japanese Journal of Applied Physics*, vol. 24(5), pp. 604-609, 1985.
- [62] S. Agnel, P. Notingher and A. Toureille, "Space charge measurements under applied dc field by the thermal step method", in *IEEE CEIDP 2000*, Victoria, Canada, 2000.
- [63] T. Pawlowski and R. J. Fleming, "LIMM study of space charge in crosslinked polyethylene", *IEEE Trans. Diel. Electr. Insul.*, vol. 13(5), pp. 1023-1029, 2006.
- [64] T. Takada, Y. Tanaka, N. Adachi, and X. Qin, "Comparison between the PEA method and the PWP method for space charge measurement in solid dielectrics," *Dielectrics and Electrical Insulation, IEEE Transactions on*, vol. 5, pp. 944-951, 1998.
- [65] D. Malec, "Technical problems encountered with the LIPP method in studies of high voltage cable insulator", *Measurement Science and Technology*, vol. 11(5), pp. 76-80, 2000.
- [66] T. Maeno, H. Kushibe, T. Takada and C. M. Cooke, "Pulsed electroacoustic method for the

- measurement of volume charges in e-beam irradiated PMMA", in Annu. Rep. IEEE CEIDP, 1985.
- [67] K. Fukunaga, "Progress and prospects in PEA space charge measurement techniques", *IEEE Electrical Insulation Magazine*, vol. 24(3), pp. 27-37, May 2008.
- [68] T. Maeno, T. Futami, H. Kushibe and T. Takada, "Measurement of spatial charge distribution in thick dielectrics using the pulsed electroacoustic method", *IEEE Tansactions on Electrical Insulation*, vol. 23(3), pp. 433-439, June 1988.
- [69] M. Fu and G. Chen, "Space charge measurement in polymer insulated power cables using flat ground electrode pea system", *IEE Proi-Sci. Meas. Technol.*, vol. 150(2), pp. 89-96, March 2003.
- [70] J. Zhao, "Dynamics of space charge and electroluminescence modelling in polyethylene", Doctoral, Electronics and Computer Science, University of Southampton, 2012.
- [71] PD IEC/TS 62758:2012 Calibration of space charge measuring equipment based on the pulsed electroacoustic (PEA) measurement principle, 2012.
- [72] T. J. Sonnonstine and M. M. Perlman, "Surface potential decay in insulators with field dependent mobility and injection efficiency", *J. Appl. Phys.*, vol. 46, no. 9, pp. 3975–3981, 1975.
- [73] P. W. M. Blom, M. J. M. De Jong, and M. G. Van Munster, "Electric-field and temperature dependence of the hole mobility in poly (p-phenylene vinylene)", *Phys. Rev. B*, vol. 55, no. 2, p. R656, 1997.
- [74] G. C. Montanari, "Dielectric material properties investigated through space charge measurements", *Dielectrics and Electrical Insulation, IEEE Transactions on*, vol. 11, no. 1, pp. 56-64, 2004.
- [75] J. M. Alison, G. Mazzanti, G. C. Montanari and F. Palmieri, "Mobility estimation in polymeric insulation through space charge profiles derived by PEA measurements", in *CEIDP*, 2002.
- [76] R. Ciobanu, I. Prisecaru and C. Schreiner, "Space charge evolution in thermally aged cellulose materials", in *Solid Dielectrics*, 2004. ICSD 2004, Taulorw, France, 2004.
- [77] G. Mazzanti, G. C. Montanari, and J. M. Alison, "A space-charge based method for the estimation of apparent mobility and trap depth as markers for insulation degradation-theoretical basis and experimental validation", *Dielectr. Electr. Insul. IEEE Trans.*, vol. 10, no. 2, pp. 187–197, 2003.
- [78] D. Van der Born, I. A. Tsekmes, P. H. F. Morshuis, J. J. Smit, T. J. Person, and S. J. Sutton, "Evaluation of apparent trap-controlled mobility and trap depth in polymeric HVDC mini-cables", in *Solid Dielectrics (ICSD)*, 2013 IEEE International Conference on, 2013, pp. 242–245.
- [79] C. Tang, R. Liao, G. Chen and L. Yang, "Research on the feature extraction of dc space charge behavior of oil-pape insulation", *SCIENCE CHINA Technological Sciences*, vol. 54(5), pp. 1315-1324, 2011.
- [80] Y. Zhang, B. Yang and D. Tu, "Measuring distribution of carrier trap energy state density at interface of dielectric with step pressure wave method", in *CEIDP*, USA, 1989.
- [81] J. G. Simmons and M. C. Tam, "Theory of isothermal currents and the direct determination of trap parameters in semiconductors and insulators containing arbitrary trap distributions", *J. Phys. D: Appl. Phys.*, vol. 7, pp. 3706-3713, 1973.
- [82] J. Hao, G. Chen and R. Liao, "Effect of thermally aged oil on space charge dynamics in oil/paper insulation system", in *Joint Colloquium on Transformers, Materials and Emerging Test Techniques*, Kyoto, Japan, 2011.
- [83] G. Chen, T. Y. G. Tay, A. E. Davies, Y. Tanaka, and T. Takada, "Electrodes and charge injection in low-density polyethylene using the pulsed electroacoustic technique", *Dielectr. Electr. Insul. IEEE Trans.*, vol. 8, no. 6, pp. 867–873, 2001.
- [84] R. Liu and G. Wahlstrom, "Measurements of the DC electric field in liquid impregnated pressboard using the pressure wave propagation technique", *Conference Record of the 1994 JEEE International Symposium on Electrical Insulation*, Pittsburgh, PA USA, June 5-8, 1994.
- [85] R. Liu, C. Tornkvist, and U. Gafvert, "Pressure wave propagation technique to measure the space charge distribution in pressboard impregnated with aged transformer oil", in *Properties and Applications of Dielectric Materials*, 1994., Proceedings of the 4th International Conference on, 1994, vol. 1, pp. 139–142.
- [86] R. Liu and A. Jaksts, "Moisture and space charge in oil-limpregnated pressboard under HVDC", in

- IEEE International Conference on Condudion and Breakdown in Solid Dielectrics, 1998.
- [87] R. Liu, C. Tornkvist and K. Nsson, "Charge storage and transport in oil-impregnated pressboard at polarity reversal under HVDC", in *Electrical Insulation and Dielectric Phenomena*, Virginia Beach, VA, 1995.
- [88] C. Tornkvist, K. Johansson, and A. Gustafsson, "Measurements of charge distributions: comparison of the PWP and the PEA techniques", in *Conduction and Breakdown in Solid Dielectrics*, 1995. ICSD'95., Proceedings of the 1995 IEEE 5th International Conference on, 1995, pp. 571–574.
- [89] K. C. Kao, Dielectric phenomena in solids, Academic press, 2004.
- [90] R. Ciobanu, I. Prisecaru and S. Aradoaei, "PEA measurements upon cellulose materials submitted to gamma radiation", in *International Conference on Solid Dielectrics*, France, 2004.
- [91] R. Ciobanu, C. Schreiner, W. Pfeiffer and B. Baraboi, "Space charge evolution in oil-paper insulation for dc cables application", in *IEEE 14th Intern. Conf. Dielectr. Liquids (ICDL)*, Massachusetts, USA, 2002.
- [92] R. C. Ciobanu, W. Pfeiffer and C. Schreiner, "Charge packet evolution in paper-oil insulation and derived technological considerations", in *the 7th International Conference on Properties and Applications*, Nagoya, Japan, 2003.
- [93] Y. Zhou, Q. Sun, G. Li, Y. Wang, X. Jiang, Y. Qiu, J. Li and X. Wang, "Effects of space charge on breakdown strength and creeping flashover in oil-paper insulation", *Power System Technology*, vol. 33(5), 2009.
- [94] M. Huang, Y. Zhou, W. Chen, Y. Sha, and F. Jin, "Influence of voltage reversal on space charge behavior in oil-paper insulation", *Dielectrics and Electrical Insulation, IEEE Transactions on*, Vol.21 (1), pp:331-339, 2014.
- [95] D. Wang, S.-Q. Wang, M. Lei, H.-B. Mu, and G.-J. Zhang, "Temperature effect on space charge behavior in oil-impregnated paper insulation", in *Electrical Insulating Materials (ISEIM)*, *Proceedings of 2011 International Conference on*, 2011, pp. 378–382.
- [96] S.-Q. Wang, G.-J. Zhang, H.-B. Mu, D. Wang, M. Lei, S. Suwarno, Y. Tanaka, and T. Takada, "Effects of paper-aged state on space charge characteristics in oil-impregnated paper insulation", *Dielectr. Electr. Insul. IEEE Trans.*, vol. 19, no. 6, pp. 1871–1878, 2012.
- [97] D. Wang, S. Wang, M. Lei, H. Mu, and G.-J. Zhang, "Space charge behavior in oil-paper insulation under polarity reversed voltage", in 2012 IEEE International Conference on Condition Monitoring and Diagnosis, 2012.
- [98] K. Wu, Z. Lv, Q. Zhu, X. Wang, Y. Cheng, and L. A. Dissado, "Space charge formation and conductivity characteristics of PE and oil impregnated paper under a temperature gradient", in *Electrical Insulating Materials (ISEIM), Proceedings of 2014 International Conference on*, 2014, pp. 93–96.
- [99] J. M. Alison and R. M. Hill, "A model for bipolar charge transport, trapping and recombination in degassed crosslinked polyethene", *J. Phys. D. Appl. Phys.*, vol. 27, no. 6, p. 1291, 1994.
- [100] M. J. P. Jeroense, "Charges and discharges in HVDC Cables-in particular in mass-impregnated HVDC cables", TU Delft, Delft University of Technology, 1997.
- [101] M. Huang, Y. Zhou, Q. Sun, Y. Sha and L. Zhang, "Effect of interface on space charge behavior in multi-layer oil-paper insulation", in *CEIDP*, Montreal, QC, 2012.
- [102] Q. Zhu, X. Wang, K. Wu, Y. Cheng, Z. Lv, and H. Wang, "Space charge distribution in oil impregnated papers under temperature gradient", *Dielectr. Electr. Insul. IEEE Trans.*, vol. 22, no. 1, pp. 142–151, 2015.
- [103] Y. Li, Y. Yasuda and T. Takada, "Pulsed electroacustic method for measurement of charge accumulation in solid dielectrics", *IEEE Trans. DEI*, vol. 1, no. 2, pp. 188-195, 1994.
- [104] Z. Xu and G. Chen, "Interfacial characteristics of space charge in multi-layer LDPE", in *CMD*, Beijing, 2008.
- [105] T. Tanaka and M. Uchiumi, "Characteristics of interfacial space charge in several lanminated

- dielectrics", in ICSD, 1998.
- [106] T. Maeno and K. Fukunaga, "Space charge accumulation in multilayer insulators", *Proc. IEEE Int. Symp. Electrets*, pp. 397-402, 1992.
- [107] J. Beyer, P. Morshuis and J. J. Smith, "Space charge phenomena in laminated HVDC insulation", in *Eelectrical insulating materials*, Toyohashi, 1998.
- [108] R. Liu, C. Tornkvist, and K. Johansson, "Space charge distribution in composite oil/cellulose insulation", in *Electrical Insulation and Dielectric Phenomena*, 1994., IEEE 1994 Annual Report., Conference on, 1994, pp. 316–321.
- [109] K. Wu, Q. Zhu, H. Wang, X. Wang, and S. Li, "Space charge behavior in the sample with two layers of oil-immersed-paper and oil", *Dielectr. Electr. Insul. IEEE Trans.*, vol. 21, no. 4, pp. 1857–1865, 2014.
- [110] I. Kitani, Y. Tsuji, and K. Arii, "Analysis of anomalous discharge current in low-density polyethylene", *Jpn. J. Appl. Phys.*, vol. 23, no. 7R, p. 855, 1984.
- [111]Data sheet for HTS 50-08-UF MOSFET switch, BEHLKE.
- [112] P. K. Waston, "The transport and trapping of electrons in polymers", *IEEE Trans. DEI*, vol. 2, pp. 915-924, 1995.
- [113] S. Le Roy, G. Teyssedre, C. Laurent, G. C. Montanari, and F. Palmieri, "Description of charge transport in polyethylene using a fluid model with a constant mobility: fitting model and experiments", *J. Phys. D. Appl. Phys.*, vol. 39, no. 7, p. 1427, 2006.
- [114] G. Chen, Y. Tanaka, T. Takada, and L. Zhong, "Effect of polyethylene interface on space charge formation", *Dielectr. Electr. Insul. IEEE Trans.*, vol. 11, no. 1, pp. 113–121, 2004.
- [115] J. Bird, Electrical circuit theory and technology. Routledge, 2010.
- [116] J. Beyer, "Space charge and partial discharge phenomena in high voltage DC devices", TU Delft, Delft University of Technology, 2002.
- [117] IEC 61378-2:2001 Convertor transformers. Transformers for HVDC applications, 2001.
- [118] M. Fu, L. A. Dissado, G. Chen and J. C. Fothergill, "Space charge formation and its modified electric field under applied voltage reversal and temperature gradient in XLPE cable", *Dielectrics and Electrical Insulation, IEEE Transactions on*, vol. 15, no. 3, pp. 851-860, 2008.
- [119] X. Wang, N. Yoshimura, Y. Tanaka, K. Murata, and T. Takada, "Space charge characteristics in cross-linking polyethylene under electrical stress from dc to power frequency", *J. Phys. D. Appl. Phys.*, vol. 31, no. 16, p. 2057, 1998.
- [120] A. See, J. C. Fothergill, L. A. Dissado, and J. M. Alison, "Measurement of space-charge distributions in solid insulators under rapidly varying voltage using the high-voltage, high-speed pulsed electroacoustic (PEA) apparatus", *Meas. Sci. Technol.*, vol. 12, no. 8, p. 1227, 2001.
- [121] J. Zhao, Z. Xu, G. Chen, and P. L. Lewin, "Numeric description of space charge in polyethylene under AC electric fields", *J. Appl. Phys.*, vol. 108, no. 12, p. 124107, 2010.
- [122] IEC 61378-3:2015 Converter transformers. Application guide, 2015.
- [123] J. Zhao, G. Chen, and L. Zhong, "Space charge in polyethylene under combined AC and DC voltages", *Dielectr. Electr. Insul. IEEE Trans.*, vol. 21, no. 4, pp. 1757–1763, 2014.